NASA TECHNICAL NOTE

NASA TN D-8128

NASA TN D-8128

A SUMMARY OF THE SKYLAB CREW/VEHICLE DISTURBANCES EXPERIMENT T-013

Bruce A. Conway and T. C. Hendricks

Langley Research Center
Hampton, Va. 23665

NATIONAL AERONAUTICS AND SPACE ADMINISTRATION • WASHINGTON, D. C. • MARCH 1976

1. Report No.	2. Government Accession No.	3. Recipient's Catalog No.
NASA TN D-8128		

4. Title and Subtitle	5. Report Date
A SUMMARY OF THE SKYLAB CREW/VEHICLE DISTURBANCES EXPERIMENT T-013	March 1976
	6. Performing Organization Code
7. Author(s)	8. Performing Organization Report No.
Bruce A. Conway and T. C. Hendricks	L-10415
	10. Work Unit No.
9. Performing Organization Name and Address	506-19-13-02
NASA Langley Research Center Hampton, Va. 23665	11. Contract or Grant No.
	13. Type of Report and Period Covered
12. Sponsoring Agency Name and Address	Technical Note
National Aeronautics and Space Administration Washington, D.C. 20546	14. Sponsoring Agency Code

15. Supplementary Notes

Bruce A. Conway: Langley Research Center.
T. C. Hendricks: Marietta Aerospace, Denver, Colorado.

16. Abstract

A manned space flight experiment (designated experiment T-013) to assess the characteristics of astronaut crew-motion disturbances was conducted on the second manned Skylab mission. A brief description of the experiment hardware utilized is given, and a comprehensive discussion of the experiment data reduction and analysis is presented. This report describes data obtained from a force-measuring system, an astronaut limb-motion measuring system, motion-picture film, and the Skylab attitude and pointing control system. Results show that astronaut crew members can produce significant disturbance inputs to a spacecraft's attitude control system. Total forces of up to 400 N were exerted during vigorous soaring activities, whereas "restrained" motions by the experiment subject generated total forces of up to 300 N. A discussion of potential applications of the experiment results is given and appendixes provide additional detail with respect to experiment operations and results. The initial results presented are expected to lead to improved criteria for consideration of crew-motion disturbances in manned spacecraft attitude and experiment pointing control system design.

17. Key Words (Suggested by Author(s))	18. Distribution Statement
Crew-motion disturbance Attitude control Skylab	Unclassified – Unlimited Subject Category 18

19. Security Classif. (of this report)	20. Security Classif. (of this page)	21. No. of Pages	22. Price*
Unclassified	Unclassified	240	$7.50

*For sale by the National Technical Information Service, Springfield, Virginia 22161

Page intentionally left blank

Page intentionally left blank

PREFACE

The Skylab program has resulted in the generation of scientific and engineering data which can be expected to influence manned space flight technology for the next few decades. In setting initial endurance levels for man in space, Skylab also produced an enormous amount of information on the Sun, the planet Earth, the universe, and on man himself. This information will require several years to be completely analyzed and digested. The Skylab crew/vehicle disturbances experiment, experiment T-013, represents a small part of the experience gained in carrying out the ambitious missions of Skylab. The intent of this report is to present the initial results of experiment T-013; it is recognized that future work in the field of astronaut crew-motion disturbances can only improve on the knowledge gained thus far.

Bruce A. Conway, Principal Investigator
Skylab Experiment T-013, Crew/Vehicle Disturbances
NASA Langley Research Center, Hampton, Va.

Page intentionally left blank

Page intentionally left blank

CONTENTS

A SUMMARY OF THE SKYLAB CREW/VEHICLE DISTURBANCES EXPERIMENT T-013

Bruce A. Conway and T. C. Hendricks*
Langley Research Center

SUMMARY

A manned space flight experiment (designated experiment T-013) to assess the characteristics of astronaut crew-motion disturbances was conducted on the second manned Skylab mission. A brief description of the experiment hardware utilized is given, and a comprehensive discussion of the experiment data reduction and analysis is presented. This report describes data obtained from a force-measuring system, an astronaut limb-motion measuring system, motion-picture film, and the Skylab attitude and pointing control system. Results show that astronaut crew members can produce significant disturbance inputs to a spacecraft's attitude control system. Total forces of up to 400 N were exerted during vigorous soaring activities, whereas "restrained" motions by the experiment subject generated total forces of up to 300 N. A discussion of potential applications of the experiment results is given and appendixes provide additional detail with respect to experiment operations and results. The initial results presented are expected to lead to improved criteria for consideration of crew-motion disturbances in manned spacecraft attitude and experiment pointing control system design.

INTRODUCTION

The consideration and analysis of the effects of astronaut crew-motion disturbances on a manned spacecraft's stabilization and control system have been topics of interest since the early 1960's. Initial studies considered crew members as point masses and investigated the effect on a spacecraft of translating one or more of these masses from one point to another within the spacecraft. Later, consideration of man himself as a dynamic system was begun and culminated in a dynamic anthropometric model (see appendixes A and B of ref. 1) developed by using previous U.S. Air Force studies. Both the point mass and anthropometric models were deterministic and required completely time-dependent specification of model inputs. Still more recent effort has been devoted to the description of so-called "stochastic models" of crew-motion disturbances. (See refs. 2

*Martin Marietta Aerospace, Denver, Colorado.

and 3.) Reference 4 presents several of the models noted above, along with a new technique for easy digital computer use of stochastic models.

Confident use of any crew-motion disturbance model depends in part on the extent to which the model can be verified. A mathematical model based in whole or in part on human performance or characteristics requires some understanding of actual performance in an environment comparable with that in which the model is supposed to act. Based on this philosophy, the concept of an experiment to assess the characteristics and effects of astronaut crew-motion disturbances in a manned spacecraft was developed. An experiment proposal was submitted in 1965, based on the simultaneous measurement of an astronaut subject's motions, his applied forces and moments, and the response of the spacecraft to the disturbance inputs. After approval of the experiment concept, development of the required flight hardware was carried out by using results of a contractual experiment definition study. Performance of the experiment (ref. 5) on Skylab 3 (second manned mission of the Skylab program) occurred in August 1973.

The intent of this report is to present a definitive summary of the methods used and the data obtained by experiment T-013. Some interpretation of the experiment data is contained herein; however, detailed analysis and application of experimental results are omitted as being not within the scope of the present effort. The report includes a description of the flight hardware utilized in the Skylab crew/vehicle disturbances experiment (designated experiment T-013). A synopsis of the experiment protocol is also furnished, and data results are included along with the methods and techniques used in the data reduction. The report concludes with a section on applications of the T-013 data and a discussion of conclusions derived from preliminary analyses of the experiment results. Appendixes A to D present additional detail on experiment operations and results.

All data obtained and reduced for this experiment have been recorded on digital magnetic tape. A description of this tape is given in appendix E of this report along with information on requesting any of the T-013 data.

Portions of the experiment T-013 data reduction efforts reported herein were carried out by Martin Marietta Aerospace, Denver, Colorado (NASA contract NAS 1-12734).

SYMBOLS

b	film plane x-coordinate of target point
b'	corrected film plane x-coordinate of target point

C_1, C_2 origins of cameras 1 and 2 coordinate system

CM torso center of mass

d distortion

E_{xj}, E_{yj} residual errors from measurement and film reading inaccuracies, used in resection problem

F force

F_X, F_Y, F_Z forces measured at FMU

F_X', F_Y', F_Z' corrected FMU forces

F_{XV}, F_{YV}, F_{ZV} crew disturbance forces on vehicle

F_1, F_2 film plane image of target for cameras 1 and 2

F1,F2 total (RSS) force, FMU 1 and FMU 2

f focal length of camera lens

g acceleration due to gravity

H_1, H_2, H_3 transformations (see appendix B)

h element of transformation matrix

K_R, K_D gains (see fig. 32)

K_1, K_2, K_3 load cell array geometry constants

$L_1, L_2, \ldots, L_6$ load cell 1, 2, . . ., 6 on an FMU

$M_{T,V}$ total moment on vehicle

M_X, M_Y, M_Z moments measured at FMU

M_X', M_Y', M_Z' corrected FMU moments

M_{XV}, M_{YV}, M_{ZV} crew disturbance moments on vehicle

n film plane y-coordinate of target point

n' corrected film plane y-coordinate of target point

R_1, R_2 vectors from OWS center of mass to FMU 1 and FMU 2 centroids

r radius to target point in film plane

S sum of least-squares solution

s Laplace variable

T_j target point for jth target

TCM,TUP points in torso surface system used in film data reduction

V sum of sum of squares of residual errors

X,Y,Z OWS (ATM) coordinate system

X_M, Y_M, Z_M astronaut overall center-of-mass coordinate system

X_{C1}, Y_{C1}, Z_{C1}; X_{C2}, Y_{C2}, Z_{C2} OWS (ATM) coordinates for center of lens for cameras 1 and 2

X_1, Y_1, Z_1; X_2, Y_2, Z_2 coordinate system for camera 1 and camera 2, respectively

X_1^*, Y_1^*, Z_1^*; X_2^*, Y_2^*, Z_2^* OWS (ATM) coordinates for film plane images of target

γ limb segment Euler angle

ϵ error quantity from measured film data

θ	angle used in film distortion correction
λ	matrix of unknown film target coordinates
σ	standard deviation
ϕ,θ,ψ	Euler angles
$\left.\begin{matrix}\phi_1,\theta_1,\psi_1;\\ \phi_2,\theta_2,\psi_2\end{matrix}\right\}$	OWS (ATM) to cameras 1 and 2 transformation Euler angles
ϕ_3,θ_3,ψ_3	OWS (ATM) to astronaut torso transformation Euler angles
$\omega_X,\omega_Y,\omega_Z$	spacecraft angular rates

Subscripts:

C	with respect to camera coordinate system
j	jth target point; for j = 2 to 9, jth limb segment
i	summation index
M	man's center-of-mass coordinate system
o	initial condition
T	total
V	vehicle
$\left.\begin{matrix}x,y,z\\ X,Y,Z\end{matrix}\right\}$	with respect to x, y, and z (or X, Y, and Z) axes
1,2	with respect to camera 1 or camera 2 (with respect to FMU 1 or FMU 2)

Superscript:

T	transpose

Abbreviations:

AM	airlock module
ANSI	American National Standards Institute
ATM	Apollo telescope mount
CAL	calibration voltage
CMG	control moment gyro
DOY	day of year
DAC	data acquisition camera
EDS	experiment data system
ESRO	European space research organization
FM/PCM	frequency modulation/pulse code modulation
FMS	force measuring system
FMU	force measuring unit
LIMS	limb motion sensing system
OWS	orbital workshop
PCS	pointing control system
PSD	power spectral density
PCM	pulse code modulation
RSS	square root of the sum of squares

An arrow indicates a vector.

DESCRIPTION OF EXPERIMENT

The objectives of the Skylab experiment T-013 (crew/vehicle disturbances) were to assess the characteristics and effects of astronaut crew-motion disturbances aboard a manned spacecraft, and to investigate the response of the Apollo telescope mount (ATM) pointing control system (PCS) to known crew disturbance inputs.

To meet the objectives of the experiment, the following information was required. To verify and extend analytical models of crew motions produced by dynamic human body movements, measurements of the body and limb movements associated with a given crew activity were needed. In order to correlate these body and limb motions with the disturbances produced (and to develop data for stochastic models), measurements of applied forces and moments for the activity were necessary.

Then, to investigate spacecraft attitude response (and specifically for this experiment that of the ATM PCS) as well as to provide an additional verification of analytical model predictions, data from spacecraft angular rate and attitude sensors, along with control actuator response information, were required.

Experiment Hardware

The development of special hardware was carried out to satisfy these objectives. The experiment hardware used in conducting experiment T-013 consisted of three major systems (ref. 1): a limb motion sensing system, a force measuring system, and an experiment data system. In addition, operational spacecraft equipment and subsystems were utilized to carry out the experiment activities in the areas of astronaut position and attitude determination, spacecraft response, and data transmission from the spacecraft to the ground. The three experiment hardware systems are discussed first.

Limb motion sensing system (LIMS).- The LIMS (fig. 1) is an external skeletal structure (exoskeleton) with pivots at 16 principal body rotation points. Each pivot contains a linear potentiometer whose output is directly proportional to the magnitude of joint rotation. The LIMS provided a continuous measurement of body limb position relative to the torso as the crew subject performed the experiment movements. The exoskeleton was fabricated of aluminum and was designed to measure Euler angles (roll, pitch, and yaw sequence) at the shoulders and hips, and a single pitch angle at the elbows and knees. There are a total of 16 potentiometers on the LIMS, 12 at hinge joints and 4 at ring joints.

To simplify donning and doffing by the subject, and to insure correct alinement of the exoskeleton members with principal body members whose rotation was being measured, the exoskeletal structure was mated to a one-piece, coverall-type, form-fitting

suit, fabricated of polybenzimidazole (PBI). PBI was selected for its flammability resistance, minimum outgassing properties, strength, wear resistance, thermal conductivity, and comfort. In addition, use of the one-piece suit for the LIMS permitted the accurate location of photographic targets on the subject for later use in torso center-of-mass and attitude determination. Figure 2 depicts the complete LIMS as worn by a subject.

Power to the potentiometers (at 4.8 V dc), as well as data return, was supplied through a flexible umbilical cable, which mated to connectors on the LIMS and the experimental data system. For protection from launch vibration loads and dust or debris during periods of nonuse, the LIMS was stowed in a container (which was located on the orbital workshop (OWS) wall), shown open in figure 3.

Force measuring system (FMS).- The FMS consists of two force measuring units (FMU's) each of which is comprised of a sense plate, a base plate, an array of six load cells, load cell caging devices, a calibration check mechanism, and signal conditioning electronics. The sense plates were fabricated of aluminum honeycomb, with solid inserts for load cell attachments. One sense plate contained foot restraints, whereas both provided for attachment of a portable handhold. The base plate consisted of a machined aluminum shape designed for the maximum ratio of stiffness to weight. Isolation flexures at both ends of each load cell provided isolation from nonaxial loading. Caging pins provided protection to the load cells from launch and boost vibration loads. Figure 4 depicts the FMU features. Figure 5 is a schematic of the load cell array geometry and gives the orientation of the axis system used.

The signal conditioner for each FMU provided (regulated) 3 V dc to the load cell bridge circuits, along with load cell output signal amplification to the 0- to 5-V dc level required for processing by the experiment data system. Figure 6 presents a circuit schematic typical for each of the load cells in an FMU.

Experiment data system (EDS).- The data system used for T-013 (fig. 7) consists basically of a pulse code modulation (PCM) encoder to accept data from 31 analog channels (LIMS and FMS data) and 24 channels of bilevel inputs representing a time code from the Skylab airlock module (AM) timing reference system. (See table I.) The inputs to the encoder are formatted in a single PCM bit stream for onboard recording and subsequent telemetry to ground. Output bit rate (0 to 5 V dc) to the AM experiment tape recorders was 5760 bits/sec. Figure 8 is a simplified diagram of the electronics within the EDS.

Spacecraft equipment and systems.- The conduct of experiment T-013 required the use of certain data handling instrumentation. One of three tape recorders dedicated to experiment use was employed to record all data coming from the EDS, along with a voice track from the orbital workshop (OWS) intercom system. This voice and data information was transmitted to ground stations at a 22:1 playback ratio during station overpasses by the Skylab vehicle, by one of three FM/PCM telemetry channels.

TABLE I.- T-013 TELEMETRY DATA LIST

Skylab measurement number	Description	LIMS angle (fig. 1)
G7017 T-013	LIMS angle, right shoulder, rear	1
G7023 T-013	LIMS angle, right shoulder, forward	2
G7024 T-013	LIMS angle, right upper arm	3
G7055 T-013	LIMS angle, left shoulder, rear	4
G7054 T-013	LIMS angle, left shoulder, forward	5
G7021 T-013	LIMS angle, left upper arm	6
G7022 T-013	LIMS angle, right elbow	7
G7057 T-013	LIMS angle, left elbow	8
G7058 T-013	LIMS angle, right hip, rear	9
G7056 T-013	LIMS angle, right hip, forward	10
G7059 T-013	LIMS angle, right thigh	11
G7060 T-013	LIMS angle, left hip, rear	12
G7061 T-013	LIMS angle, left hip, forward	13
G7063 T-013	LIMS angle, left thigh	14
G7062 T-013	LIMS angle, right knee	15
G7052 T-013	LIMS angle, left knee	16
S7005 T-013	FMU 1, load cell 1	
S7004 T-013	FMU 1, load cell 2	
S7003 T-013	FMU 1, load cell 3	
S7007 T-013	FMU 1, load cell 4	
S7006 T-013	FMU 1, load cell 5	
S7009 T-013	FMU 1, load cell 6	
S7008 T-013	FMU 2, load cell 1	
S7001 T-013	FMU 2, load cell 2	
S7000 T-013	FMU 2, load cell 3	
S7011 T-013	FMU 2, load cell 4	
S7010 T-013	FMU 2, load cell 5	
S7002 T-013	FMU 2, load cell 6	
M7075 T-013	FMU 1, calibration voltage	
M7076 T-013	FMU 2, calibration voltage	
M7077 T-013	LIMS, calibration voltage	
K7328 T-013	Airlock module timing reference	
K7329 T-013	T-013 identification word	

Two data acquisition cameras (DAC's), operating at 6 frames per second, with 5-mm lenses monitored the experiment subject's center of mass and torso attitude. By using the targets on the LIMS suit, photogrammetric techniques have been employed to obtain subject's torso motion histories. These techniques, and the results obtained, are discussed subsequently.

Finally, to obtain the necessary spacecraft response information for the experiment, a series of measurements from the ATM PCS were taken. These measurements were existing ATM "housekeeping" data and were obtained both in real time during portions of the experiment and in the record/dump mode. A discussion of these measurements may also be found in the section "Results."

As a further note, parts of the experiment activities were recorded on video tape, which was subsequently dumped to the ground. Figure 9 shows the OWS area of experiment operations with certain T-013 equipment identified.

Experiment Operation and Protocol

The crew/vehicle disturbances experiment was performed in the forward (dome) area of the Skylab orbital workshop during the Skylab-3 mission (second manned mission). Alan L. Bean, spacecraft commander, served as the primary experiment subject, with Jack R. Lousma, spacecraft pilot, as a secondary subject for some of the experiment tasks. All experiment activities were conducted on day-of-year (DOY) 228 (mission day 20), with some additional experiment-related activities performed on other days in efforts to resolve anomalies noted on day 228. Appendix A to this report presents an excerpt from the Skylab maneuvering experiments checklist, which describes the T-013 operations and activities carried out by the flight crew. Table II summarized the days and activities of experiment T-013 operations on the Skylab-3 mission. The tasks performed by the subject included the following primary categories.

Gross body motions.- These motions included simple arm and leg movements, breathing and coughing exercises, and soaring translations between the two force measuring units. The limb motions included single- and double-pendulum arm and leg movements and body bending at the waist. These body motions were designed primarily to reproduce types of activities performed in earlier ground simulations (ref. 6) and to allow comparisons by use of the mathematical models discussed previously. The arm and leg movements and breathing and coughing exercises were performed with the subject attached to FMU 1 with foot restraints.

Simulated console operations.- This activity consisted of the subject performing motions typically associated with a console operation, such as the flipping of switches, hand-controller inputs, and keyboard entries. This exercise lasted approximately 3 minutes, and its purpose was to provide a baseline for stochastic model definition.

TABLE II.- OPERATIONS CHRONOLOGY

Day of year	Activity
226	Ten-minute checkout operations to ascertain that the force measuring system was operational
228	Performance of T-013
240 and 241	Performance of malfunction procedure to investigate anomaly occurring in one force measuring unit during T-013 performance
242	Repeat of task 3, "Worst Case Control System Input," in order to obtain camera/PCS real-time data correlation
247	Repeat of task 3 to obtain camera/PCS real-time data correlation

Worse case control system inputs.- Included in this category were movements chosen for their potentially large force and moment inputs to the ATM pointing control system; examples of these activities are one- and two-man soaring motions (utilizing the primary and secondary subjects along the paths indicated in fig. 10), and vigorous one-man exercise-type motions performed with the subject restrained to FMU 1.

Hardware Performance Assessment and Anomalies

Hardware operation.- In general, operations with the T-013 experiment hardware were carried out satisfactorily. Stowage and unstowage and donning and doffing of the LIMS garment and exoskeleton were performed smoothly. Uncaging of the FMU's and operation of the calibration lever were also performed with no problems. All other experiment hardware and related operations performed by the crew in conjunction with T-013 were likewise conducted successfully and without difficulty.

Force measuring unit anomaly.- On DOY 228 an apparently severe loading condition on FMU 2 (without foot restraints) caused two of the six load cells to go off scale at the maximum output voltage (+5 V dc). Based on analysis of individual load cell readings immediately prior to the anomaly, it has been concluded that the unit was subjected to a severe shock bending moment during a "landing" from a vigorous soaring maneuver. The two load cells continued to read off scale during the remainder of the T-013 performances. The other four load cells in the FMU 2 array exhibited a "zero shift" but appeared to function in a nominal manner throughout T-013 activities. On DOY 240 and 241 a malfunction procedure, which had been devised after discovery of

the load cell anomaly, was carried out by the crew to determine the cause of the off-scale readings. The procedure consisted primarily of using a push-pull force indicator to apply calibrated loadings to selected locations and in specified directions on the unit while recording and transmitting the FMU data back to ground. As a result of these procedures, and by considering all data from FMU 2, the most probable cause of the anomalous readings appears to be a failure in the bond between the load cell beam and the strain gage produced by a mechanical deformation of the FMU assembly which, in turn, caused (at least momentary) high loading input to the load cells. A hysteresis effect of this mechanical deformation may also be involved in the "zero shifts" noted in the other four load cells.

Attempts were made to reduce data from FMU 2 by using an algorithm to synthesize "correct" data from the two damaged load cells. However, it was found that (based on a check of the algorithm with FMU 1 data) accuracy of the reconstructed force profiles varied from 0 to 25 percent of full-scale values. It was thus determined that such data could be used only to indicate trends and to provide event time correlation of T-013 activities.

DATA REDUCTION

Skylab experiment T-013 data consisted of 16-mm motion-picture film and telemetry data. As noted previously, two data acquisition cameras (DAC's) were positioned in the OWS to record T-013 astronaut activities. (See fig. 10.) One camera was located in the OWS dome, the other to the side of the OWS. The T-013 telemetry data were recorded in digital form and were comprised of force and moment time profiles measured by the FMU's, the LIMS voltages, and the airlock module timing reference. The reduction of the telemetry data involved scaling, bias removal, and appropriate formatting of the data. Reduction of the 16-mm motion-picture film data was a more complex task that required explicit points to be read from each frame of the film. Each frame required reading three points on the astronaut and three background points. The background points were used to remove lens distortion and the astronaut points were transformed by appropriate equations to yield astronaut center-of-mass and torso-attitude time histories. Initially, it was assumed that the DAC locations and orientations were known. Preliminary data analysis results indicated that the DAC locations were in error and a photogrammetric resection was required to determine camera location and orientation. Appendix B presents the coordinate systems, the appropriate transformations, and the analysis used in the photogrammetric reduction of the T-013 film data.

Film Data Reduction

The purpose of this analysis was to reduce experiment T-013 motion-picture film data to obtain astronaut position and attitude in orbital workshop (OWS) coordinates. (See appendix B.) The film data consisted of two cameras photographing three noncollinear targets on an astronaut over the same time period. The analysis converted the film plane images of the three targets to their corresponding OWS coordinates, and then computed astronaut center of mass and attitude from the OWS target coordinates.

Because of poor image quality of much of the film, some uncertainty in locating the targets was encountered. Two types of image enhancement, spatial frequency filtering and spectral filtering, were employed in attempts to improve the resolution. Neither method produced satisfactory results, and the raw data film was used for all reduction activities discussed herein.

Error correction of raw film data.- Raw data were modified to account for lens distortion. The radial distance from the center of the film to the film image was computed; the distortion was then found by linear interpolation from a table of the variation of distortion with radial distance. The data were then corrected by the (radius-distortion)/radius factor.

Let

b_j film plane x-coordinate of target

n_j film plane y-coordinate of target

$\theta = \tan^{-1} \frac{n_j}{b_j}$

$r = \sqrt{b_j^2 + n_j^2}$

d table lookup value based on r

then

$$r' = r - d$$

and

$$b_j' = \frac{b_j r'}{r} = r' \cos \theta = \text{Corrected x-coordinate of film plane target image}$$

$$n_j' = \frac{n_j r'}{r} = r' \sin \theta = \text{Corrected y-coordinate of film plane target image}$$

Film data readout.- For the film data readout, the film was projected onto a sonic screen to an image size of approximately 0.3048 m by 0.4064 m. A sonic stylus was then used to locate the four corners and center of the film. A key punch recorded the stylus locations for each of the three targets on a card. To convert from stylus coordinates to camera coordinates, the center of the frame was subtracted out and the value scaled to the actual film frame size of 7.2 mm by 10.0 mm. Let g_x and g_y be the stylus-read coordinates. The camera coordinates are b, n, and -f where

$$b = -(g_x - 1146)(0.009354537)$$

$$n = (g_y - 884)(0.009354537)$$

f = Distance from center of camera lens to film plane, 5 mm

Telemetry Data Reduction

Data acquisition during the execution of experiment T-013 consisted not only of photographic data as discussed previously, but also of telemetry data from the force measuring units (FMU) and the limb motion sensors (LIMS).

The total measurements transmitted to ground as telemetry data are presented in table I.

Limb motion data.- Analysis of experiment T-013 in part required that the time orientation of the subject's limbs with respect to his torso be known. This motion was obtained by the use of the limb motion sensor (LIMS) assembly. For more clarity, the LIMS shoulder and hip joints are shown in figure 11. (See also fig. 1.)

The angular motion of each limb relative to the torso can be described by two Euler angles per segment. (See ref. 1.) These Euler angles can then be used to relate the motion of the man's limbs to vehicle disturbances.

The man's torso coordinate system (X_M, Y_M, Z_M) and identification of each limb segment are shown in figure 12. The desired Euler angles for each segment are shown in figure 13 for segments 2 to 9. The rotation sequence is 0, γ_{j2}, and γ_{j1}.

The gamma angles for each segment are defined in terms of the scaled potentiometer outputs as follows:

For $j = 2,6$,

$$\gamma_{j1} = \sin^{-1} 0.7071(S\theta_j + S\phi_j C\theta_j)$$

$$\gamma_{j2} = \tan^{-1} \frac{0.7071(S\theta_j - S\phi_j C\theta_j)}{C\phi_j C\theta_j}$$

where $S\theta$, $C\theta$, and so forth, are shorthand notations for $\sin\theta$, $\cos\theta$, and so forth.

For $j = 3,7$,

$$\gamma_{j1} = \sin^{-1} 0.7071(-S\theta_j + S\phi_j C\theta_j)$$

$$\gamma_{j2} = \tan^{-1} \frac{0.7071(S\theta_j + S\phi_j C\theta_j)}{C\phi_j C\theta_j}$$

For $j = 4,8$,

$$\gamma_{j1} = \sin^{-1} \left\{0.7071\left[(C\theta_i C\psi_i - C\phi_i S\psi_i - S\phi_i S\theta_i C\psi_i)S\theta_j + (S\theta_i + S\phi_i C\theta_i\, C\theta_j\right]\right\}$$

$$\gamma_{j2} = \tan^{-1} \left\{\frac{0.7071\left[(C\theta_i C\psi_i + C\phi_i S\psi_i + S\phi_i S\theta_i C\psi_i)S\theta_j + (S\theta_i - S\phi_i C\theta_i)C\theta_j\right]}{(S\phi_i S\psi_i - C\phi_i S\theta_i C\psi_i)S\theta_j + C\phi_i C\theta_i C\theta_j}\right\}$$

For $j = 5,9$,

$$\gamma_{j1} = \sin^{-1} \left\{0.7071\left[(C\theta_i C\psi_i + C\phi_i S\psi_i - S\phi_i S\theta_i C\psi_i)S\theta_j + (S\theta_i - S\phi_i C\theta_i)C\theta_j\right]\right\}$$

$$\gamma_{j2} = \tan^{-1} \left\{\frac{0.7071\left[(C\theta_i C\psi_i - C\phi_i S\psi_i - S\phi_i S\theta_i C\psi_i)S\theta_j + (S\theta_i + S\phi_i C\theta_i)C\theta_j\right]}{(S\phi_i S\psi_i - C\phi_i S\theta_i C\psi_i)S\theta_j + C\phi_i C\theta_i C\theta_j}\right\}$$

where $i = j - 2$.

The LIMS voltages as obtained from the telemetry data tape were biased, scaled, and calibrated. The bias terms represent the output of each potentiometer when the subject was in an attitude, as determined by observing the film data, similar to that shown in figure 2. This reference attitude occurred on DOY 228 at 15:55:24.

The angles were then divided by the LIMS calibration voltages (CAL = 4.8 V) and converted to radians by the following constants:

$$\theta_i = \frac{5.58029\theta_i}{CAL} \qquad (i = 2 \text{ to } 9)$$

$$\phi_i = \frac{5.58029\phi_i}{CAL} \qquad (i = 2, 3, 6, 7)$$

$$\psi_i = \frac{7.59520\psi_i}{CAL} \qquad (i = 2, 3)$$

$$\psi_i = \frac{5.81760\psi_i}{CAL} \qquad (i = 6, 7)$$

A representative display of gamma angles from certain activities is given in the "Results" section.

Force measuring system data.- Figure 14 describes the coordinate system and orientation of each load cell in an FMU, whereas figure 15 shows the orientation of each FMU as installed in the orbital workshop and the conversion to the analysis coordinate system. Forces and moments sensed at an FMU are

$$F_X = \cos 45^\circ \cos 30^\circ \left(L_2 - L_3 - L_4 + L_5\right)$$

$$F_Y = \sin 45^\circ \left(L_1 + L_2 + L_3 + L_4 + L_5 + L_6\right)$$

$$F_Z = \cos 45^\circ \sin 30^\circ \left(L_3 - L_2 + L_5 - L_4\right) + \cos 45^\circ \left(L_6 - L_1\right)$$

$$M_X = K_1 \sin 45^\circ \left(L_2 + L_3 - L_4 - L_5\right)$$

$$M_Y = K_2 \cos 45^\circ \left(L_5 - L_4 + L_3 - L_2 + L_1 - L_6\right)$$

$$M_Z = K_2 \sin 45^\circ \left(L_1 + L_6\right) - K_3 \sin 45^\circ \left(L_2 + L_3 + L_4 + L_5\right)$$

Since the sensing plate is relatively stiff, any force applied to it will be sensed by all load cells. This cross coupling determined by FMU calibration is accounted for by a series of equations, one of which is presented here:

$$F'_X = F_X + 0.016732F_Y - 0.012130F_Z + 0.0013370M_X + 0.0028717M_Y$$
$$- 0.0071968M_Z - 0.000047152F_XF_Z - 0.0010625F_YF_Z$$
$$+ 0.00028291F_ZM_Z + 0.00015890F_XF_Y + 0.00017863F_YF_Y$$

The final set of equations, scaling equations, to give the forces and moments about each FMU coordinate system is given for FMU 1,

$$F_{X,1} = 38.139456F'_X, \text{ newtons}$$

$$F_{Y,1} = 38.103968F'_Y, \text{ newtons}$$

$$F_{Z,1} = 39.850579F'_Z, \text{ newtons}$$

$$M_{X,1} = 0.9698586M'_X, \text{ newton-meters}$$

$$M_{Y,1} = 0.9871221M'_Y, \text{ newton-meters}$$

$$M_{Z,1} = 1.0174757M'_Z, \text{ newton-meters}$$

and for FMU 2,

$$F_{X,2} = 38.402497F'_X, \text{ newtons}$$

$$F_{Y,2} = 37.958804F'_Y, \text{ newtons}$$

$$F_{X,2} = 38.31944F'_Z, \text{ newtons}$$

$$M_{X,2} = 0.9874284M'_X, \text{ newton-meters}$$

$$M_{Y,2} = 0.9695604M'_Y, \text{ newton-meters}$$

$$M_{Z,2} = 0.9891317M'_Z, \text{ newton-meters}$$

The conversion to vehicle coordinates can be obtained directly from figure 15. These equations are:

$$F_{XV} = -F_{Z,1} + F_{Z,2}$$

$$F_{YV} = -F_{Y,1} + F_{Y,2}$$

$$F_{ZV} = -F_{X,1} - F_{X,2}$$

$$M_{XV} = -R_{1,Y}F_{X,1} + R_{1,Z}F_{Y,1} - R_{2,Y}F_{X,2} - R_{2,Z}F_{Y,2} - M_{Z,1} + M_{Z,2}$$

$$M_{YV} = -R_{1,Z}F_{Z,2} + R_{1,X}F_{X,1} + R_{2,Z}F_{Z,2} + R_{2,X}F_{X,2} - M_{Y,1} + M_{Y,2}$$

$$M_{ZV} = -R_{1,X}F_{Y,1} + R_{1,Y}F_{Z,1} + R_{2,X}F_{Y,2} - R_{2,Y}F_{Z,2} - M_{X,1} + M_{X,2}$$

RESULTS

Results of the data reduction efforts described in the section "Data Reduction" are presented in this section. Included are the center-of-mass time histories from the film data and the LIMS and FMS results from the experiment telemetry data. Also, the vehicle response results, as obtained from the experiment and as calculated by using mathematical models of the Skylab vehicle dynamics, are reported.

Astronaut Center-of-Mass Time Histories

An objective of the T-013 optical film data reduction was to determine the time histories of the astronaut's center of mass and attitude. Because of the volume and nature of this data, no tabular representation is presented. However, specific plots are useful in that qualitative assessments may be made of the various soaring activities. A summary of the reduced soaring film data presented herein is given as table III.

TABLE III.- SOARING DATA

Figure	Start time	Duration, sec	Film frames	Direction of motion
16(a)	16:06:43.57	2.0	1 to 15	To FMU 2
16(b)	16:06:52.24	1.7	53 to 63	To FMU 1
16(c)	16:07:03.57	2.7	121 to 137	To FMU 2
16(d)	16:07:10.07	2.7	160 to 176	To FMU 1

The computed results for astronaut position during soaring activities are displayed in figure 16. In each plot, FMU 1 is on the right and FMU 2 is on the left. The grid represents a cross-sectional plane of the OWS located at the base of the FMU's and viewed from the side of the OWS opposite the FMU's. Grid spacing is approximately 0.185 m.

It is interesting to note that for each soaring activity, the center-of-mass trajectory tends to slope toward the OWS dome as FMU 1 is approached. Careful visual analysis of this film indicates that there is an obstruction above FMU 2 which results in the observed trajectories.

Of additional interest are the velocities achieved by the subject while soaring. From figure 16 and by also noting the durations of various soaring movements (obtainable from table III), it is seen that soaring velocities of up to 1.9 m/sec are routinely observable. Inspection of video tape records of portions of the T-013 experiment confirm this calculated value.

Correlation of Film and Telemetry Data

Five of the eight periods of soaring activity can be correlated with the film data for day 228. The soaring in this tabulation corresponds to intervals of no measurable force on either FMU. The duration of soaring appears to be shorter on the telemetry tape than on the film. This is probably due to the fact that the crewman is still in contact with an FMU during part of the soaring motion. If FMU-hold plus soaring times are compared, then the time reference is good to within 5 percent and major activities (long hold periods, etc.) can be correlated.

This correlation is presented in table IV. The first column (Start time) is the time in hours and minutes of DOY 228 that a particular activity started as determined from the film data with an initial time reference from the telemetry data. The second column (Activity) describes the particular activity observed on the film. The third column (Duration) is the duration in seconds of that activity as determined from the film data.

These times are relatable to the Start times of table XI and the times (sec) shown in figure 60. Time correlation between film and telemetry was obtained with a sequence whereby the observer "knocked" on an FMU at specified intervals. This visual sequence, and the force spikes resulting in the telemetry from the "knocks" enabled the film and telemetry data to be correlated to within one frame (or 1/6 second). Sequence 3 of task 1, as outlined in appendix A, presents details of the time correlation sequence.

TABLE IV.- TELEMETRY/FILM SOARING ACTIVITY SUMMARY

(a) Soaring activity 4; day 228 (15:41:4.25 to 15:41:42.35)

Start time	Activity	Duration, sec
41:04.25	Soar to FMU 2	0.8
41:04.05	Hold FMU 2	4.3
41:09.35		1.1
41:10.45	FMU 1	4.2
41:14.65	Soar	1.0
41:15.65	FMU 2	4.8
41:20.45	Soar	1.0
41:21.45	FMU 1	3.9
41:25.35	Soar	.8
41:26.15	FMU 2	4.3
41:30.45	Soar	.9
41:31.35	FMU 1 only	5.2
41:36.55	Activity on both FMUs	3.3
41:39.85	FMU 1 only	2.5
Summary: 38.1 seconds activity; 6 soarings		

(b) Soaring activity 5; day 228 (16:06:43.57 to 16:07:19.77)

Start time	Activity	Duration, sec
6:43.57	Soar to FMU 2	0.5
6:44.07	Hold FMU 2	7.5
6:51.57	Soar	.8
6:52.38	FMU 1	10.39
7:02.77	Soar	2.0
7:04.77	FMU 2	4.5
7:09.27	Soar	1.7
7:10.97	Hold FMU 1	8.8
Summary: 36.2 seconds activity; 4 soarings		

TABLE IV.- Concluded

(c) Soaring activity 6; day 228 (16:14:55.57 to 16:15:52.87)

Start time	Activity	Duration, sec
14:55.57	Soar to FMU 2	0.4
14:55.97	Hold FMU 2	5.2
15:01.17	Soar	.7
15:01.87	Hold FMU 1	5.2
15:07.07	Soar	.6
15:07.67	FMU 2	4.5
15:12.17	Soar	.7
15:12.87	FMU 1	6.8
15:19.67	Soar	1.3
15:20.97	FMU 2	5.41
15:26.38	Soar	1.09
15:27.47	FMU 1	5.7
15:33.17	Soar	1.0
15:34.17	FMU 2	6.1
15:40.27	Soar	1.1
15:41.37	Hold FMU 1	11.5
Summary: 57.3 seconds activity; 8 soarings		

(d) Soaring activity 7; day 228 (16:17:14.37 to 16:18:01.17)

Start time	Activity	Duration, sec
17:14.37	Soar to FMU 2	0.7
17:15.07	Hold FMU 2	7.4
17:22.47	Soar	.7
17:23.17	FMU 1	5.5
17:28.67	Soar	.6
17:29.27	FMU 2	6.7
17:35.97	Soar	.7
17:36.37	FMU 1	15.0
17:51.67	Soar	.4
17:52.07	FMU 2	8.2
18:00.27	Soar	.9
Summary: 46.8 seconds activity; 6 soarings		

(e) Soaring activity 8; day 228 (16:26:04 to 16:26:56)

Start time	Activity	Duration, sec
26:04.3	Hold FMU 1	9.6
26:13.9	Soar to FMU 2	.9
26:14.8	FMU 2	5.8
26:20.6	Soar	1.1
26:21.7	FMU 1	9.9
26:31.6	Soar	2.7
26:34.3	FMU 2	3.6
26:37.9	Soar	3.3
26:41.2	FMU 1	3.9
26:45.1	Soar	3.2
26:48.3	FMU 2	3.7
26:52.0	Soar	4.2
Summary: 52 seconds activity; 6 soarings		

LIMS "Gamma" Angles

For all the DOY 228 experiment activities, measurements of body limb motions of the subject astronaut were carried out. The limb Euler angles (referred to herein as "gamma" angles) are contained on the digital magnetic tape described in appendix E. Examples of these results are given in figure 17, which shows γ_{31},γ_{32} and γ_{51},γ_{52}, respectively, for motion of the left arm during part 9(c) of task 1. (See appendix A.) The "gamma" angles may be utilized in dynamic crew motion models such as that presented in reference 1. (Additional segment "gamma" angles may be found in figs. 40, 43, 49, 51, and 53.

FMU Forces and Moments

Crew motion force and moment profiles are useful in the design of future spacecraft pointing control systems, in the verification of existing crew motion models, and in the development of new models. Accordingly, a primary output of the Skylab T-013 crew motion experiment was the determination of astronaut force and moment profiles for a range of activities. Typical activities include flapping arms, squat thrust, forceful soaring, console operations, and specific arm and leg motions. Telemetry obtained during the performance of experiment T-013 on day of year 228 was analyzed during this study. The time periods for which data were available are given in table V.

TABLE V.- TELEMETRY DATA COVERAGE – DOY 228

Start (a)	Finish (a)	Duration
13:19:29 (19747169)	13:24:03 (19747443)	0:04:34
15:17:31 (19754251)	15:28:15 (19754895)	0:10:44
15:29:18 (19754958)	16:02:38 (19756958)	0:33:20
16:03:43 (19757023)	16:19:21 (19757961)	0:15:38
16:20:18 (19758018)	16:27:54 (19758474)	0:07:36
Total data		1:11:52

[a]Numerical value of accumulated seconds from 01 January 1973 denoted in parentheses.

The total force time profiles exerted on each FMU during the execution of T-013 on day 228 are displayed in appendix C.

Force and Moment Spectrum Analysis

A crew-motion force-time profile can be viewed as a stochastic process. One manner in which the process can be analyzed is by its corresponding power spectral density (PSD). The PSD of a time series gives an indication of the relationship between frequency and energy and, as such, is a useful analysis technique. Since extensive ground-based simulations have been both analyzed and modeled by using the concepts of spectrum analysis, it is useful to compare the results from both ground-based and flight data. Three T-013 flight activities have been analyzed to date for signal frequency content. The three activities are crouch and pushoff, console operation, and flapping arms (like a bird).

In all cases except for the flapping arms, the PSD peaks are in the range of 1.0 to 2.0 rad/sec. The amplitudes, of course, are very different, the maximum force of 400 newtons being generated by the crouch and pushoff activity.

Figures 18 to 25 present the time functions and corresponding PSD's which were subjected to this analysis. The PSD's were generated from the time function by using standard digital computer Fourier transform routines. From the crouch and pushoff activity, 256 samples were used; and from the console operations and arm-flapping activities, 512 samples each were used. It is noted that for the console operations activity, the force along the X-axis was predominant, and F_X is used; total force is analyzed for the other two activities, its total moment being shown for the crouch and straighten motion also.

Vehicle Dynamic Response

Analysis of the Skylab vehicle dynamic response to experiment T-013 crew motion disturbances will provide a control system analysis baseline for future manned space vehicles. This baseline consisting of expected control system and vehicle response to various crew motions and activities can be utilized to determine some of the vehicle control system parameters.

This section deals with the comparisons between flight data as obtained by telemetry and simulation data where the FMU forces and moments as obtained from the T-013 telemetry system were used as the disturbance.

Detailed vehicle dynamic model.- The model used for this study consists mainly of a dynamic model of the vehicle and the attitude and pointing control system (APCS). This model (see fig. 26) was developed as part of the verification and performance assessment of the APCS dynamics which did not deal directly with all APCS hardware-related aspects.

The effects of filtering and unique hardware effects (such as sun sensor, star tracker, and control moment gyro (CMG) dynamics) were integrated into the simulation models and were considered in processing of the data. A band-limited white-noise generator was used to simulate the rate-gyro noise characteristics. No attempt was made to simulate the telemetry noise because of the varied effects caused by the different ground receiving stations and the data processing and handling involved prior to utilization in the verification and assessment task.

The APCS dynamics of primary interest is defined as the rotational motion of the vehicle in response to control moments under the influence of crew-motion disturbances. APCS dynamics are influenced by flexible body characteristics, mass distribution, control logic, vehicle configuration control authority, and subsystem hardware characteristics.

The digital simulation program utilized to assess the Skylab vehicle dynamic response is generated in the context of a general modular digital simulation program consisting of three groups of subroutines: (1) the executive program, (2) the general program-related subroutines, and (3) the specific, applications-oriented subroutines or modules. The particular functions of the three groups of routines are as follows:

(a) The executive program initializes program parameters and controls the flow of the simulation for the basic integration loop by processing subroutines and modules in the input-specified sequence.

(b) The functions of the subroutines include processing for printout, plotting, statistical computations, and other auxiliary operations not directly related to the simulated system.

(c) The applications modules pertain to the simulation of the actual problem or physical situation. For this particular application, the concern is for the dynamic behavior of the Skylab cluster, treated as a single flexible body, in response to disturbances and under the control of the control moment gyro (CMG) system. Individual modules are programed, where possible, to be independent entities to permit the ready substitution or exchange with one having the same function but of different complexity. The applications modules provide the following functions:

(a) Rotational dynamics of a rigid body

(b) Flexible body dynamics using the normal mode method

(c) Gravity gradient moment

(d) Crew-motion disturbance

(e) Sensor characteristics consisting of noise and bandwidth limiting filter

(f) Control computations

(g) CMG dynamics (low-frequency model)

(h) Telemetry processing.

The flow diagram of these applications modules is shown in figure 26. It should be noted that the vehicle model did not include the experiment pointing control system (EPCS) used to isolate the ATM experiment package from the primary vehicle inputs. Observations during the experiment performance indicated that the EPCS was capable of providing necessary isolation during most of the T-013 operations, although some slight motion was detected in watching the ATM control console TV monitor during solar pointing activities occurring during the experiment.

By using this model, the degree that the flexible-body dynamics influences the APCS dynamics in the presence of the T-013 disturbance torques was assessed. Figure 27 shows the measured disturbance torques during one of the soaring exercises. Figures 28 to 30 show the rigid-body vehicle rates, the flexible-body vehicle rates, and the total vehicle rates, all from the simulation depicted in figure 26. Points A, B, and C in figure 26 are the respective model pick-off points. The flexible-body rates add approximately 3.3 percent, 6 percent, and 2.9 percent to the X-, Y-, and Z-axis rigid-body rates. It was deemed that these small percentages did not warrant the additional computer expense (approximately 44 percent). Therefore, all runs utilizing the detailed simulation excluded the flexible-body dynamics. The rigid-body vehicle attitude during this period is shown in figure 31.

Simplified vehicle dynamic model.- In an attempt to reduce analysis costs further, a simplified model of the vehicle dynamics developed during the Skylab program was utilized. This model, in the form of a first-order transfer function, represented the controlling torque generated by the CMG's. This control torque in each axis was then subtracted from the disturbance torque vector and the result was multiplied by the inverse inertia matrix and integrated to produce the vehicle rates about the three axes. A block diagram of this model is shown in figure 32.

In order to validate this simplified model, the same disturbance torque profiles as those used in the detailed simulation were applied to the simplified model. (See fig. 27.) The resulting vehicle rates are shown in figure 33, whereas figure 34 gives the vehicle attitude. A comparison of the computed vehicle rates is given in table VI. Peak-to-peak values of the rates show that the simplified model produces rates on the order of 10 to 25 percent lower.

The attitude excursions for the detailed and simplified models are very small, and therefore are difficult to compare in magnitude. The basic profiles (figs. 31 and 34) are very similar. The simplified vehicle dynamic model was utilized in subsequent simulations.

TABLE VI.- VEHICLE RATES

	Vehicle rates (peak-to-peak values), deg/sec, for –		
	X	Y	Z
Detailed simulation:			
Rigid body	-0.0167 to 0.0223	-0.0027 to 0.0023	-0.0095 to 0.0138
Total vehicle	-0.0165 to 0.0226	-0.0027 to 0.0022	-0.0100 to 0.0066
Simplified simulation:			
Total vehicle	-0.0154 to 0.0203	-0.0018 to 0.0019	-0.0078 to 0.0056
As a percentage of detailed simulation for –			
Rigid body, percent	91.5	74.0	57.5
Total vehicle, percent	91.3	75.5	80.7

TABLE VII.- WALL PUSH-OFF FORCING FUNCTION

Time, sec	Force, N	Time, sec	Force, N	Time, sec	Force, N	Time, sec	Force, N
0	0	2.44	0	4.717	0	7.157	0
.397	53.2	2.53	-39.5	5.114	53.2	7.166	-39.5
.579	105.0	2.579	-112.0	5.296	105.0	7.215	-112.0
.619	95.0	2.82	-58.8	5.336	95.0	7.456	-58.8
.698	0	2.975	0	5.415	0	7.611	0

Preflight predictions.- The studies performed prior to the Skylab mission in the area of crew-motion disturbances utilized a wall pushoff function based on aircraft flight data. This forcing function was applied in the Y-axis at the FMU location to produce torques about the X- and Z-axis. (See table VII and fig. 35.) The rate-gyro and vehicle-attitude responses to this disturbance are shown in figures 36 and 37, respectively. By comparing figures 27 and 35, it is seen that the actual disturbance torques obtained from the T-013 telemetry data are much larger than those predicted before the mission. Also, since the predicted force function was applied in the Y-axis only, there was not any torque about the Y-axis. Consequently, the resulting predicted rates and attitude excursions are less than those actually experienced.

Comparisons with measured response.- In general, excellent time correlation has been obtained between measured vehicle response and disturbance inputs. However, because of the low values, noise, and quantization effects of the measured data, it was difficult to establish exact rate profiles from the measured Skylab data. The rate amplitudes obtained from both the detailed and simplified simulations appear to be lower than those measured.

Seven different time periods or activities were investigated. These periods are identified in table VIII. For each time period, the vehicle disturbance torque as determined from the FMU data is presented and is followed by the measured vehicle rates. The period is completed with plots of the LIMS "gamma" angles. LIMS data are not presented for the soaring periods.

Measured vehicle data are not available for the last three time periods because the Skylab vehicle was not in contact with a ground station during those periods. The vehicle rate and sun sensor data were not recorded on the ATM telemetry system at a usable sample rate.

For comparison purposes, the rate-gyro output for the soaring activity is displayed with the crew-motion input in figure 54. From this figure, which combines parts of figures 44 and 45, the correlation between input and output is clearly indicated.

TABLE VIII.- ACTIVITIES INVESTIGATED

[NP denotes not presented; NA denotes not available]

	DOY 228 Start time hr:min:sec	Figure for –		
		Disturbance torques	Vehicle rates	Gamma angles
Flapping arms (task 3 – part 6)	15:26:00	38	39	40
Crouch and pushoff (task 3 – part 6)	15:28:00	41	42	43
Soaring (normal and forceful) (task 3 – part 8)	15:29:50	44	45	NP
Two men soaring (task 3 – part 9)	15:33:45	46	47	NP
Both arms in motion (task 1 – part 9)	15:55:00	48	NA	49
Console operation (task 2 – part 4)	16:10:00	50	NA	51
Flapping arms like a bird (task 3 – part 6)	16:13:45	52	NA	53

DISCUSSION

This section discusses certain observations and interpretations of the T-013 experiment data from analyses to date. Consideration of some applications of the experiment results is also included.

Experiment Data

In reducing the motion-picture film data, it was noted (and confirmed by analysis of the FMS telemetry data) that soaring velocities of up to twice those observed in ground simulations were achieved. Velocities of approximately 2 m/sec were noted, compared with 1 m/sec or less in ground simulations. (See ref. 6, for example.) Examination of videotapes made of other routine in-flight Skylab activities support this observation, which indicates that previous assessments of crew locomotion capabilities are conservative. An obvious implication of this result is that higher input forces to a spacecraft (and its attitude-control system) may result from the apparently normal soaring velocities seen in Skylab.

In addition to the just-noted observation, the motion-picture films, in conjunction with Skylab voice transcripts (which have not been included herein), were useful in establishing the time correlation of events with the telemetry data and aided in the annotations of the total force profiles displayed in appendix C.

As a visual record of the experiment, the film provided yet another insight into other data results. For the "arm-flapping" motion of the worst case task, resultant force profiles seemed to be of an unusually high level, if only movement of the subject's arms was considered (because of their relatively low mass and moment of inertia when compared with those of the total body). Study of the motion-picture data film showed, however, that the entire body of the subject was extending in the "flapping" sequence and indicated that movement of the centers of mass of the torso and legs was also occurring. The movements contributed to a larger movement of the overall center of mass than expected.

Preliminary analysis of the LIMS data show that body limb motions in flight were completed approximately 35 percent faster than comparable motions simulated on the ground and reported in reference 6. This observation, with its implication of higher accelerations for the limbs, provides a basis for understanding the higher forces generated in flight, as compared with data from reference 6. The higher forces may be attributable to lack of 1g restraint. For example, the documented zero-g phenomenon of "overshooting" (see, for example, ref. 7) can contribute to higher decelerations resulting

in the higher applied forces at the end of limb rotation. Also, this lack of gravity restraint may permit (or promote) higher initial acceleration at the onset of limb motions.

Operation of the LIMS was satisfactory throughout the experiment performance on DOY 228, although the data indicate occasional "sticking" of some of the potentiometers. The LIMS data are expected to provide a good basis for the crew-motion mathematical model verification process to be carried out.

As mentioned previously, forces produced by the T-013 subject were generally higher in magnitude than those measured in ground simulations. Table IX presents a summary of maximum forces observed for the various activities of the experiment. A range of peak RSS force magnitudes is given in order to reflect the different levels attained from replicated motions.

TABLE IX.- SUMMARY OF APPLIED FORCE MAGNITUDES FROM T-013

Activity or exercise:	Maximum RSS Force Range, N
Deep breathing	8 to 100
Coughing	45 to 95
Sneezing	140 to 215
Single-pendulum arm rotation (90°):	
Sagittal plane	30 to 80
Frontal plane	80 to 95
Double-pendulum arm rotation:	
Frontal plane	40 to 80
Sagittal plane	35 to 45
Body bending at waist (80°)	70 to 200
Single-pendulum leg rotation (45°):	
Sagittal plane	60 to 85
Frontal plane	60 to 115
Double-pendulum leg rotation	40 to 50
Free soaring:	
"Normal" manner	30 to 220
Vigorous manner	60 to 400
Arm "flapping"	200 to 300
Crouch and straighten	250 to 340
Simulated console activity	7 to 20

For the respiration exercises (breathing, coughing, sneezing), only coughing had the same force levels in flight as obtained in simulation. Sneezing produced up to twice the force, and deep breathing resulted in over 25 times as much force. A lack of 1g restraint on the subject's visceral mass, allowing more acceleration and motion of this mass, appears to provide reasonable explanation for the larger in-flight forces. In considering all flight experiment motions, it should be noted that the subject was not one utilized in the ground simulations reported in reference 6. However, subject mass and status varied by less than 8 percent between flight and simulation; this variation suggests that comparison of flight and simulation results is permissible.

In general, flight force data results indicate levels greater than simulations. The lack of gravity restraint, as mentioned previously, is postulated as the predominant factor in producing this phenomenon. The experiment was performed approximately 3 weeks into the Skylab 3 mission; it is assumed that the crew had become well adapted to its environment. This adaptation may explain why the preflight zero-g aircraft soaring force data, contained in table VII, were not as high as the flight levels; short periods of zero-g interspersed with periods of greater than 1g would seem to preclude a complete zero-g adaptation and development of the large translation capabilities evidenced in Skylab.

The vigorous soaring produced the largest forces (up to 400 N) and resulted in applied disturbance torques on the order of 1000 N-m as seen by the attitude control system. Vehicle rates on the order of 0.02 deg/sec were observed because of these torques. During the two-man soaring portion of task 3 (see appendix A), observed vehicle rates or 0.03 to 0.04 deg/sec were noted; this result implies that the secondary subject was providing disturbance inputs comparable with that of the primary subject.

The arm-flapping motion resulted in about 800 N-m of disturbance torque, but only 0.005 deg/sec of observed vehicle rates. The higher frequency of the "flapping" may have been "ignored" by the bending filters present in the attitude-control system; as a result, there was little control system activity. The crouch and straighten motion, on the other hand, resulted in vehicle rate excursions of 0.03 deg/sec.

Console operations, as expected, produced the lowest forces and moments and resulted in minimal disturbance torques and negligible rates. Agreement with ground simulation for this activity was very good.

For virtually all experiment motions, ATM console observations by the mission science pilot indicated that the Skylab experiment pointing control system (EPCS) acted satisfactorily to isolate the ATM experiment package from T-013 disturbances.

Applications

Future missions of the Shuttle era will have varied pointing requirements. One classification of pointing requirements for the Spacelab is given in table X. Classes II

and III of this table represent situations in which crew motions will be a significant factor. Even in Class I, some requirements, such as stability rate, must take into account activities such as the soaring maneuvers of T-013. The possible constraints on crew activities during critical high pointing accuracy periods must be addressed for future missions.

TABLE X.- PAYLOAD POINTING REQUIREMENTS

Characteristics	Class I (a)	Class II (a)	Class III (a)
Pointing accuracy	1800 arc-sec	1 arc-sec	1 arc-sec
Pointing stability	360 arc-sec	1 arc-sec	1 arc-sec
Stability rate	36 arc-sec/sec	0.0002 arc-sec/sec	0.1 arc-sec/sec
Stability duration	24 hr	93 min	93 min
Viewing required	Hemisphere, Earth, misc.	100^{o} cone, misc. hemisphere	100^{o} cone, hemisphere

[a]Class I: Pallet mounted, no gimbals, inertia measuring unit, vernier control system positioning

Class II: Pallet mounted, ESRO-instrument pointing system, vernier control system positioning

Class III: Pallet mounted, ESRO-instrument pointing system, control moment gyro positioning

This report has categorized some types and kinds of activities and presents force and moment profiles. A magnetic tape of DOY 228 experiment T-013 data is available. (See appendix E.) These results provide a basis for future manned mission control system design. Analyses of the type noted in the section "Vehicle Dynamic Response" can be carried out with any potential vehicle by utilizing the T-013 data as a forcing function input.

The use of spectral data, such as those outlined also in the section "Force and Momentum Spectrum Analysis" gives a potentially useful method of incorporating frequency response characteristics of crew-motion disturbances in systems analyses. Models such as those reported in reference 3, which characterize a crew-motion disturbance as an output from a linear filter driven by white noise, have been employed in the past by using ground simulation data to define the filter characteristics. Use of the flight data should provide a more accurate model.

CONCLUDING REMARKS

Analysis to date of Skylab experiment T-013 film and telemetry data leads to the following conclusions:

1. Significant control system inputs were generated on Skylab by astronaut crew movements.

2. Applied force levels from Skylab flight activities were generally notably higher than those from comparable ground (and zero-g aircraft) simulation activities.

3. The lack of 1g restraint appears to be a predominant factor in the higher force levels observed in flight.

4. Previous preflight estimates of crew locomotion capabilities are conservative. Actual translational velocities on Skylab were up to twice as high as some predictions.

5. The ATM EPCS provided adequate isolation from the T-013 experiment activities.

The degree to which crew motions affect a spacecraft is, of course, dependent on the size (inertia) of the vehicle and the magnitude of the disturbance torques as seen by the control system. The size of the crew is another consideration. It is felt that extension of the T-013 experiment results together with ground-based analyses and simulation to the disturbance problems associated with large, multiman crews will be feasible. Use of the T-013 data to develop a family of flight-verified crew-motion disturbance models could prove useful for control system design and analysis. Refinement of the existing dynamic anthropometric model is also expected to provide a valuable tool not only for crew-motion analysis on the ground, but also for other astronaut orientation, mobility, and activity studies.

In summary, it is felt that the results presented and discussed herein are a significant contribution to the understanding of the character and effects of crew-motion disturbances aboard a manned spacecraft.

Langley Research Center
National Aeronautics and Space Administration
Hampton, Va. 23665
December 30, 1975

APPENDIX A

SKYLAB MANEUVERING EXPERIMENTS CHECKLIST – T-013 ACTIVITIES

This appendix presents portions of the Skylab maneuvering experiments checklist (pp. 30-1 to 32-4) detailing crew tasks to be followed in carrying out the crew/vehicle disturbances experiment. The checklist was prepared, based on inputs from principal investigators, by personnel of the crew procedures division at the NASA Lyndon B. Johnson Space Center.

The procedures described in this appendix are grouped into integrated tasks. For the three experiment-motion tasks, order of performance was not critical and was dictated by external factors such as available ground station coverage.

In the checklist excerpts which follow, SUB refers to the primary experiment subject, OBS refers to the experiment observer (who also served as the secondary subject during the worst case inputs task), and SPT refers to the mission science pilot.

DATE 7/10/73 30-1

T013 TASK NO. 1

(GROSS BODY MOTIONS)

OBS 1 Voice record 'TASK NO. 1 - GROSS BODY MOTIONS' started and give subject identification

SUB 2 Position feet in FMU 1 restraints

OBS 3 Tell SPT not to do any gross motions during the experiment

Note: Do not block view of cameras

4 Time Correlation Sequence....
Knock on FMU 2 at the approx center of the sense plate below handhold with side of fist as follows:
Four times at 1 sec intervals with 9 in. hand travel
Three times at 1/2 sec intervals with 5 in. hand travel
Four times at 2 sec intervals with 14 in. hand travel

5 Remain stationary at FMU 2 while the subject performs the exp exercises

6 Read checklist & demonstrate maneuvers to subject

Note: After each of the following exercises, the subject will stabilize for approx 5 seconds

	TV	TV
SPT	7 Set up TV 10C - Arm/Body exercises	
	VTR - RCD	
	TV	TV

T013 TASK NO. 1

DATE 7/2/73 30-2

SUB 8 Respiration Exercises....

Breathe deeply (approx 6 times)
Cough 5 times
Simulate sneezing 5 to 6 times

9 Arm Exercises....

Perform each of the following 3 times as shown:

a With right arm straight & rigid at side, raise it out 90 deg from side and return

b With right arm straight & rigid at side, raise it in front of body 90 deg and return

T013 TASK NO. 1

DATE 7/2/73 30-3

SUB

c In one continuous movement, raise left arm out 90 deg from side & move hand toward shoulder through an angle of 150 deg. Return arm to side while straightening

d With right arm straight & rigid at side, raise arm 90 deg in front of body. Move it through 90 deg to right side, and return to side

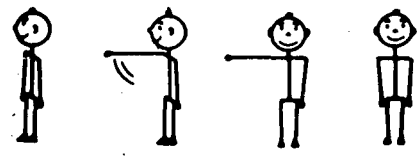

e With both arms straight & rigid at side, raise them simultaneously straight out 90 deg from each side. Move them through 90 deg to front of body then lower both arms to side simultaneously

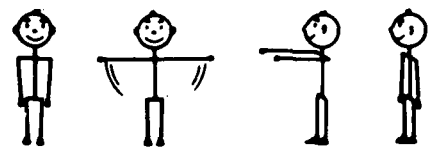

DATE 7/19/73 (PST)

30-4

SUB

f In one continuous movement, raise left arm in front of body 90 deg & move hand toward shoulder through an angle of 150 deg. Return arm to side while straightening

10 Body Exercises....

Bend upper body forward (bow) (0 to 80 deg) at waist 3 times

11 Remove right foot from restraint and stabilize

12 Leg Exercises....

Perform each of the following 3 times as shown:

a With right leg straight & rigid, raise it out to side through an angle of 35 to 45 deg and return (see picture at top of page 30-5)

DATE 7/19/73 (PEI) ~~7/10/73~~ 30-5

SUB b With right leg straight & rigid, raise it in front of body through an angle of 35 to 45 deg and return (see picture at bottom of page 30-4)

c In one continuous movement, raise right knee upward in front of body through an angle of 45 deg while keeping lower leg vertical and return gently

TV----------TV
SPT 113 Set up TV 10D - Soaring
TV----------TV

OBS 14 Stabilize at VCS Duct No. 2

Note: OBS watch LIMS cable for snagging during Soaring Exercises.

DATE 7/10/73 30-6

15 Soaring Exercises....

SUB Release left foot from restraint and crouch for free soaring (use hand-hold to keep feet on FMU 1)

a Push off from FMU 1 (with feet), soar to FMU 2, & stabilize with hands only

b Position feet on FMU 2, push off to FMU 1, & stabilize with hands only

c Push off FMU 1 with hands, turn, and stabilize at FMU 2 with hands only

```
TV------------------------------TV
SPT  I Set up TV 13E - FMU 1 closeup I
TV------------------------------TV
```

SUB d Push off FMU 2 with hands and return to FMU 1; stabilize with hands only

```
TV------------TV
SPT  I TV PWR - OFF I
TV------------TV
```

OBS 16 Voice record 'TASK NO. 1 - GROSS BODY MOTIONS' task completed and any pertinent comments

DATE 7/2/73 31-1

T013 TASK NO. 2

(SIMULATED CONSOLE OPS)

OBS 1 Voice record 'TASK NO. 2 - SIMULATED CONSOLE OPS' started and give subject identification

SUB 2 Attach self to FMU 1 foot restraints

OBS 3 Tell SPT not to do any gross motions during the experiment

4 Read the following simulated actions to the SUB for him to perform. Allow a 3 to 5 sec pause between each item:

SUB
- A Right hand - flipping switches
- B Right hand - rotating selector switches (chest height)
- C Right hand - flipping switches
- D Left hand - THC operations
- E Right hand - flipping switches
- F Left hand - keyboard entry
- G Right hand - RHC Attitude nulling sequence
- H Right hand - RHC yaw inputs
- I Left hand - keyboard entry
- J Right hand - RHC yaw inputs
- K Left hand - keyboard entry
- L Right hand - RHC pitch inputs
- M Left hand - keyboard entry
- N Right hand - flipping switches (reach up)

OBS 5 Voice record 'TASK NO. 2 - SIMULATED CONSOLE OPS' completed and any pertinent comments

DATE _____

T013 TASK NO. 2

DATE 7/2/73 32-1

T013 TASK NO. 3

(WORST CASE INPUTS)

T013 TASK NO. 3

Note: All three crewmen will be required later for this task.

OBS 1 Voice record 'TASK NO. 3 - WORST CASE INPUTS' started and give subject identification

2 Read checklist & demonstrate maneuvers to subject

SUB 3 Position feet in FMU 1 restraints

OBS 4 Tell SPT not to do any gross motions until called

5 Verify STDN acquisition

SUB 6 Fixed Position Tasks....

Rapidly move both arms up and down out from the side thru an angle of 90 deg; like a bird flapping its wings for 10 to 20 secs
Stabilize
Repeat arm movements
Stabilize
Crouch and quickly straighten body (as in push-off); stabilize
Perform 5 or 6 times (30 to 40 sec total)

7 Disengage feet from restraints

Note: OBS watch LIMS cable for snagging.

T013 TASK NO. 3

DATE 7/10/73 32-2

8 Soaring Between FMUs....

OBS Remove pg 32-3

TV----------TV
| If TV-10B is rqd, give pg 32-3 to SPT |
| & follow his direction |
TV----------TV

If TV-10B is not rqd, discard pg 32-3 & proceed thru steps 8, 9, & 10

SUB Forcefully push off (with feet) from FMU 1 and soar to FMU 2
Forcefully push off (with feet) from FMU 2 and soar to FMU 1
Repeat soaring exercise 4 times as rapidly as practical (30 to 40 sec total)

9 Worst Case Tasks....

OBS Call SPT to participate in experiment

Doff Lt Wt headset & give to SPT

SPT Read checklist

SUB & OBS Simultaneously perform the following on mark from SPT:
SUB - Soar between FMUs as in step 8
OBS - Soar from food locker to film vault & return (feet to hands)

SUB & OBS Repeat above Worst Case Tasks quickly 3 times

SPT 10 Voice record 'TASK NO. 3 - WORST CASE INPUTS' completed and any pertinent comments

DATE ~~7/10/73~~ 7/19/73 (PGI) 32-3

SPT

If TV-1CB is rqd, do the following:

a. Point H alpha 1 at any convenient target

TV----------TV

b. VTR -RCD

c. Video sel - ATM 1 or 2 (max zoom)

TV----------TV

d. Have the CDR perform step 8, pg 32-2 (Soaring Between FMUs) with the PLT describing the activity on channel B (particularly the times of 'launch' & 'landing')

TV----------TV

e. VTR - STBY

TV----------TV

f. Have the PLT doff & temp stow his comm equipment

TV----------TV

g. VTR - RCD

TV----------TV

h. Direct the CDR & PLT to simultaneously perform the following sequence 4 times & report any disturbances seen on the C&D displays:

(CDR) Soar between FMUs as in step 8, pg 32-2

(PLT) Soar from the food lockers to the film vault & return (feet to hands)

TV----------TV

i. VTR - STBY

TV----------TV

j. Select 'SI' mode

k. Reopen the H alpha 1 & 2 doors

l. If rqd, perform an 'offset' mnvr to assure that H alpha 1 is pointing at the sun

~~m. Have the PLT don his comm equipment~~

TV----------TV

n. VTR - RCD

TV----------TV

DATE ~~7/10/73~~ 7/19/73 (P&I) 32-4

SPT

o. Repeat steps d thru i

TV----------TV

Ip. VTR - STBY (verify) I

TV----------TV

q. Voice record 'TASK NO 3 - WORST CASE INPUTS' complete & give any pertinent comments

r. Discard this page

s. Have CDR & PLT proceed with the experiment as rqd (PLT don comm equip as reqd)

APPENDIX B

PHOTOGRAMMETRIC COORDINATES, TRANSFORMATIONS, AND ANALYSIS

This appendix presents the analysis required to construct the astronaut center-of-mass and torso-attitude data in orbital workshop (OWS) coordinates from the T-013 motion-picture film data. Also included is a resection analysis whereby the camera locations and orientations were determined.

Coordinate System Definitions

OWS system.- The OWS system is defined by the Y and Z axes as shown in figure 55; the X-axis completes the right-hand system. The origin is taken at the center of the OWS floor (which separated the OWS forward dome area and the crew quarters).

Camera 1 system.- The camera 1 coordinate system (fig. 56) is X_1, Y_1, and Z_1 with its origin at the center of the camera 1 lens (C_1). The Z-axis points away from the film plane along the line of sight of camera 1 and is perpendicular to the film plane. The X_1 and Y_1 axes lie in a plane parallel to the film plane and are oriented so that when the film is projected on a screen, Y_1 is up and X_1 completes the right-hand system.

Camera 2 system.- The camera 2 axis system is X_2, Y_2, and Z_2 with its origin at the center of the camera 2 lens (C_2) axes defined analogously to the camera 1 axes.

Astronaut system.- The astronaut coordinate system (shown in fig. 14) has its origin at the astronaut center of mass. Z_M is the vertical axis of the body, pointing toward the feet. Y_M points to the astronaut's right side. X_M completes the right-hand system, pointing out the front of the astronaut's body. The X_MZ_M plane is the nominal plane of symmetry of the body.

Coordinate Transformations

Coordinate transformations required in the film data analysis are given in this section.

OWS to camera 1 transformation.- Let the angles ϕ_1, θ_1, and ψ_1 denote the angles of positive[1] rotation about X, Y, and Z, respectively, so that a rotation ϕ_1 about the X-axis, followed by a rotation θ_1 about the rotated Y-axis, followed by a final rotation ψ_1 about the twice-rotated Z-axis results in a coordinate system whose X, Y, and Z axes are parallel to X_1, Y_1, and Z_1, respectively. The transformation H_1 is defined by

[1]Positive is defined to be counterclockwise when looking into the positive end of the axis.

$$[H_1] = \begin{bmatrix} C\psi_1 & S\psi_1 & 0 \\ -S\psi_1 & C\psi_1 & 0 \\ 0 & 0 & 1 \end{bmatrix} \begin{bmatrix} C\theta_1 & 0 & -S\theta_1 \\ 0 & 1 & 0 \\ S\theta_1 & 0 & C\theta_1 \end{bmatrix} \begin{bmatrix} 1 & 0 & 0 \\ 0 & C\phi_1 & S\phi_1 \\ 0 & -S\phi_1 & C\phi_1 \end{bmatrix} \tag{B1}$$

$$[H]_1 = \left[\begin{array}{c:c:c} C\theta_1 C\psi_1 & C\phi_1 S\psi_1 + S\phi_1 S\theta_1 C\psi_1 & S\phi_1 S\psi_1 - C\phi_1 S\theta_1 C\psi_1 \\ -C\theta_1 S\psi_1 & C\phi_1 C\psi_1 - S\phi_1 S\theta_1 S\psi_1 & S\phi_1 C\psi_1 + C\phi_1 S\theta_1 S\psi_1 \\ S\theta_1 & -S\phi_1 C\theta_1 & C\phi_1 C\theta_1 \end{array}\right]$$

where S and C denote sine and cosine, respectively.

If this new system is translated by C_1 (origin of the camera 1 system), the camera 1 coordinate system is obtained. Then any point (x,y,z) in the OWS coordinate system can be expressed in camera 1 coordinates by

$$\begin{bmatrix} x_1 \\ y_1 \\ z_1 \end{bmatrix} = [H_1] \begin{bmatrix} x - x_{C1} \\ y - y_{C1} \\ z - z_{C1} \end{bmatrix} \tag{B2}$$

and conversely any point (x_1,y_1,z_1) in the camera 1 coordinate system can be represented in the OWS system by

$$\begin{bmatrix} x \\ y \\ z \end{bmatrix} = [H_1]^T \begin{bmatrix} x_1 \\ y_1 \\ z_1 \end{bmatrix} + \begin{bmatrix} x_{C1} \\ y_{C1} \\ z_{C1} \end{bmatrix} \tag{B3}$$

OWS to camera 2 transformation.- Define $[H_2]$ analogously to $[H_1]$ with angles ϕ_2, θ_2, and ψ_2 to get the required transformation.

OWS to astronaut transformation.- Define $[H_3]$ analogously to $[H_1]$ with angles ϕ_3, θ_3, and ψ_3. Evaluation of $(\phi_1, \theta_1, \text{and } \psi_1)$, $(\phi_2, \theta_2, \text{and } \psi_2)$, C_1, and C_2 is outlined in a subsequent section of this appendix by using a least-squares resection method. Evaluation of ϕ_3, θ_3, and ψ_3, along with determination of astronaut center-of-mass location, is discussed next.

APPENDIX B

Photogrammetric Equations

To reduce two-dimensional film data to three-dimensional OWS coordinates, the following conditions suffice:

(a) The torso targets are within the field of view of both cameras.

(b) The location and orientation of both cameras are known in OWS coordinates.

(c) The coordinates of the film image of the torso targets are known in each camera coordinate system.

Condition (a) has been satisfied by observation of the film data. Condition (b) is determined by solving the resection problem. Condition (c) is accomplished by reading coordinates from a projected image (by using automated film-reading equipment). These coordinates must be converted to camera coordinates.

Note figure 57 and let $C_1 = (x_{C1}, y_{C1}, z_{C1})$, $C_2 = (x_{C2}, y_{C2}, z_{C2})$, $F_{1,j} = (b_{1,j}, n_{1,j}, -f)$ = Camera 1 coordinates of the target image, and $F_{2,j} = (b_{2,j}, n_{2,j}, -f)$ = Camera 2 coordinates of the target image. As can be seen from figure 57, T_j, C_1, and $F_{1,j}$ are collinear. (T_j, C_2, and $F_{2,j}$ are also collinear.)

Next, transforming $F_{1,j}$ to OWS coordinates

$$\begin{bmatrix} x \\ y \\ z \end{bmatrix}_{F_{1,j}} = [H_1]^T \begin{bmatrix} x_1 \\ y_1 \\ z_1 \end{bmatrix}_{F_{1,j}} + \begin{bmatrix} x_{C1} \\ y_{C1} \\ z_{C1} \end{bmatrix} \tag{B4}$$

For convenience of notation, let

$$\begin{bmatrix} x \\ y \\ z \end{bmatrix}_{F_{1,j}} = \begin{bmatrix} x^*_{1,j} + x_{C1} \\ y^*_{1,j} + y_{C1} \\ z^*_{1,j} + z_{C1} \end{bmatrix} \tag{B5}$$

where

$$\begin{bmatrix} x^*_{1,j} \\ y^*_{1,j} \\ z^*_{1,j} \end{bmatrix} = [H_1]^T \begin{bmatrix} b_{1,j} \\ n_{1,j} \\ -f \end{bmatrix} \tag{B6}$$

and also let

$$\begin{bmatrix} x \\ y \\ z \end{bmatrix}_j = \begin{bmatrix} x_j \\ y_j \\ z_j \end{bmatrix} \tag{B7}$$

Coordinates of the points T_j, C_1, and $F_{1,j}$ can be used in the equation defining a line in three-dimensional space to get

$$\frac{x_j - x_{C1}}{x^*_{1,j}} = \frac{y_j - y_{C1}}{y^*_{1,j}} = \frac{z_j - z_{C1}}{z^*_{1,j}} \tag{B8}$$

Similarly, for camera 2, T_j, C_2, and $F_{2,j}$ are collinear, and a relation similar to equation (B8) exists as

$$\frac{x_j - x_{C2}}{x^*_{2,j}} = \frac{y_j - y_{C2}}{y^*_{2,j}} = \frac{z_j - z_{C2}}{z^*_{2,j}} \tag{B9}$$

where (see eqs. (B4), (B5), and (B6))

$$\begin{bmatrix} x^*_{2,j} \\ y^*_{2,j} \\ z^*_{2,j} \end{bmatrix} = [H_2]^T \begin{bmatrix} b_{2,j} \\ n_{2,j} \\ -f \end{bmatrix} \tag{B10}$$

Now, use cross multiplication in equations (B8) and (B9), and collect terms to get

$$\left.\begin{aligned} z^*_{1,j}x_j + 0 - x_{i,j}z_j - \left(x^*_{1,j}z_{C1} - z^*_{1,j}x_{C1}\right) &= 0 + \epsilon_1 \\ 0 + z^*_{1,j}y_j - y^*_{1,j}z_j - \left(y^*_{1,j}z_{C1} - z^*_{1,j}y_{C1}\right) &= 0 + \epsilon_2 \\ z^*_{2,j}x_j + 0 - x^*_{2,j}z_j - \left(x^*_{2,j}z_{C2} - z^*_{C2}x_{C2}\right) &= 0 + \epsilon_3 \\ 0 + z^*_{2,j}y_j - y^*_{2,j}z_j - \left(y^*_{2,j}z_{C2} - z^*_{C2}y_{C2}\right) &= 0 + \epsilon_4 \end{aligned}\right\} \tag{B11}$$

The solution for the unknowns x_j, y_j, and z_j is overdetermined, since there are more equations than unknowns. A solution may be obtained by solving any three of the four equations. However, since the known data values are measured and therefore contain

unknown errors (resulting in the ϵ_i), a unique solution does not necessarily exist. For this reason a least-squares method was used to determine the "best" solution for x_j, y_j, and z_j.

Furthermore, since the film quality of camera 2 was found to be much better than that of camera 1, the least-squares solution was weighted to favor the camera 2 data.

The weighted least-squares solution is the value of x_j, y_j, and z_j that minimizes the quantity S, where

$$S = \sum_{i=1}^{4} \left(\frac{1}{\sigma_i} \epsilon_i \right)^2 \tag{B12}$$

where σ_i is the standard deviation of ϵ_i determined by observation of the film.

Rewriting S in matrix notation yields

$$S = W(A\lambda - D)^2 \tag{B13}$$

where

$$W = \begin{bmatrix} \frac{1}{\sigma_1^2} & 0 & 0 & 0 \\ 0 & \frac{1}{\sigma_2^2} & 0 & 0 \\ 0 & 0 & \frac{1}{\sigma_3^2} & 0 \\ 0 & 0 & 0 & \frac{1}{\sigma_4^2} \end{bmatrix} \tag{B14}$$

$$A = \begin{bmatrix} z^*_{1,j} & 0 & -x^*_{1,j} \\ 0 & z^*_{1,j} & -y^*_{1,j} \\ z^*_{2,j} & 0 & -x^*_{2,j} \\ 0 & z^*_{2,j} & -y^*_{2,j} \end{bmatrix} \tag{B15}$$

$$\lambda = \begin{bmatrix} x_j \\ y_j \\ z_j \end{bmatrix} \tag{B16}$$

$$D = \begin{bmatrix} x^*_{1,j} z_{C1} - z^*_{1,j} x_{C1} \\ y^*_{1,j} z_{C1} - z^*_{1,j} y_{C1} \\ x^*_{2,j} z_{C2} - z^*_{2,j} x_{C2} \\ y^*_{2,j} z_{C2} - z^*_{2,j} y_{C2} \end{bmatrix} \tag{B17}$$

To minimize S, solve

$$\frac{dS}{d\lambda} = 0 \tag{B18}$$

$$\frac{dS}{d\lambda} = 2W(A\lambda - D)A = 0 \tag{B19}$$

$$WA\lambda = WD \tag{B20}$$

$$A^T WA\lambda = A^T WD \tag{B21}$$

Finally λ, the matrix of the unknown coordinates, is given by

$$\lambda = \left(A^T WA\right)^{-1} A^T WD \tag{B22}$$

This technique requires no more than a matrix inversion and multiplication to obtain the unknown target coordinates in OWS coordinates. It has the additional advantage of emphasizing data from higher quality film while giving less weight to data of poorer quality.

Computation of Astronaut Center-of-Mass and Torso Attitude

Consider figure 58, which represents the torso of the subject astronaut. To compute the location of the torso center of mass, the following method was used:

(a) Find TCM, a point on the torso surface directly over the torso center of mass.

(b) Define the orientation of the torso axes X_T, Y_T, and Z_T with respect to the OWS.

(c) Torso center of mass is then equal to the location of TCM plus a scalar along X_T.

This procedure is subject to the following conditions:

(1) The astronaut torso is rigid and planar (that is, flat, as depicted in fig. 58).

(2) OWS coordinates of three noncollinear points on the astronaut torso are known.

(3) Astronaut torso coordinates of any point on the astronaut are known.

Condition (1) is assumed. Condition (2) is satisfied by solution of the photogrammetric equations outlined earlier in this appendix. Condition (3) is satisfied from actual measurements of the astronaut and a table of anthropometric measurements. (See appendix D.)

To compute TCM, let $T_j = (x_j, y_j, z_j)$ (when $j = 1, 3$) be the OWS coordinates of the three torso points. By condition 1, all points on the torso surface lie in the same plane. T_1, T_2, and T_3 determine this plane defined by $Ax + By + Cz + 1 = 0$ with $A^2 + B^2 + C^2 \neq 0$. A, B, and C can be found from

$$\begin{bmatrix} A & B & C \end{bmatrix} = \begin{bmatrix} -1, & -1, & -1 \end{bmatrix} \begin{bmatrix} x_1 & x_2 & x_3 \\ y_1 & y_2 & y_3 \\ z_1 & z_2 & z_3 \end{bmatrix}^{-1} \tag{B23}$$

Since TCM is on the torso surface,

$$Ax_{TCM} + By_{TCM} + Cz_{TCM} + 1 = 0 \tag{B24}$$

By condition (3) all the distances (therefore all the angles) between T_1, T_2, T_3, and TCM are known. (See fig. 59.) By using T_1 and T_2,

$$\overrightarrow{T_2TCM} \cdot \overrightarrow{T_2T_1} = \left|\overrightarrow{T_2TCM}\right| \left|\overrightarrow{T_2T_1}\right| \cos \alpha_2 \tag{B25}$$

$$\overrightarrow{T_1T_3} \cdot \overrightarrow{T_1TCM} = \left|\overrightarrow{T_1T_3}\right| \left|\overrightarrow{T_1TCM}\right| \cos \alpha_1 \tag{B26}$$

Using equation (B24) along with expansion of equations (B25) and (B26) and multiplying and collecting terms gives

$$\begin{bmatrix} A & B & C \\ x_1 - x_2 & y_1 - y_2 & z_1 - z_2 \\ x_3 - x_1 & y_3 - y_1 & y_3 - z_1 \end{bmatrix} \begin{bmatrix} x_{TCM} \\ y_{TCM} \\ z_{TCM} \end{bmatrix}$$

$$= \begin{bmatrix} -1 \\ x_2(x_1 - x_2) + y_2(y_1 - y_2) + z_2(z_1 - z_2) + \left|\overrightarrow{T_2TCM}\right| \left|\overrightarrow{T_2T_1}\right| \cos \alpha_2 \\ x_1(x_3 - x_1) + y_1(y_3 - y_1) + z_1(z_3 - z_1) + \left|\overrightarrow{T_1T_3}\right| \left|\overrightarrow{T_1TCM}\right| \cos \alpha_1 \end{bmatrix} \tag{B27}$$

which can be solved for the OWS coordinates of TCM.

The next step is to define the orientation of the X_T, Y_T, and Z_T axes with respect to the OWS X, Y, and Z system (and, hence, determine torso attitude).

By using the method just outlined to determine the coordinates of TCM, find the coordinates of TUP, a point on the torso so that a vector $\overrightarrow{TCM\ TUP}$ is anti-parallel to X_T (TUP must not be coincident with T_3). By using TX (see fig. 59), let

$$\overrightarrow{TCM\ TX} = \overrightarrow{TCM\ T_3} \times \overrightarrow{TCM\ TUP} \tag{B28}$$

The vector $\overrightarrow{TCM\ TX}$ is perpendicular to the torso surface and passes through TCM. By definition of the X_T-axis, $\overrightarrow{TCM\ TX}$ is coincident with X_T. (To insure that $\overrightarrow{TCM\ TX}$ has the proper direction, relative positions on the torso of T_3 and TCM must be known and the cross product taken in the appropriate order.)

Calculate the vector cross product, $-\left(\overrightarrow{TCM\ TUP}\right) \times \overrightarrow{TCM\ TX}$. This cross product yields a vector parallel to Y_T and since $-\left(\overrightarrow{TCM\ TUP}\right)$ is parallel to z_T, also yields a right-handed system of three vectors parallel to X_T, Y_T, and Z_T which have an origin at TCM. The torso center of mass will lie along the line defined by the $\overrightarrow{TCM\ TX}$ vector, at a scalar distance $-x_{TCM}$ from TCM, where x_{TCM} is determined from anthropometric measurements and models of the human body. (See appendix A of ref. 1, for example.) This center of mass is the origin of the X_T, Y_T, and Z_T coordinate system.

The orientation of the X_T, Y_T, and Z_T system in the OWS is given by the $\overrightarrow{TCM\ TX}$, $-\left(\overrightarrow{TCM\ TUP}\right) \times \overrightarrow{TCM\ TX}$, $-\left(\overrightarrow{TCM\ TUP}\right)$ triad orientation. The torso attitude is defined by the angles ϕ_3, θ_3, and ψ_3 which rotate the OWS axes into the torso axes (parallel to X_M, Y_M, and Z_M) by the transformation $[H_3]$. These angles may be calculated by solving for $[H_3]$.

Assume a vector $\vec{B}$ whose components in the torso axis system are unit vectors, but which is defined in OWS coordinates (that are easily obtainable from the calculations just discussed). In matrix form

$$B_{OWS} = \left[B_x, B_y, B_z\right]_{OWS} = \begin{bmatrix} b_{xx} & b_{yx} & b_{zx} \\ b_{xy} & b_{yy} & b_{zy} \\ b_{xz} & b_{yz} & b_{zz} \end{bmatrix} \tag{B29}$$

where, for example, b_{xx} is the projection of the unit vector along X_T upon the OWS X-axis.

Now, B in the torso system is given by

$$B_{torso} = \begin{bmatrix} 1 & 0 & 0 \\ 0 & 1 & 0 \\ 0 & 0 & 1 \end{bmatrix} = [H_3] \begin{bmatrix} b_{xx} & b_{yx} & b_{zx} \\ b_{xy} & b_{yy} & b_{zy} \\ b_{xz} & b_{yz} & b_{zz} \end{bmatrix} \tag{B30}$$

By proceeding piecemeal,

$$\begin{bmatrix} 1 \\ 0 \\ 0 \end{bmatrix} = [H_3] \begin{bmatrix} b_{xx} \\ b_{xy} \\ b_{xz} \end{bmatrix} \tag{B31}$$

and

$$[H_3]^T \begin{bmatrix} 1 \\ 0 \\ 0 \end{bmatrix} = \begin{bmatrix} b_{xx} \\ b_{xy} \\ b_{xz} \end{bmatrix} \tag{B32}$$

Relations similar to equation (B32) can be written for the unit vectors along Y_T and Z_T. Solving for the attitude angles by solving the calculated values of $[H_3]$ elements in terms of the b's for ϕ_3, θ_3, and ψ_3 yields

$$\left.\begin{aligned} \phi_3 &= -\tan^{-1} \frac{b_{zy}}{b_{zz}} \\ \theta_3 &= \sin^{-1} b_{zx} \\ \psi_3 &= -\tan^{-1} \frac{b_{xy}}{b_{xx}} \end{aligned}\right\} \tag{B33}$$

Torso attitude with respect to OWS axes has thus been determined, and location of the torso center of mass has been found. Determination of the overall astronaut center of mass, and hence the origin of the X_M, Y_M, and Z_M system requires use of the LIMS data discussed in the section "Experiment Results." These data are used to define the subject's mass moments of inertia and his overall center of mass dynamic motion (by using methods outlined in appendix B of ref. 1).

APPENDIX B

Resection Solution Using a Method of Least Squares

This subsection describes the techniques used to define the exact position and orientation of the T-013 data acquisition cameras in the OWS coordinate system. A resection solution was required because placement and alinement of the cameras for the experiment were known only to within a few inches and degrees. The procedure is described for one camera; identical steps are followed for the second camera.

Let x_C, y_C, and z_C be the unknown OWS coordinates of the camera. Let ϕ, θ, and ψ be unknown angles of rotation defined by the transformation $[H]$ between OWS axes and camera orientation. $[H]$ is analogous to $[H_1]$ and $[H_2]$

$$[H] = \begin{bmatrix} h_{11} & h_{12} & h_{13} \\ h_{21} & h_{22} & h_{23} \\ h_{31} & h_{32} & h_{33} \end{bmatrix} \tag{B34}$$

Assume the camera coordinates of (at least) three film images b_j, n_j, and $-f$ ($j = 1$ to 3) to be given along with the OWS coordinates of the corresponding objects, x_j, y_j, and z_j ($j = 1, 3$).

From the photogrammetric equations (see eq. (B8)),

$$\left.\begin{aligned} x_j^* &= \frac{(x_j - x_C)z_j^*}{z_j - z_C} \\ y_j^* &= \frac{(y_j - y_C)z_j^*}{z_j - z_C} \\ z_j^* &= \frac{(z_j - z_C)z_j^*}{z_j - z_C} \end{aligned}\right\} \tag{B35}$$

where (as in eq. (B6))

$$\begin{bmatrix} x_j^* \\ y_j^* \\ z_j^* \end{bmatrix} = [H]^T \begin{bmatrix} b_j \\ n_j \\ -f \end{bmatrix} \tag{B36}$$

Solving equation (B36) for b_j, n_j, and $-f$, and substituting for x_j^*, y_j^*, and z_j^* from equation (B35) yields

$$
\left.
\begin{aligned}
b_j &= \frac{z_j^*}{z_j - z_C}\Big[(x_j - x_C)C\theta C\psi + (y_j - y_C)(C\phi S\psi + S\phi S\theta C\psi) \\
&\quad + (z_j - z_C)(S\phi S\psi - C\phi S\theta C\psi)\Big] \\
n_j &= \frac{z_j^*}{z_j - z_C}\Big[(x_j - x_C)(-C\theta S\psi) + (y_j - y_C)(C\phi C\psi - S\phi S\theta S\psi) \\
&\quad + (z_j - z_C)(S\phi C\psi + C\phi S\theta S\psi)\Big] \\
-f &= \frac{z_j^*}{z_j - z_C}\Big[(x_j - x_C)S\theta + (y_j - y_C)(-S\phi C\theta) + (z_j - z_C)(C\phi C\theta)\Big]
\end{aligned}
\right\} \qquad \text{(B37)}
$$

Divide b_j and n_j by $-f$ and, for notational convenience, replace the transformation trigonometric elements with the matrix elements as given in equation (B34)

$$\frac{b_j}{-f} = \frac{(x_j - x_C)h_{11} + (y_j - y_C)h_{12} + (z_j - z_C)h_{13}}{(x_j - x_C)h_{31} + (y_j - y_C)h_{32} + (z_j - z_C)h_{33}} = 0 + E_{xj} \qquad \text{(B38)}$$

$$\frac{n_j}{-f} = \frac{(x_j - x_C)h_{21} + (y_j - y_C)h_{22} + (z_j - z_C)h_{23}}{(x_j - x_C)h_{31} + (y_j - y_C)h_{32} + (z_j - z_C)h_{33}} = 0 + E_{yj} \qquad \text{(B39)}$$

The quantities E_{xj} and E_{yj} are residual errors resulting from measurement and film reading inaccuracies.

The use of three known OWS points yields six equations in the form of equations (B38) and (B39). With six unknowns (x_C, y_C, z_C, ϕ, θ, and ψ), the six equations would be sufficient to yield a solution. However, the equations are nonlinear, and an iterative method starting with an initial estimate for the unknowns was used.

Approximate E_{xj} and E_{yj} by their first-degree Taylor expansions as

$$
\left.
\begin{aligned}
E_{xj} &= E_{xj,o} + \frac{\partial E_{xj,o}}{\partial x_C}dx_C + \frac{\partial E_{xj,o}}{\partial y_C}dy_C + \frac{\partial E_{xj,o}}{\partial z_C}dz_C \\
&\quad + \frac{\partial E_{xj,o}}{\partial \phi}d\phi + \frac{\partial E_{xj,o}}{\partial \theta}d\theta + \frac{\partial E_{xj,o}}{\partial \psi}d\psi \\
E_{yj} &= E_{yj,o} + \frac{\partial E_{yj,o}}{\partial x_C}dx_C + \frac{\partial E_{yj,o}}{\partial y_C}dy_C + \frac{\partial E_{yj,o}}{\partial z_C}dz_C \\
&\quad + \frac{\partial E_{yj,o}}{\partial \phi}d\phi + \frac{\partial E_{yj,o}}{\partial \theta}d\theta + \frac{\partial E_{yj,o}}{\partial \psi}d\psi
\end{aligned}
\right\} \qquad \text{(B40)}
$$

where $E_{xj,o}$ and $E_{yj,o}$ are the values of E_{xj} and E_{yj} for the initial estimates of x_C, y_C, z_C, ϕ, θ, and ψ $(x_{C,o}, y_{C,o}$, etc.).

The approximations for E_{xj} and E_{yj} are linear in dx_C, dy_C, dz_C, $d\phi$, $d\theta$, and $d\psi$. A least-squares method can be used to solve for dx_C, dy_C, etc.

It is desired to minimize V where

$$V = \sum_j E_{xj}^2 + \sum_j E_{yj}^2 \tag{B41}$$

Rewriting equation (B41) in matrix notation yields

$$V = \sum_j (G\eta - P)^2$$

where

$$G = \begin{bmatrix} \frac{\partial E_{xj,o}}{\partial x_C} & \frac{\partial E_{xj,o}}{\partial y_C} & \cdots & \frac{\partial E_{xj,o}}{\partial \psi} \\ \frac{\partial E_{yj,o}}{\partial x_C} & \frac{\partial E_{yj,o}}{\partial y_C} & \cdots & \frac{\partial E_{yj,o}}{\partial \psi} \end{bmatrix}$$

$$\eta = \begin{bmatrix} dx_C \\ dy_C \\ dz_C \\ d\phi \\ d\theta \\ d\psi \end{bmatrix}$$

and

$$P = \begin{bmatrix} -E_{xj,o} \\ -E_{yj,o} \end{bmatrix}$$

Solve

$$\frac{d\left[\sum_j (G\eta - P)^2\right]}{d\eta} = 0 \tag{B42}$$

$$\sum_j 2G^T(G\eta - P) = 0 \tag{B43}$$

$$\left(\sum_j G^T G\right)\eta = \left(\sum_j G^T P\right) \tag{B44}$$

and

$$\eta = \left(\sum_j G^T G\right)^{-1} \sum_j G^T P \tag{B45}$$

The estimates of x_C, y_C, z_C, ϕ, θ, and ψ are then updated by using the corrections given by equation (B45)

$$\begin{bmatrix} x_C \\ y_C \\ z_C \\ \phi \\ \theta \\ \psi \end{bmatrix} = \begin{bmatrix} x_{C,o} \\ y_{C,o} \\ z_{C,o} \\ \phi_o \\ \theta_o \\ \psi_o \end{bmatrix} + \begin{bmatrix} dx_C \\ dy_C \\ dz_C \\ d\phi \\ d\theta \\ d\psi \end{bmatrix} \tag{B46}$$

Equations (B38) to (B45) are reevaluated by using the values for x_C, y_C, etc., given by equation (B46); the method is repeated until all the values of the corrections, given by η, approach zero.

For T-013, six known OWS points were used to determine x_C, y_C, z_C, ϕ, θ, and ψ for each camera. The film coordinates for the six image points were determined by using automated film reading equipment (as discussed in the section "Data Reduction"), and the OWS object coordinates were determined from OWS manufacturing blueprints. When compared, the OWS points obtained by using camera coordinates from the resection analysis just described were in agreement with blueprint locations to an accuracy of 1 cm and indicated a position and orientation determination for the cameras of 1 cm and 1^o, respectively.

APPENDIX C

EXPERIMENT T-013 TOTAL FORCE TIME PROFILES

The total force time profiles exerted on each FMU during the execution of T-013 on day 228 are shown in figure 60. For this figure, the total force was computed as

$$F1 = \left(\text{sign } F_{Y,1}\right)\left(F_{X,1}^2 + F_{Y,1}^2 + F_{Z,1}^2\right)^{1/2}$$

$$F2 = \left(\text{sign } F_{Y,2}\right)\left(F_{X,2}^2 + F_{Y,2}^2 + F_{Z,2}^2\right)^{1/2}$$

The resulting force profiles represent the maximum force that could be exerted on the FMU for the particular activity taking place.

For convenience, the major activities are given in table XI.

APPENDIX C

TABLE XI.- DOY 228 ACTIVITIES

Start time, hr:min:sec	Activity
15:19:25	Calibrate FMU 1
15:19:47	Calibrate FMU 2
15:20:30	Task 3, trial run, fixed to FMU 1
15:21:35	End task 3
15:26:00	Time correlation on FMU 2
15:26:50	Task 3, part 6, flapping arms
15:27:20	Task 3, part 6, flapping arms
15:28:01	Task 3, part 6, forceful squat thrust
15:28:15	Data gap
15:29:19	Task 3, part 6, normal thrust
15:29:50	Task 3, part 8, forceful soaring (soaring 1)
15:30:35	Task 3, part 8, normal soaring
15:33:45	Task 3, part 9, forceful soaring, two men (soaring 2)
15:33:57	Strain gages 4-2 and 5-2 go off-scale and stay off-scale
15:38:05	Task 3, part 10, forceful soaring with two men (soaring 3)
15:40:00	Film coverage starts
15:41:00	Task 3, part 10, forceful soaring with two men (soaring 4)
15:45:12	Calibrate FMU 1
15:46:04	Calibrate FMU 2
15:46:55	Unscheduled swaying motion
15:51:48	Time reference on FMU 2
15:43:35	Start task 1, part 8, deep breathing
15:54:07	Task 1, part 8, 5 coughs
15:54:25	Task 1, part 8, 5 sneezes
15:55:24	Subject at attention for LIMS reference
15:55:25	Task 1, part 9-A, wave right arm
15:56:15	Task 1, part 9-C, wave left arm
15:56:40	Task 1, part 9-D, wave right arm
15:57:56	Task 1, part 10, bowing motion
15:58:35	Task 1, part 12-A, swing right leg
15:59:13	Task 1, part 12-C, bend right knee
16:02:38	Data gap
16:06:40	Task 1, part 15, one man soaring
16:09:35	Start task 2, console operation
16:12:20	Finish task 2, console operation
16:13:25	Task 3, part 6, flapping arms
16:13:47	Second LIMS reference, arms straight, knees bent 10^{o}
16:14:02	Task 3, part 6, forceful pushoffs
16:14:22	Task 3, part 6, normal pushoffs
16:14:53	Task 3, part 8, one man, worst case soaring
16:17:12	Task 3, part 9, two men soaring
16:18:10	Subject uncoils LIMS cable
16:19:21	Data gap
16:20:30	Task 1, part 4, time reference on FMU 2
16:22:32	Task 1, part 8, coughs, sneezes
16:23:30	Task 1, part 9, arm movements
16:25:15	Task 1, part 12, leg lifts
16:26:10	Task 1, part 15, one man soaring
16:26:44	Double somersault
16:27:54	End of telemetry

APPENDIX D

ANTHROPOMETRY OF EXPERIMENT T-013 PRIMARY AND SECONDARY SUBJECTS

Some forms of modeling of astronaut crew-motion disturbances require a knowledge of the anthropometric measurements of a modeled subject (or subjects). For experiment T-013, the requisite data for both the primary and secondary subjects are presented in table XII. Use of the data for the primary subject (with LIMS) is made in verifying the analytical model described in reference 1. Data for the secondary subject (who participated in the two-man soaring part of the worst-case control system input task) are presented for information and completeness of reporting, although no limb motion measurements were made. It is noted that certain quantities have been estimated; these estimates were either derived from other measurements based on geometric relations given in appendix A of reference 1 or represent approximations based on averages for measurement subjects with similar mass and stature. It is also noted that all anthropometric measurements (except for body mass) represent preflight values and do not account for variations attributable to conditions of prolonged "weightlessness." Appendix A of reference 1 describes the measurements whose values (in centimeters) are given in table XII.

APPENDIX D

TABLE XII.- ANTHROPOMETRIC MEASUREMENTS

Measurement	Primary subject	Secondary subject
Ankle circumference, cm	21.9	27.6
Axillary arm circumference, cm	[a]29.2	33.7
Buttock depth, cm	[a]30.0	31.0
Chest breadth, cm	[a]31.0	34.6
Chest depth, cm	22.8	31.0
Elbow circumference, cm	30.1	33.7
Fist circumference, cm	[a]28.9	[a]31.0
Forearm length, cm	27.0	29.2
Foot length, cm	24.8	26.7
Knee circumference, cm	[a]37.0	41.4
Head circumference, cm	56.9	59.1
Hip breadth, cm	33.4	34.0
Shoulder (acromial) height, cm	142.9	150.5
Sitting height, cm	91.1	[a]97.2
Sphyrion height, cm	[a]7.0	[a]7.5
Stature, cm	174.2	183.4
Substernale height, cm	[a]126.0	[a]132.0
Thigh circumference, cm	54.7	61.0
Tibiale height, cm	48.4	[a]48.5
Trochanteric height, cm	87.9	95.2
Upper arm length, cm	33.9	35.6
Waist breadth, cm	32.9	[a]29.0
Waist depth, cm	[a]24.6	[a]20.5
Wrist circumference, cm	16.5	18.7
Mass, kg	69.4	88.9

[a]Estimated value.

APPENDIX E

EXPERIMENT T-013 DATA TAPE DESCRIPTION

A digital magnetic tape of much of the reduced T-013 data has been prepared and is described in this appendix. Inquiries concerning availability of these data should be addressed to:

National Space Sciences Data Center
National Aeronautics and Space Administration
Goddard Space Flight Center
Code 601
Greenbelt, MD 20771

Reference: NSSDC ID 73-027A-42A

The data tape was prepared by use of Control Data Corporation's (CDC) Model 6000 series digital computers and is described herein.

Data generated from processing the raw data from experiment T-013 are recorded in seven files on the magnetic tape designated W0045. This tape is a labeled, nine-track, 1600 bits per inch, phase encoded, CDC SCOPE 3.4 internal format tape. The tape has an ANSI-standard 80 character label. The "label" internal to the label is T-013, and the creation date is given as "75232" which means day 232 (20 August) of 1975. The seven files group as three logical units: a descriptive header file and a long data stream of FMU and vehicle forces and moments and astronaut body Euler angles; three files of smoothed astronaut center-of-mass and attitude data as functions of time; and a descriptive header file and a short stream of raw ATM rate gyro data.

The first two files are a header and a long data stream. The first file contains one 70-word record which was written with an unformatted write statement, and so may be read with an unformatted read statement, and may be interpreted with an A10 format,

```
      DIMENSION HEADER (70)
                .
                .
                .
      READ (9) HEADER
                .
                .
                .
      PRINT 400, HEADER
  400 FORMAT (5X, 7A10)
```

The second file, the data stream file, contains 3074 records of 512 words each, written by an unformatted write statement.

```
DIMENSION A (512)
      .
      .
      .
WRITE (9) A
```

Each record contains 14 contiguous blocks of 35 words per time point (490 words of data in each 512 word record). The blocks of 35 words contain the values of the following forces, moments, and body Euler angles.

Word	Parameter
1	Time, in seconds from beginning of year (TGMT)
2-4	F_X, F_Y, and F_Z for FMU 1, in newtons
5-7	M_X, M_Y, and M_Z for FMU 1, in newton-meters
8-13	F_X, F_Y, F_Z, M_X, M_Y, and M_Z for FMU 2, in newtons and newton-meters
14-19	F_X, F_Y, F_Z, M_X, M_Y, and M_Z for vehicle, in newtons and newton-meters
20-35	γ_{21}, γ_{22}, γ_{31}, γ_{32}, γ_{41}, γ_{42}, γ_{51}, γ_{52}, γ_{61}, γ_{62}, γ_{71}, γ_{72}, γ_{81}, γ_{82}, γ_{91}, and γ_{92}, in degrees

If these records are read by an unformatted read statement, they can be interpreted as in an E-format.

```
      DIMENSION A (512)
            .
            .
            .
      READ (9) A
      PRINT 200, (A(I), I = 1, 490)
  200 FORMAT (7 (5E25.15/)/)
```

Table XIII correlates certain activities of the T-013 experiment with time points in the data stream and record numbers in the second file of tape W0045. The data stream in the second file has had short data gaps filled by linear interpolation; the time span runs from 13:19:29 to 16:27:54 on day 228 (from TGMT 19747169 to 19758474).

APPENDIX E

TABLE XIII.- DOY 228 ACTIVITIES

Start time	Time, sec	Activity	Initial record in file 2
15:19:25	19754365	Calibrate FMU 1	277
15:19:47	19754387	Calibrate FMU 2	293
15:20:30	19754430	Task 3, trial run	324
15:21:35	19754495	End trial run	370
15:26:00	19754760	Time correlation on FMU 2	559
15:26:50	19754810	Flapping arms	595
15:27:20	19754840	Flapping arms	617
15:28:01	19754881	Forceful squat thrust	646
15:29:19	19754959	Normal thrust	657
15:29:50	19754990	Forceful soaring	678
15:30:35	19755035	Normal soaring	711
15:33:45	19755225	Forceful soaring, two men	846
15:38:05	19755485	Forceful soaring, two men	1032
15:40:00	19755600	Film coverage starts	1114
15:45:12	19755912	Calibrate FMU 1	1337
15:46:04	19755964	Calibrate FMU 2	1374
15:46:55	19756015	Unscheduled swaying motion	1410
15:51:48	19756308	Time reference on FMU 2	1620
15:53:35	19756415	Start deep breathing	1696
15:54:07	19756447	5 coughs	1719
15:54:25	19756465	5 sneezes	1732
15:55:24	19756524	Astronaut at attention, LIMS reference	1774
15:55:25	19756525	Wave right arm	1775
15:56:15	19756575	Wave left arm	1810
15:56:40	19756600	Wave right arm	1828
15:57:56	19756676	Bowing motion	1883
15:58:35	19756715	Swing right leg	1910
15:59:13	19756753	Bend right knee	1938
16:06:40	19757200	One man soaring	2210
16:09:35	19757375	Console operations, start	2335
16:12:20	19757540	Console operations, end	2452
16:13:25	19757605	Flapping arms	2498
16:13:47	19757627	Second LIMS reference, arms straight, knees bent 10^{o}	2513
16:14:02	19757642	Forceful pushoffs	2524
16:14:22	19757662	Normal pushoffs	2538
16:14:53	19757693	Worst case soaring, one man	2560
16:17:12	19757832	Two men soaring	2660
16:18:10	19757890	Astronaut uncoils LIMS cable	2701
16:20:30	19758030	Time reference on FMU 2	2758
16:22:32	19758152	Coughs, sneezes	2845
16:23:30	19758210	Arm movements	2886
16:25:15	19758315	Leg lifts	2961
16:26:10	19758370	One man soaring	3001
16:26:44	19758404	Double somersault	3025
16:27:53	19758473	End of telemetry	3074

APPENDIX E

The middle files, files number 3, 4, and 5, each contain an initial Hollerith identification record followed by several data records (215 in file 3, 311 in file 4, 310 in file 5) of seven 60-bit words containing values of the following parameters (at 6 samples/sec):

Word	Parameter
1	Time of day 228 in seconds
2-4	X, Y, and Z coordinates of astronaut center of mass, cm
5-7	ϕ, θ, and ψ astronaut attitude angles, deg

The files contain the smoothed data for soaring activities 5, 6, and 7 as detailed in tables XIV, XV, and XVI. All records were written by an unformatted write statement; they may be read with an unformatted read statement.

```
      DIMENSION C (7)
      .
      .
      .
      READ (9) C
```

The header record may be printed with an A10 format

```
      PRINT 100, C
  100 FORMAT (1X, 8A10)
```

and the data records printed with an E-format

```
      PRINT 300, C
  300 FORMAT (1X, 5E25.15)
```

APPENDIX E

TABLE XIV.- SOARING ACTIVITY 5 FOR DAY 228

[16:06:43.57 to 16:07:19.77]

Start time	Activity	Duration, sec
6:43.57	Soar to FMU 2	0.5
6:44.07	Hold FMU 2	7.5
6:51.57	Soar	.8
6:52.38	FMU 1	10.39
7:02.77	Soar	2.0
7:04.77	FMU 2	4.5
7:09.27	Soar	1.7
7:10.97	Hold FMU 1	8.8
Summary: 36.2 seconds activity; 4 soarings		

TABLE XV.- SOARING ACTIVITY 6 FOR DAY 228

[16:14:55.57 to 16:15:52.87]

Start time	Activity	Duration, sec
14:55.57	Soar to FMU 2	0.4
14:55.97	Hold FMU 2	5.2
15:01.17	Soar	.7
15:01.87	Hold FMU 1	5.2
15:07.07	Soar	.6
15:07.67	FMU 2	4.5
15:12.17	Soar	.7
15:12.87	FMU 1	6.8
15:19.67	Soar	1.3
15:20.97	FMU 2	5.41
15:26.38	Soar	1.09
15:27.47	FMU 1	5.7
15:33.17	Soar	1.0
15:34.17	FMU 2	6.1
15:40.27	Soar	1.1
15:41.37	Hold FMU 1	11.5
Summary: 57.3 seconds activity; 8 soarings		

APPENDIX E

TABLE XVI.- SOARING ACTIVITY 7 FOR DAY 228

[16:17:14.37 to 16:18:01.17]

Start time	Activity	Duration, sec
17:14.37	Soar to FMU 2	0.7
17:15.07	Hold FMU 2	7.4
17:22.47	Soar	.7
17:23.17	FMU 1	5.5
17:28.67	Soar	.6
17:29.27	FMU 2	6.7
17:35.97	Soar	.7
17:36.37	FMU 1	15.0
17:51.67	Soar	.4
17:52.07	FMU 2	8.2
18:00.27	Soar	.9
Summary: 46.8 seconds activity; 6 soarings		

The last two files (files 6 and 7) contain 512-word records, file 6 is another header and contains one record with 35 words of alphameric information and 477 words of blanks. It may be read with an unformatted read statement and interpreted by an A10 format; only the first 35 words need to be printed.

```
      DIMENSION D (512)
              .
              .
              .
      READ (9) D
              .
              .
              .
      PRINT 500, (D(I), I = 1, 35)
  500 FORMAT (5X, 7A10)
```

The 21 records in file 7 may also be read with an unformatted read statement, but should be interpreted with an E-format.

```
      DIMENSION D(512)
                .
                .
                .
      READ (9) D
                .
                .
                .
      PRINT 600, (D(I), I = 1, 510)
  600 FORMAT (5X, 5E 20.10)
```

Each record in file 7 contains 102 contiguous groups of 5 data words; in each group, the words contain the following variable values:

Word	Parameter
1	Time from beginning of year (1973), sec
2	Time from a reference time point, sec (this word is non-T-013 related)
3	OWS rate gyro output from X2 gyro, deg/sec
4	OWS rate gyro output from Y1 gyro, deg/sec
5	OWS rate gyro output from Z3 gyro, deg/sec

These groups of data occur at 12 samples/sec.

REFERENCES

1. Conway, Bruce A. (appendix A by Charles T. Woolley; appendix B by Peter R. Kurzhals and Robert B. Reynolds): Development of Skylab Experiment T-013 Crew/Vehicle Disturbances. NASA TN D-6584, 1972.

2. Groom, Nelson J.; Shaughnessy, John D.; and Nene, Vilas D.: On the Stability and Pointing of an Attached Double-Gimbal Experiment Package. NASA TN D-6676, 1972.

3. Hendricks, T. C. ; and Johnson, C. H.: Stochastic Crew Motion Modeling. J. Spacecraft & Rockets, vol. 8, no. 2, Feb. 1971, pp. 150-154.

4. Conway, Bruce A.: Mathematical Crew Motion Disturbance Models for Spacecraft Control System Design. M.S. Thesis, George Washington Univ., 1974. (Available as NASA TM X-70342.)

5. Conway, Bruce A.: Investigation of Crew Motion Disturbances on Skylab-Experiment T-013. AAS Paper 74-139, American Astronaut. Soc., Aug. 1974.

6. Murrish, C. H.; and Smith, G. W.: Apollo Applications Program Crew Motion Experiment – Program Definition and Design Development. Contract NAS 1-7276, Martin Marietta Corp., Mar. 1968. (Available as NASA CR 66599.)

7. Parker, James F., Jr.; and West, Vita R., eds.: Bioastronautics Data Book. Second ed. NASA SP-3006, 1973.

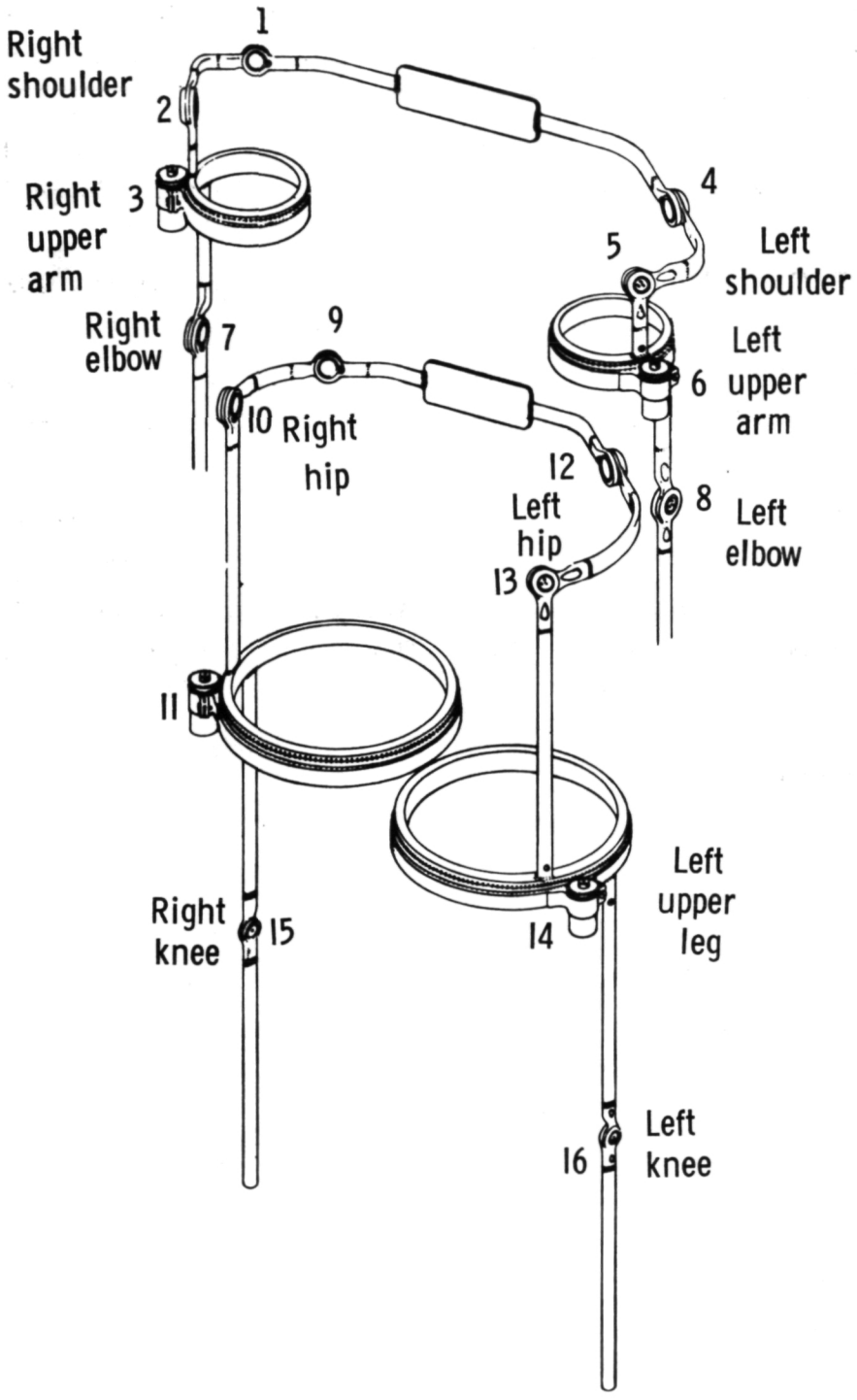

Figure 1.- Limb motion sensor exoskeleton showing potentiometer identification.

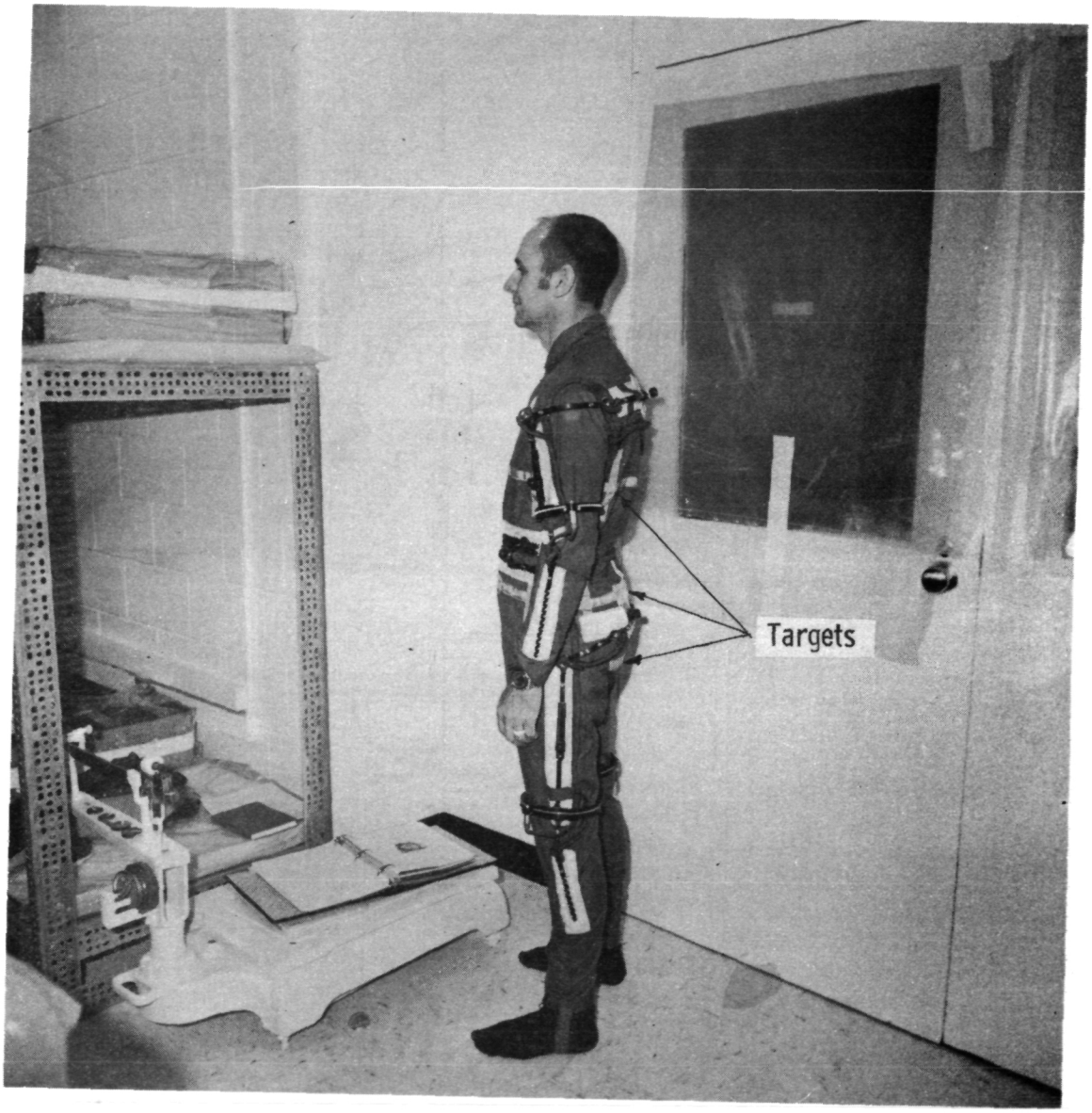

L-75-275

Figure 2.- LIMS as worn by subject.

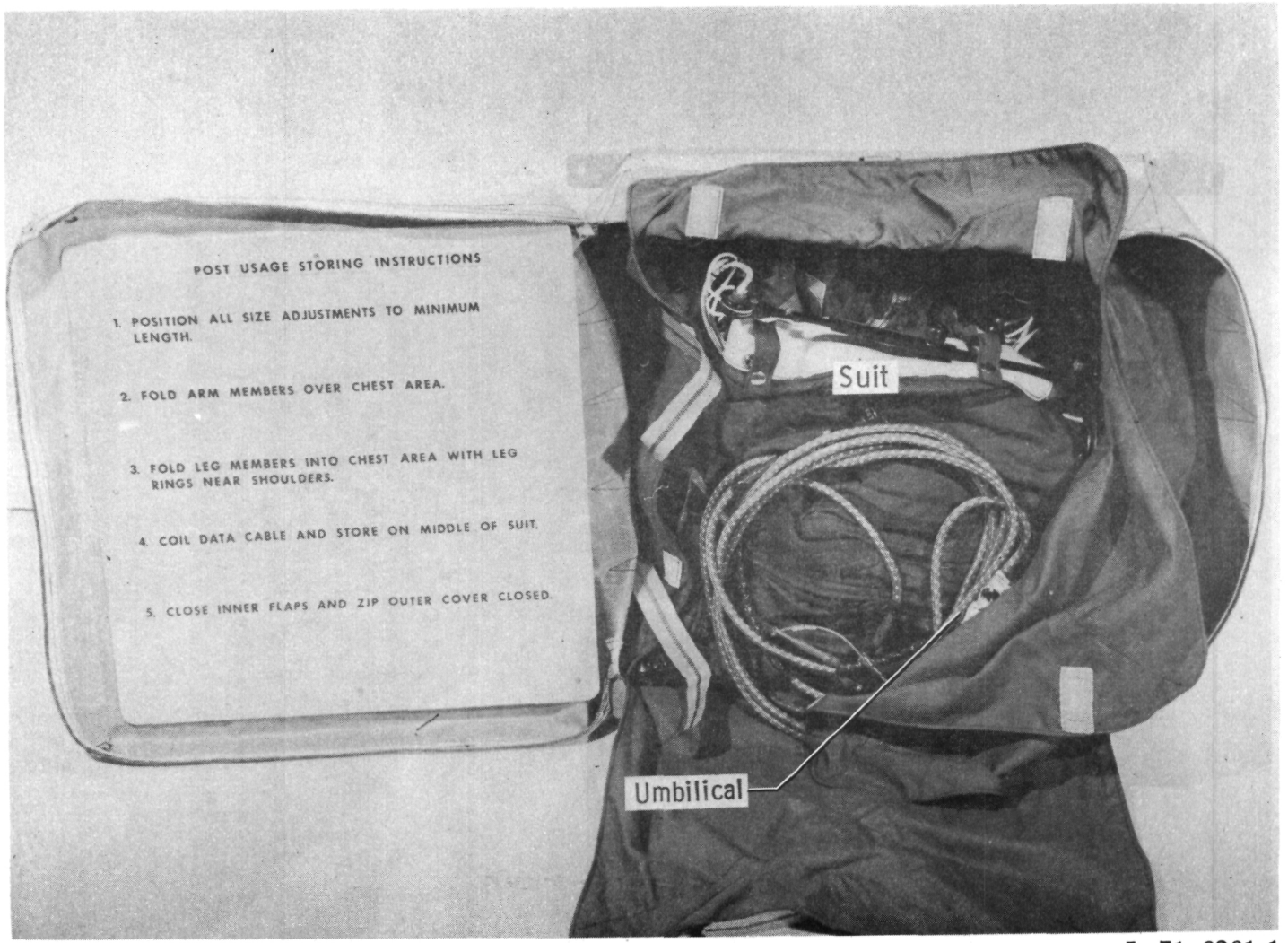

L-71-6261.1

Figure 3.- View of LIMS stowage container.

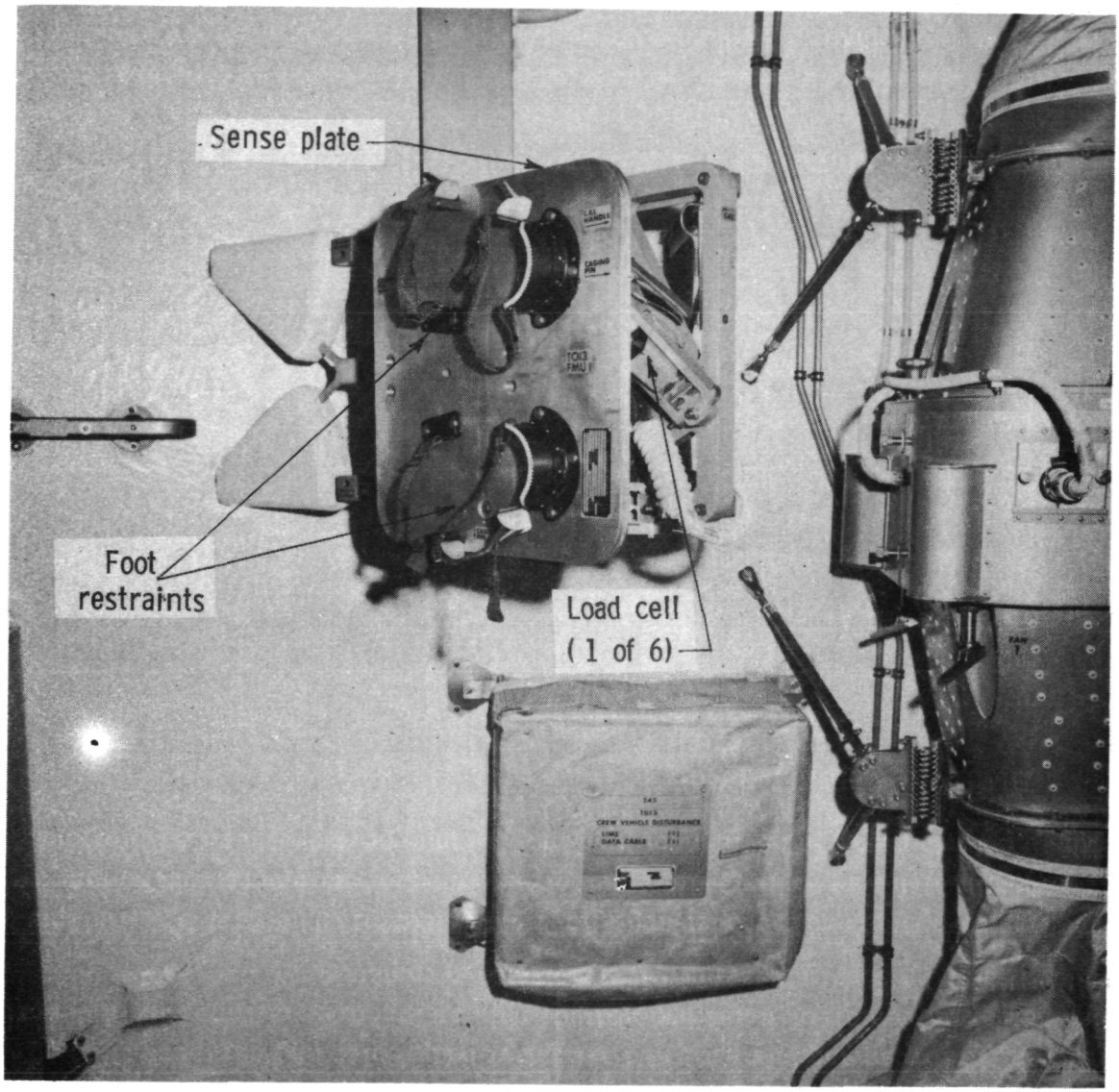

(a) FMU 1.

Figure 4.- View of force measuring units mounted in OWS.

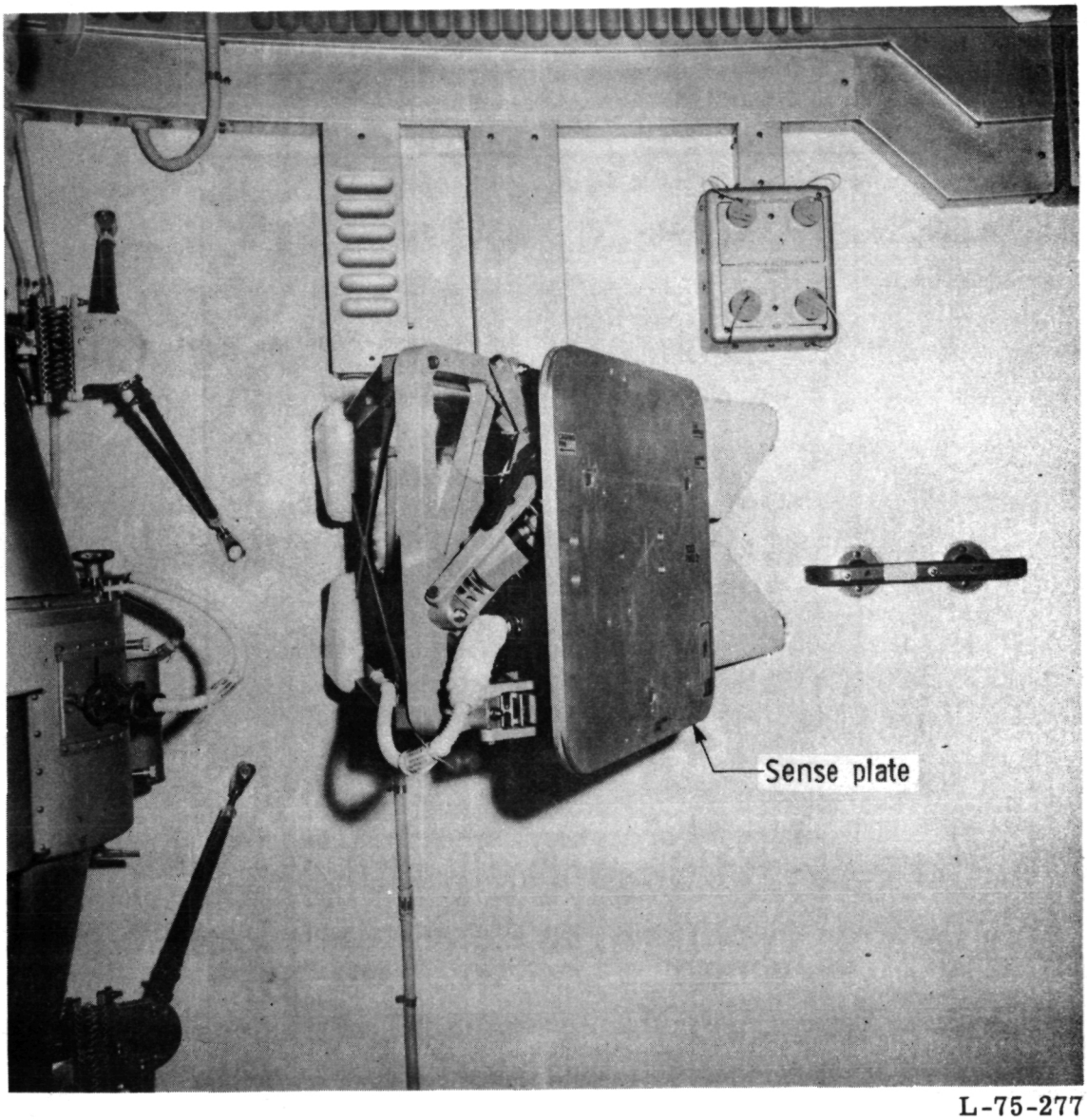

L-75-277

(b) FMU 2.

Figure 4.- Concluded.

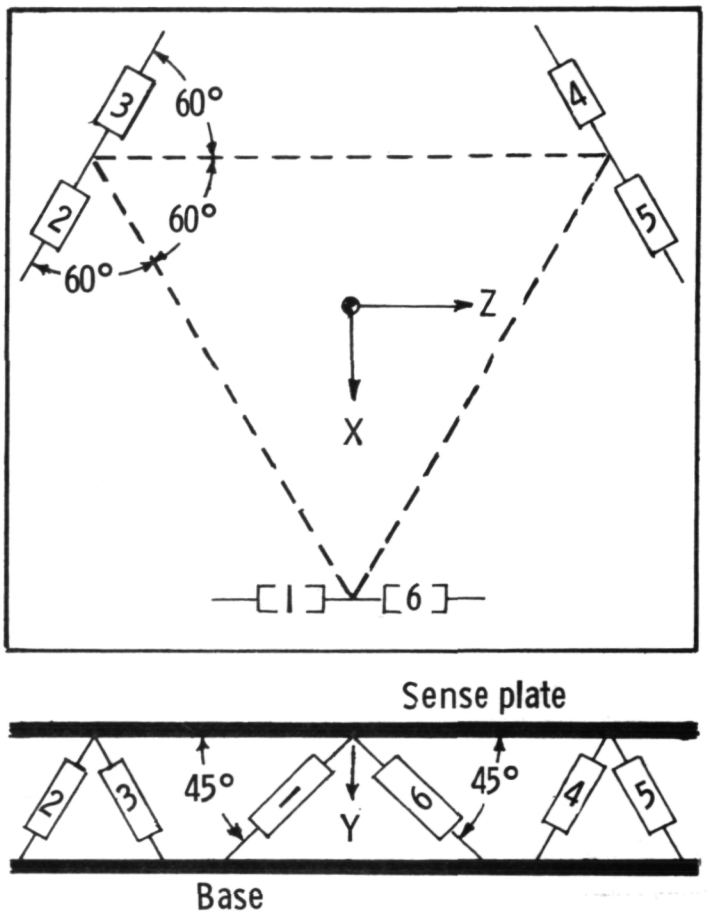

Figure 5.- Load cell array schematic with axis system.

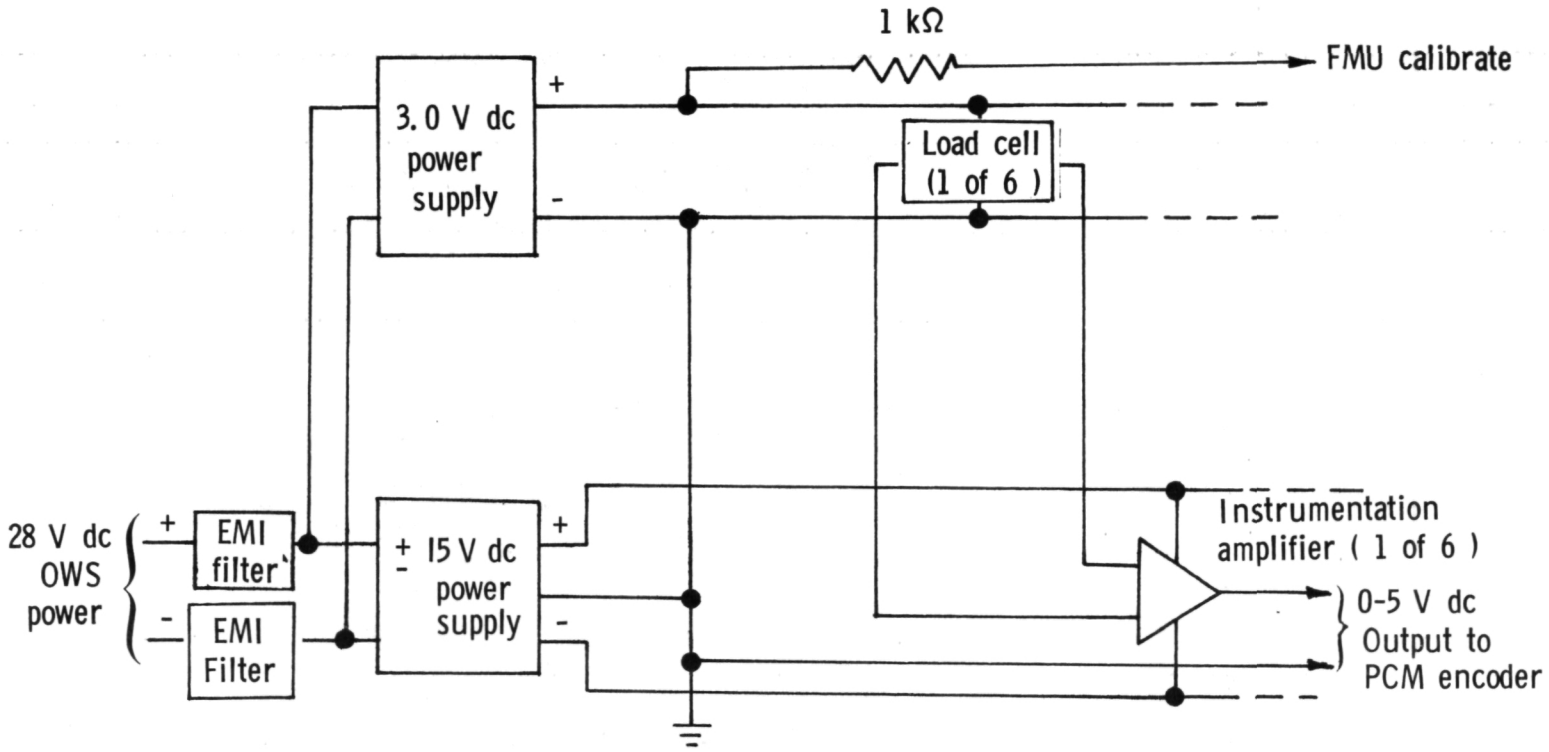

Figure 6.- Schematic of typical load cell circuit.

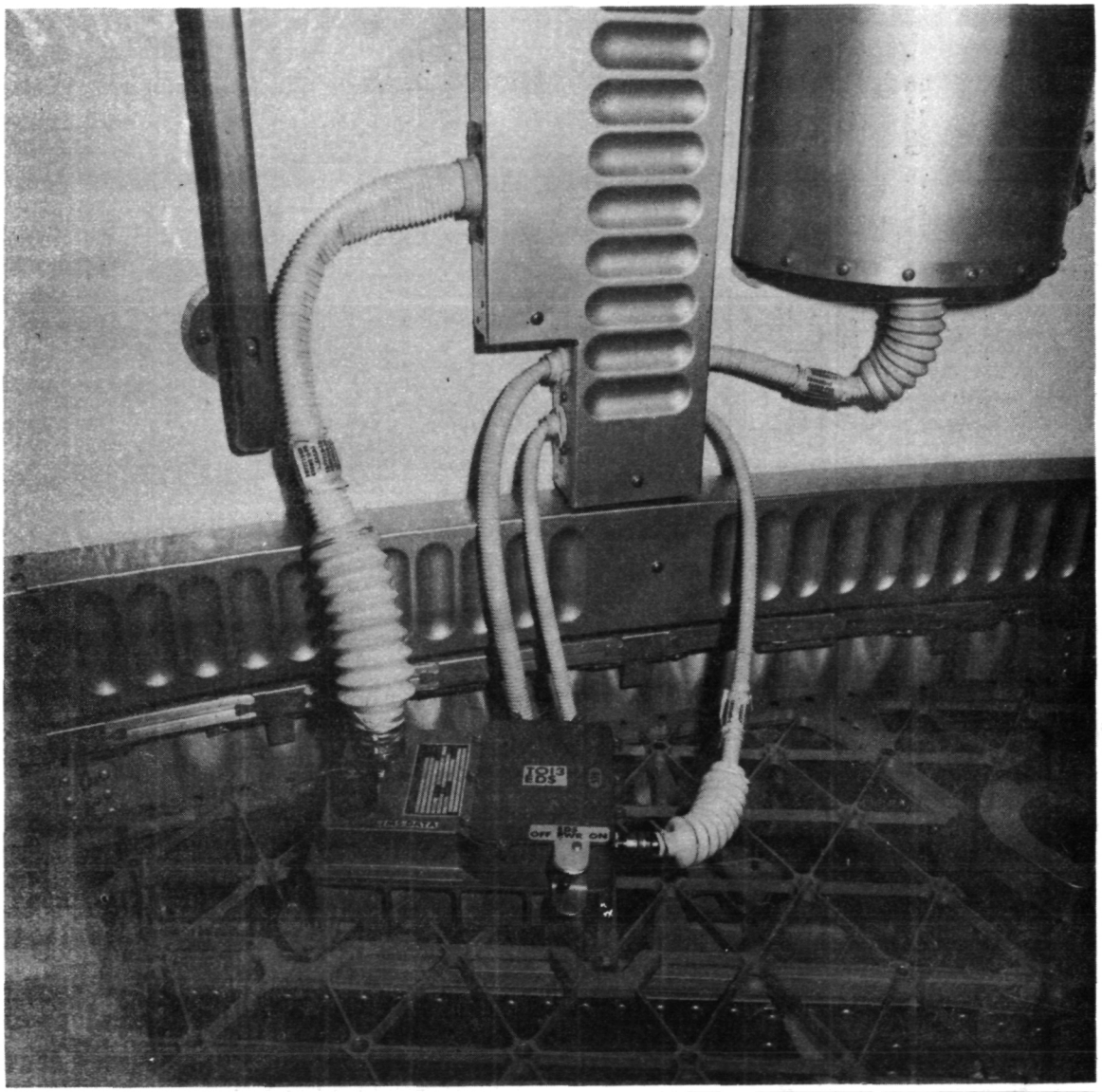

L-75-278

Figure 7.- View of experiment data system in OWS.

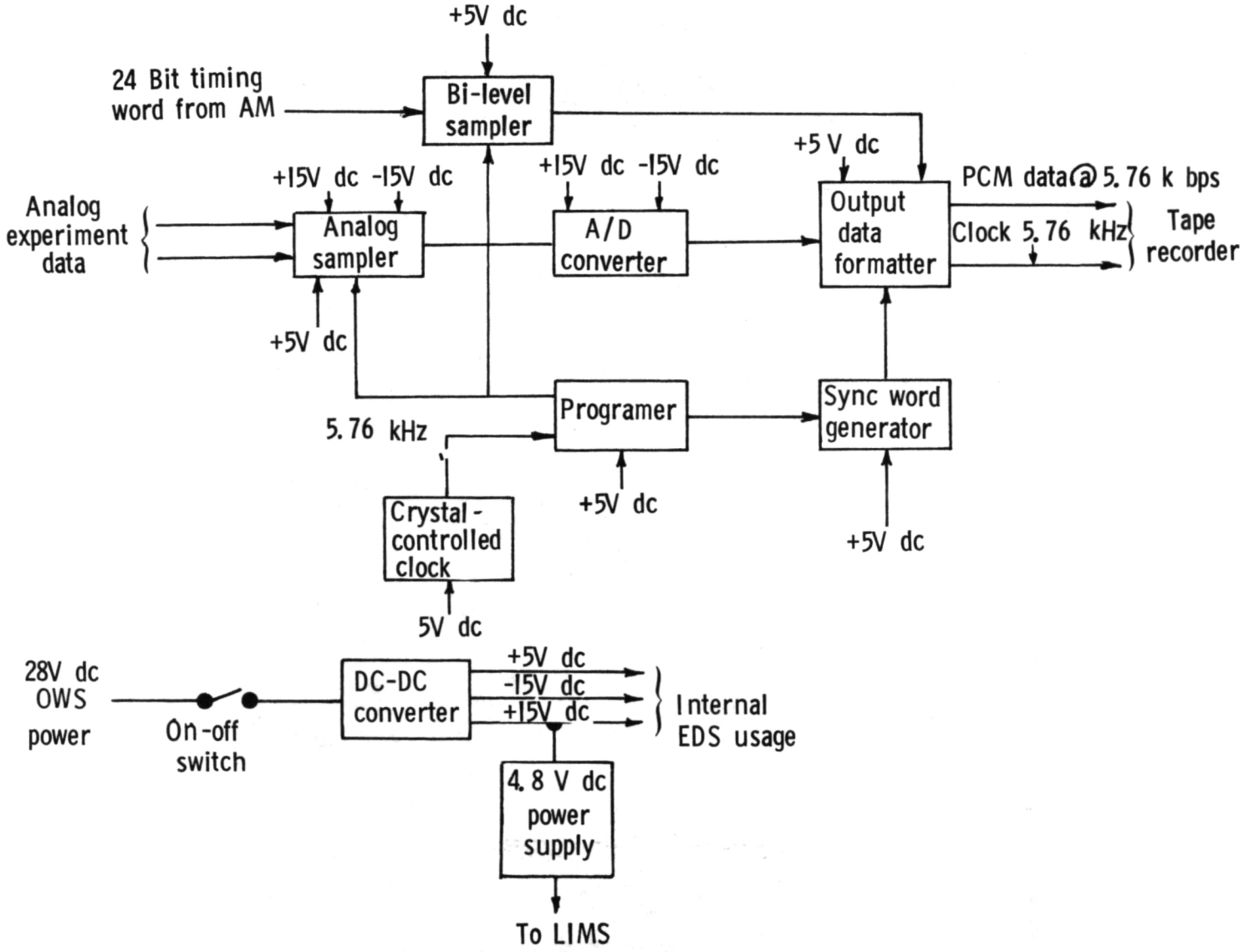

Figure 8.- Simplified EDS electronics diagram.

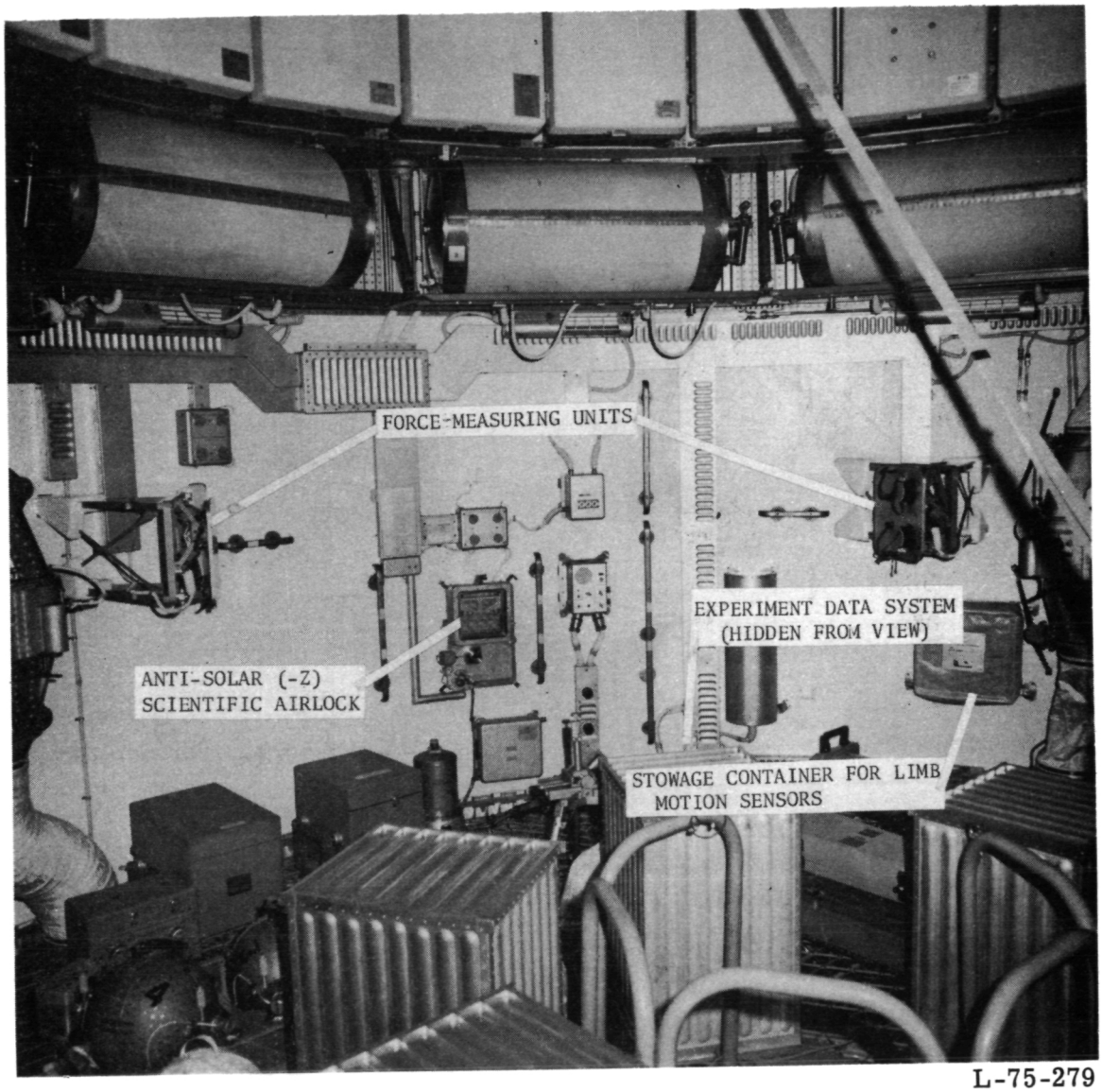

Figure 9.- Photograph of T-013 operations area in OWS (taken prior to launch) showing hardware locations.

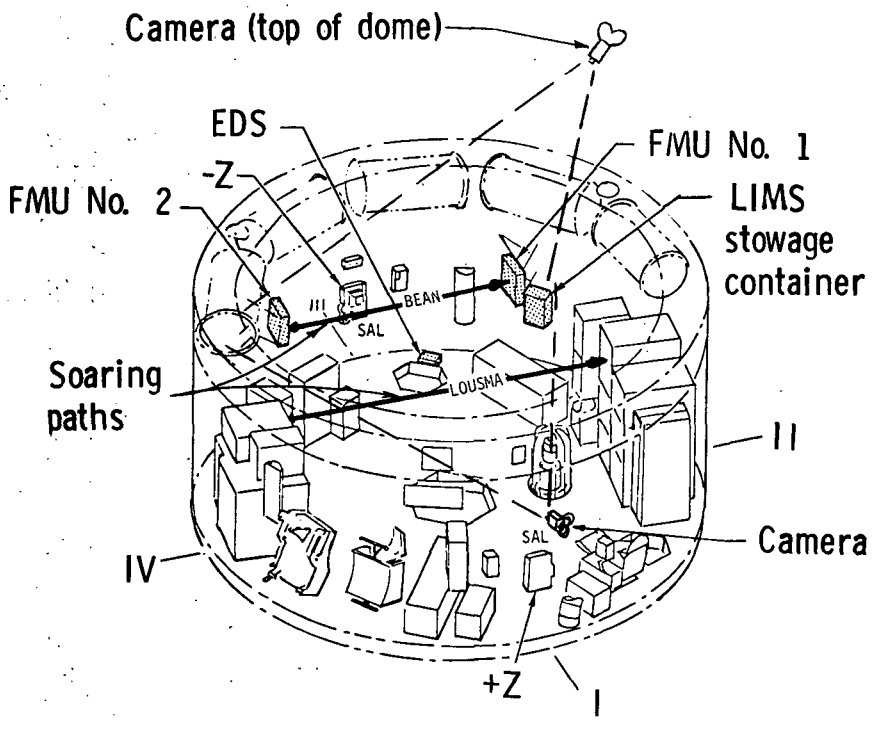

Figure 10.- T-013 operations area of OWS indicating soaring paths.

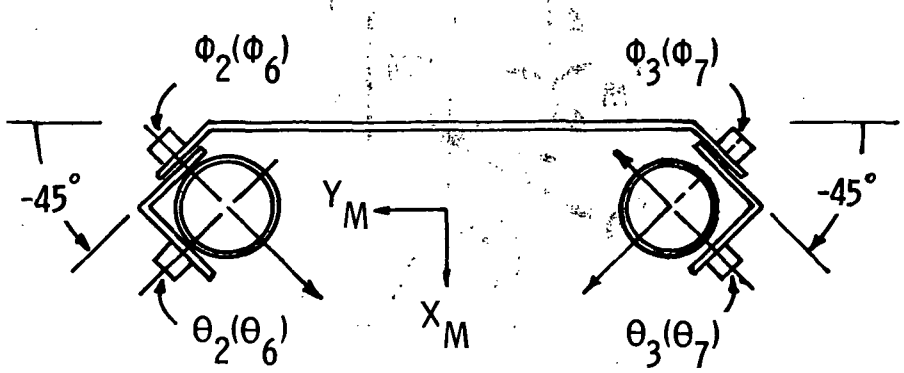

Figure 11.- LIMS shoulder and hip joint detail.

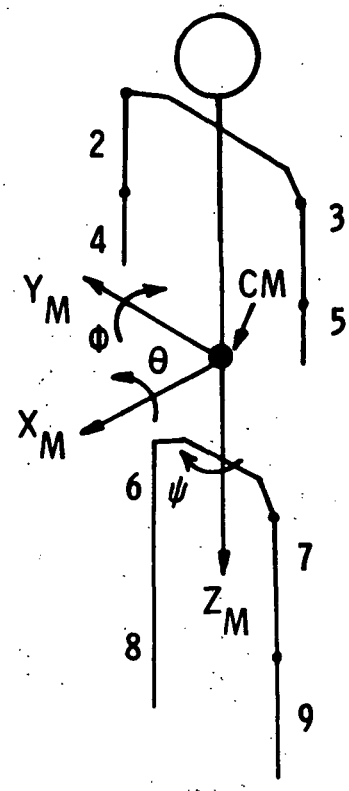

Figure 12.- Torso coordinate system and limb designation.

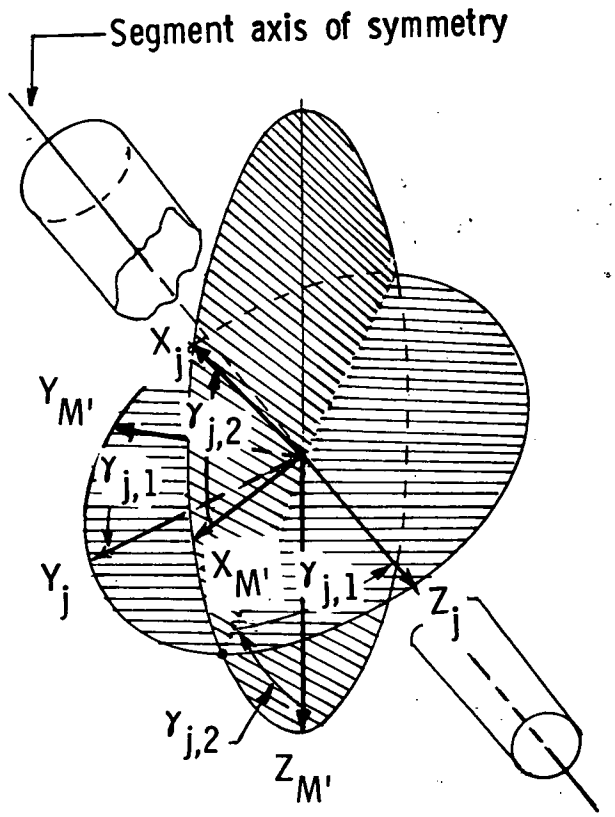

Figure 13.- Euler angles for segments 2 to 9. $X_{M'}$, $Y_{M'}$, and $Z_{M'}$ axes are parallel to the X_M, Y_M, and Z_M axes, respectively.

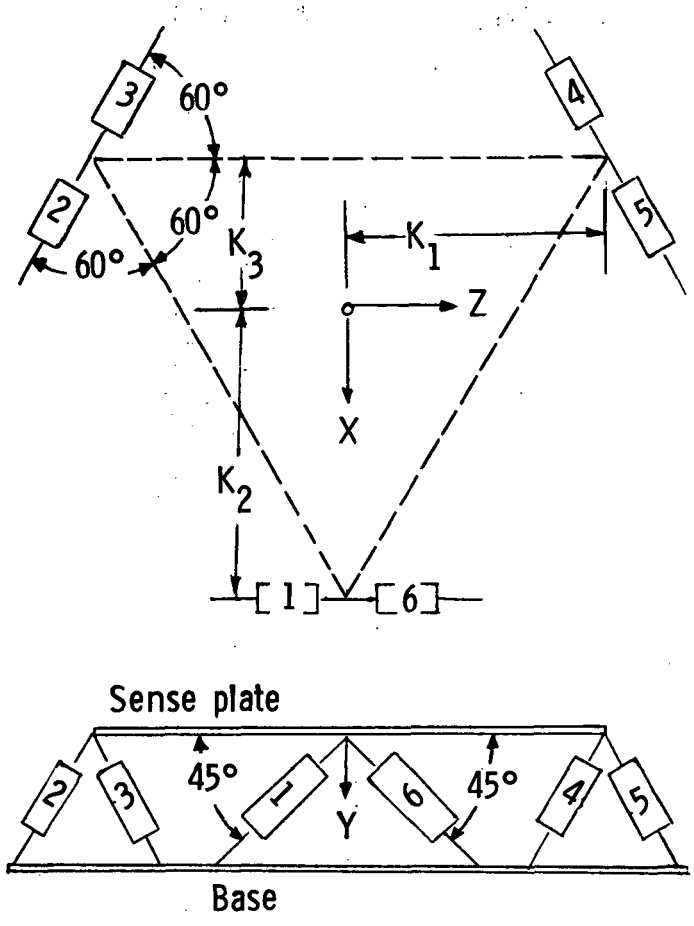

Figure 14.- Load cell array schematic.

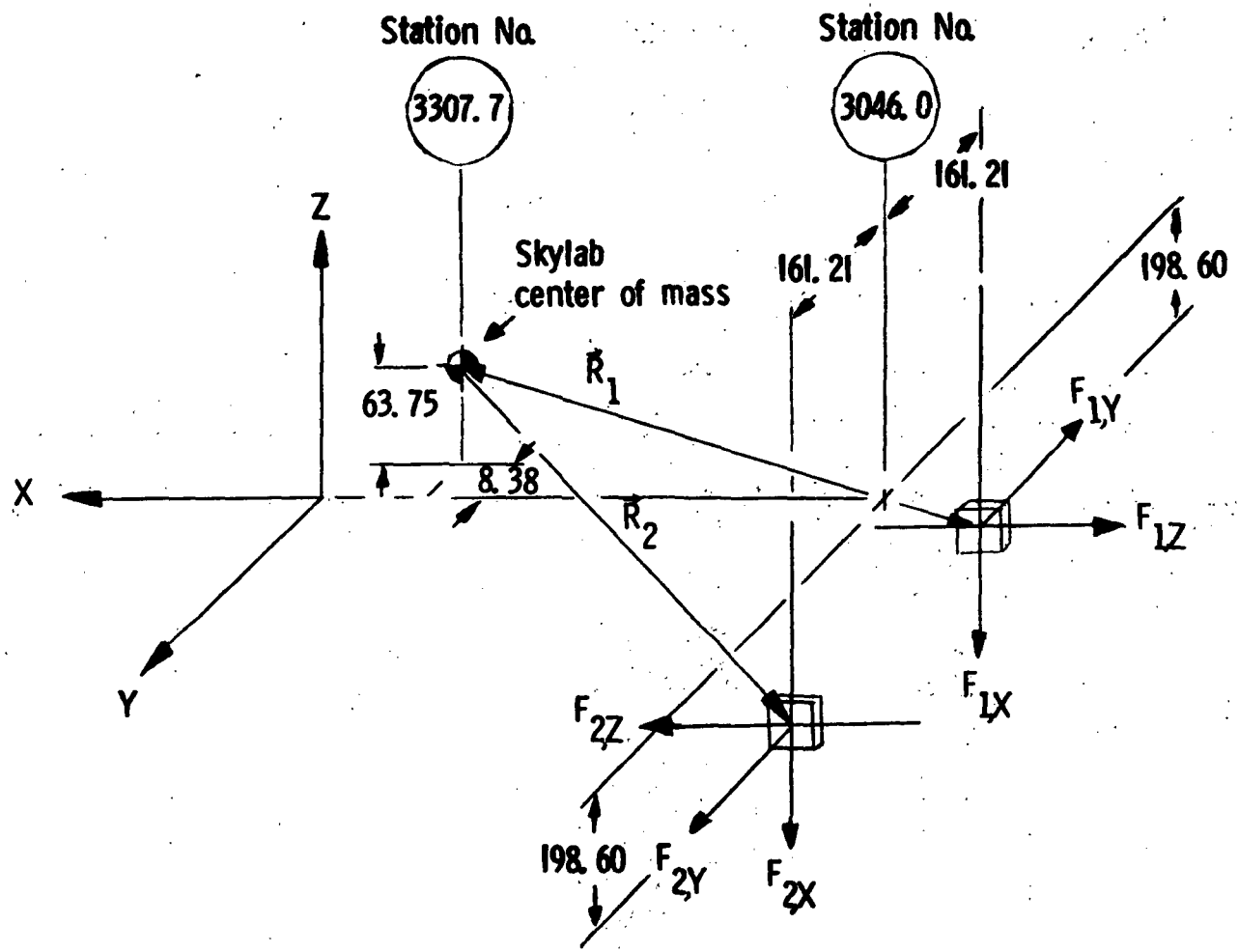

Figure 15.- FMU locations in OWS. Center-of-mass location is obtained from "Skylab orbital mass properties" MSFC/Sand E-ASTN-SAE (74-1) of 7 Jan 1974, event II. All dimensions are in centimeters.

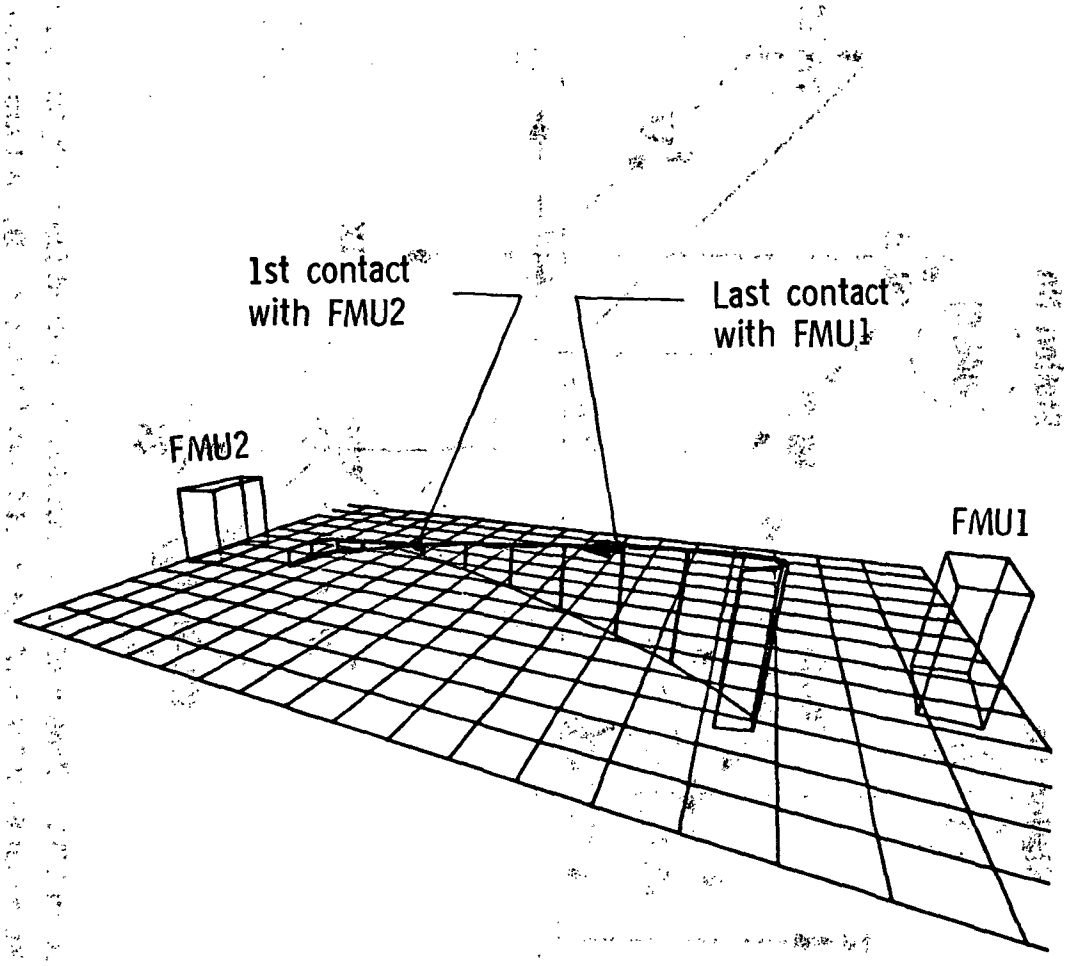

(a) Frames 1 to 15.

Figure 16.- Torso center-of-mass trajectory for activity 5.

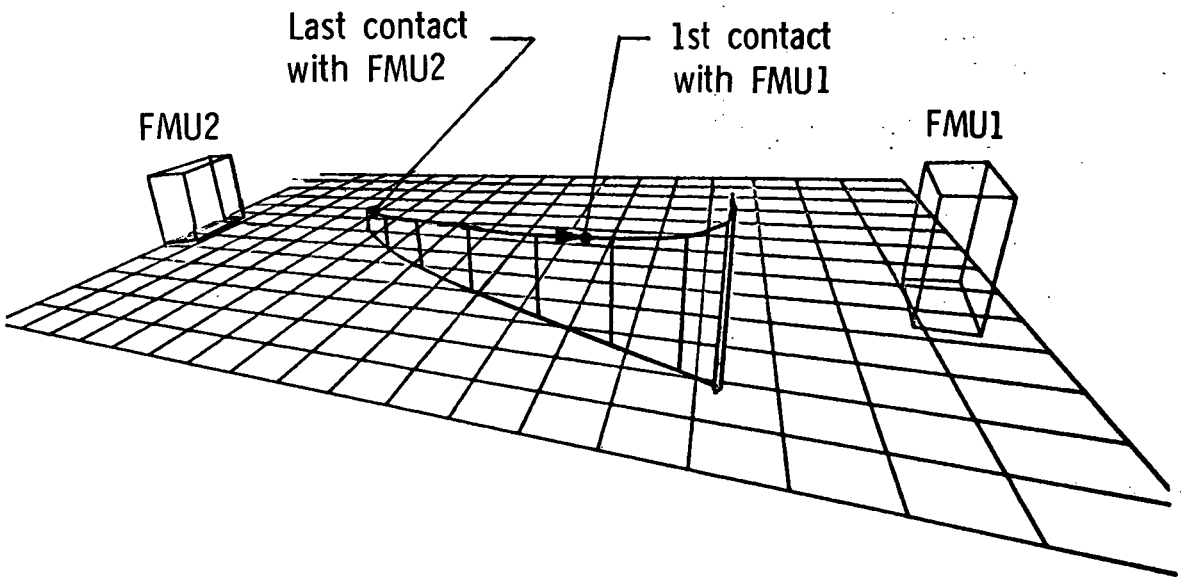

(b) Frames 53 to 63.

Figure 16.- Continued.

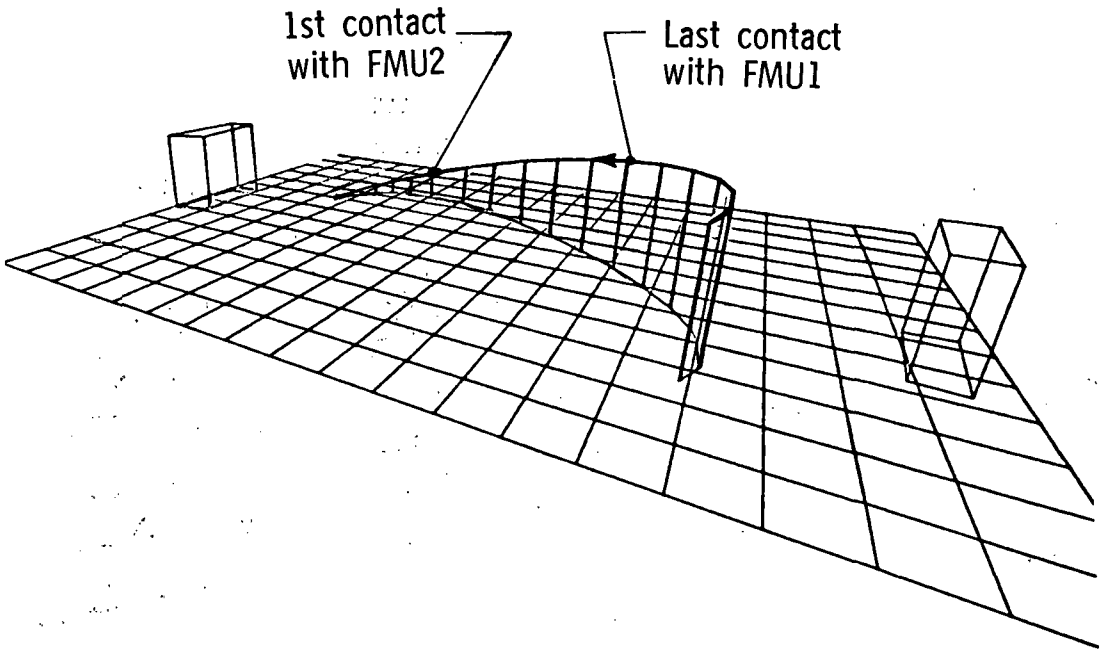

(c) Frames 121 to 137.

Figure 16.- Continued.

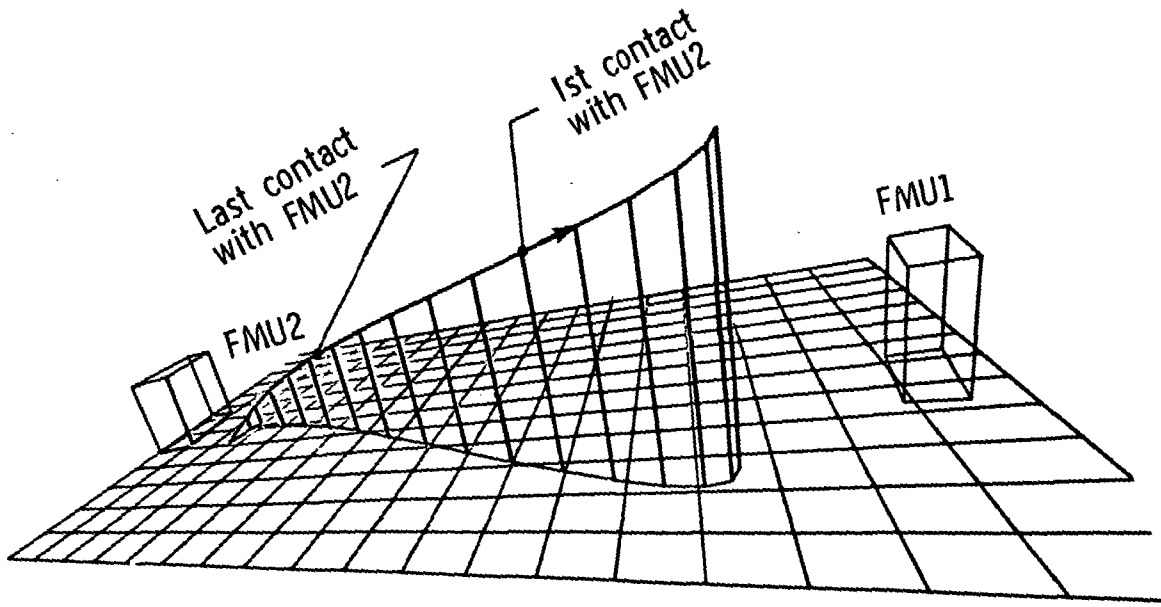

(d) Frames 160 to 176.

Figure 16.- Concluded.

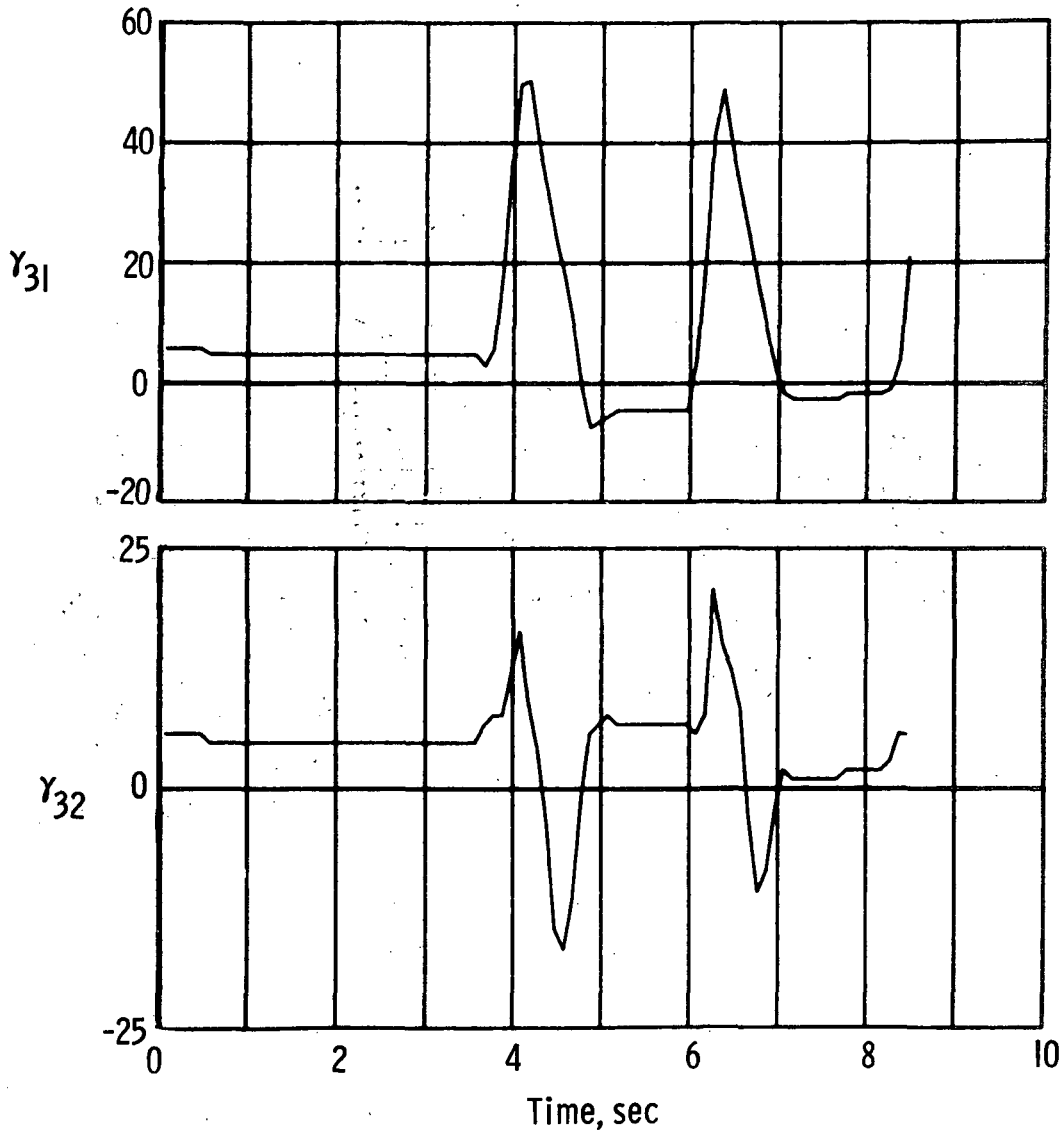

(a) Upper left arm (15:56:12).

Figure 17.- Gamma angles.

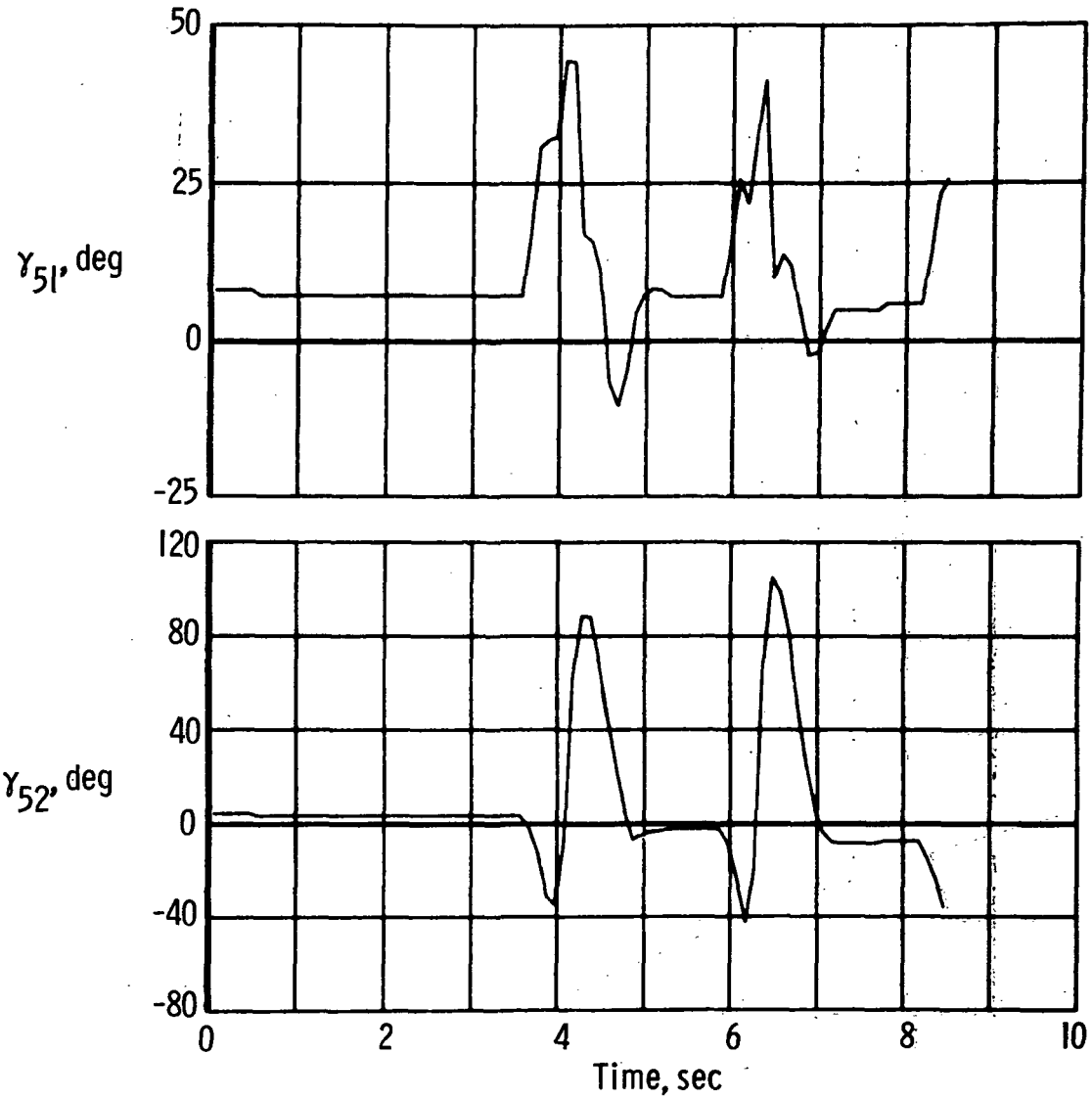

(b) Lower left arm (15:56:12).

Figure 17.- Concluded.

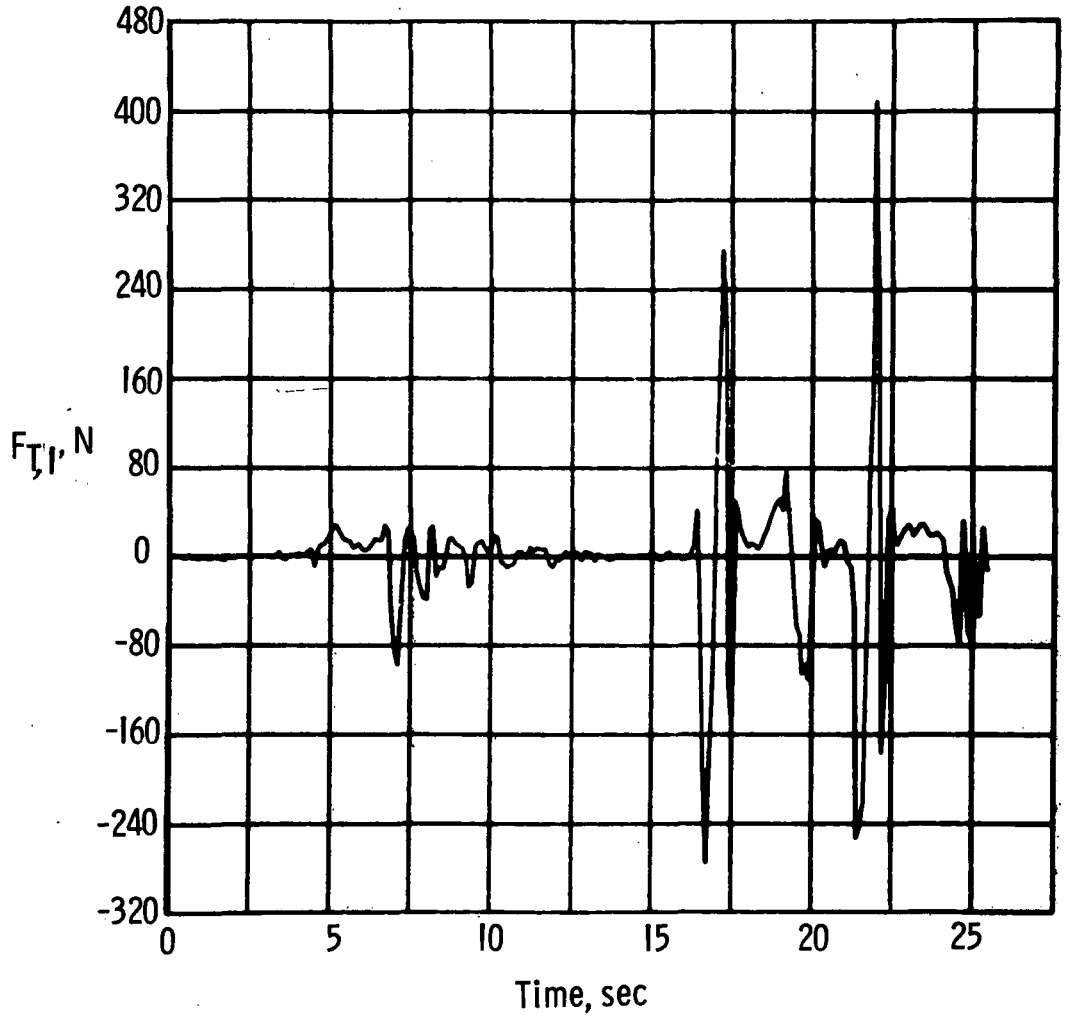

Figure 18.- $F_{T,1}$ time function. Crouch and pushoff (15:27:45).

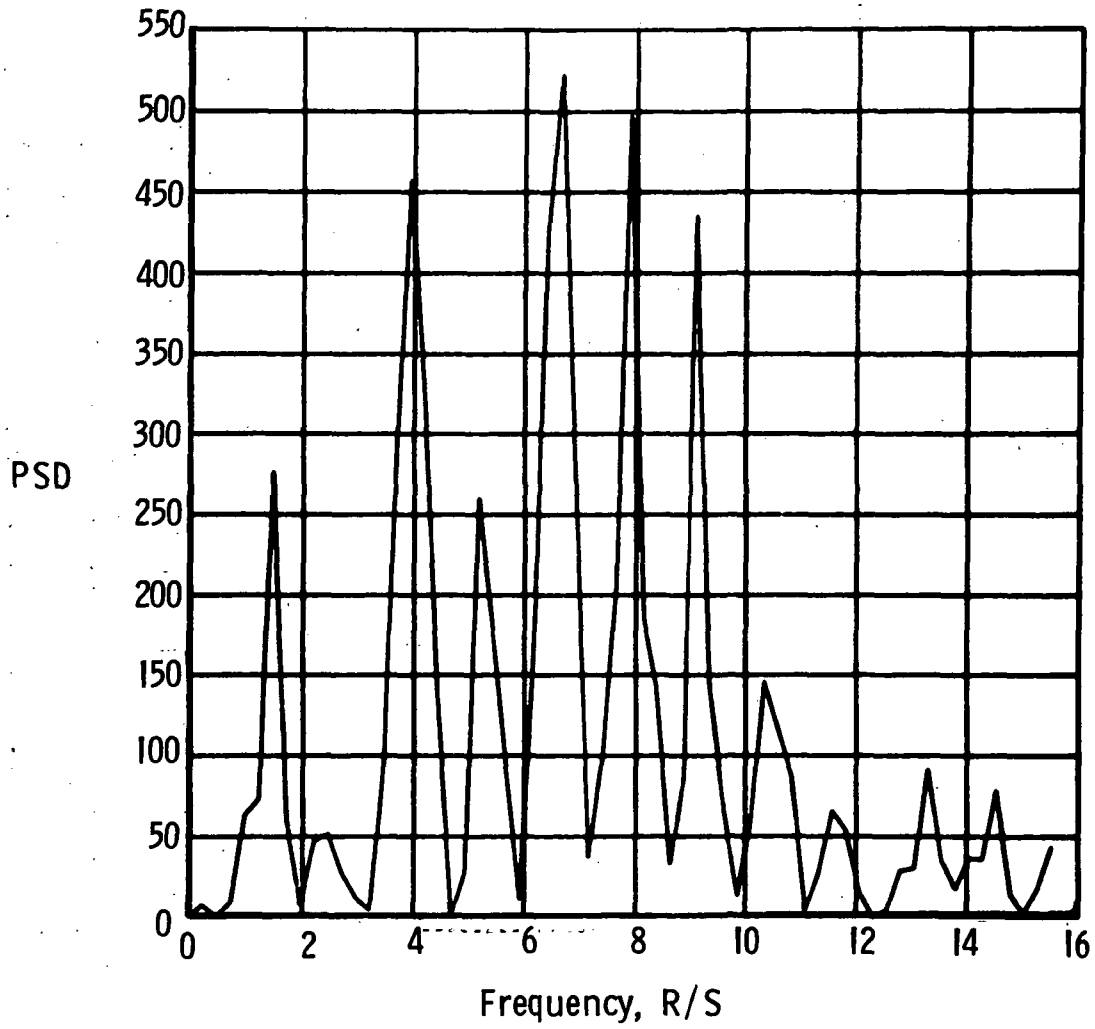

Figure 19.- $F_{T,1}$ power spectral density (15:27:45).

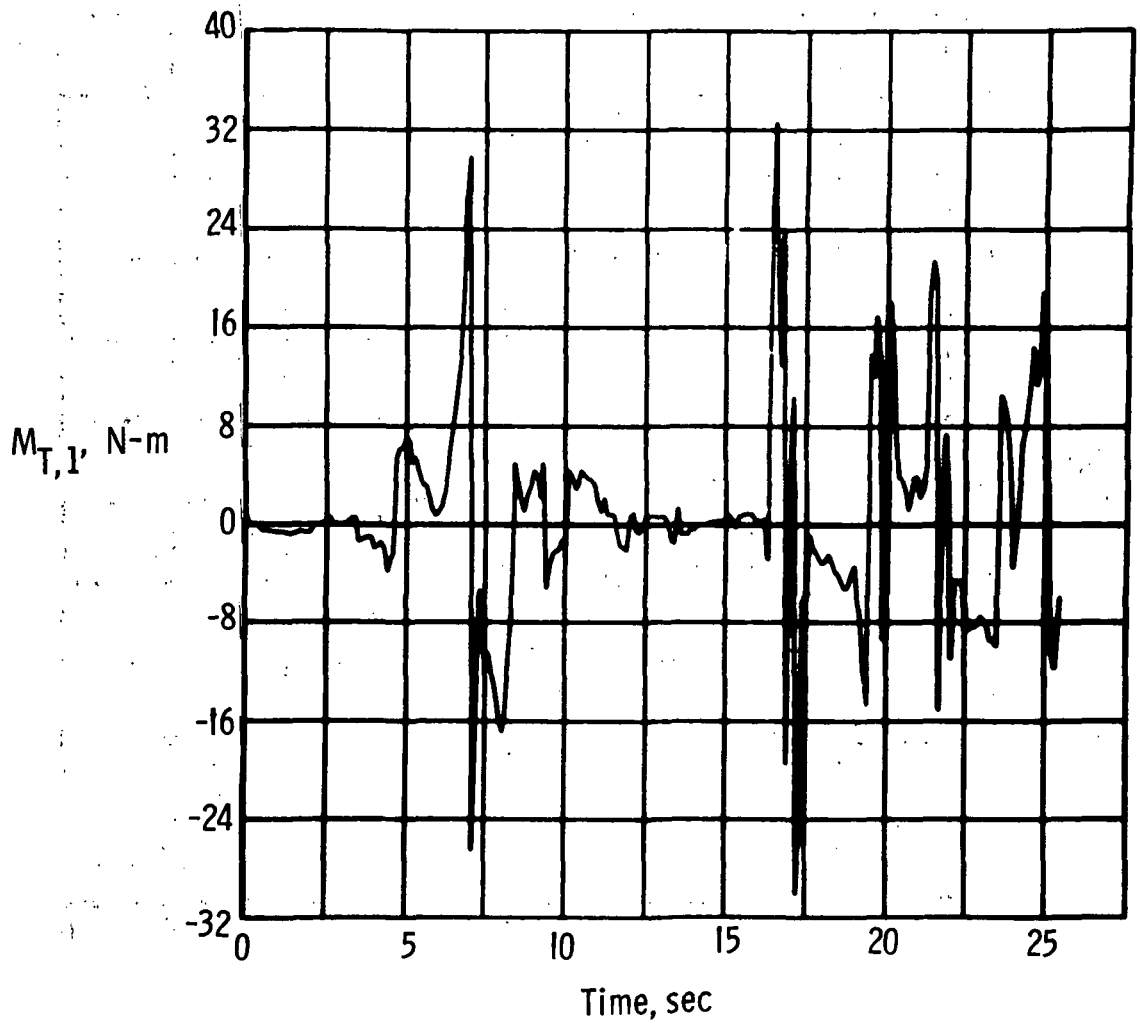

Figure 20.- $M_{T,1}$ time function. Crouch and pushoff (15:27:45).

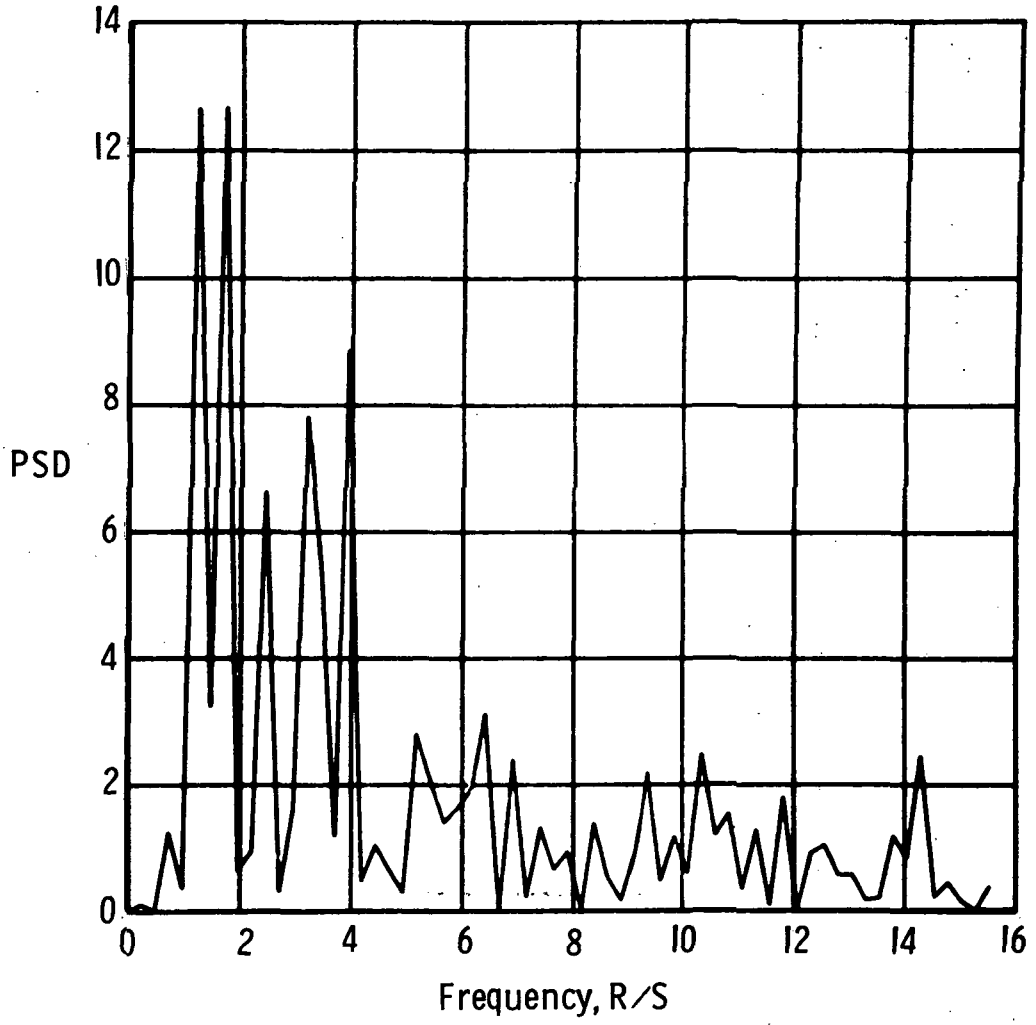

Figure 21.- $M_{T,1}$ power spectral density (15:27:45).

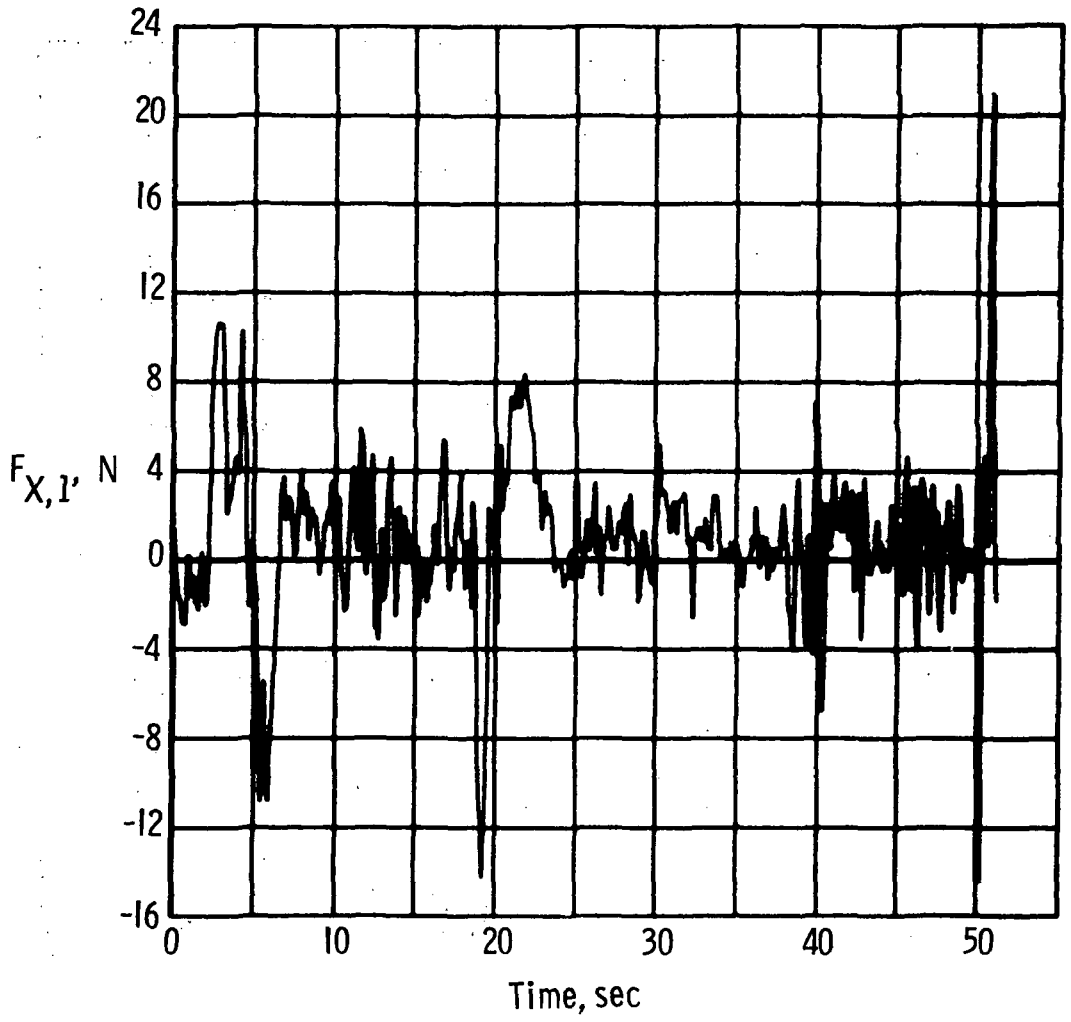

Figure 22.- $F_{X,1}$ time function. Console operations (16:10:00).

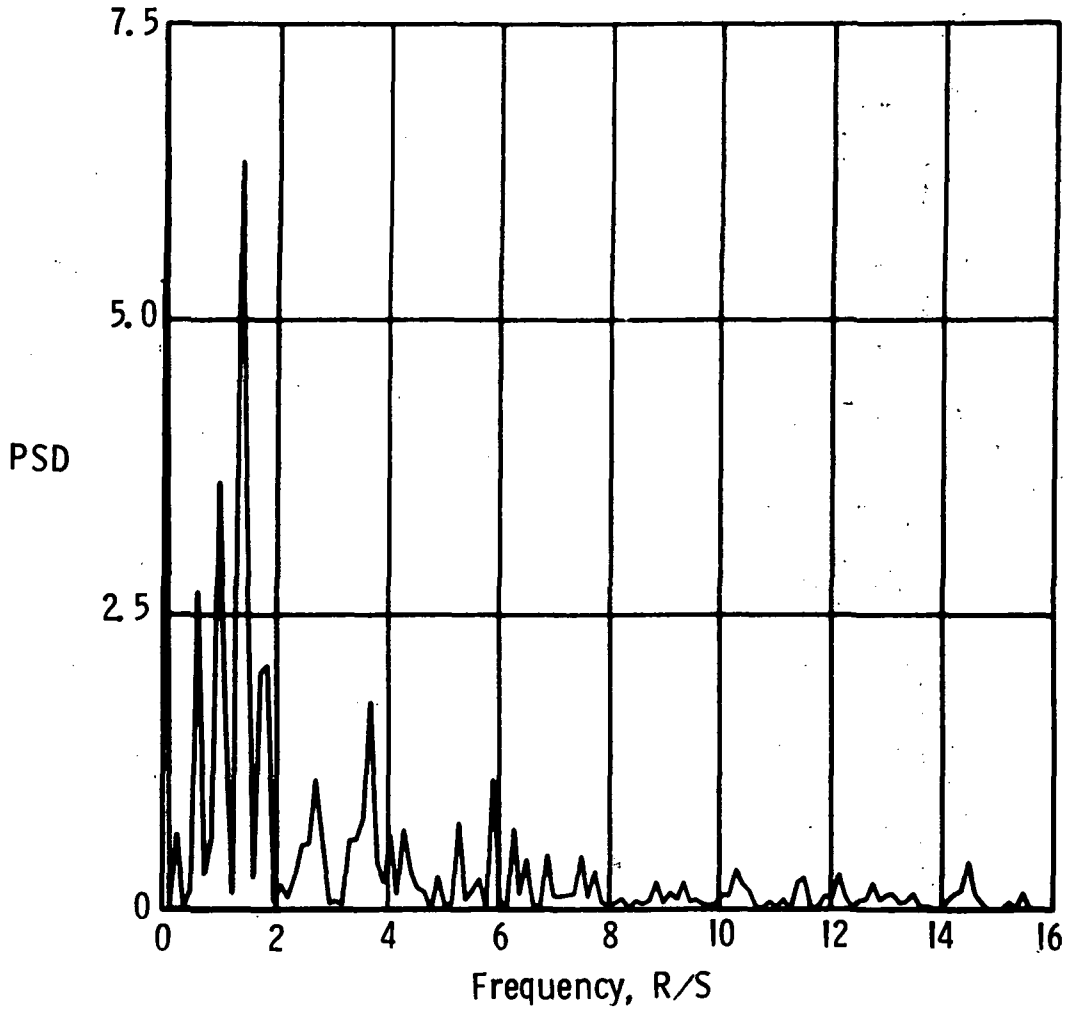

Figure 23.- $F_{X,1}$ power spectral density (16:10:00).

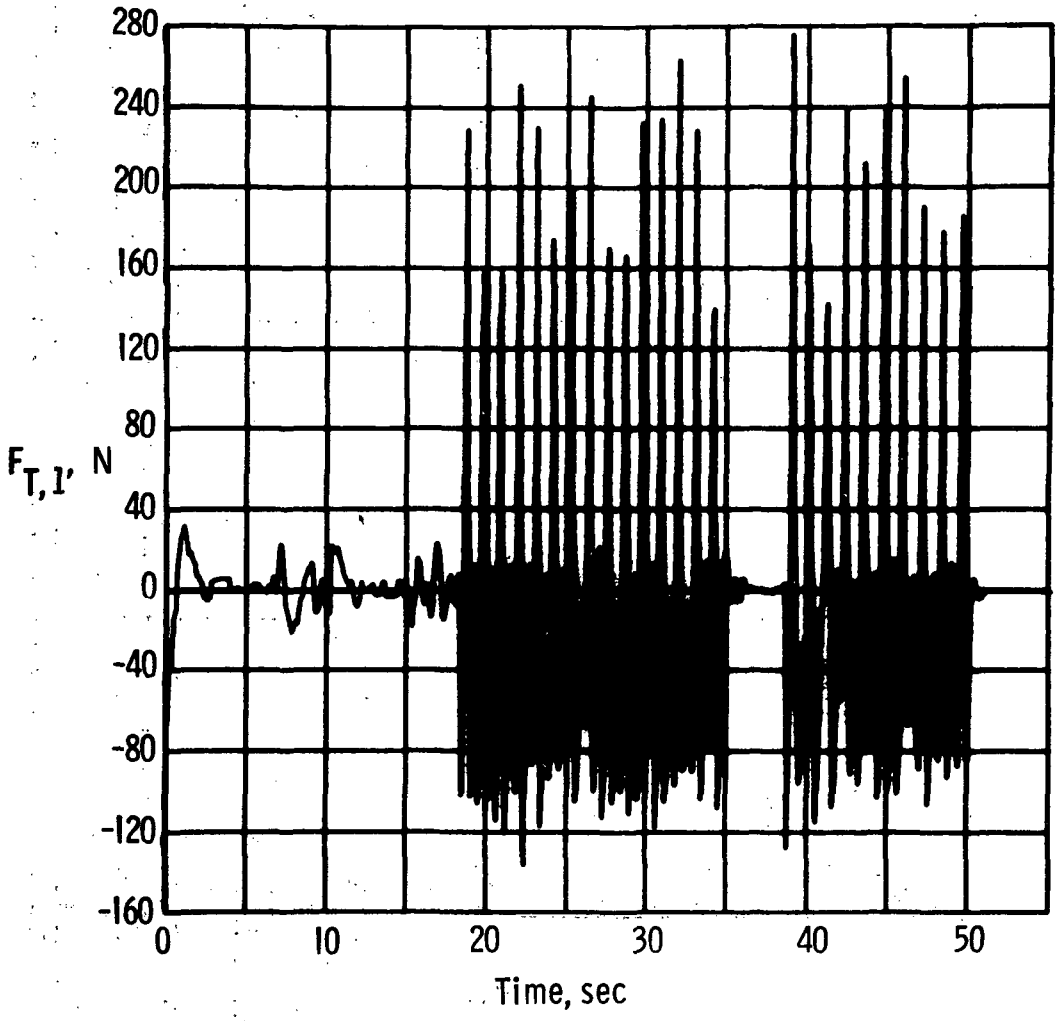

Figure 24.- $F_{T,1}$ time function. Arm flapping (16:13:10).

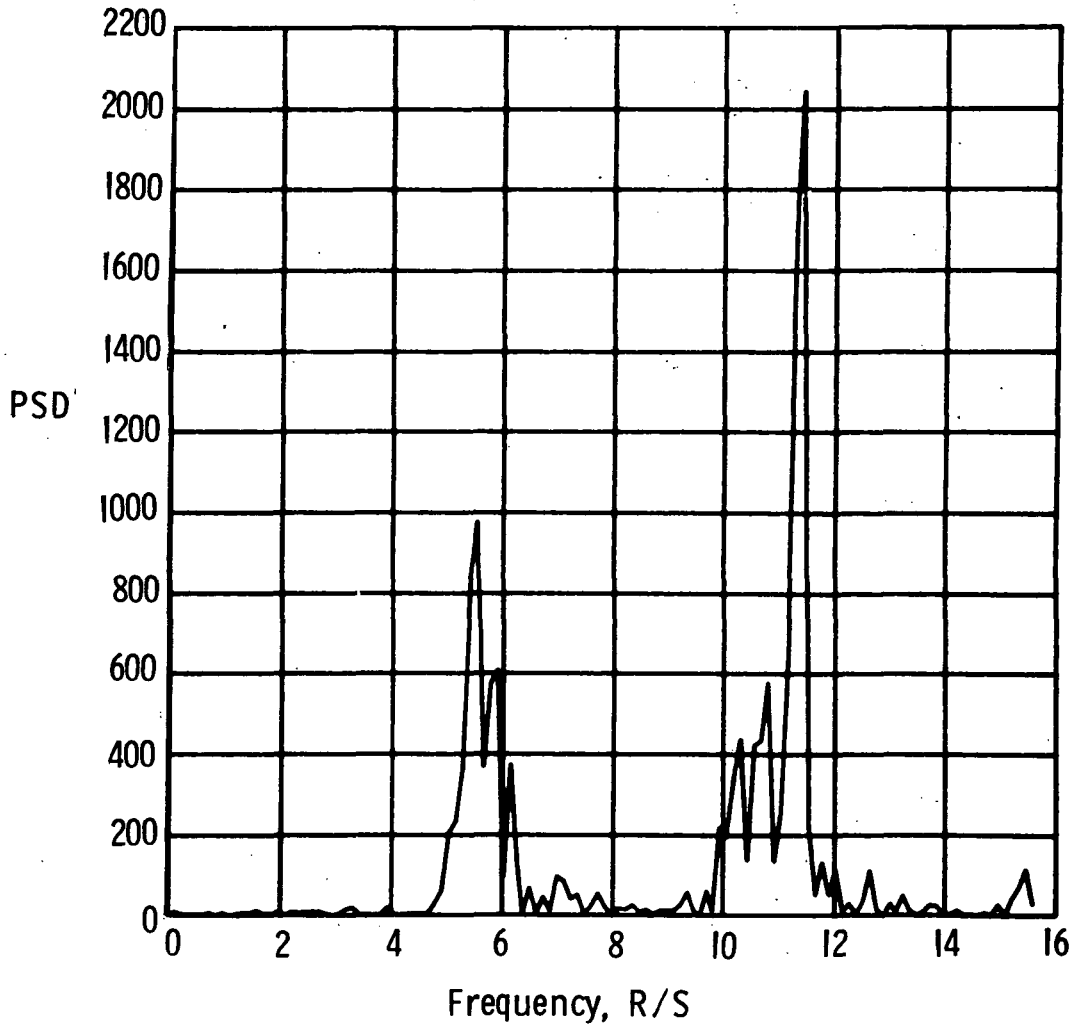

Figure 25.- $F_{T,1}$ power spectral density (16:13:10).

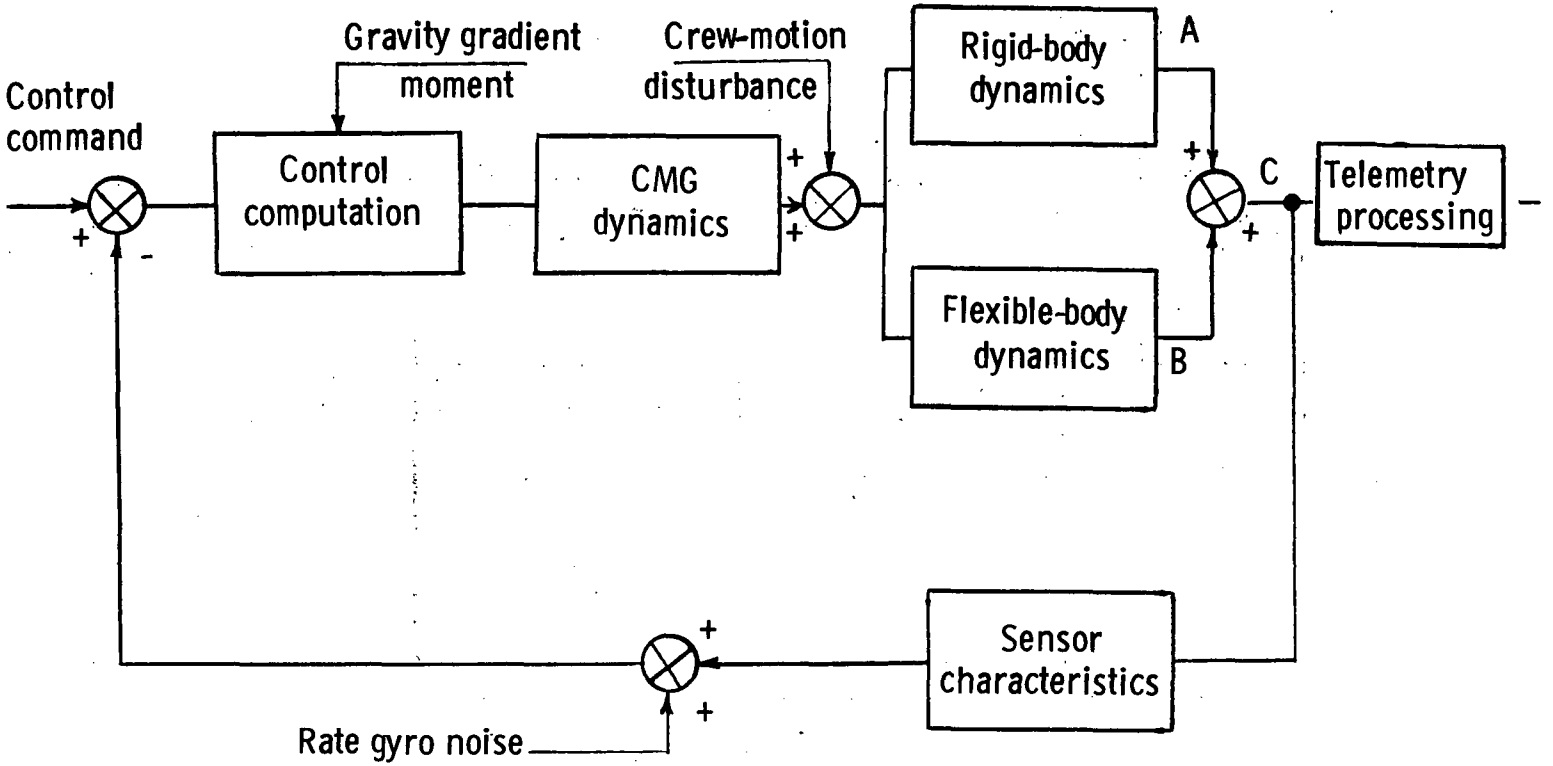

Figure 26.- Vehicle dynamics response simulation.

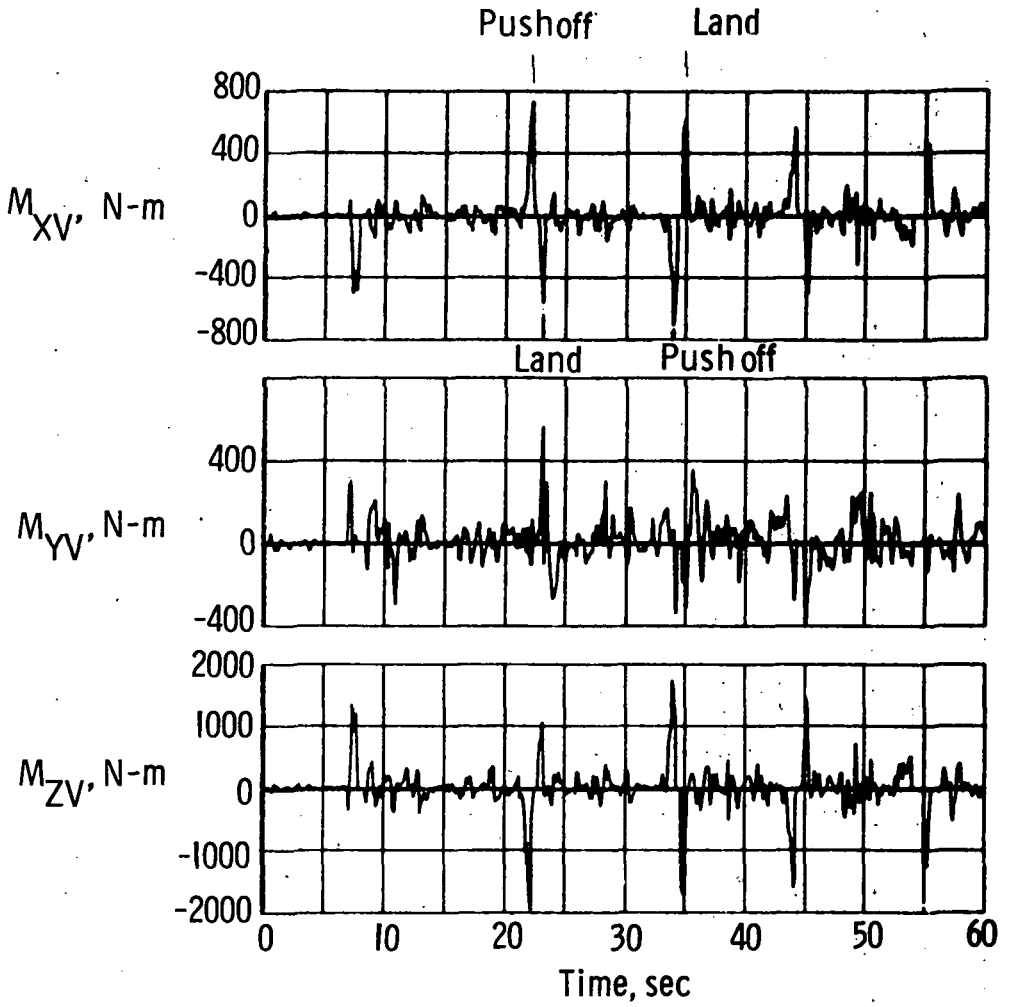

Figure 27.- Disturbance torques. Soaring (15:29:45).

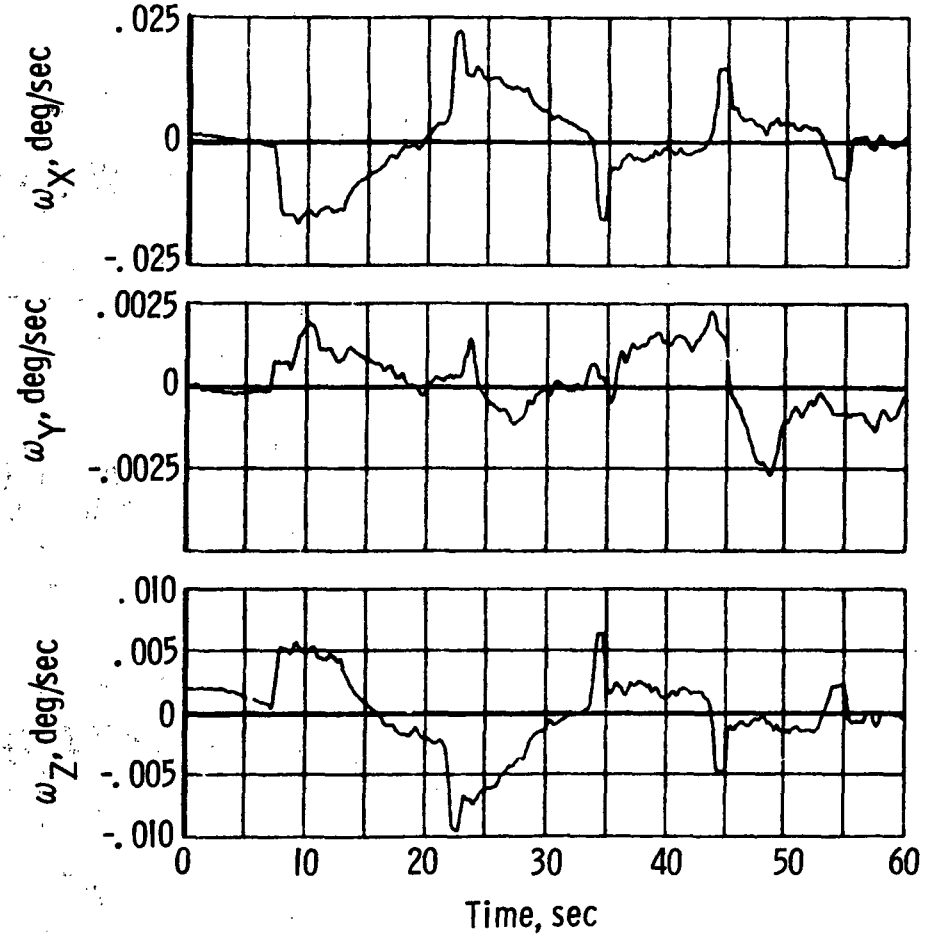

Figure 28.- Simulation rigid-body rates (15:29:45).

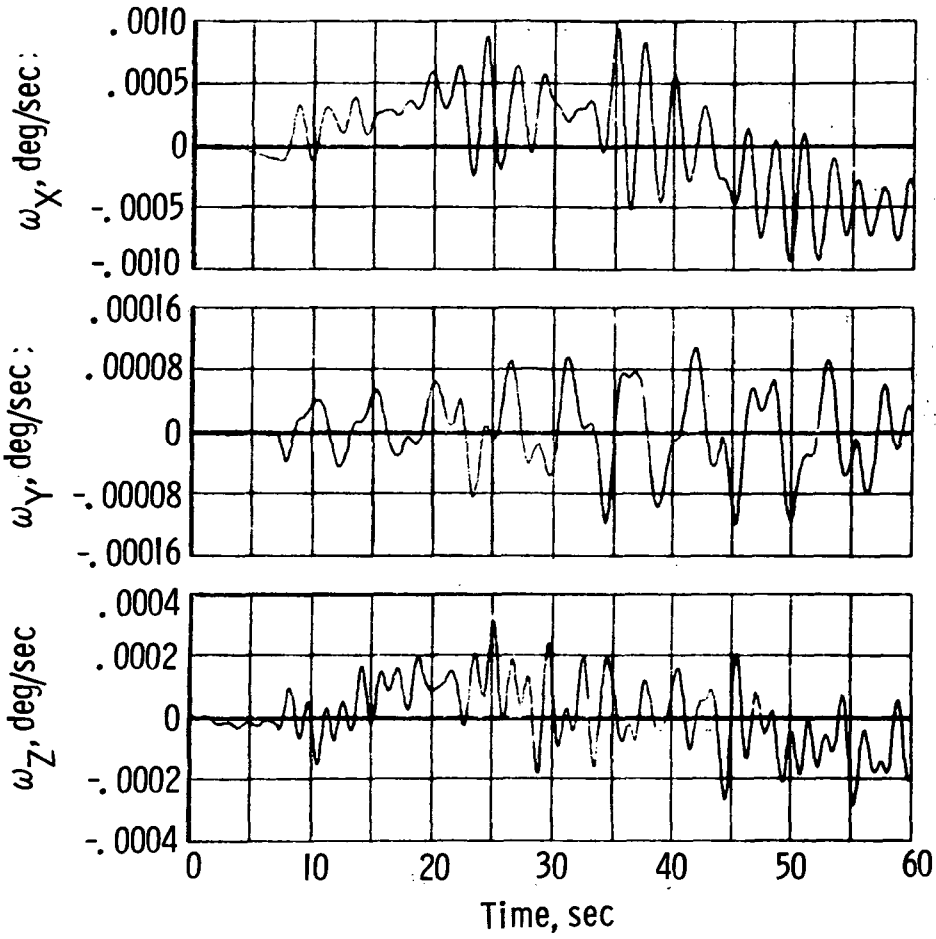

Figure 29.- Simulation flexible-body rate components (15:29:45).

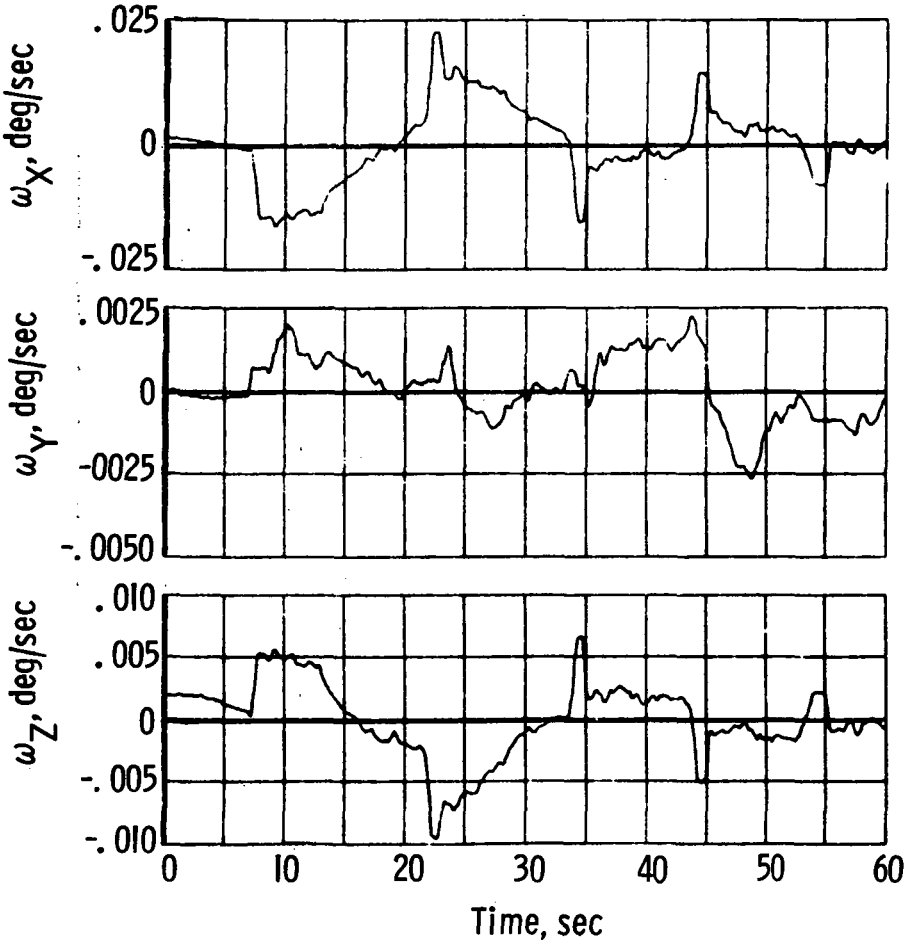

Figure 30.- Simulation total vehicle rates (15:29:45).

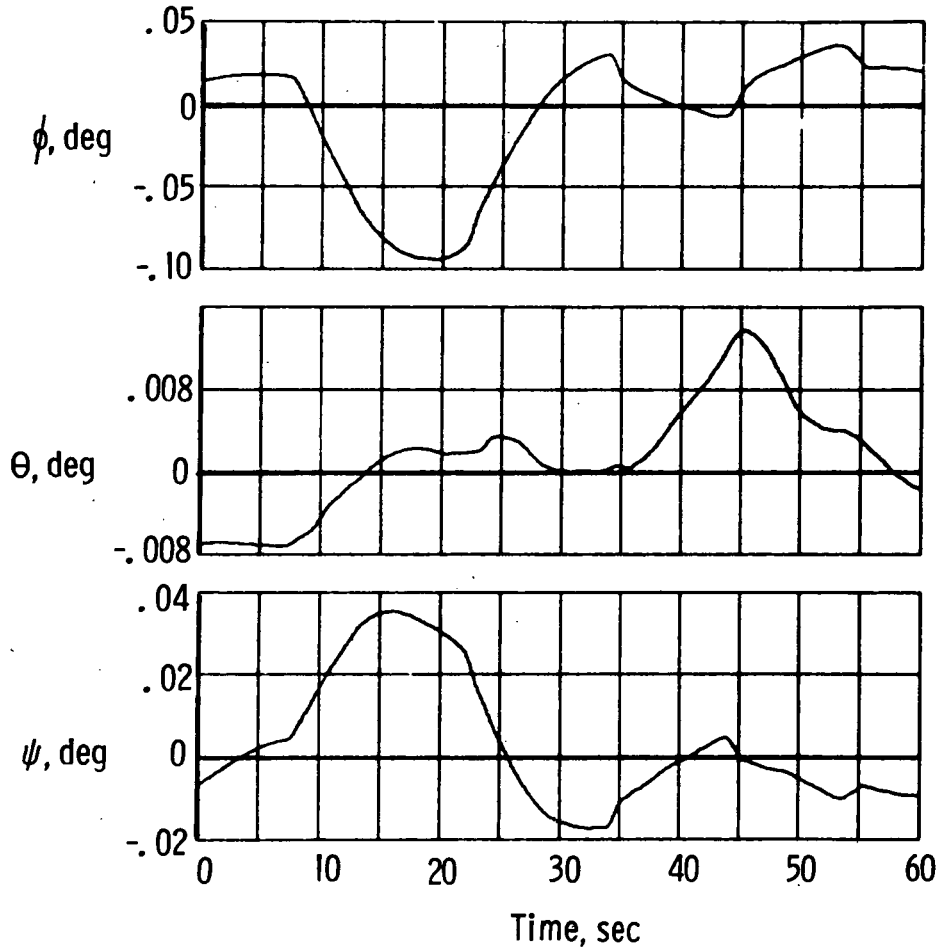

Figure 31.- Simulation vehicle attitude (15:29:45).

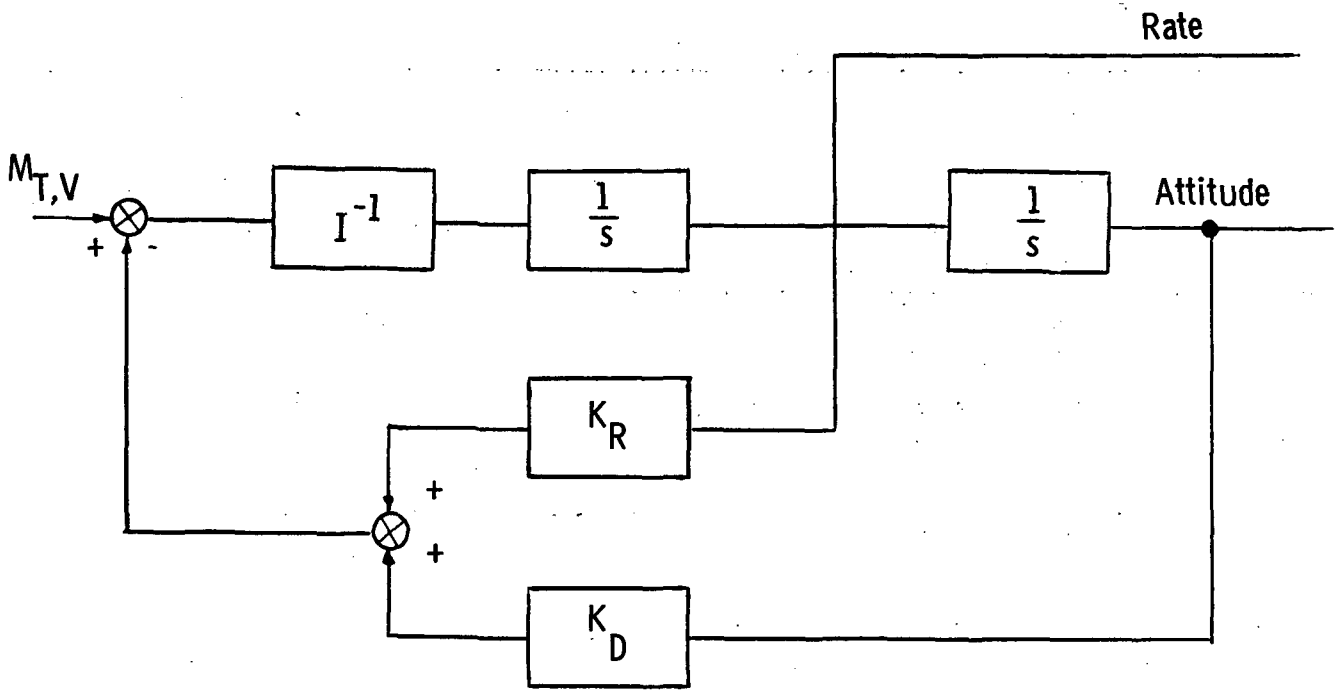

Figure 32.- Simplified vehicle dynamic response model.

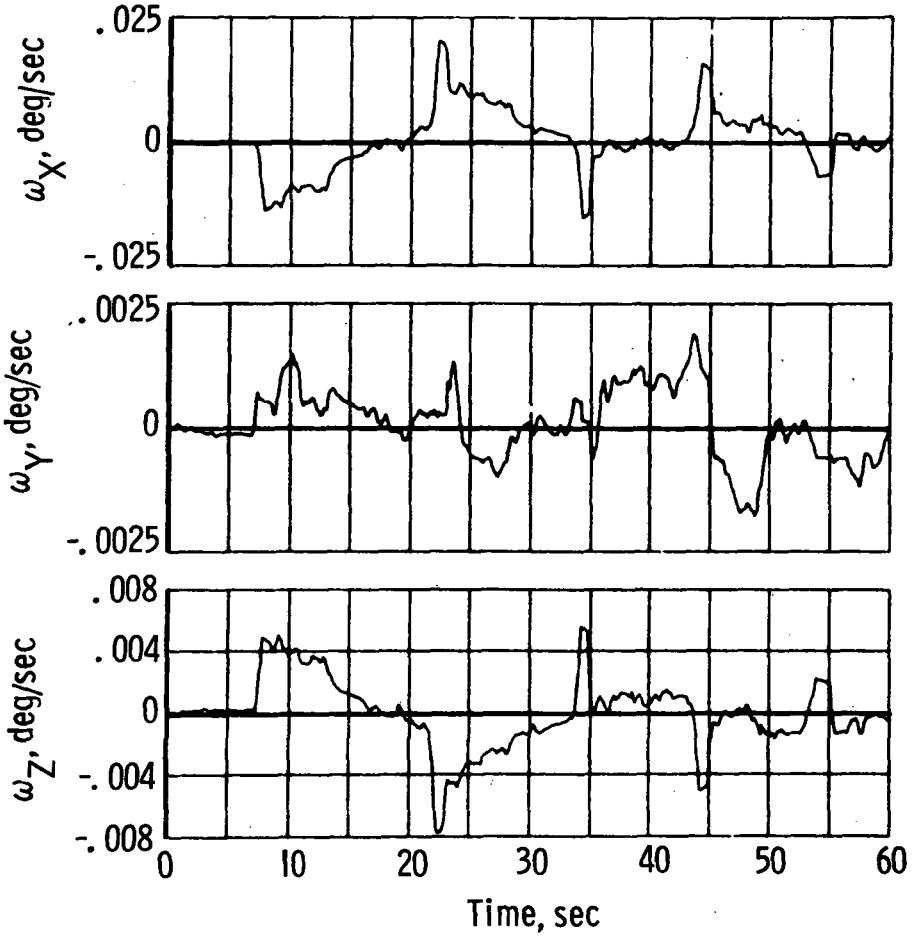

Figure 33.- Vehicle rates. Simplified model (15:29:45).

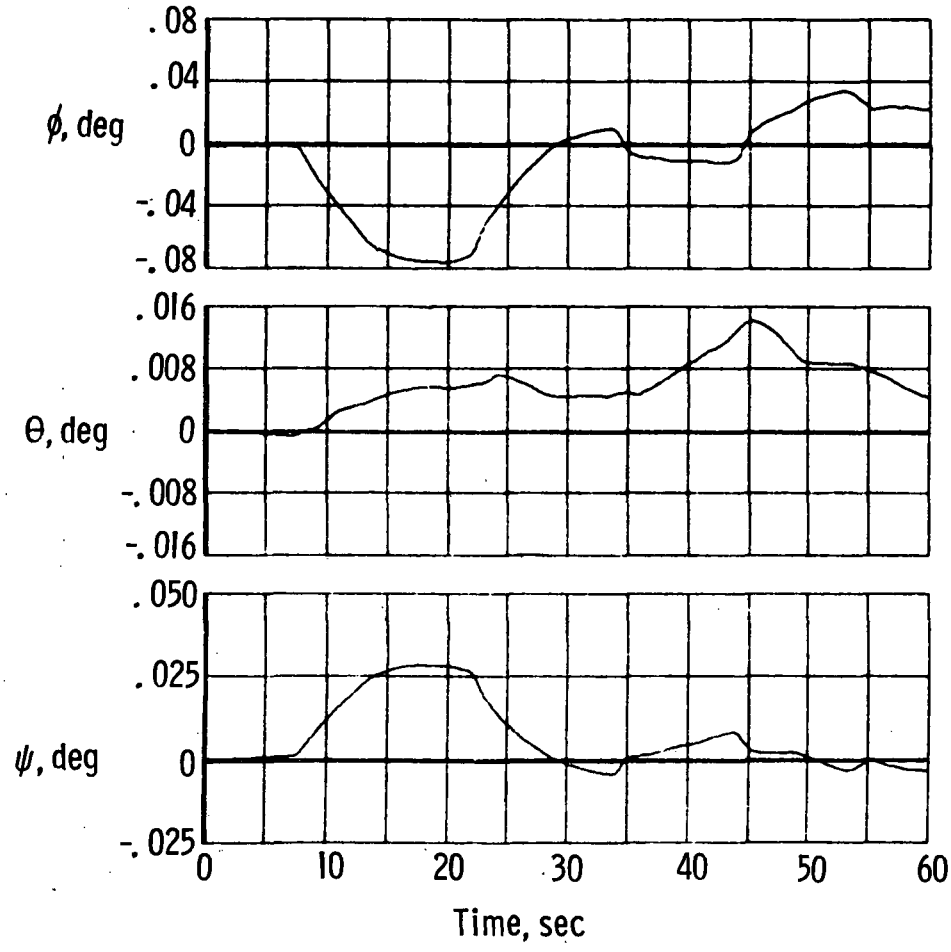

Figure 34.- Vehicle attitude. Simplified model (15:29:45).

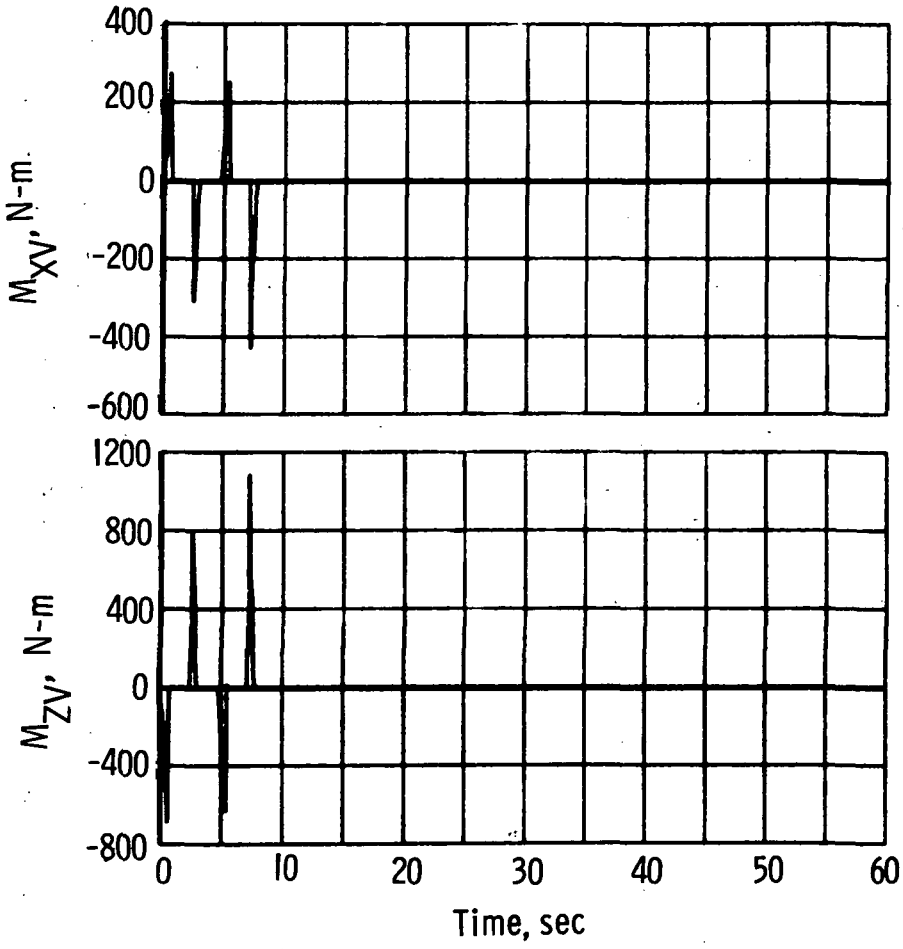

Figure 35.- Preflight disturbance torque (wall pushoff).

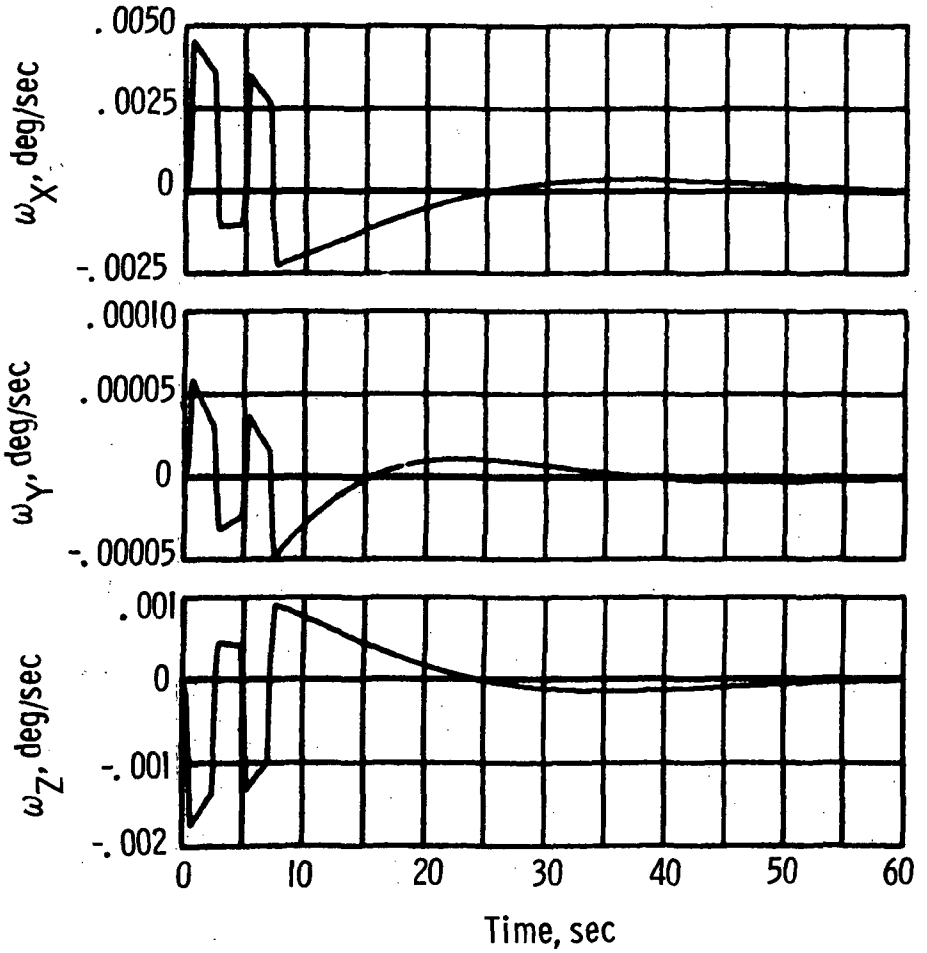

Figure 36.- Preflight rates (wall pushoff).

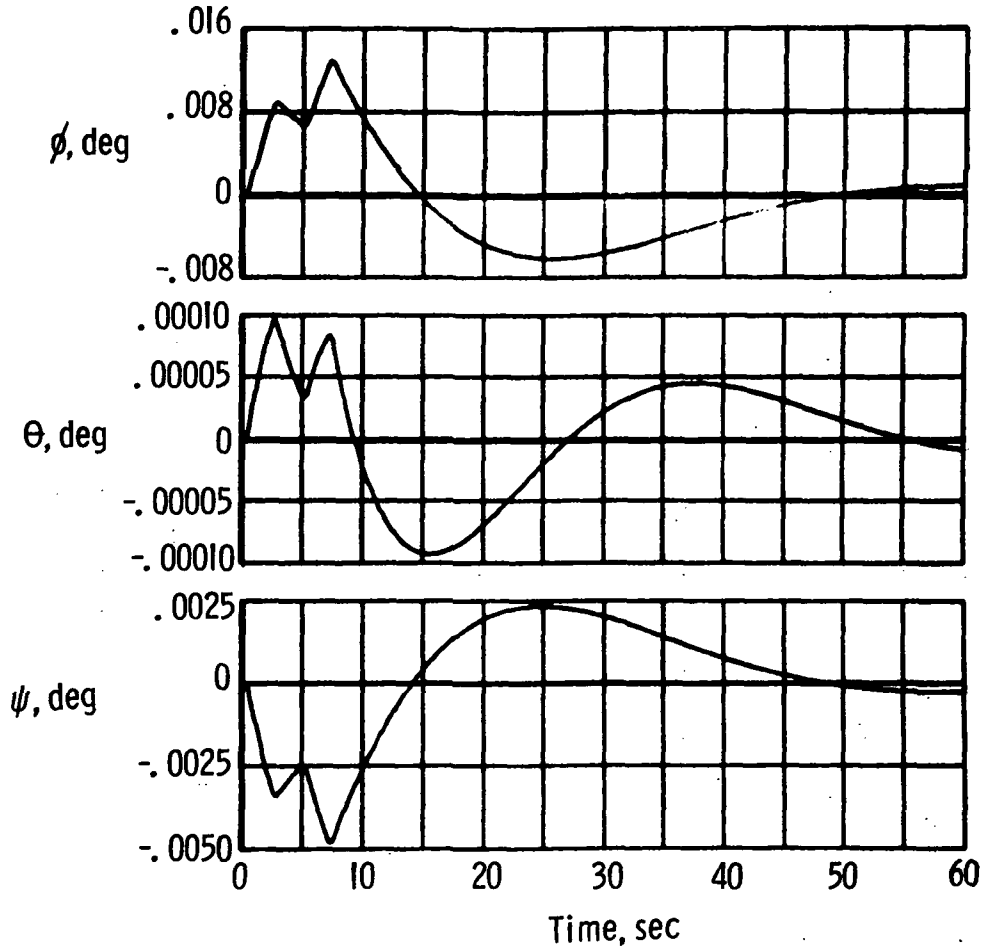

Figure 37.- Preflight attitude (wall pushoff).

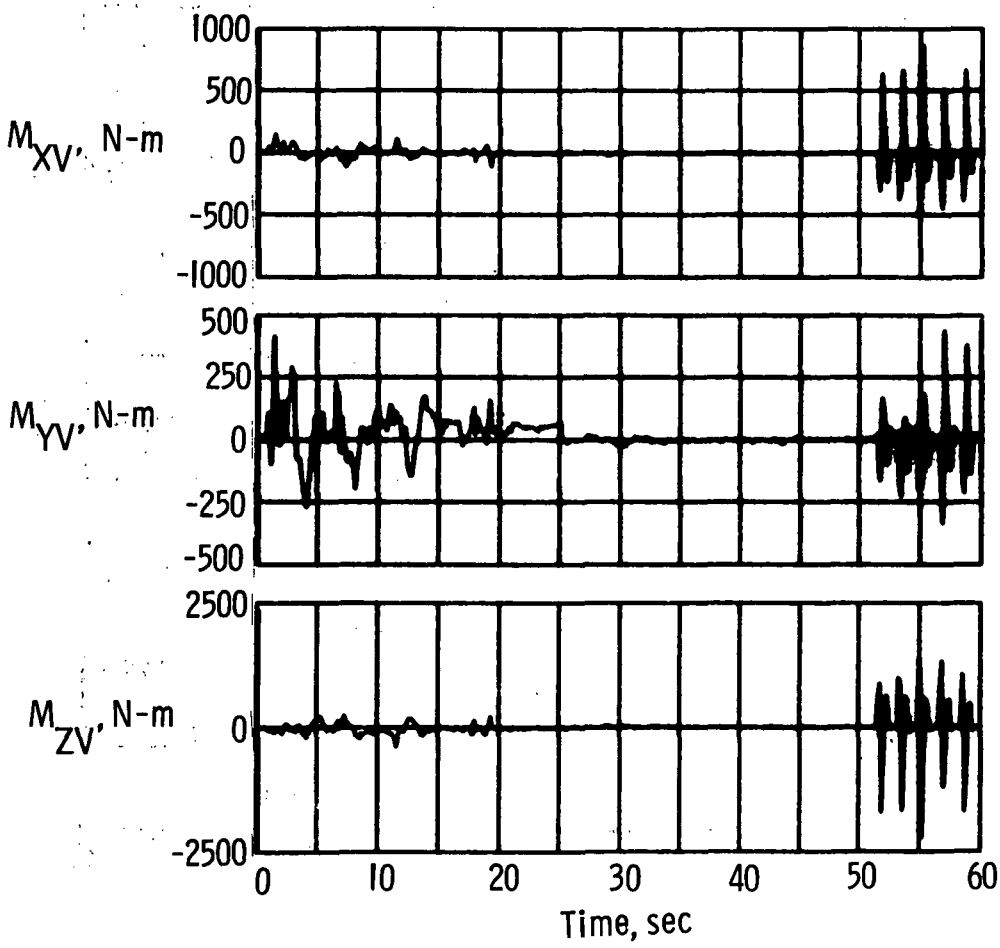

Figure 38.- Disturbance torques. Flapping arms (15:26:00).

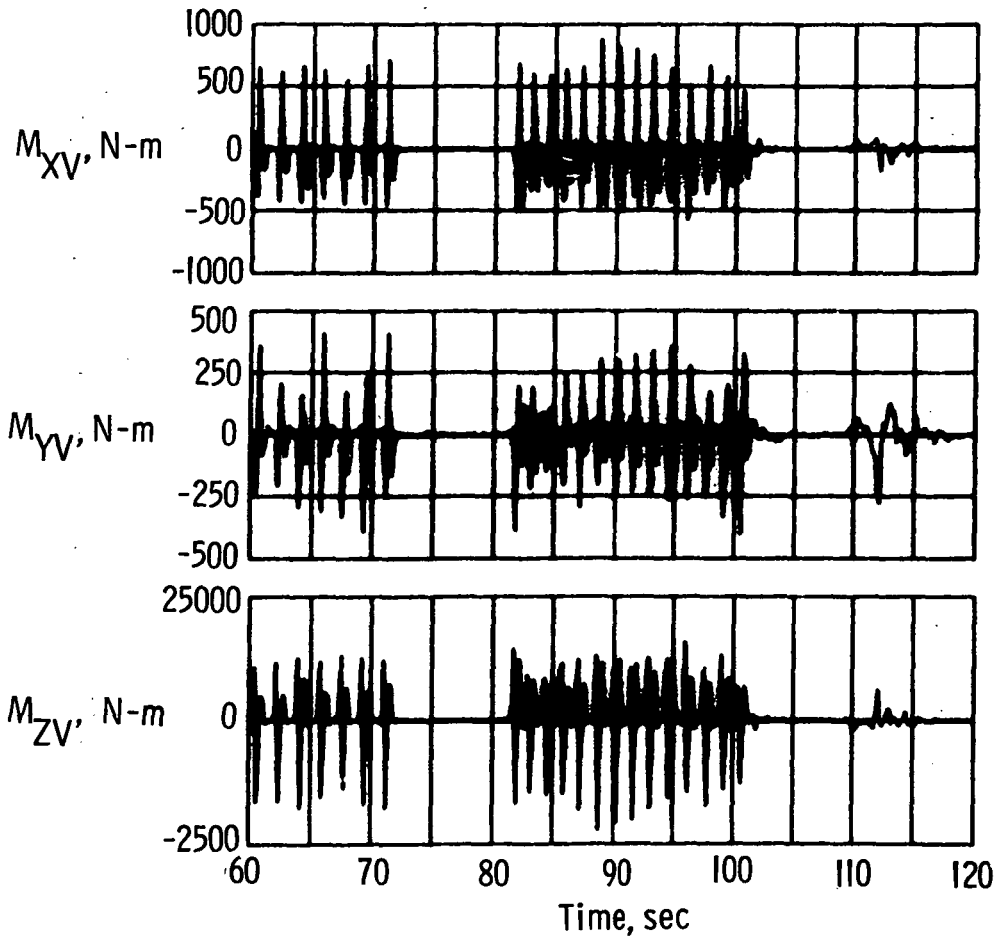

Figure 38.- Concluded.

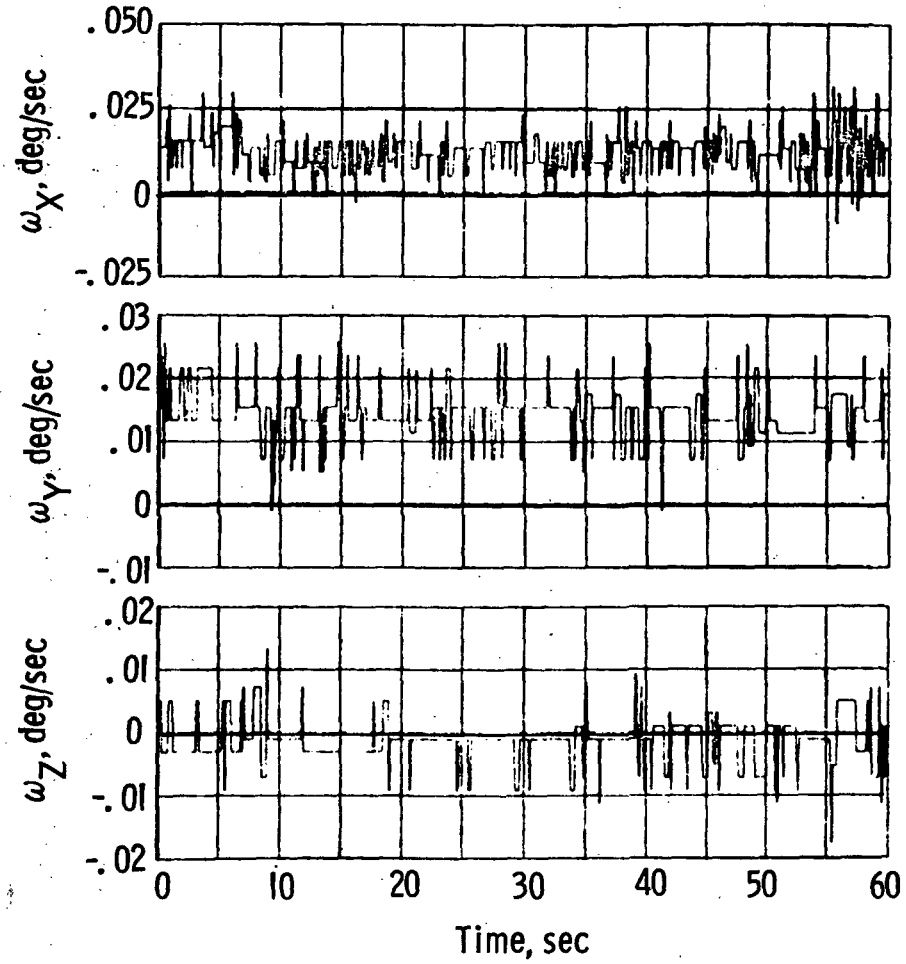

Figure 39.- Measured vehicle rates (15:26:00).

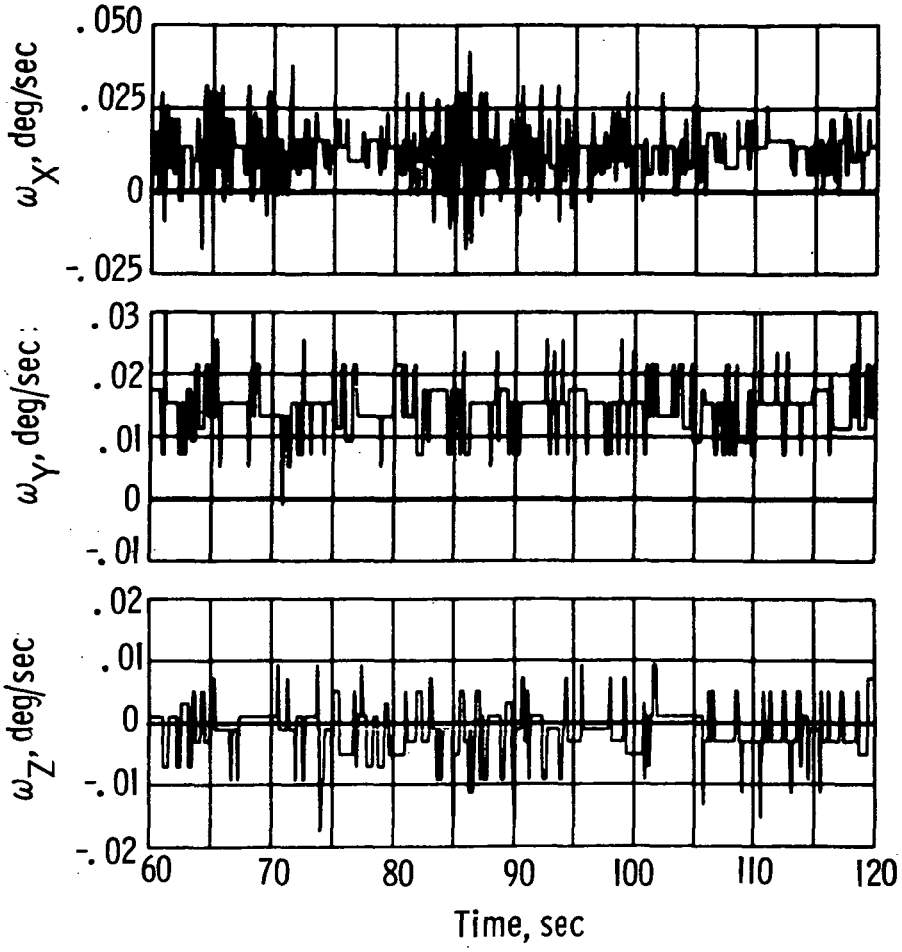

Figure 39.- Concluded.

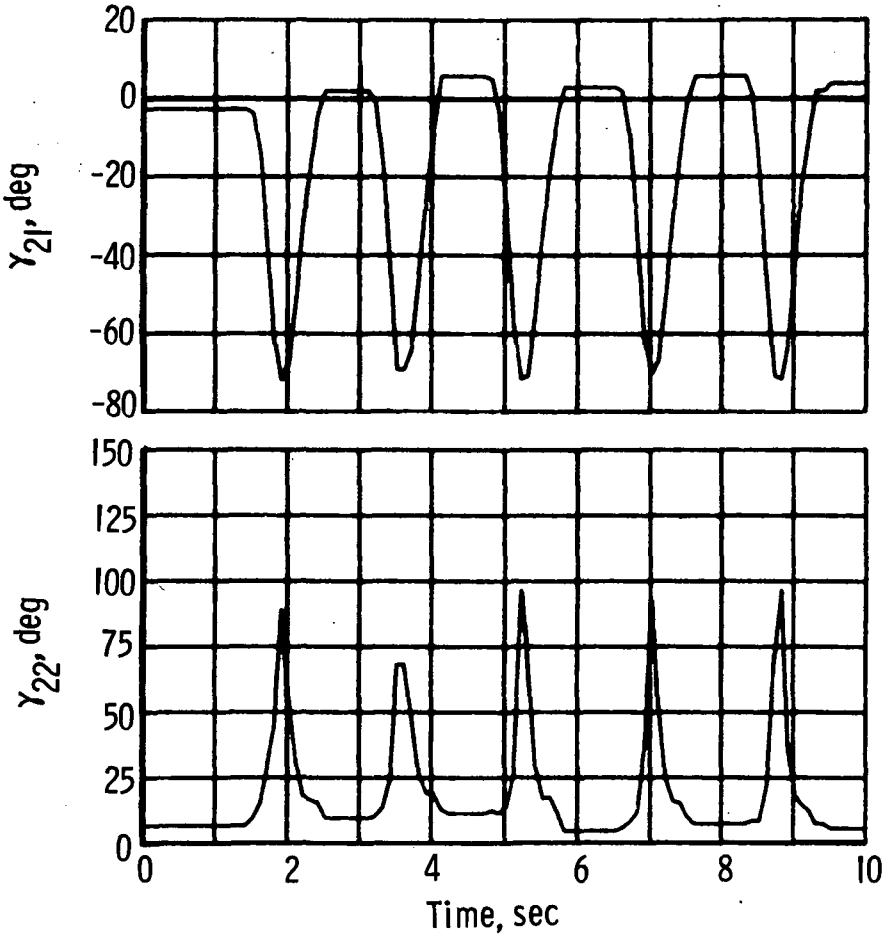

(a) Upper right arm (15:26:50).

Figure 40.- Gamma angles.

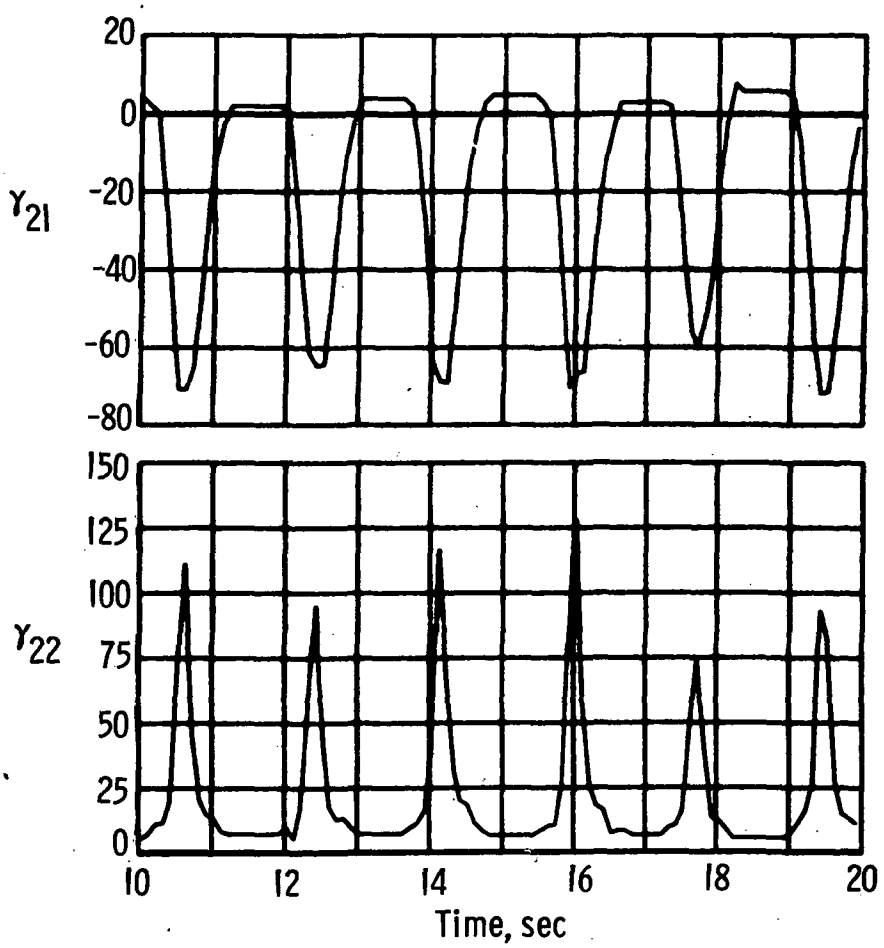

(a) Concluded.

Figure 40.- Continued.

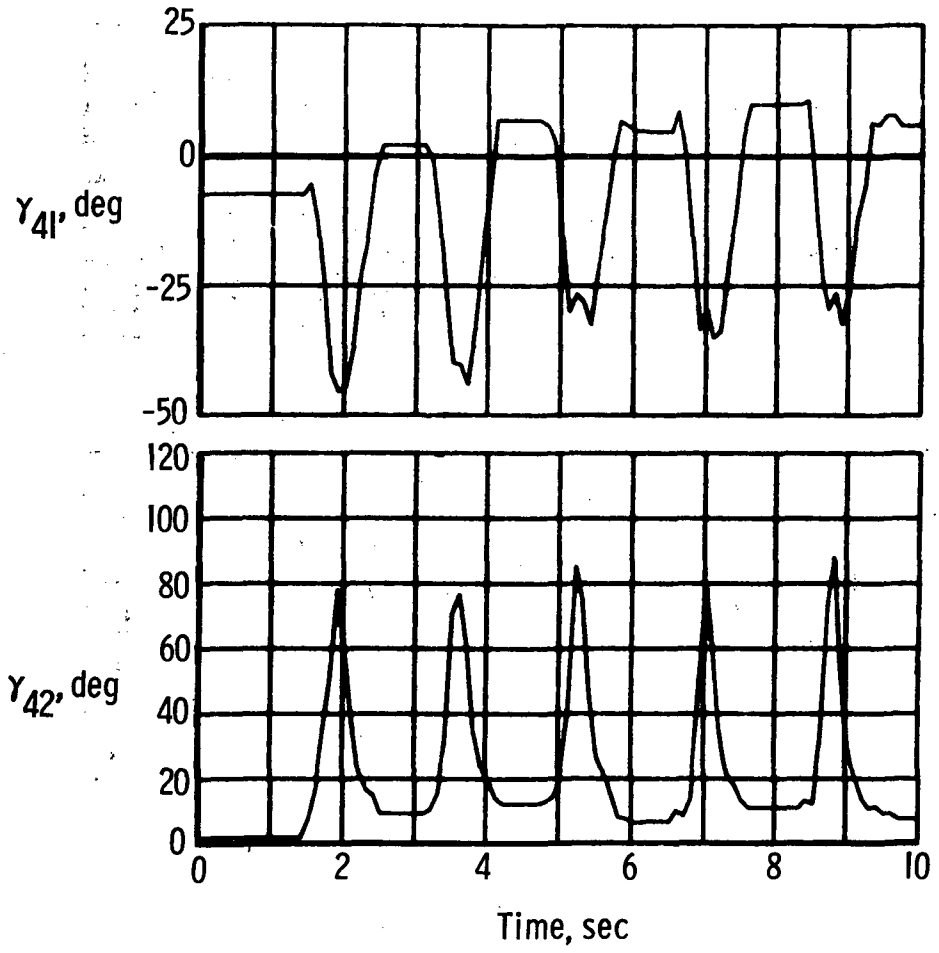

(b) Lower right arm (15:26:50).

Figure 40.- Continued.

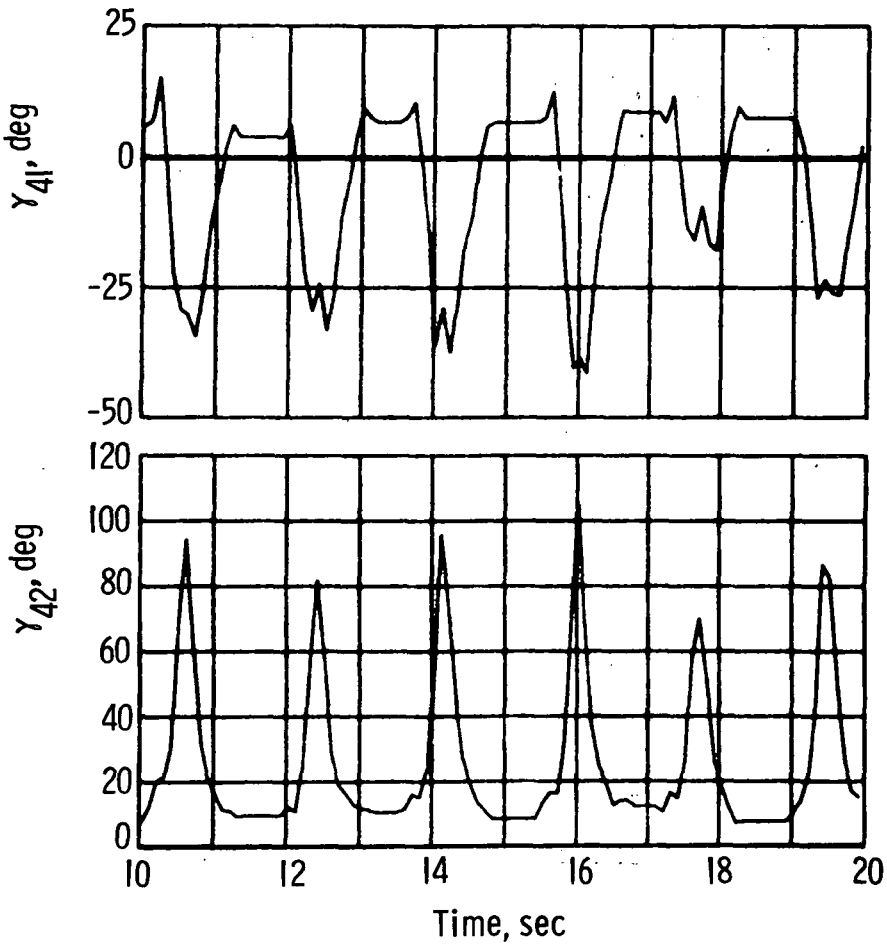

(b) Concluded.

Figure 40.- Continued.

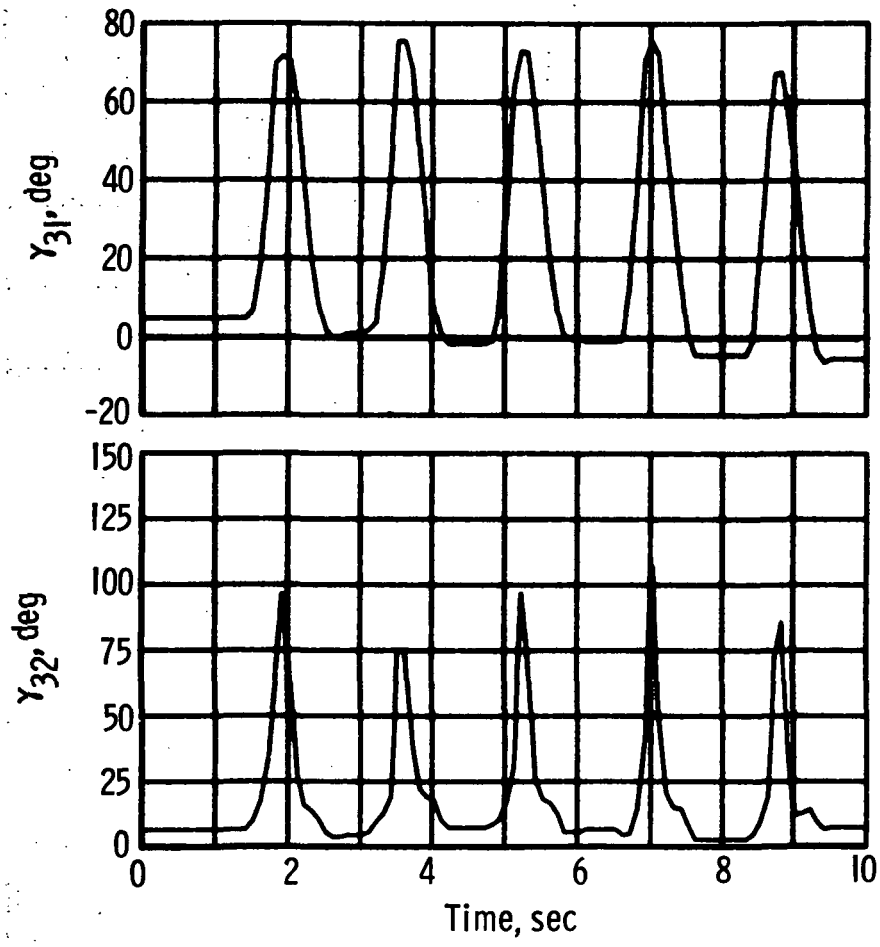

(c) Upper left arm (15:26:50).

Figure 40.- Continued.

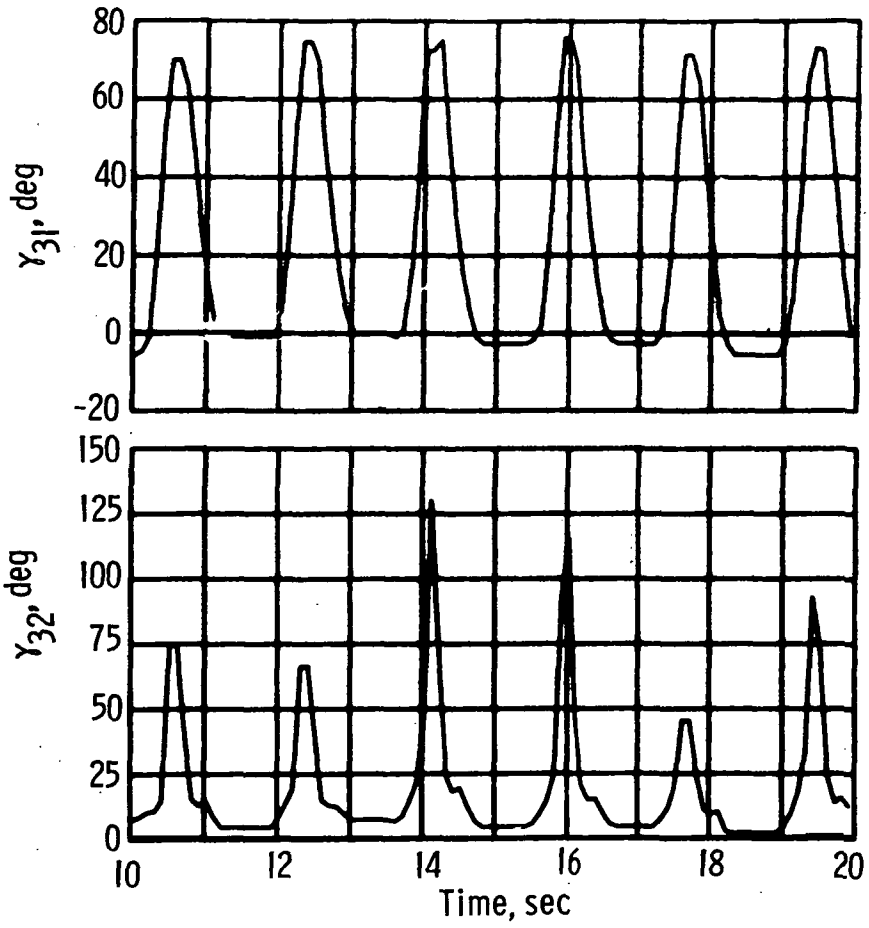

(c) Concluded.

Figure 40.- Continued.

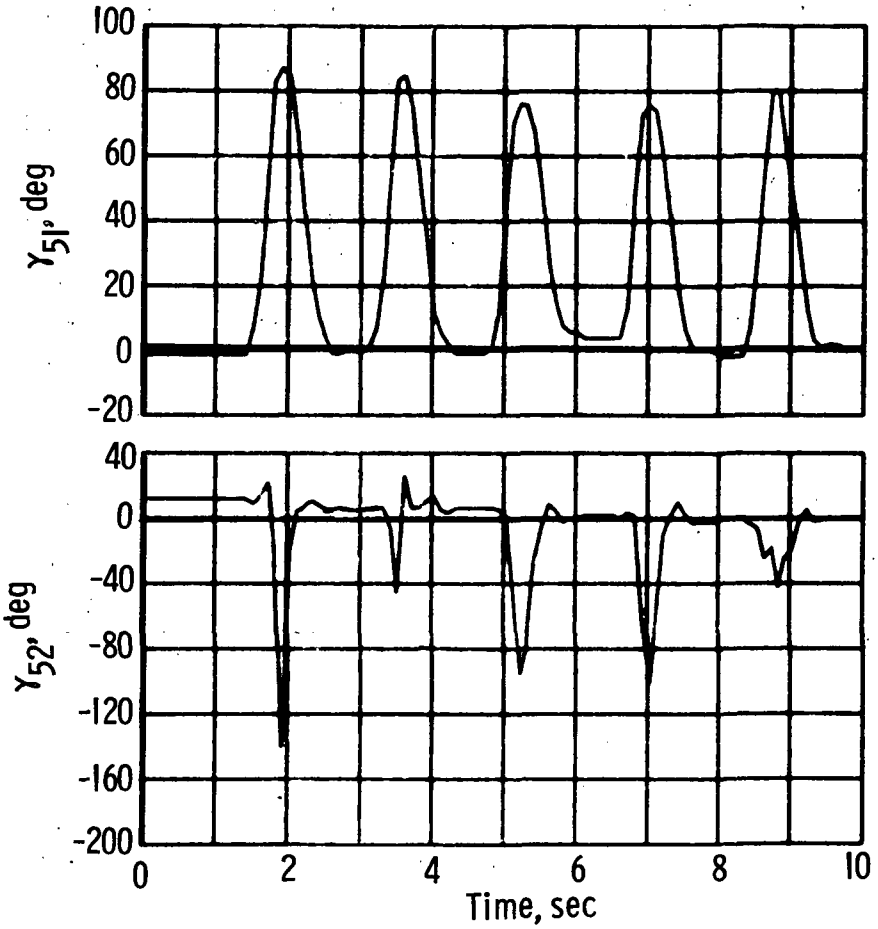

(d) Lower left arm (15:26:50).

Figure 40.- Continued.

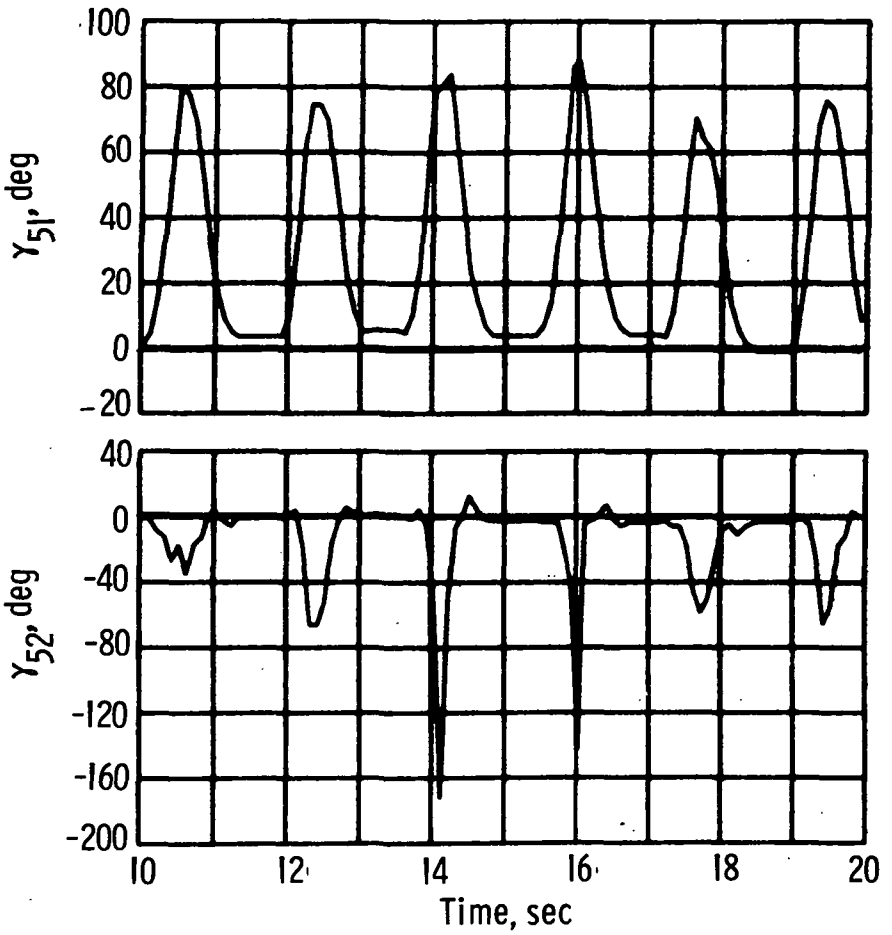

(d) Concluded.

Figure 40.- Concluded.

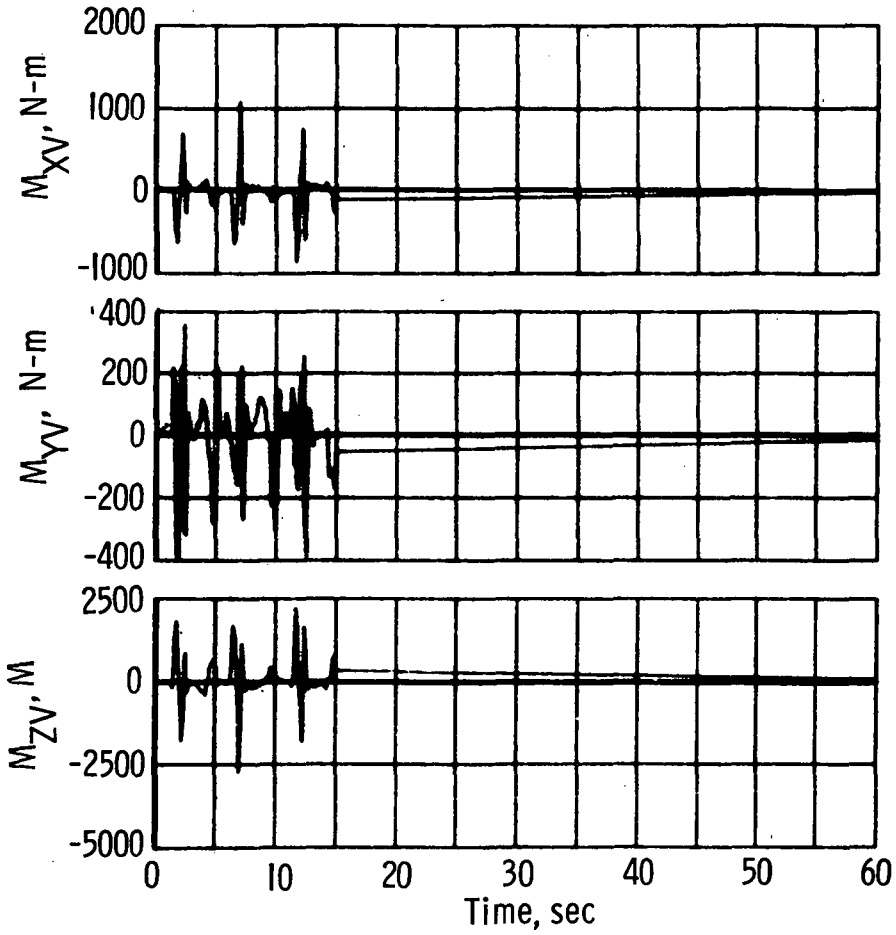

Figure 41.- Disturbance torques. Crouch and pushoff (15:28:00).

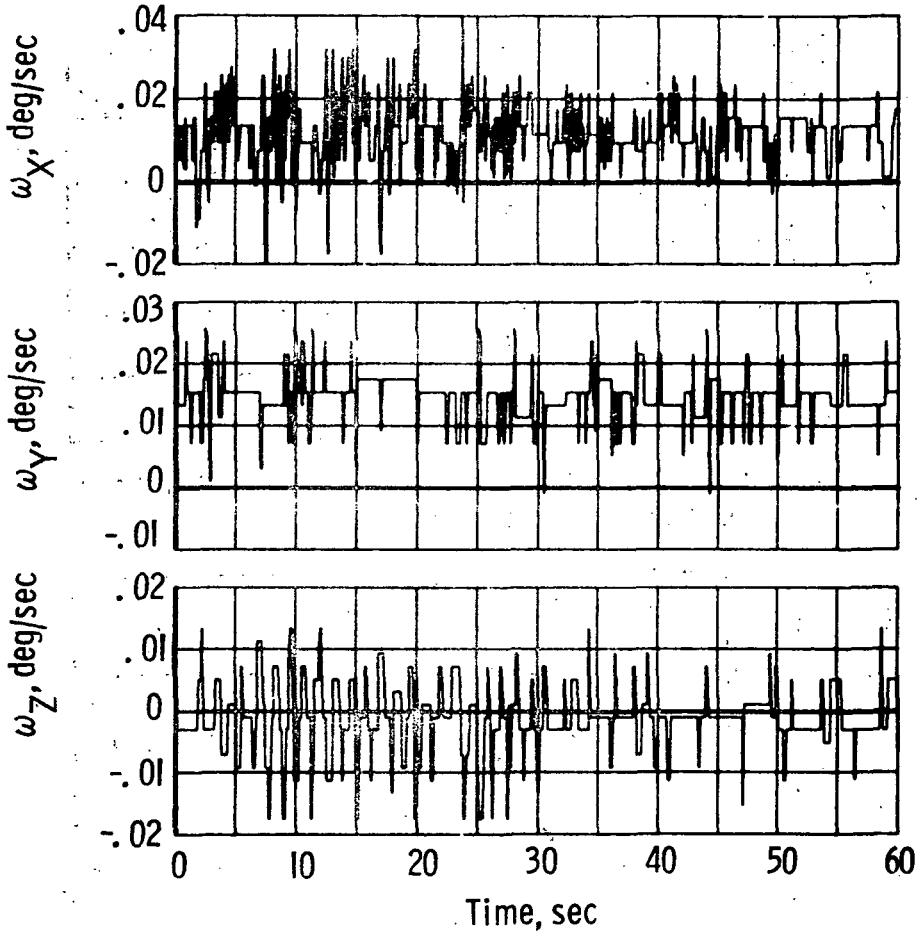

Figure 42.- Measured vehicle rates (15:28:00).

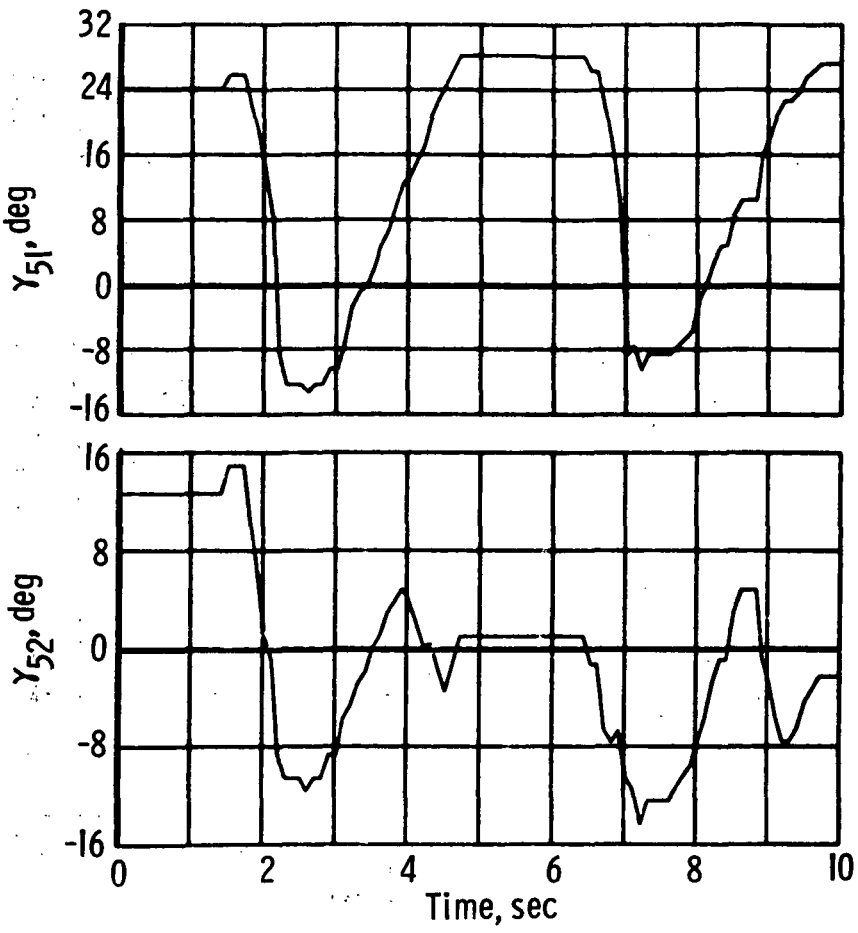

(a) Upper right leg (15:28:00).

Figure 43.- Gamma angles.

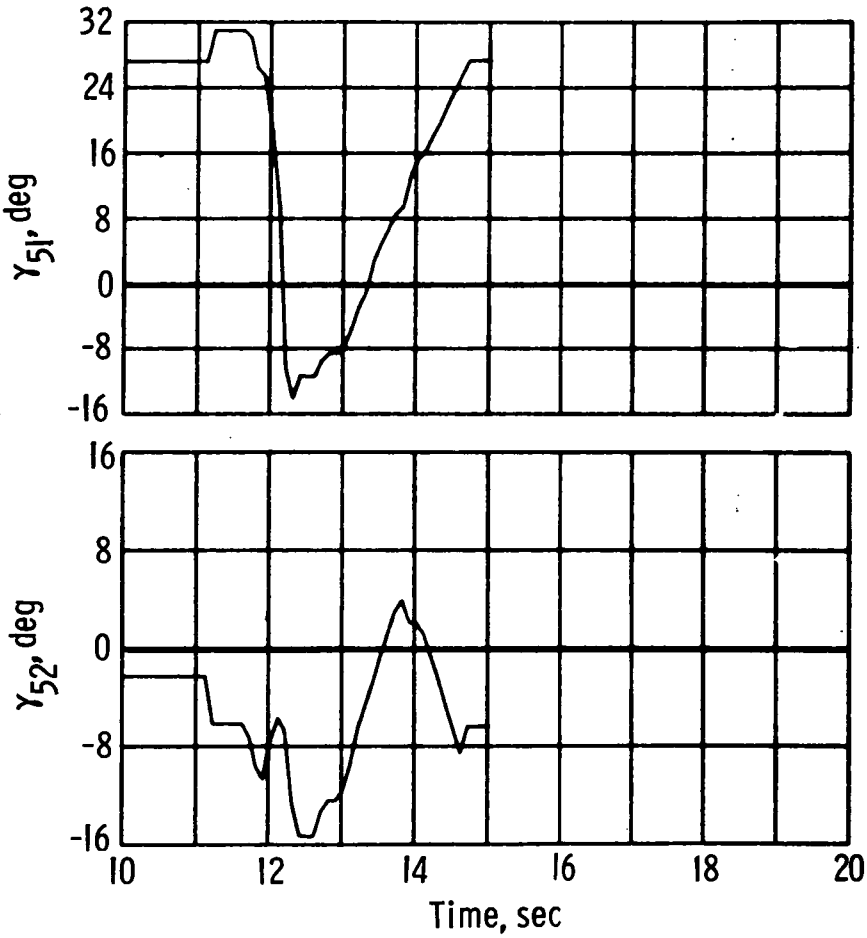

(a) Concluded.

Figure 43.- Continued.

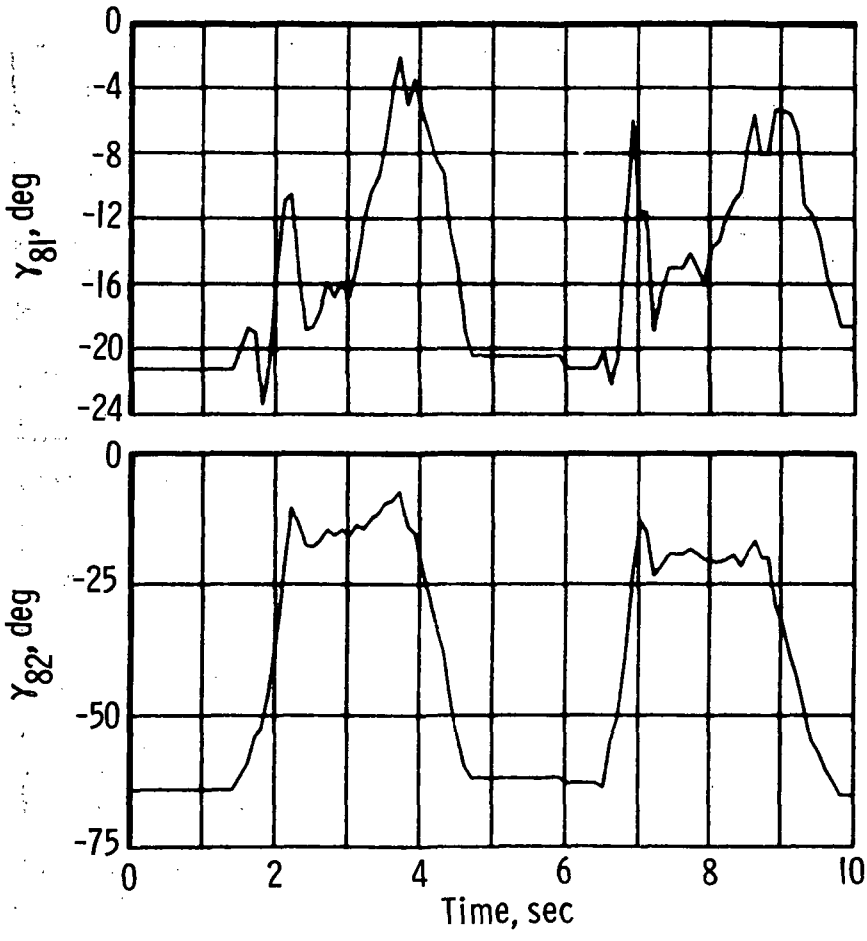

(b) Lower right leg (15:28:00).

Figure 43.- Continued.

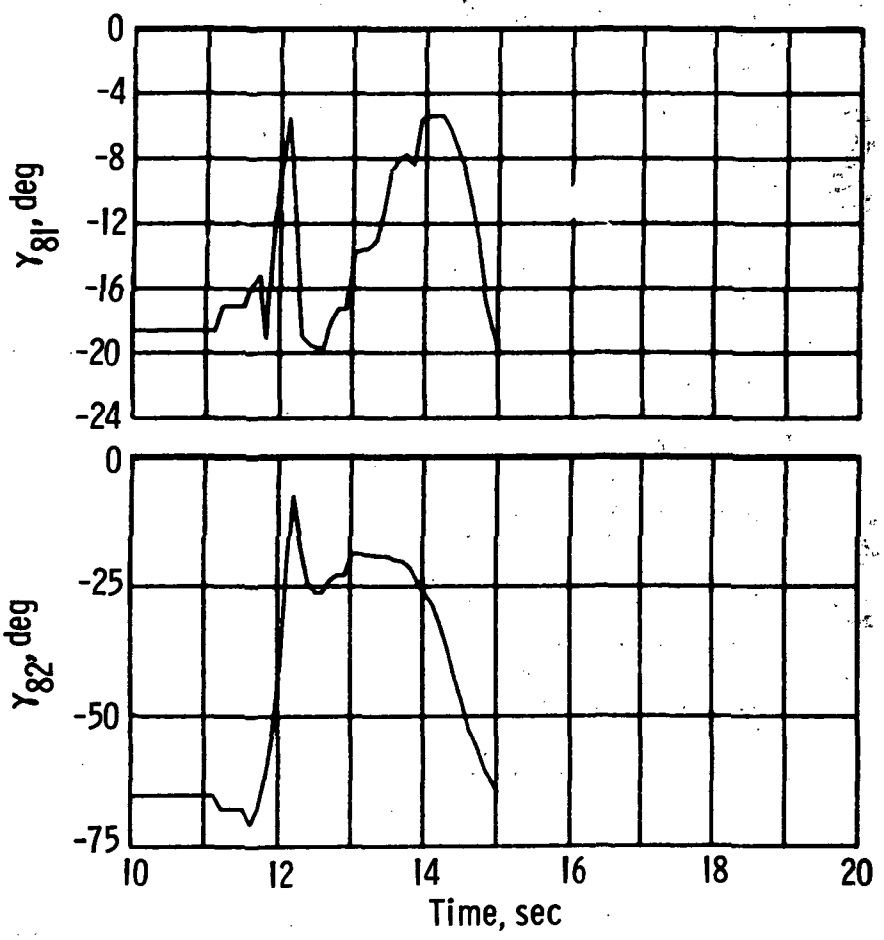

(b) Concluded.

Figure 43.- Continued.

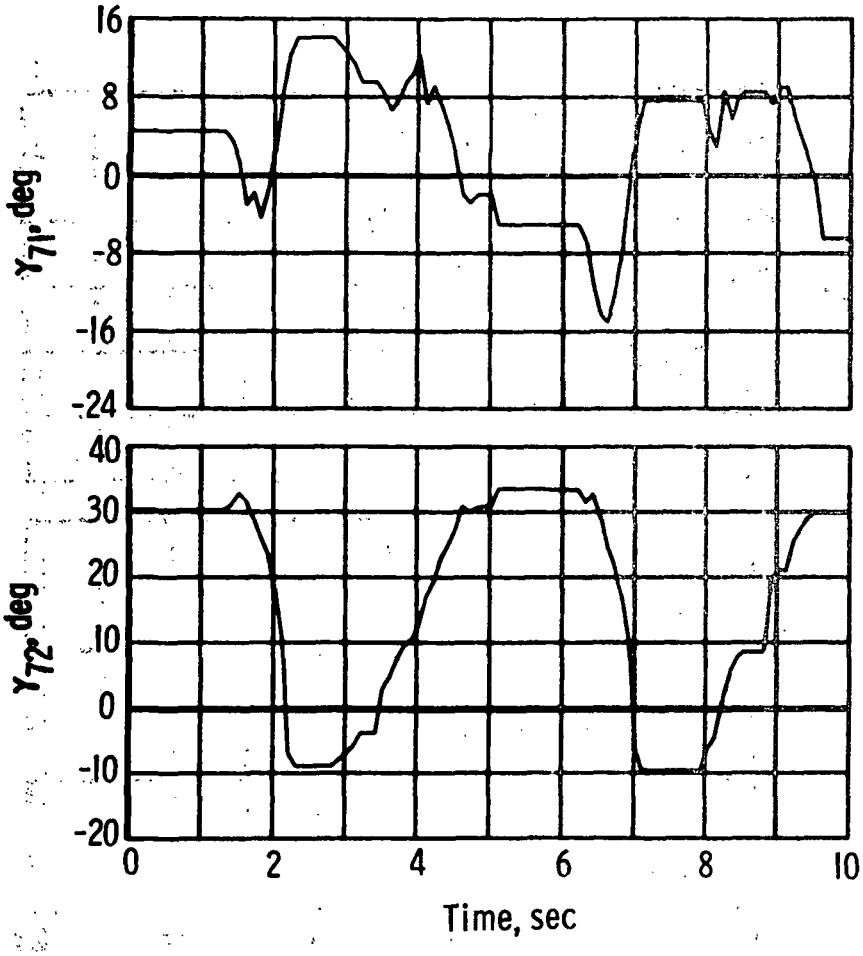

(c) Upper left leg (15:28:00).

Figure 43.– Continued.

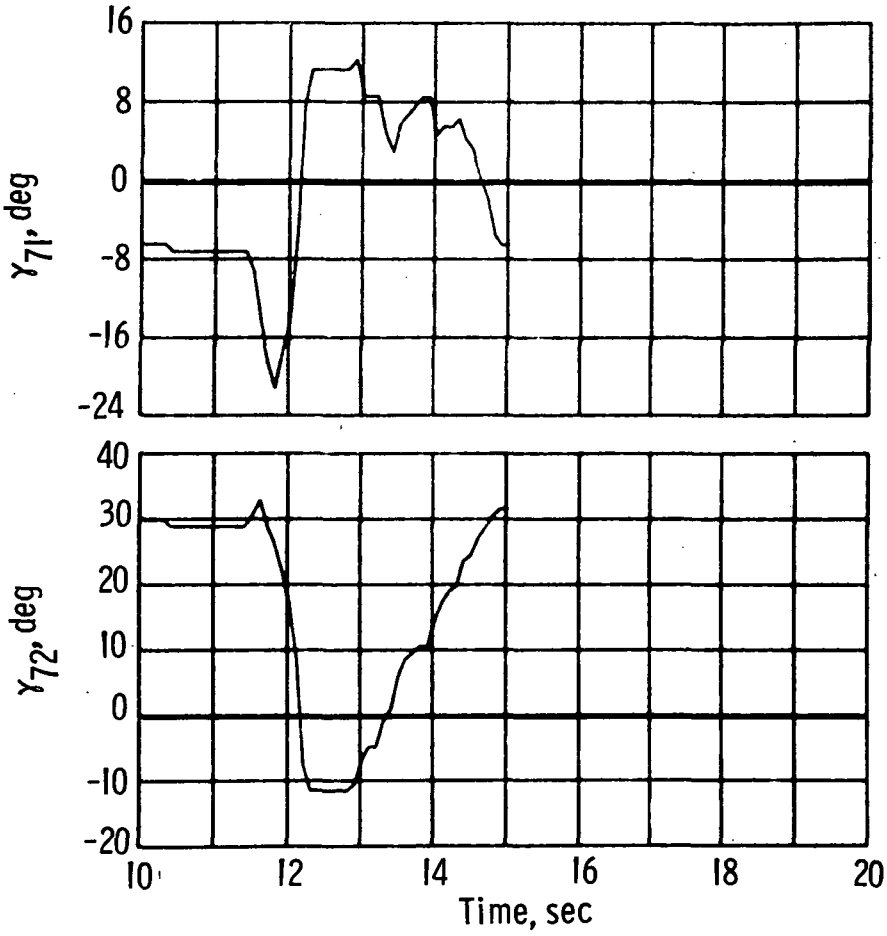

(c) Concluded.

Figure 43.- Continued.

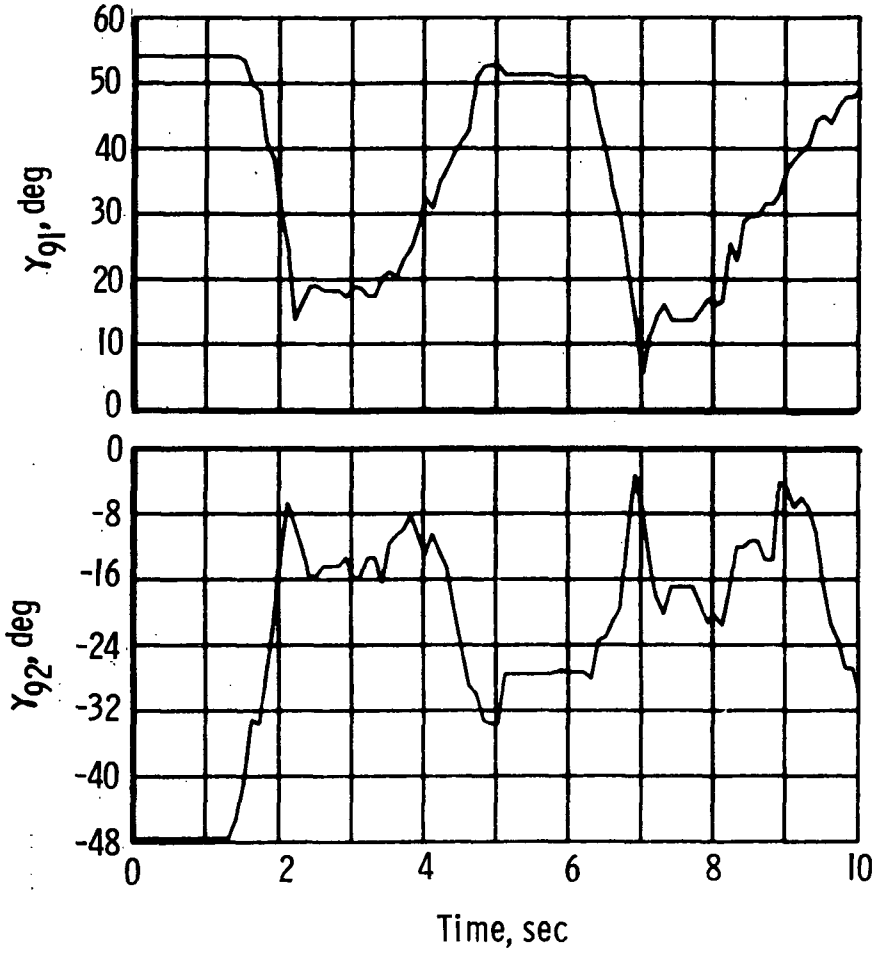

(d) Lower left leg (15:28:00).

Figure 43.- Continued.

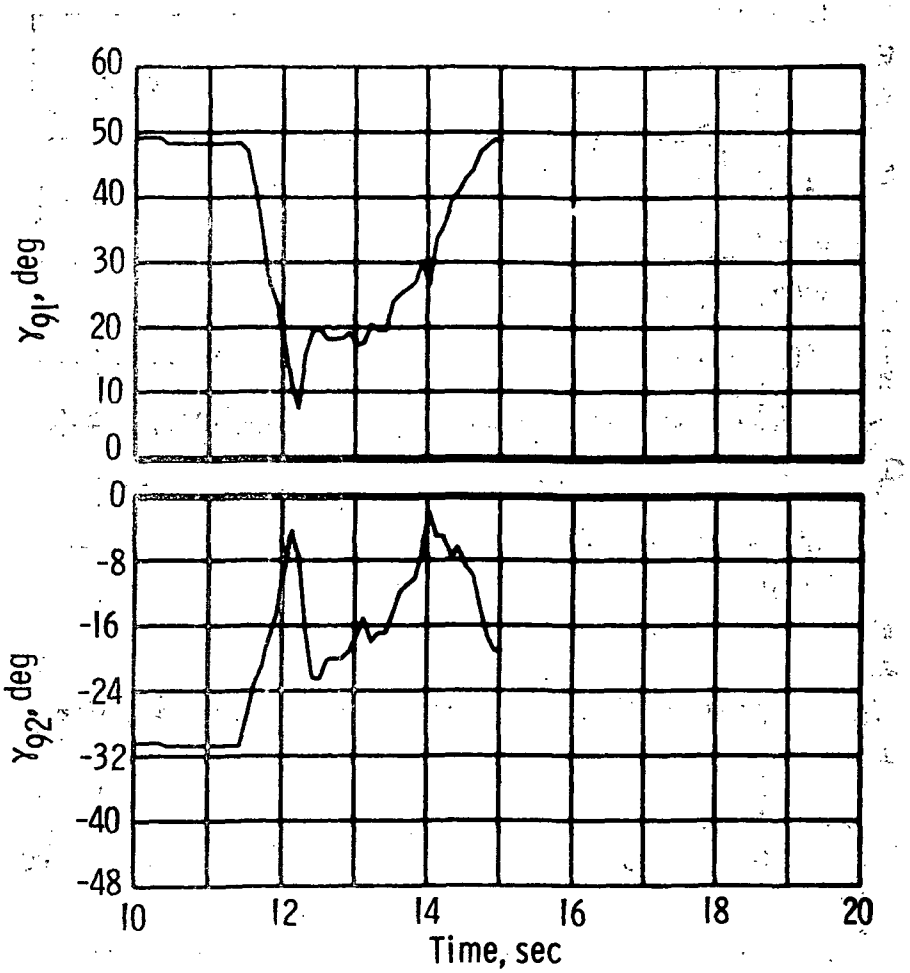

(d) Concluded.

Figure 43.- Concluded.

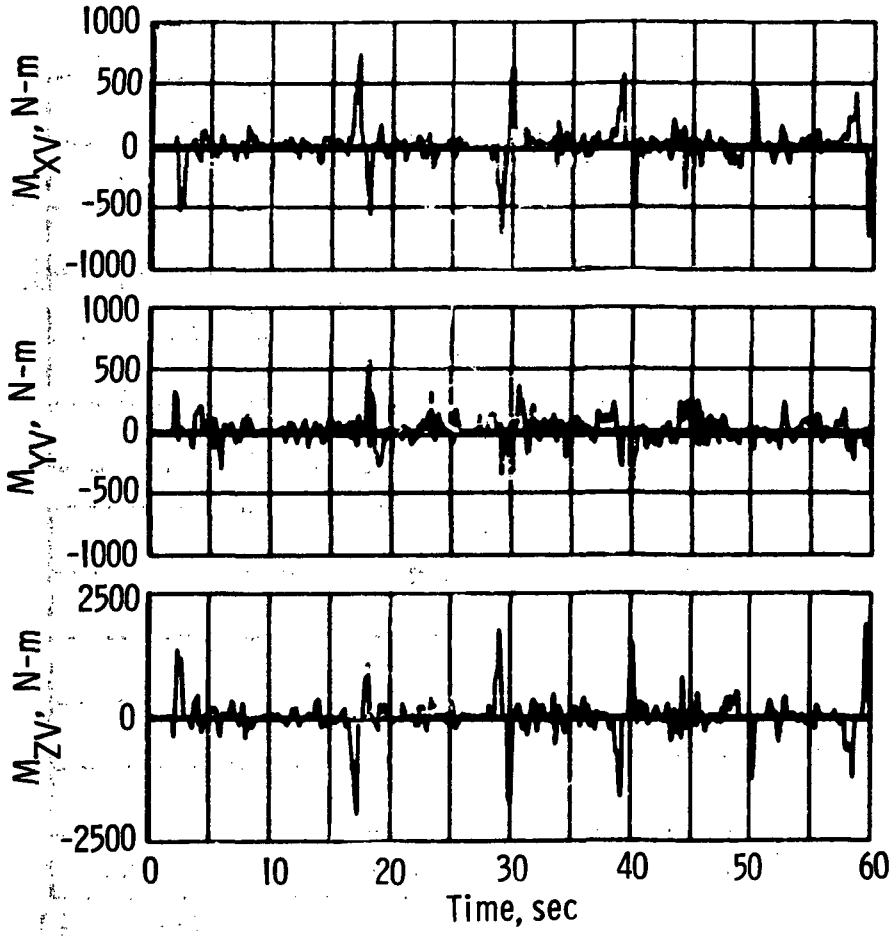

Figure 44.- Disturbance torques. Soaring (15:29:50).

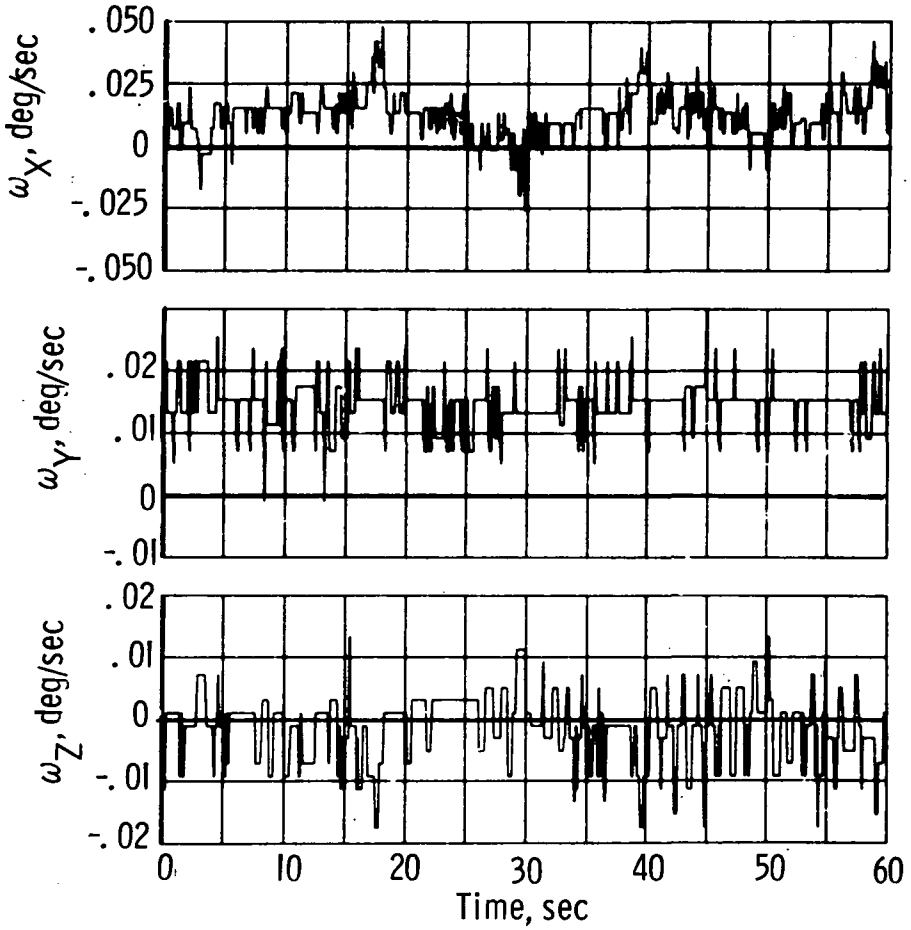

Figure 45.- Measured vehicle rates (15:29:50).

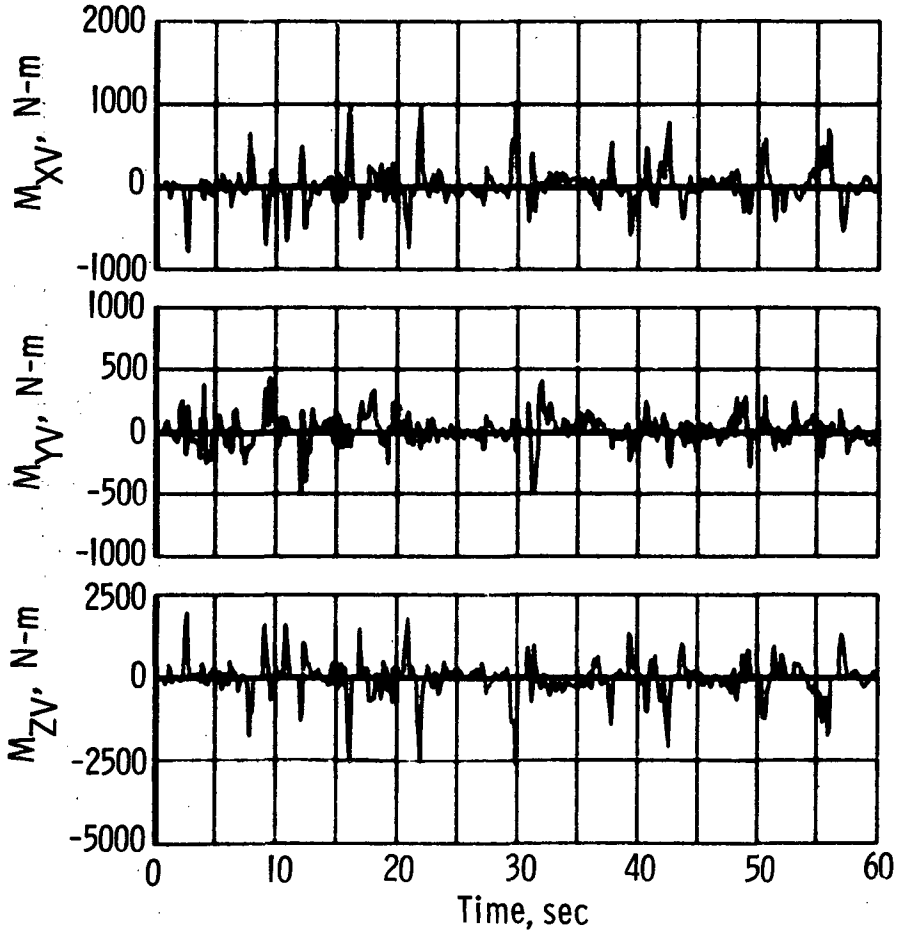

Figure 46.- Disturbance torques (15:33:45).

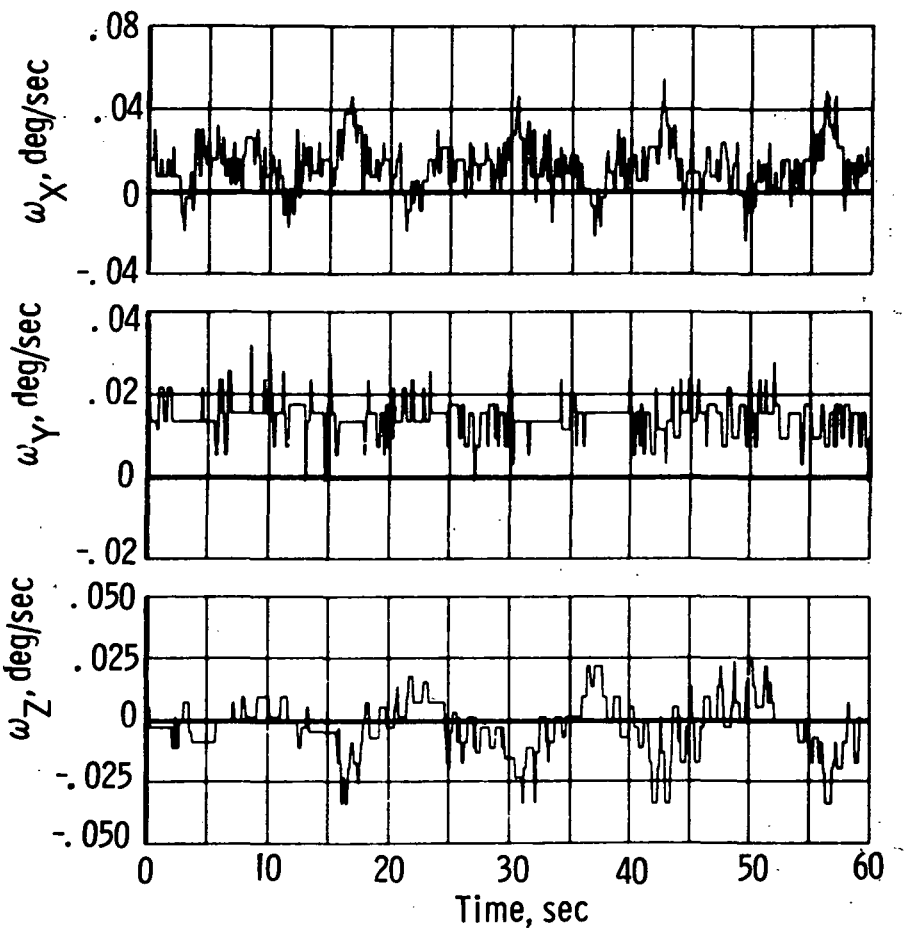

Figure 47.- Measured vehicle rates (15:33:45).

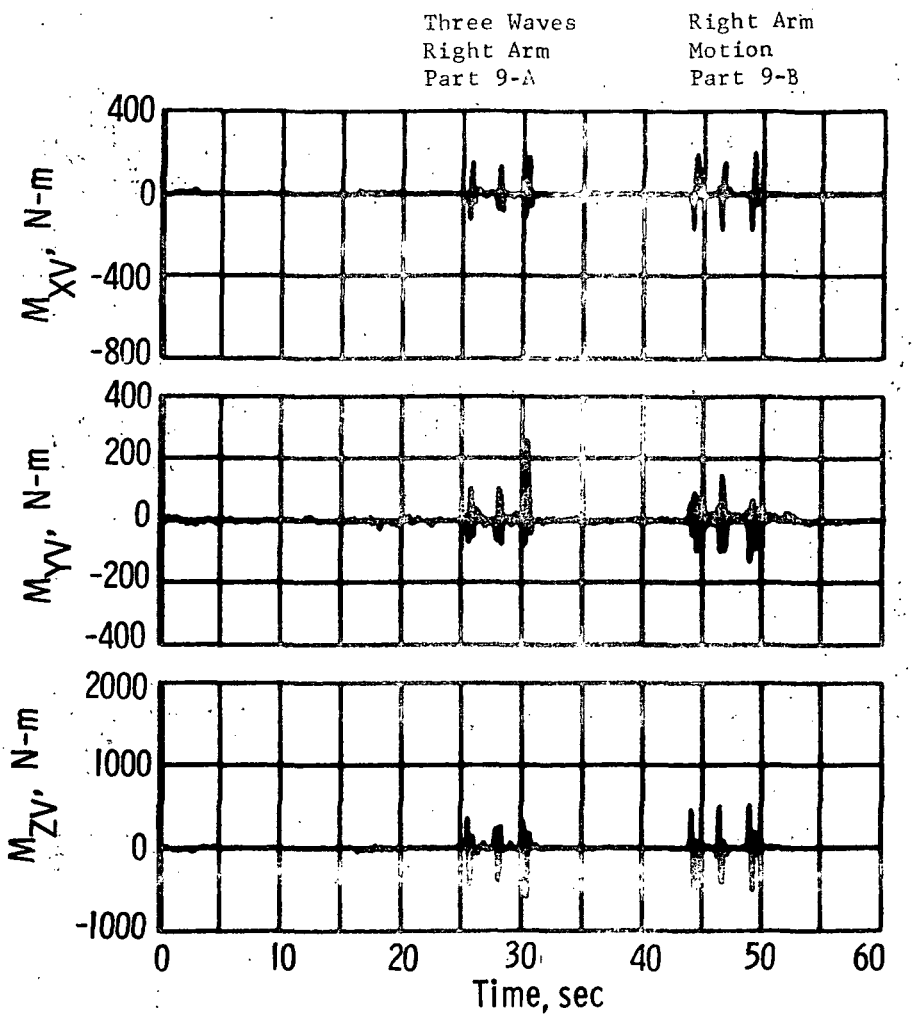

Figure 48.- Disturbance torques (15:55:00).

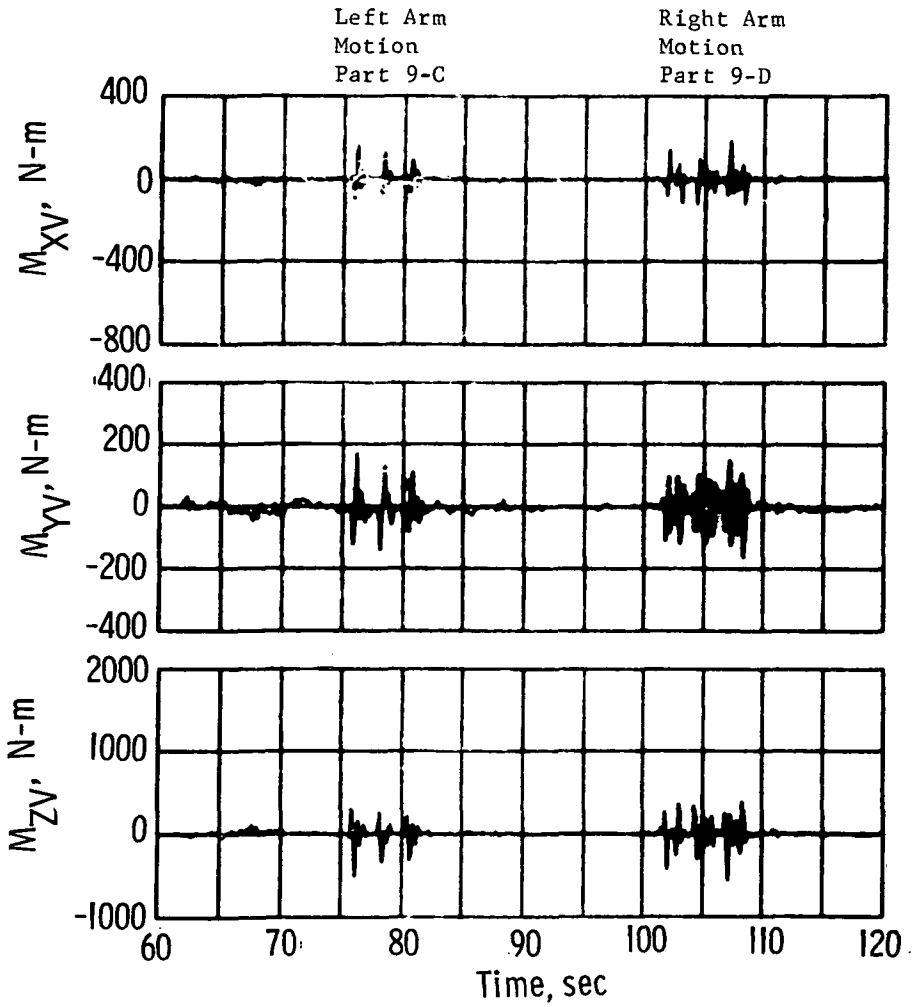

Figure 48.- Continued.

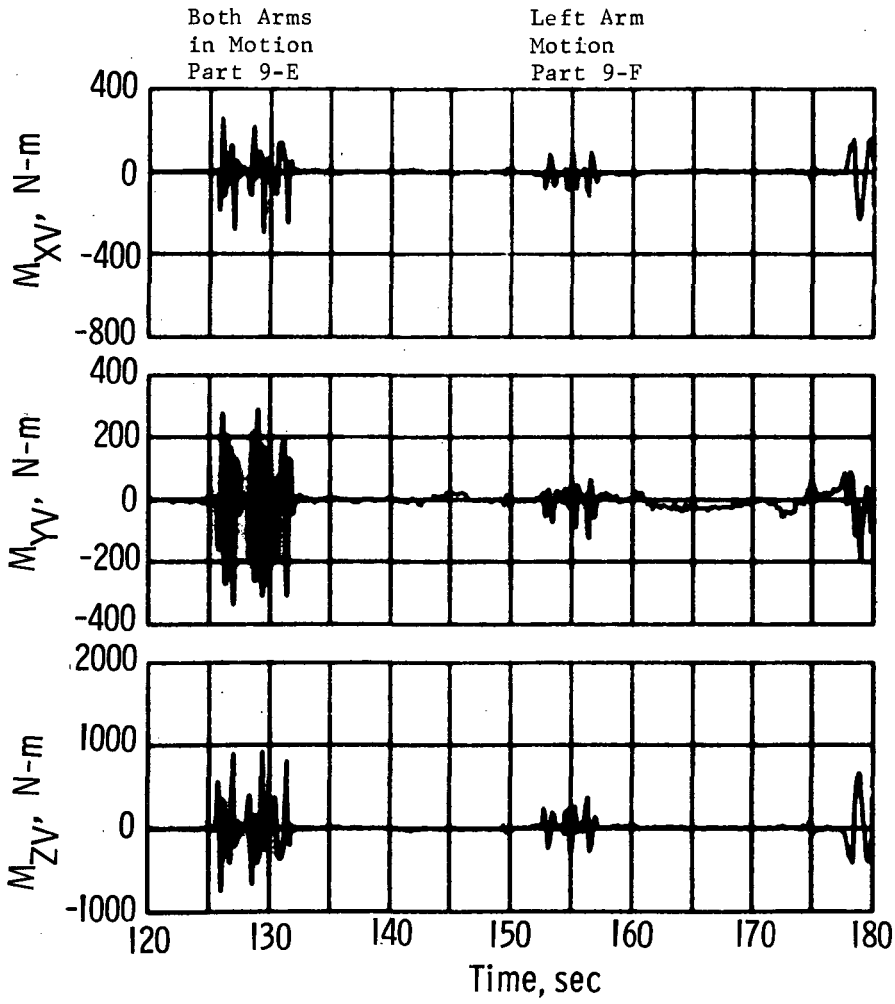

Figure 48.- Continued.

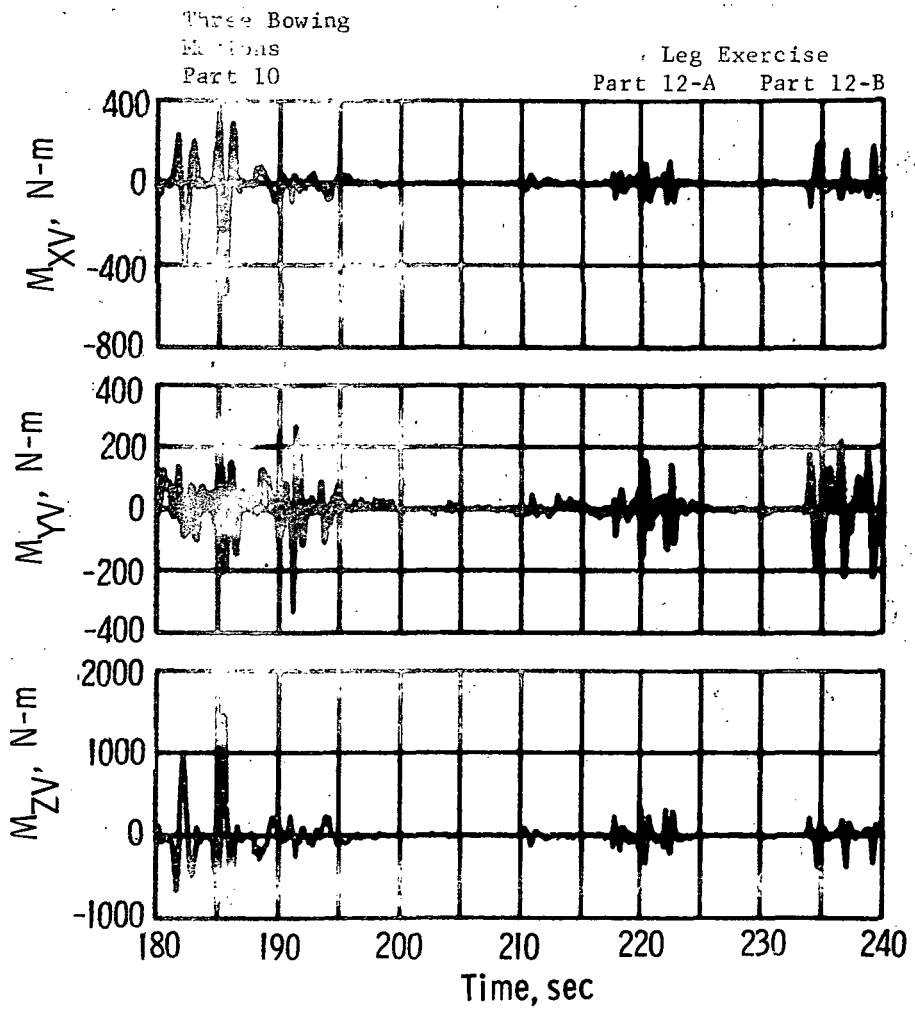

Figure 48.- Concluded.

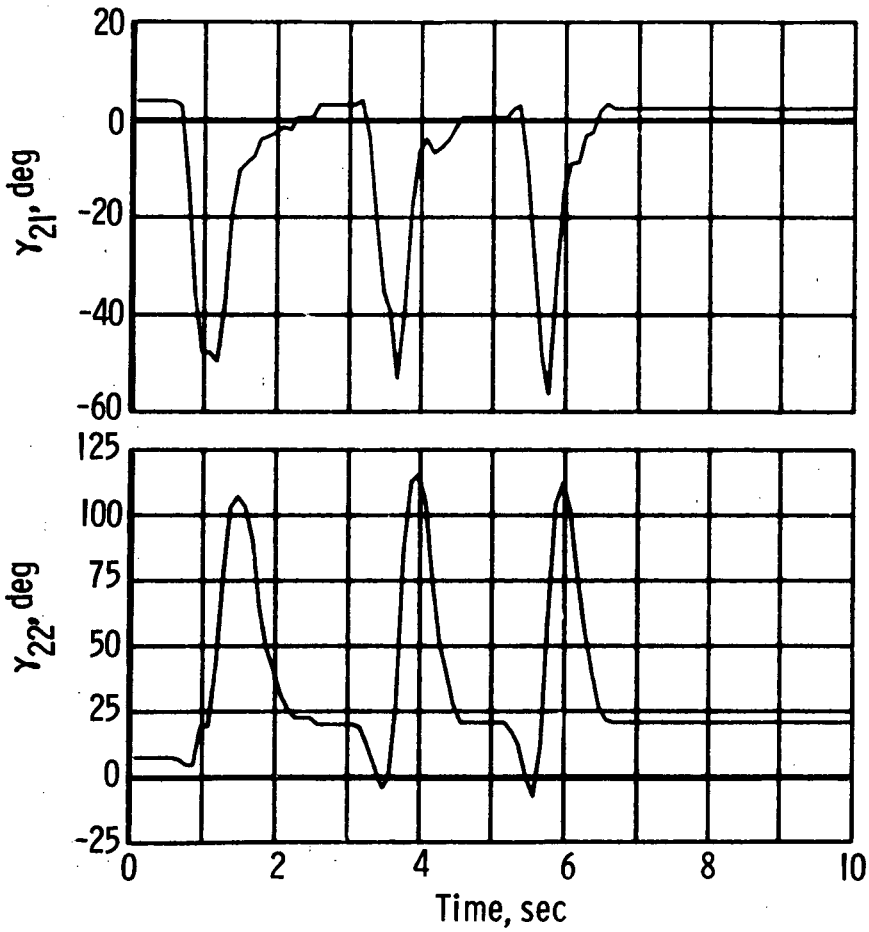

(a) Upper right arm (15:57:05).

Figure 49.- Gamma angles.

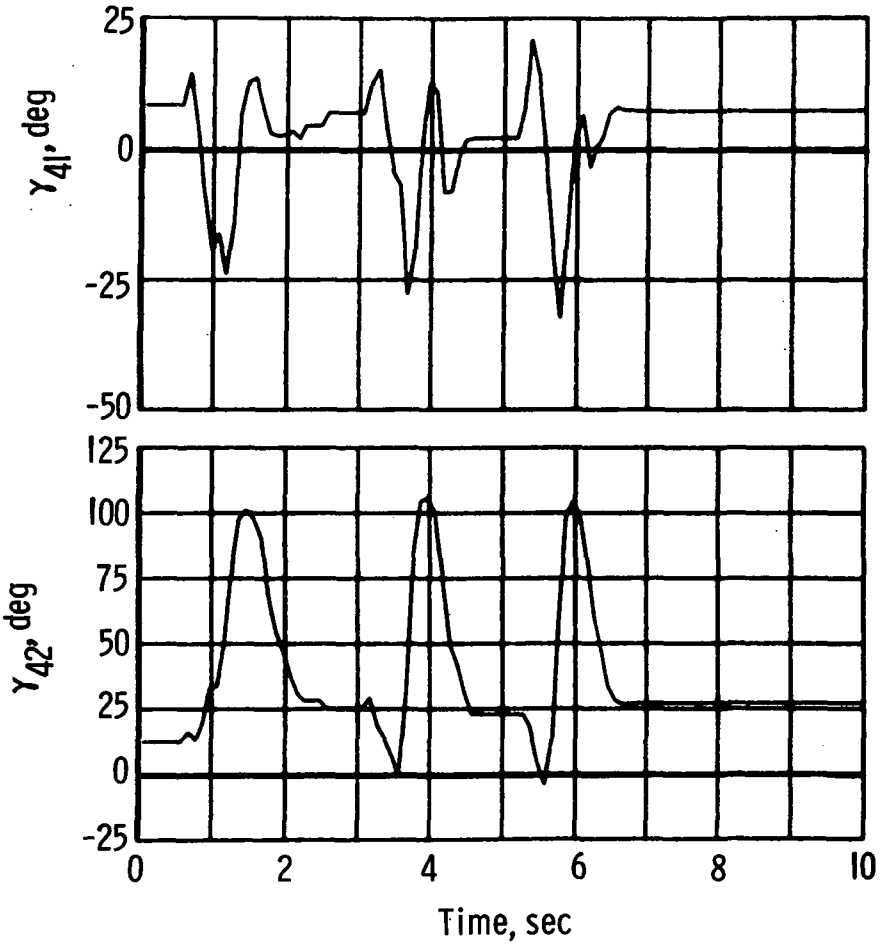

(b) Lower right arm (15:57:05).

Figure 49.- Continued.

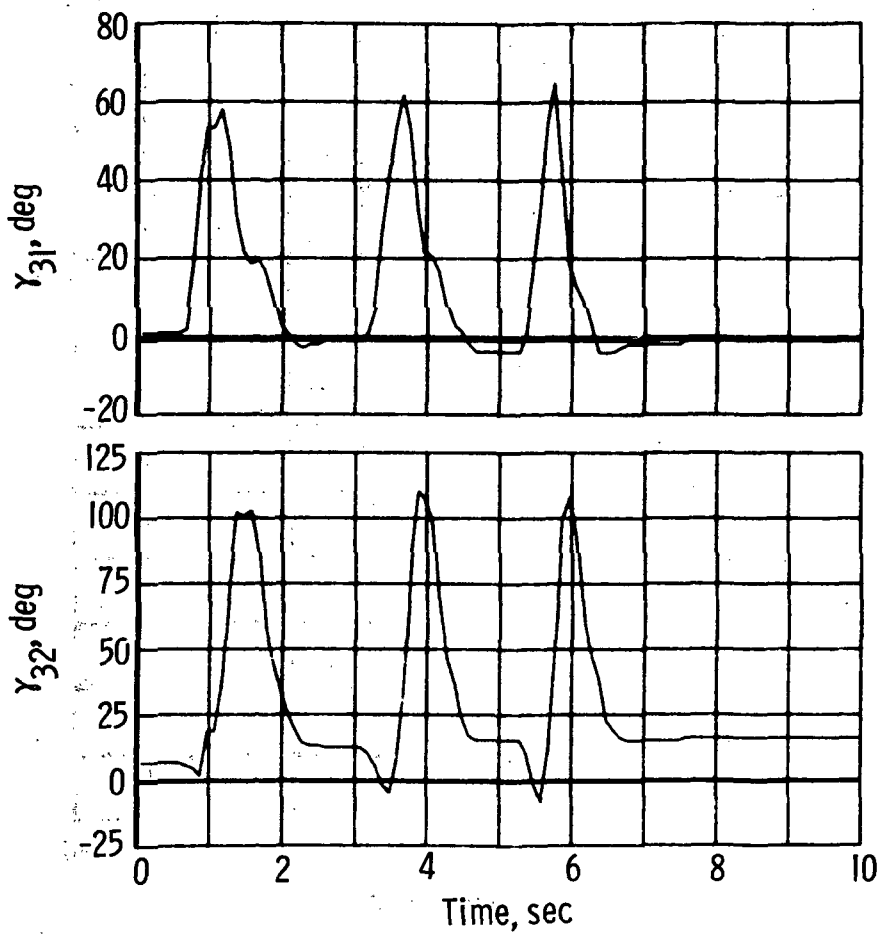

(c) Upper left arm (15:57:05).

Figure 49.- Continued.

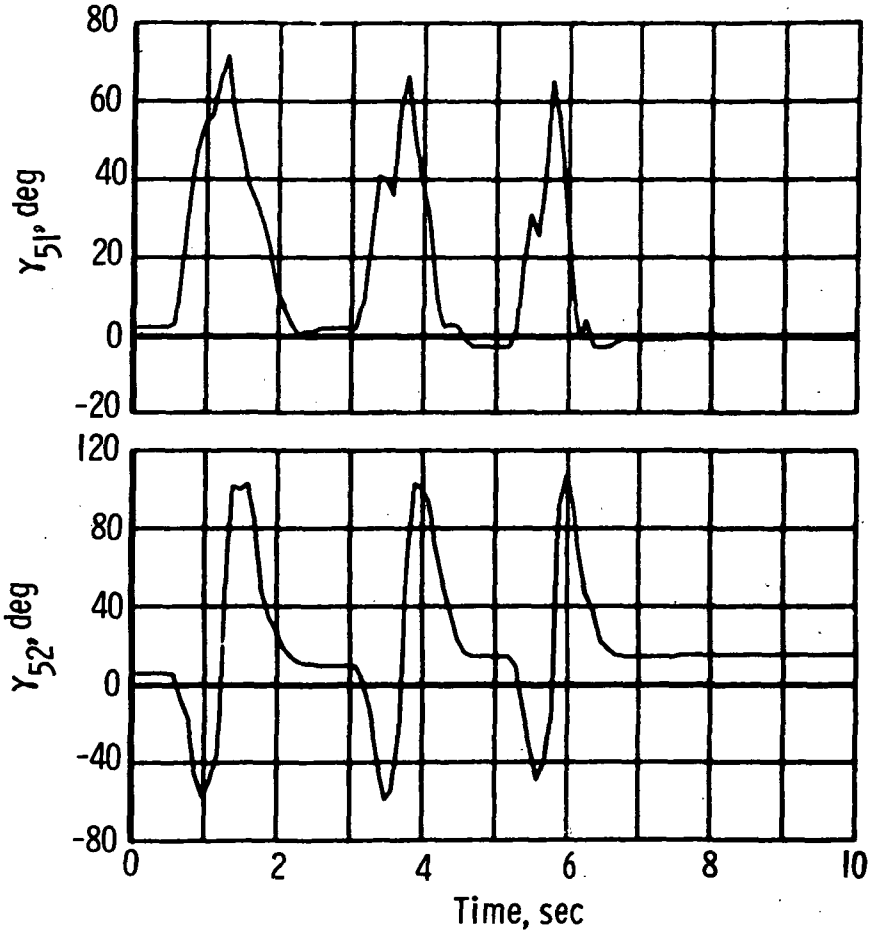

(d) Lower left arm (15:57:05).

Figure 49.- Concluded.

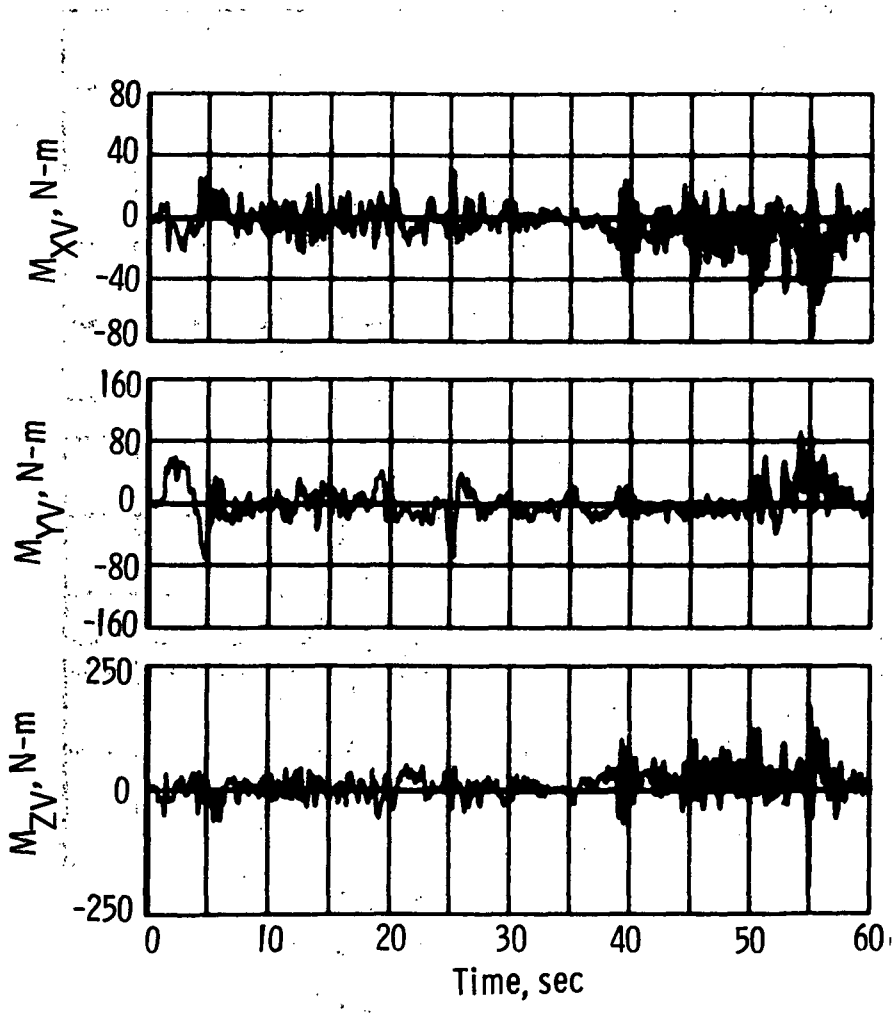

Figure 50.- Disturbance torques. Console operations (16:10:00).

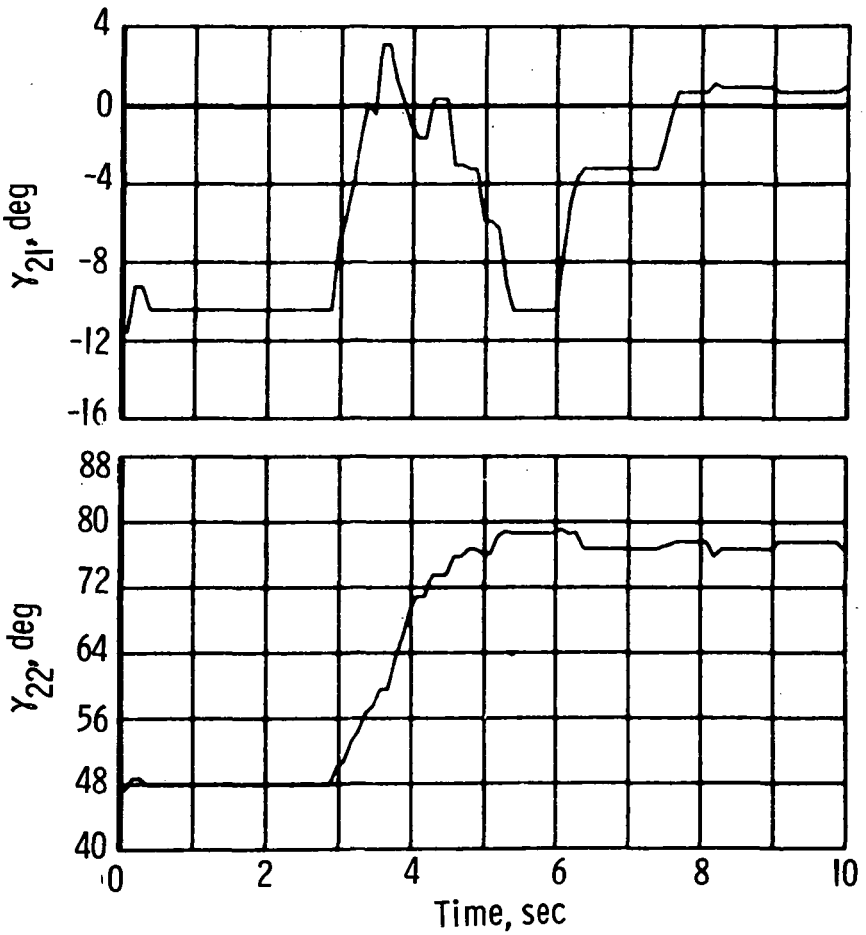

(a) Upper right arm (16:10:00).

Figure 51.- Gamma angles.

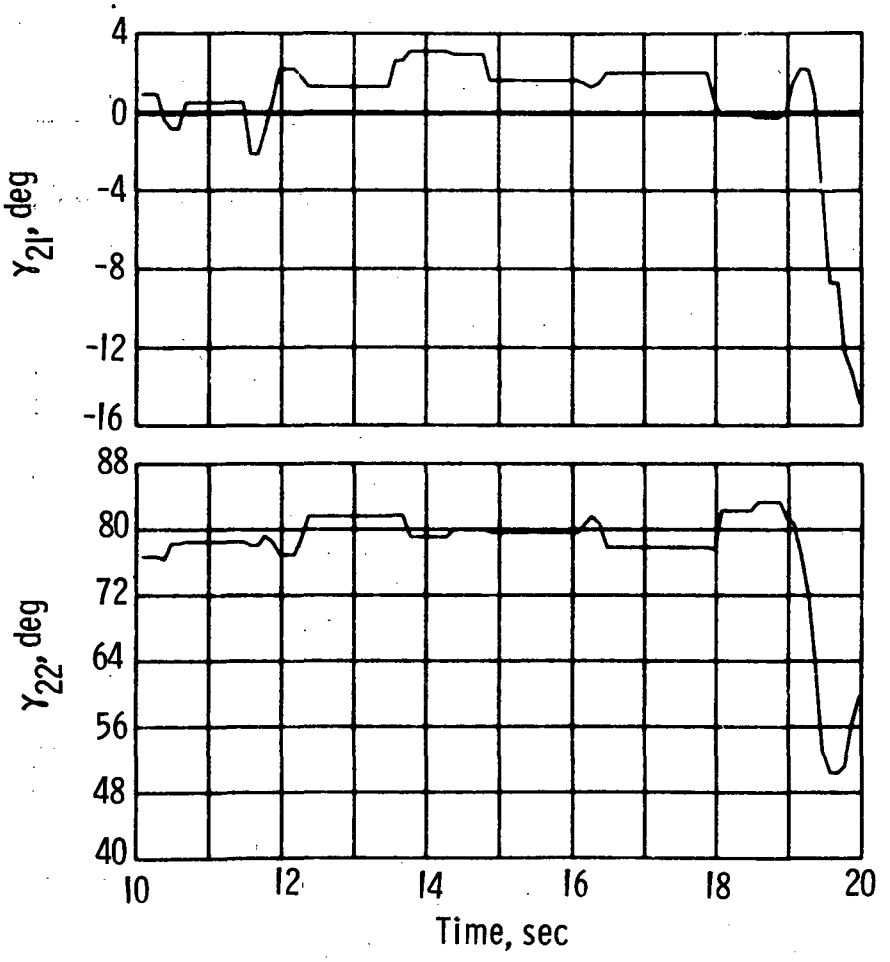

(a) Concluded.

Figure 51.- Continued.

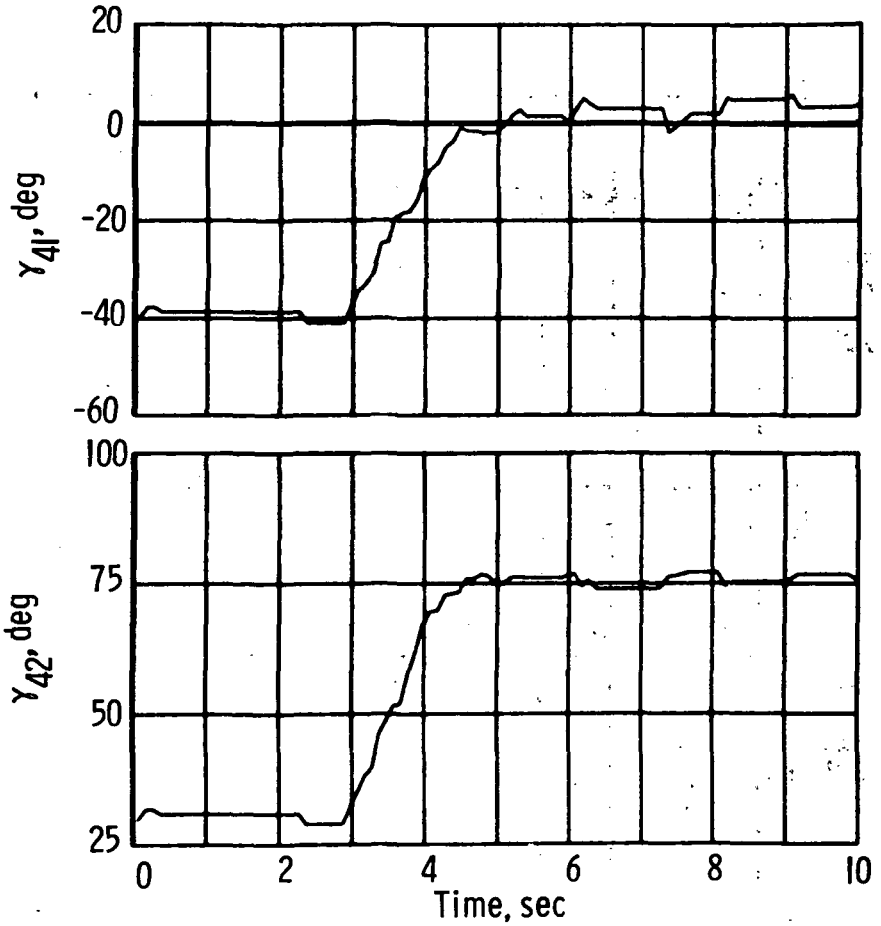

(b) Lower right arm (16:10:00).

Figure 51.- Continued.

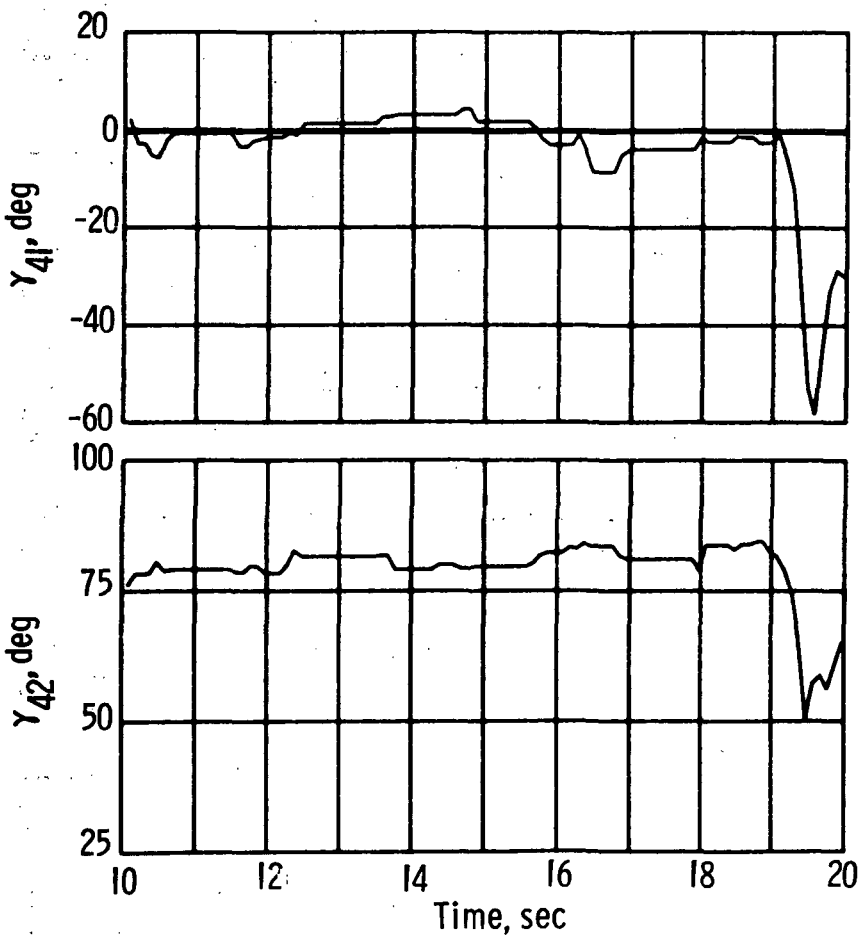

(b) Concluded.

Figure 51.- Continued.

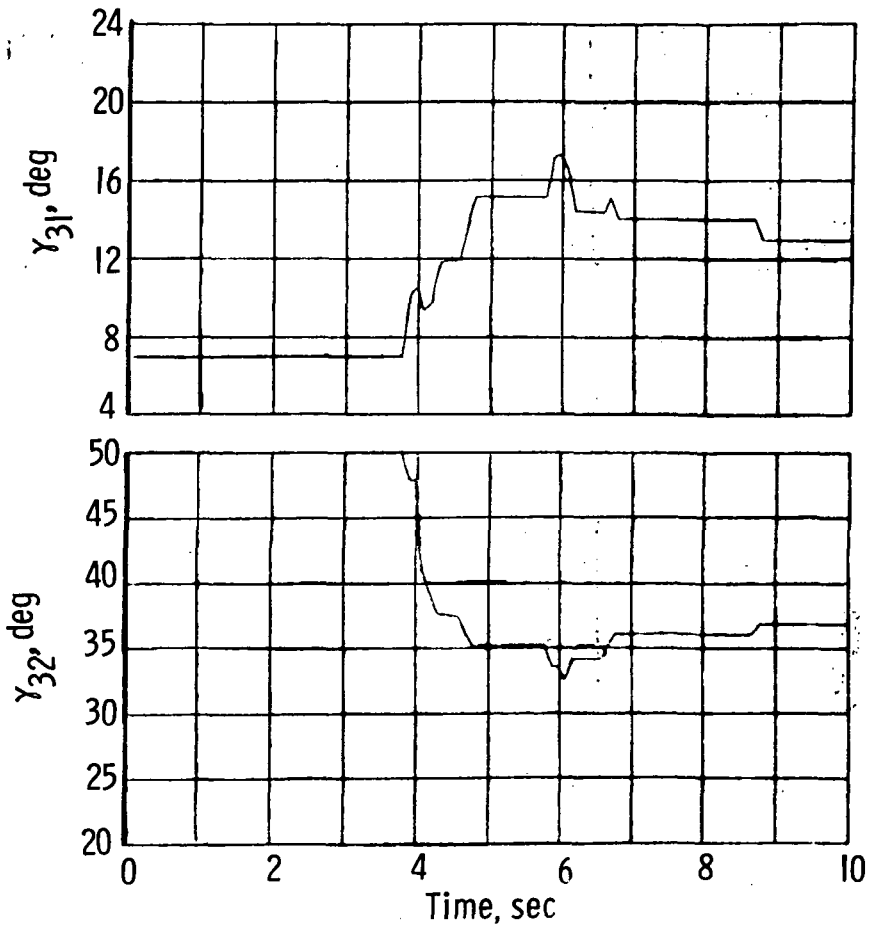

(c) Upper left arm (16:10:00).

Figure 51.- Continued.

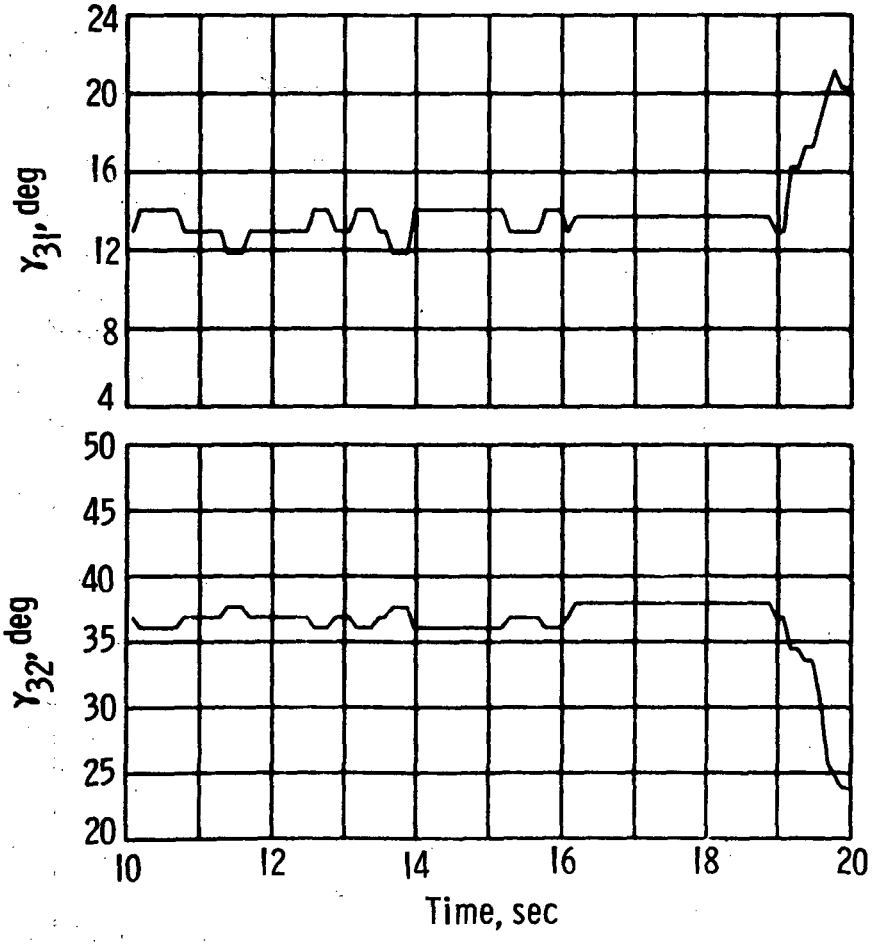

(c) Concluded.

Figure 51.- Continued.

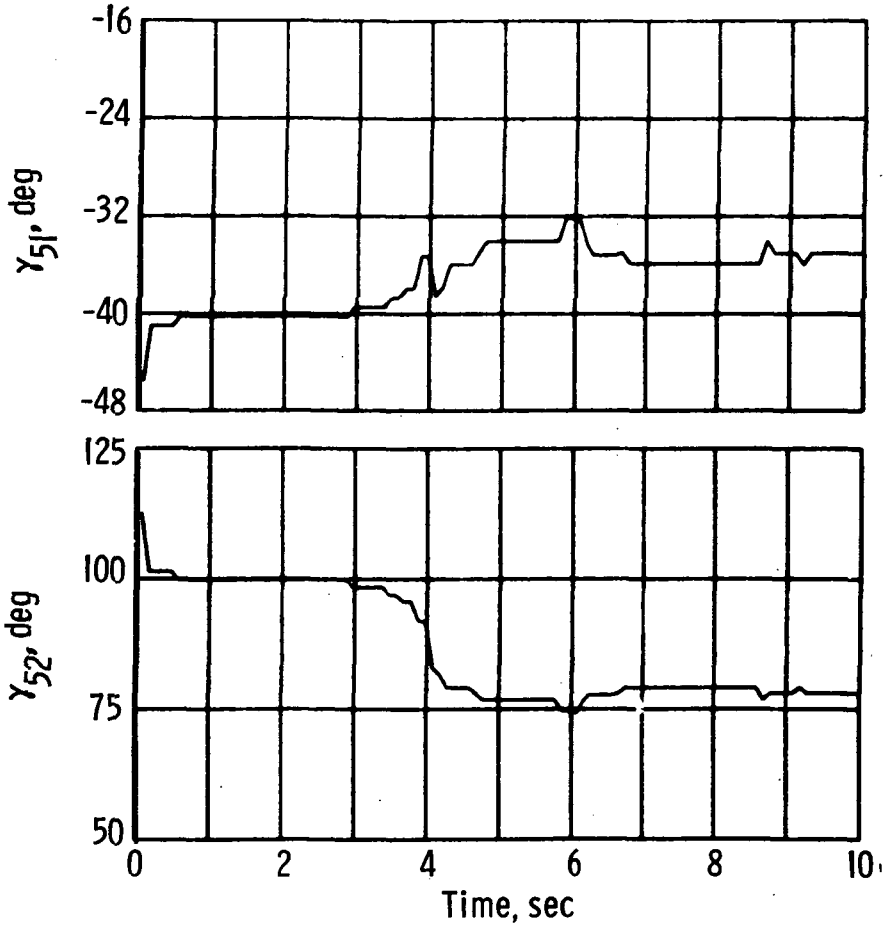

(d) Lower left arm (16:10:00).

Figure 51.- Continued.

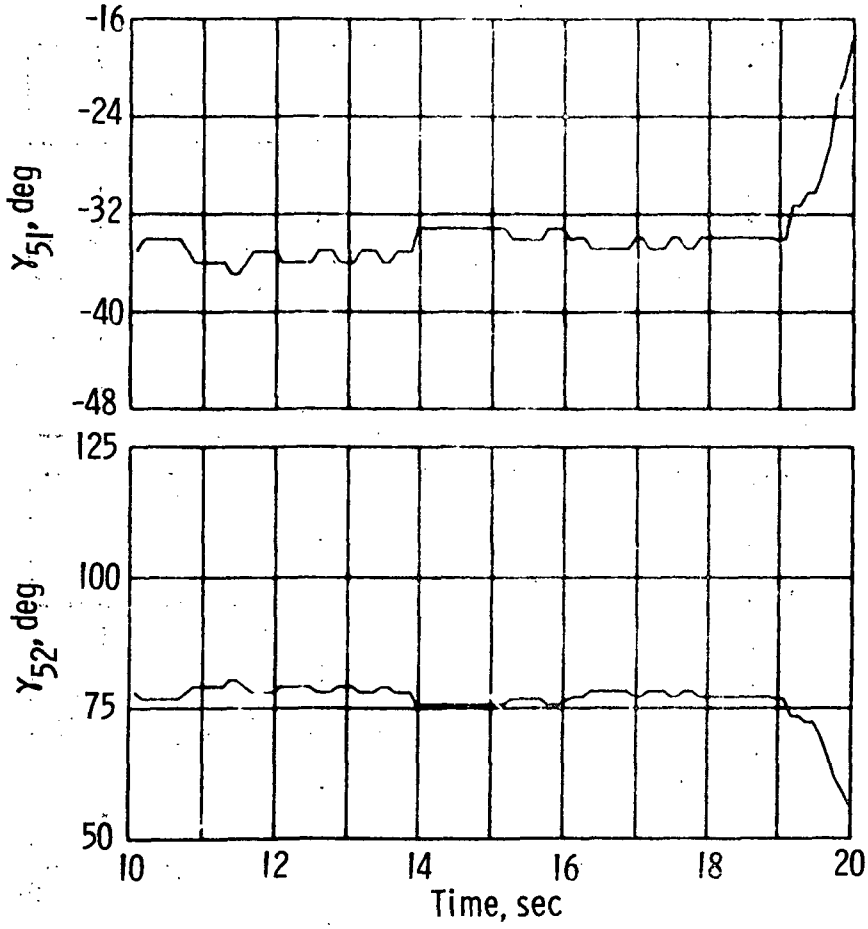

(d) Concluded.

Figure 51.- Concluded.

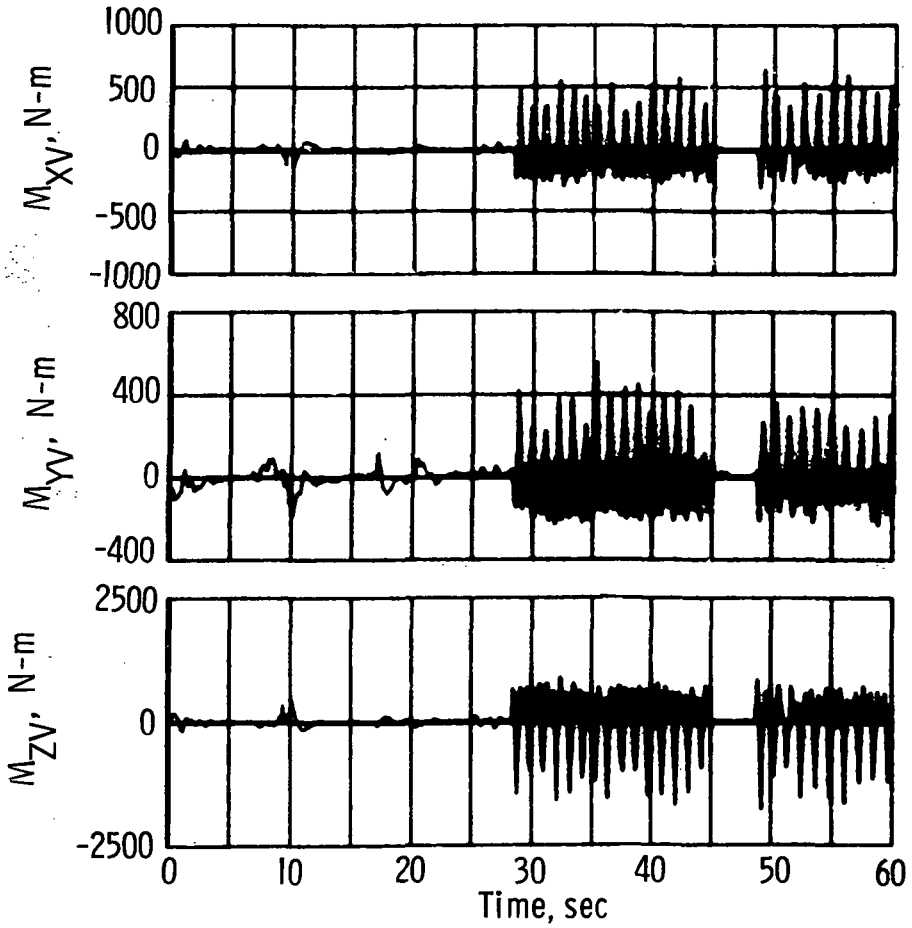

Figure 52.- Disturbance torques. Flapping arms (16:13:00).

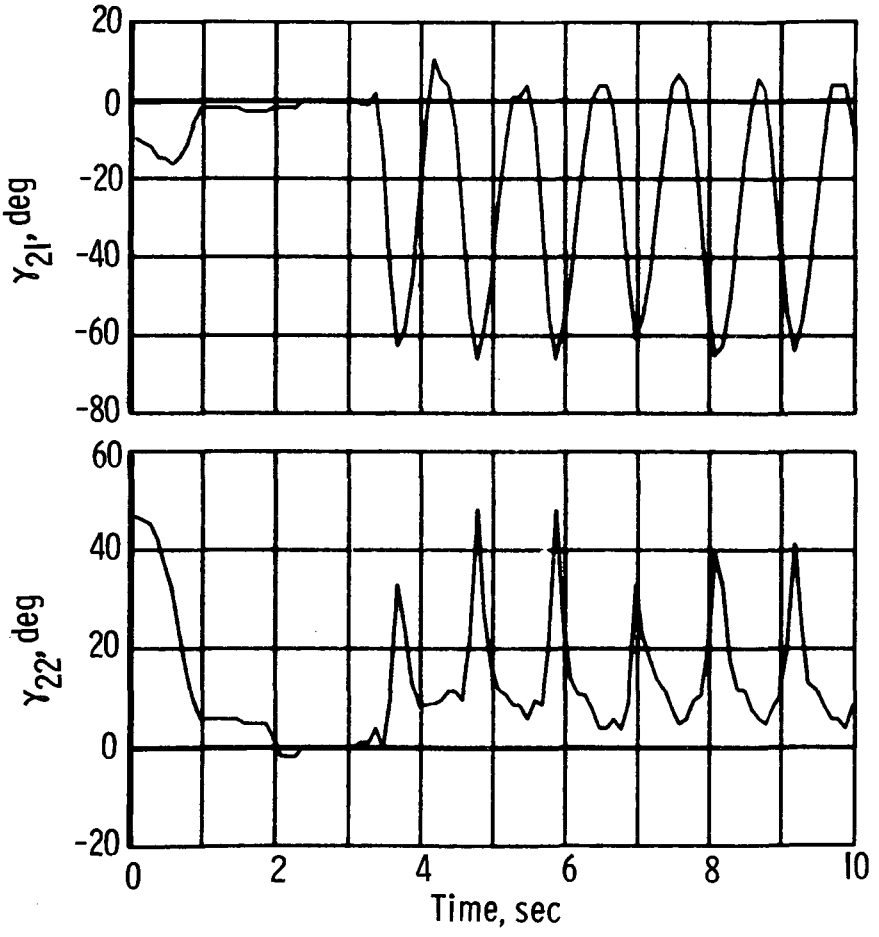

(a) Upper right arm (16:13:25).

Figure 53.- Gamma angles.

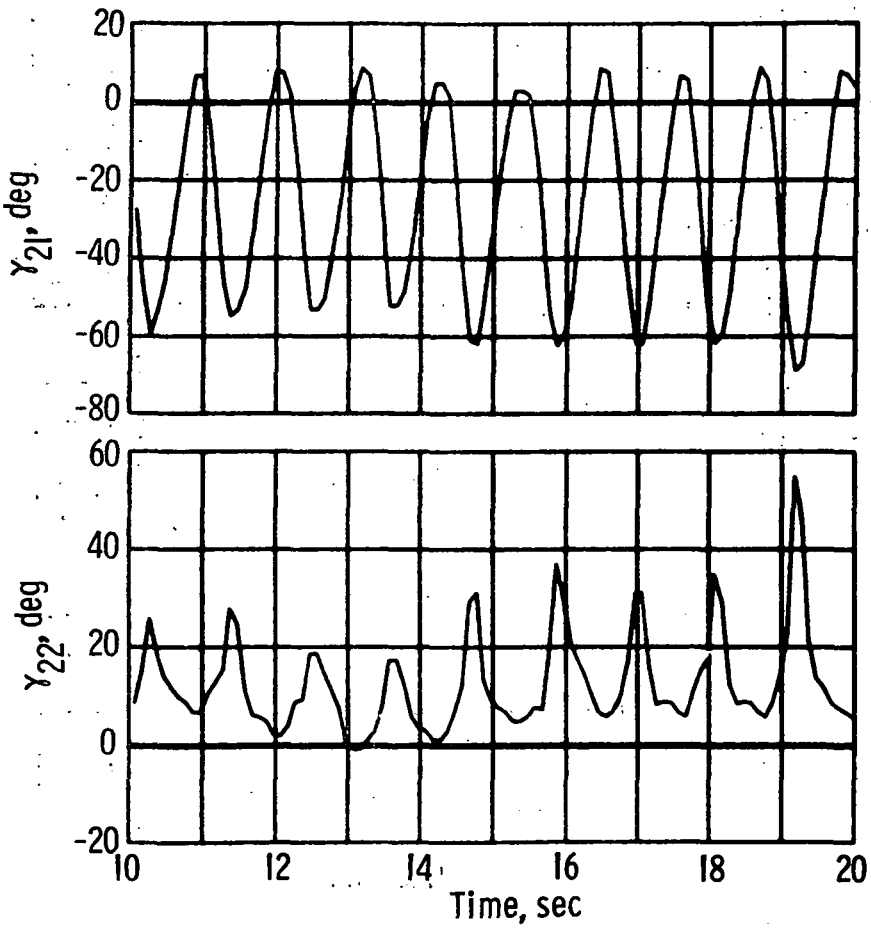

(a) Concluded.

Figure 53.- Continued.

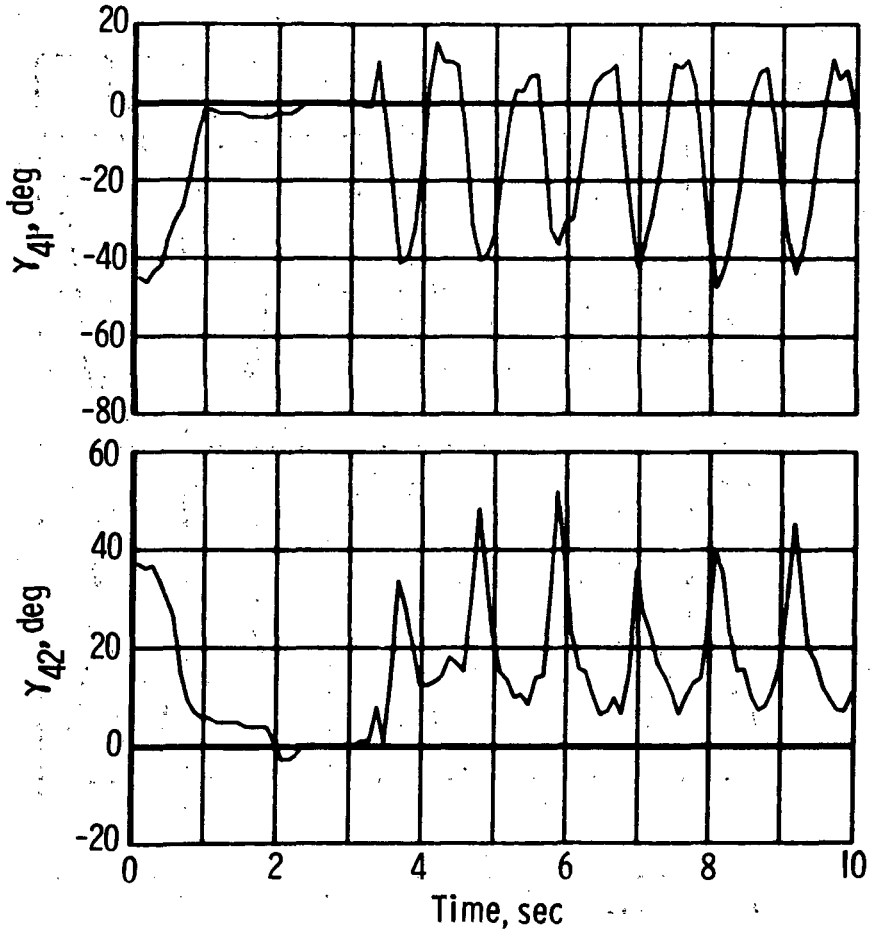

(b) Lower right arm (16:13:25).

Figure 53.- Continued.

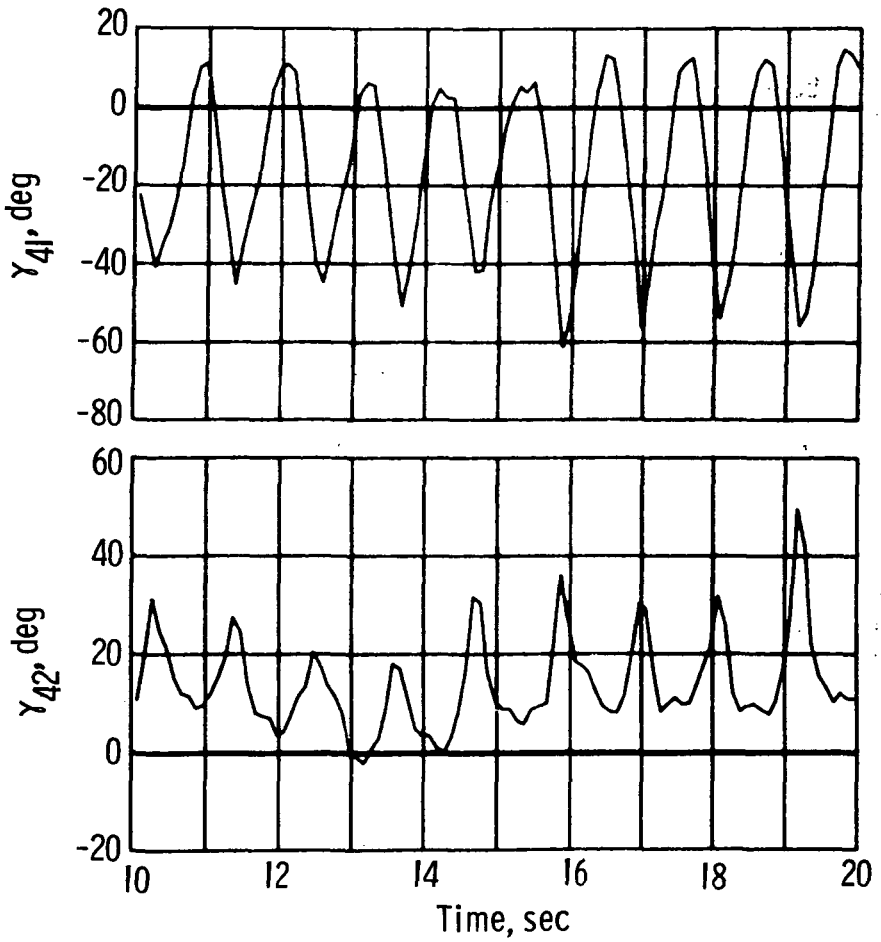

(b) Concluded.

Figure 53.- Continued.

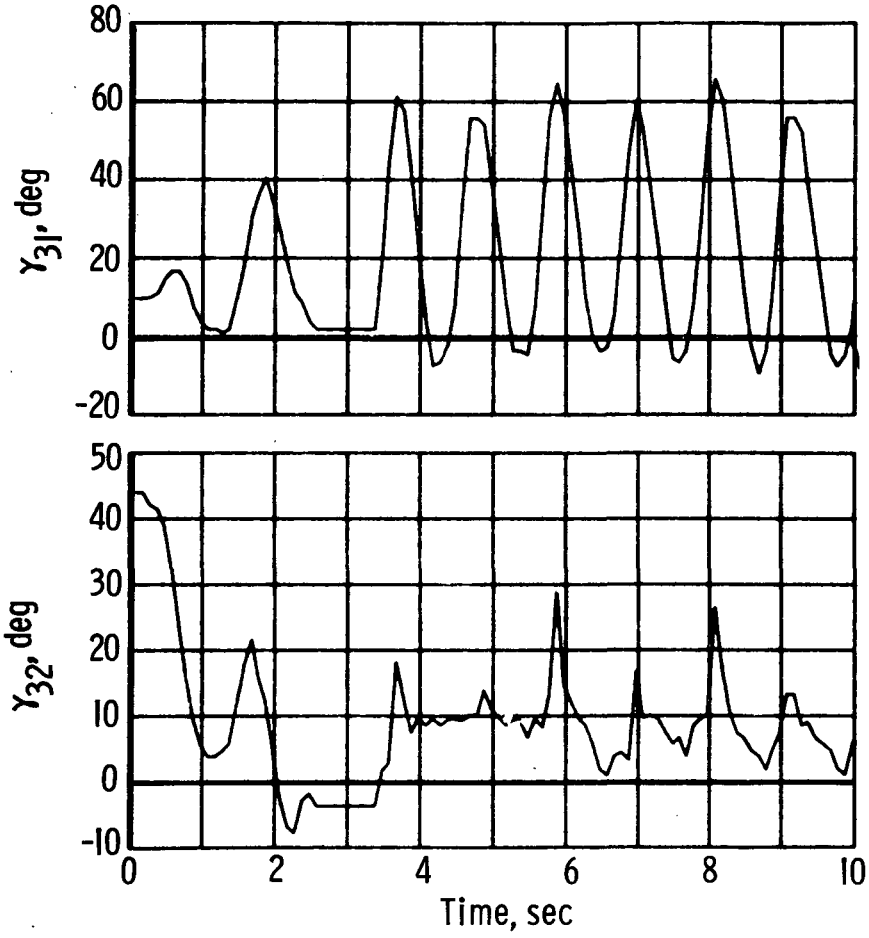

(c) Upper left arm (16:13:25).

Figure 53.- Continued.

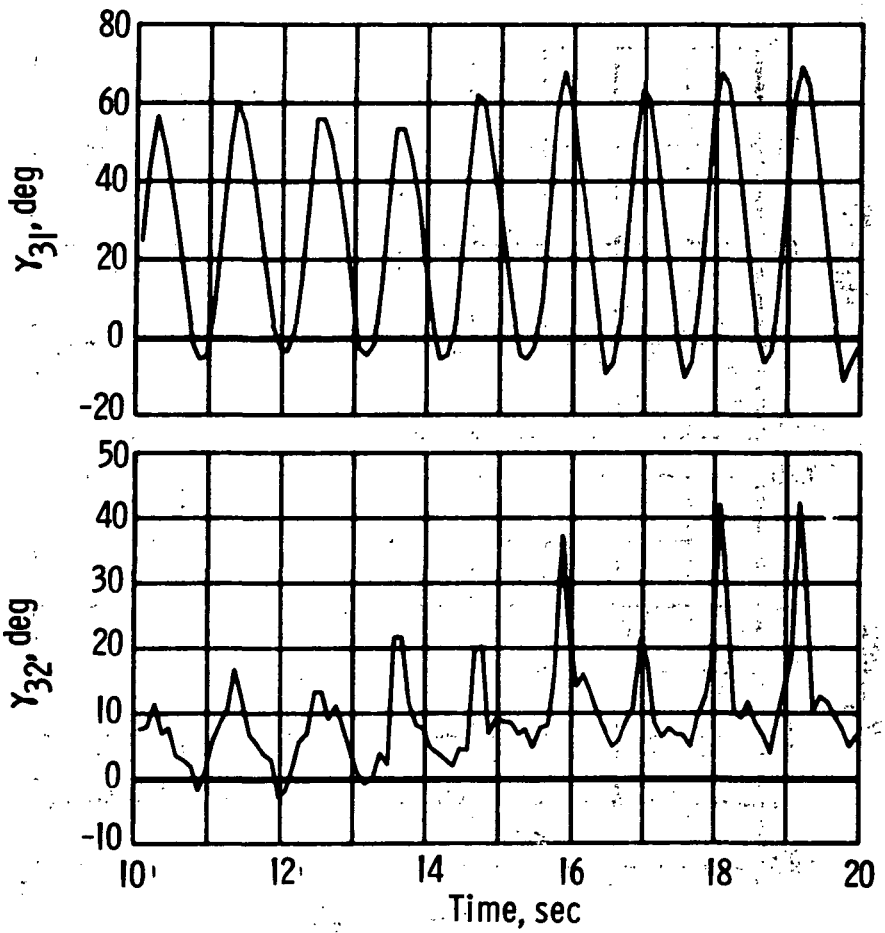

(c). Concluded.

Figure 53.- Continued.

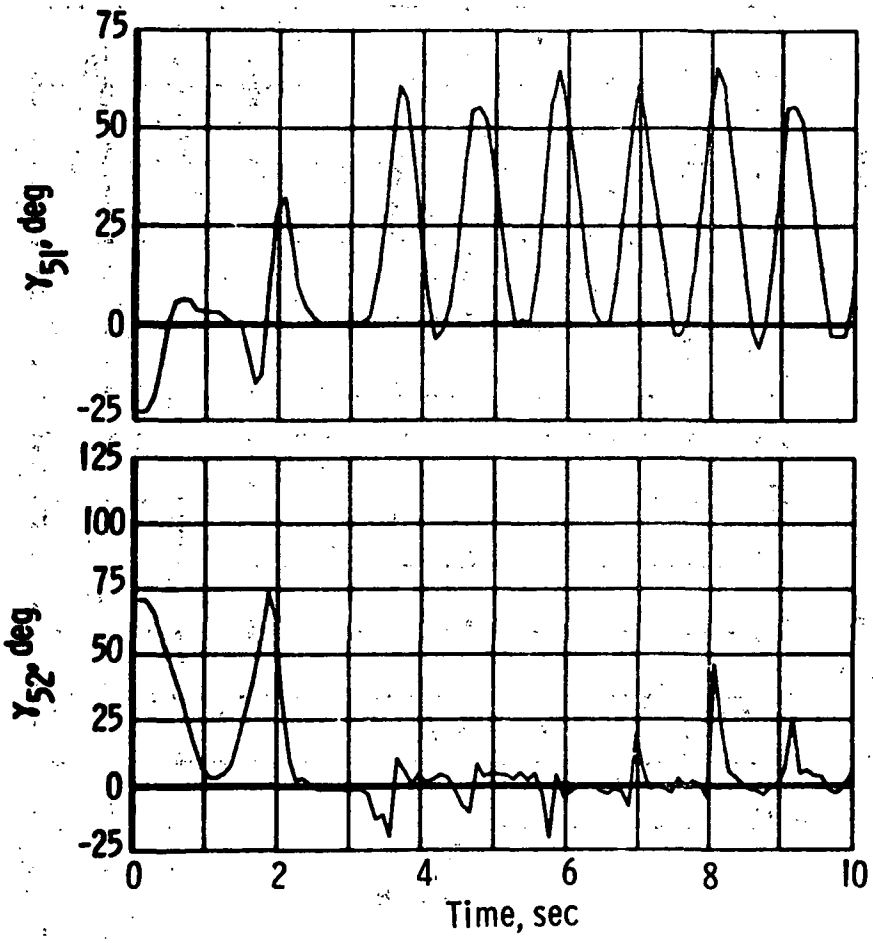

(d) Lower left arm (16:13:25).

Figure 53.- Continued.

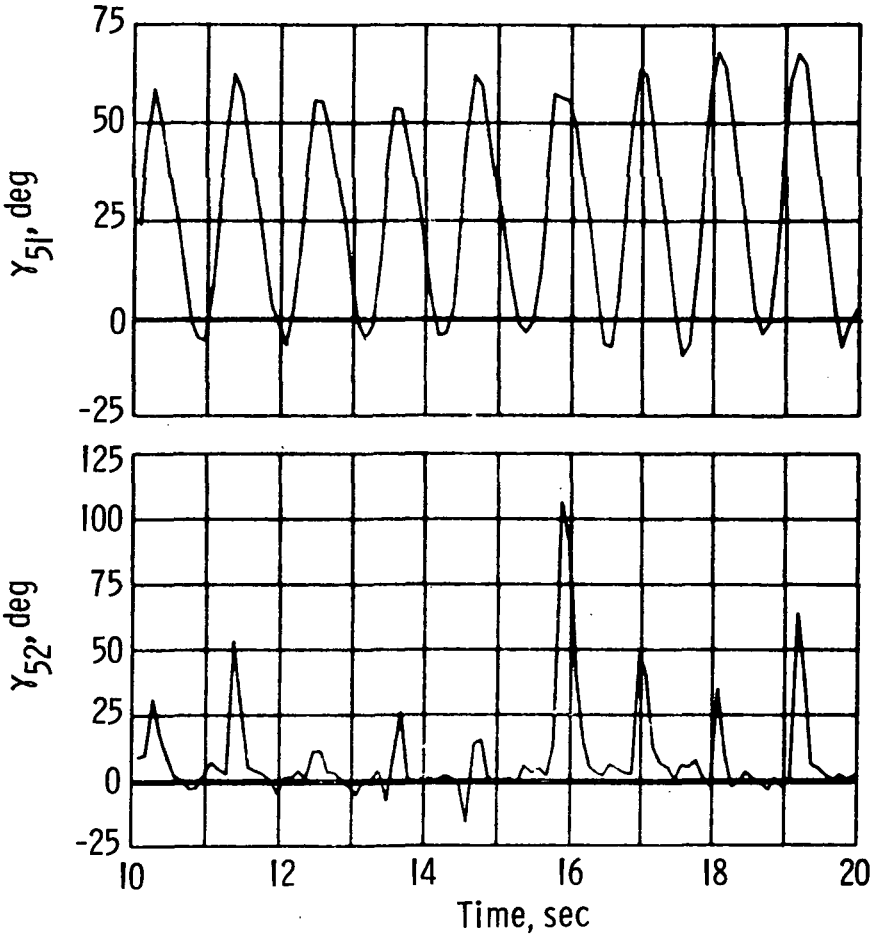

(d) Concluded.

Figure 53.- Concluded.

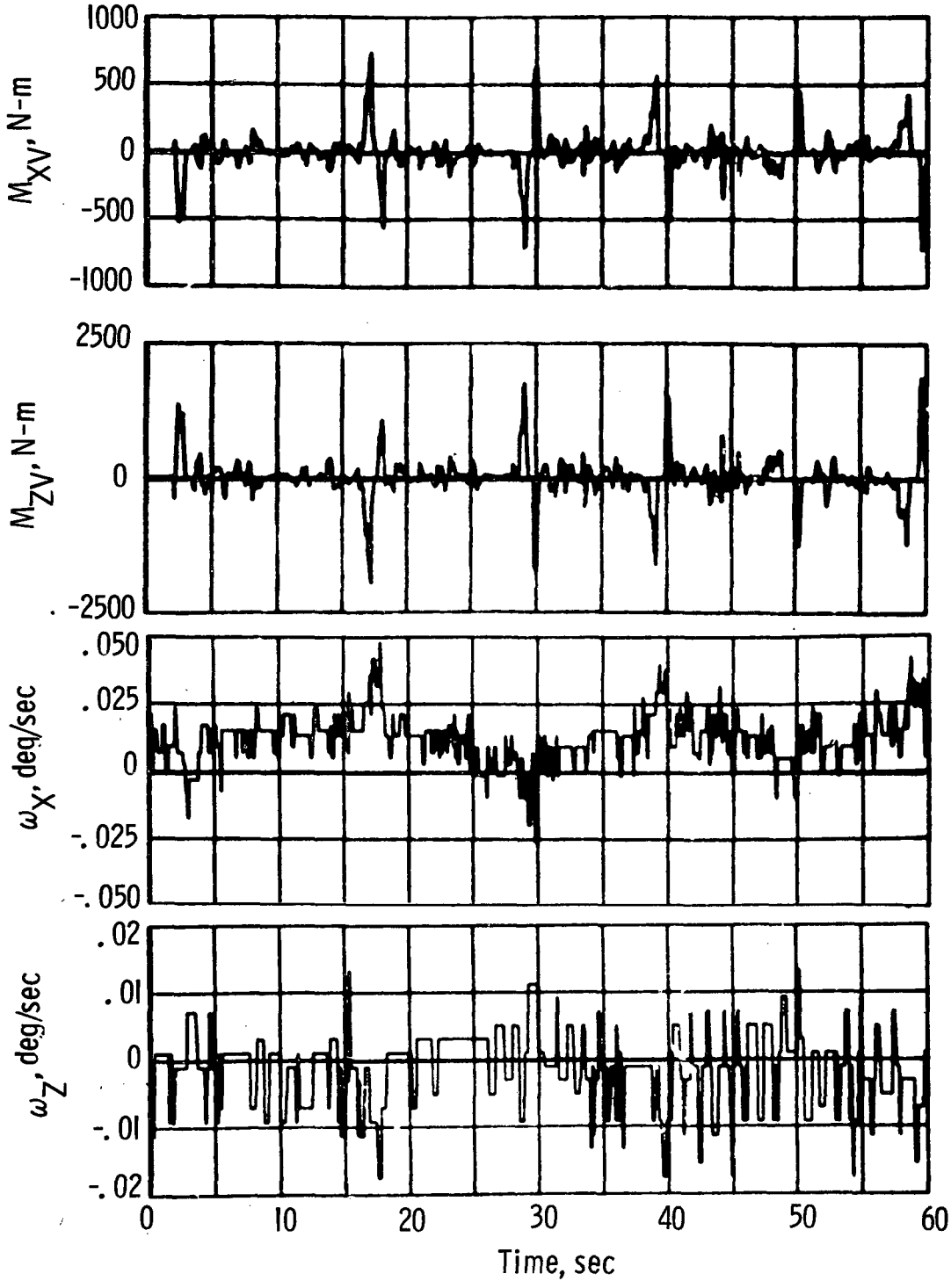

Figure 54.- Forceful soaring input compared with rate gyro output.

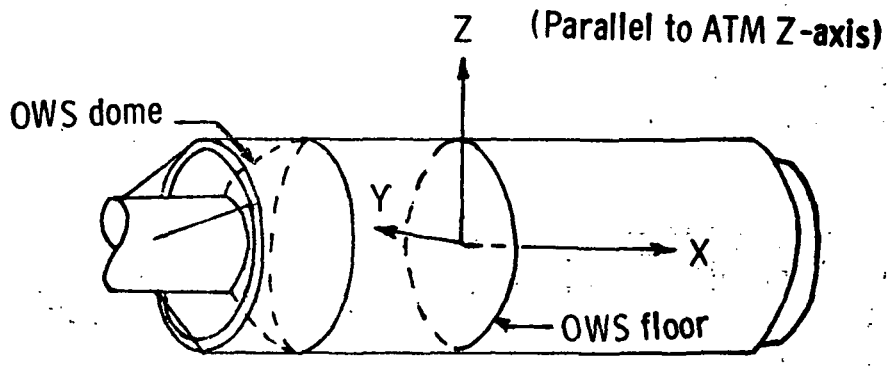

Figure 55.- Orbital workshop axes.

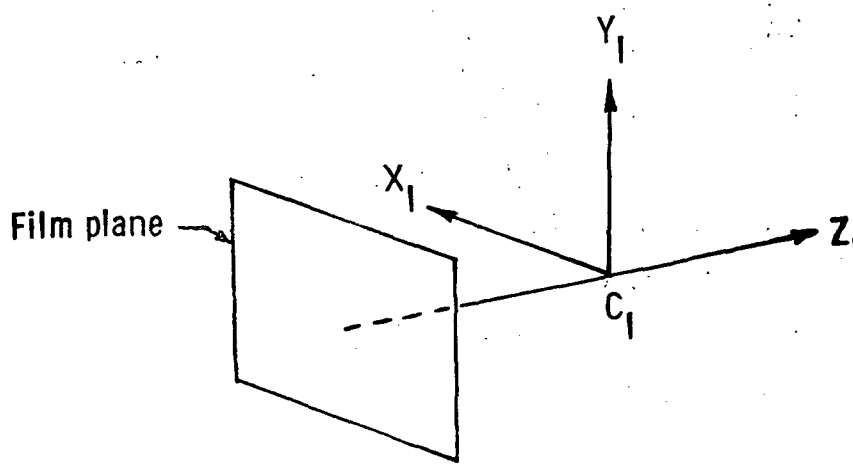

Figure 56.- Camera 1 axis system.

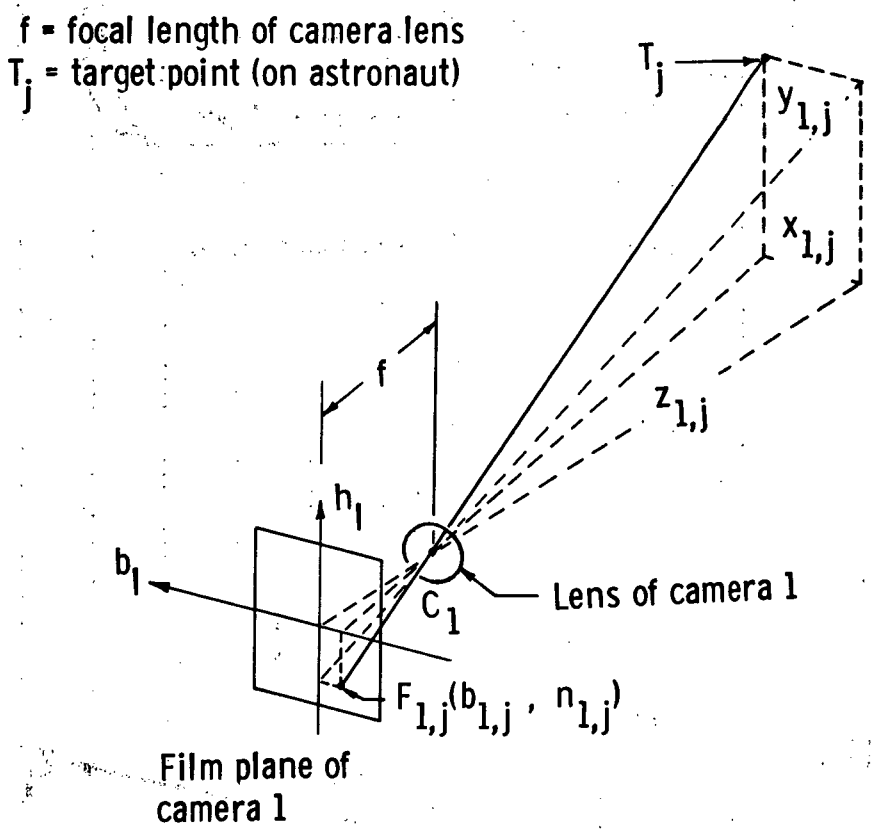

Figure 57.- Camera 1 target geometry.

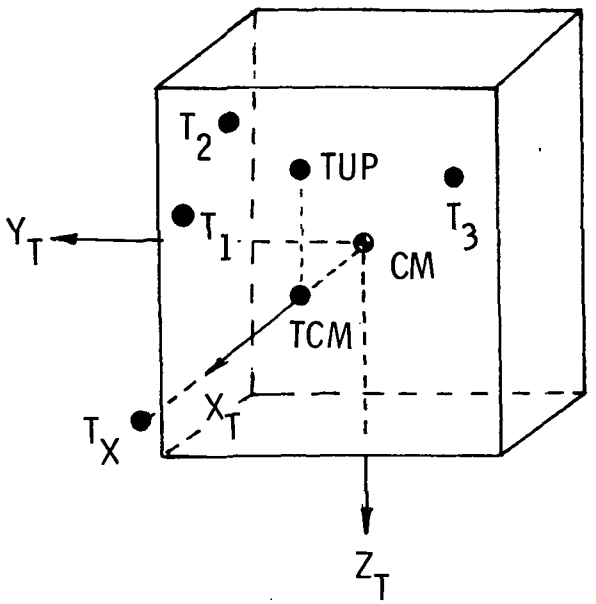

Figure 58.- Astronaut torso schematic. X_T, Y_T, and Z_T axes are parallel to X_M, Y_M, and Z_M axes (fig. 12) with origin at torso center of mass.

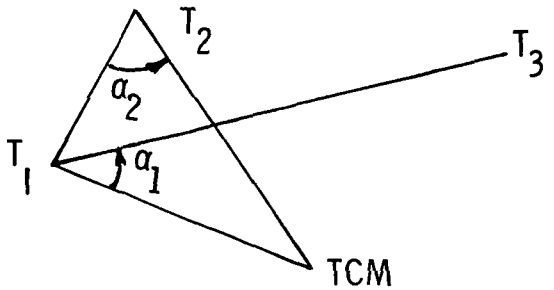

Figure 59.- Torso target geometry.

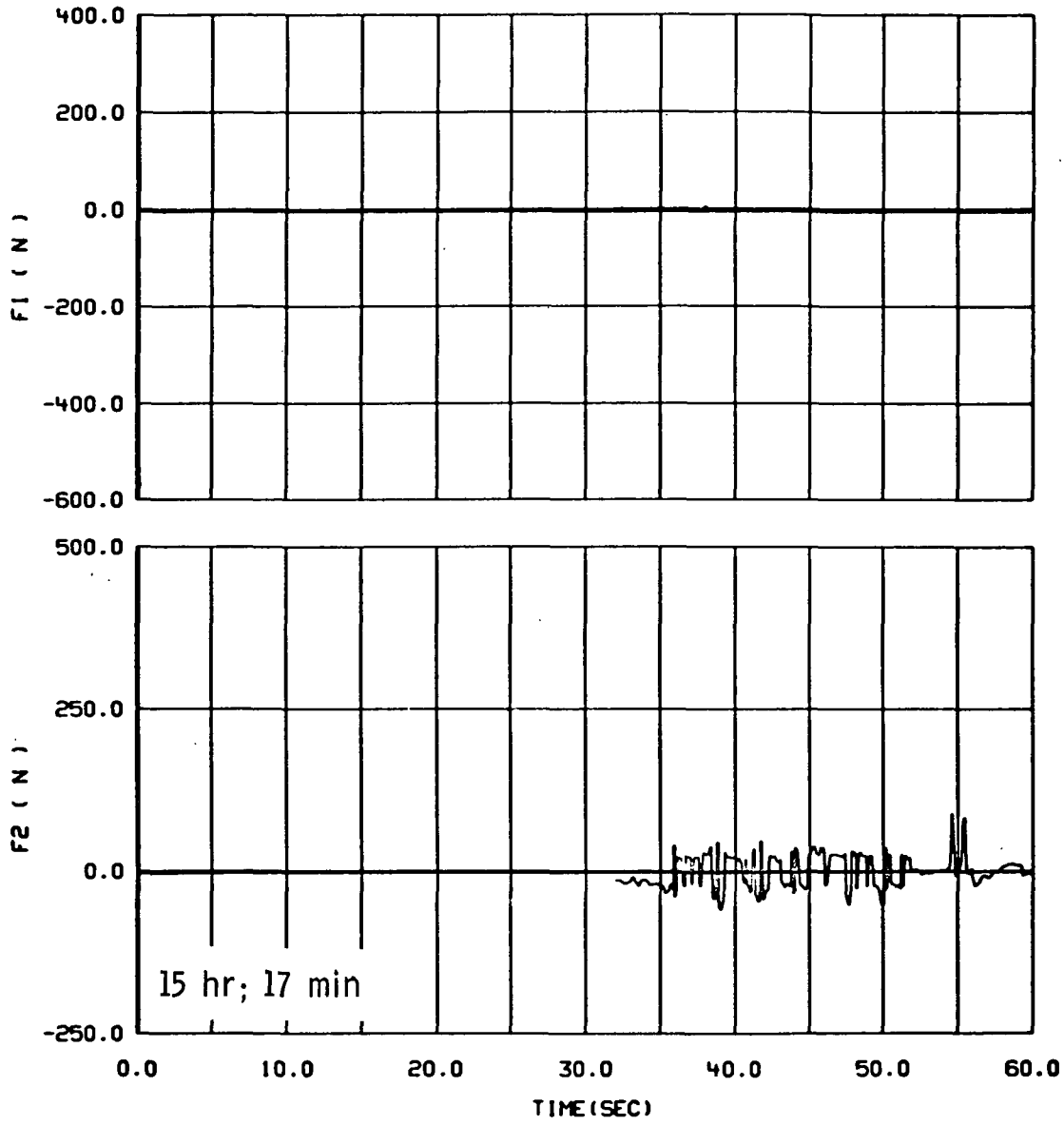

Figure 60.- FMU total forces.

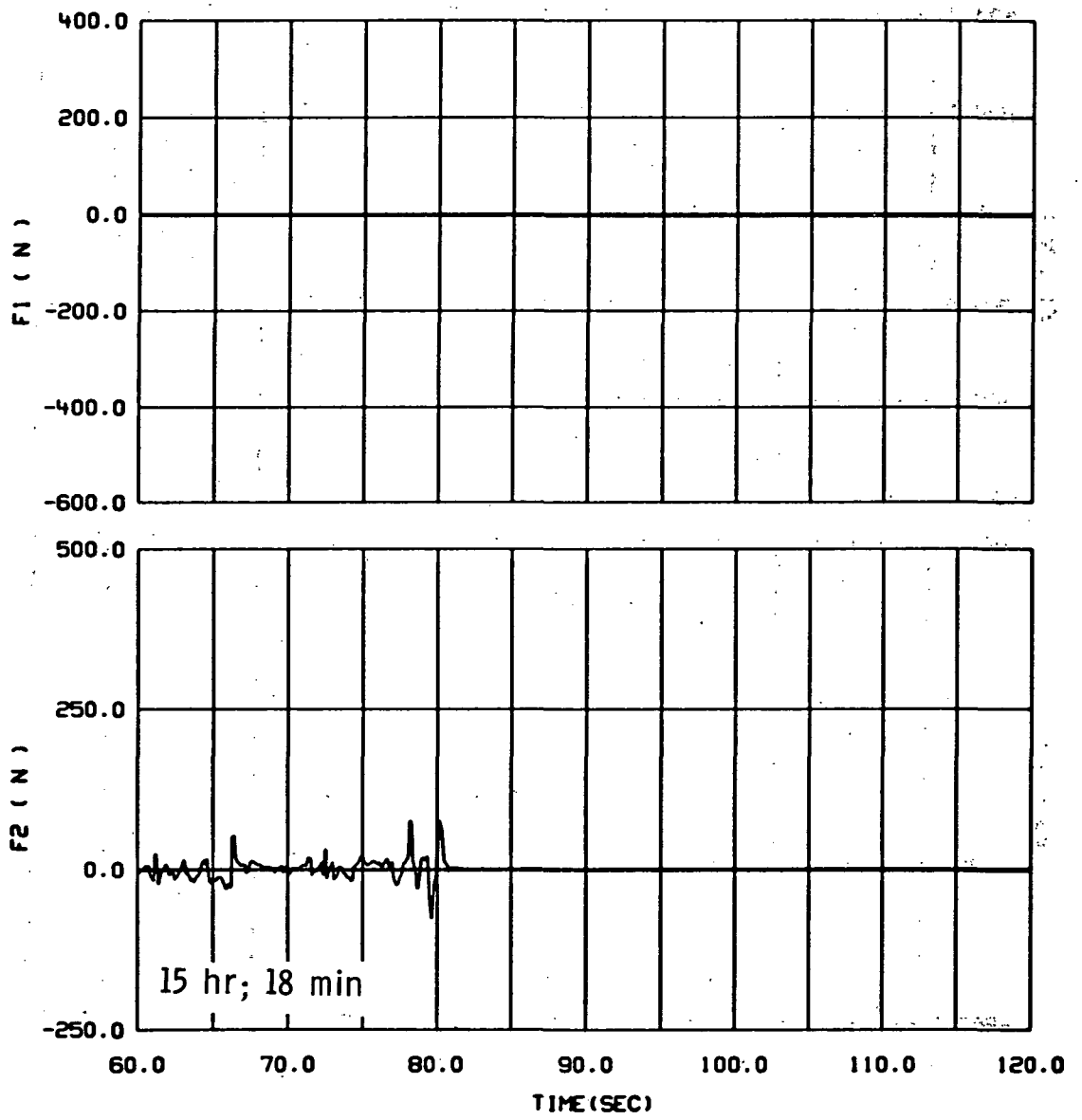

Figure 60.- Continued.

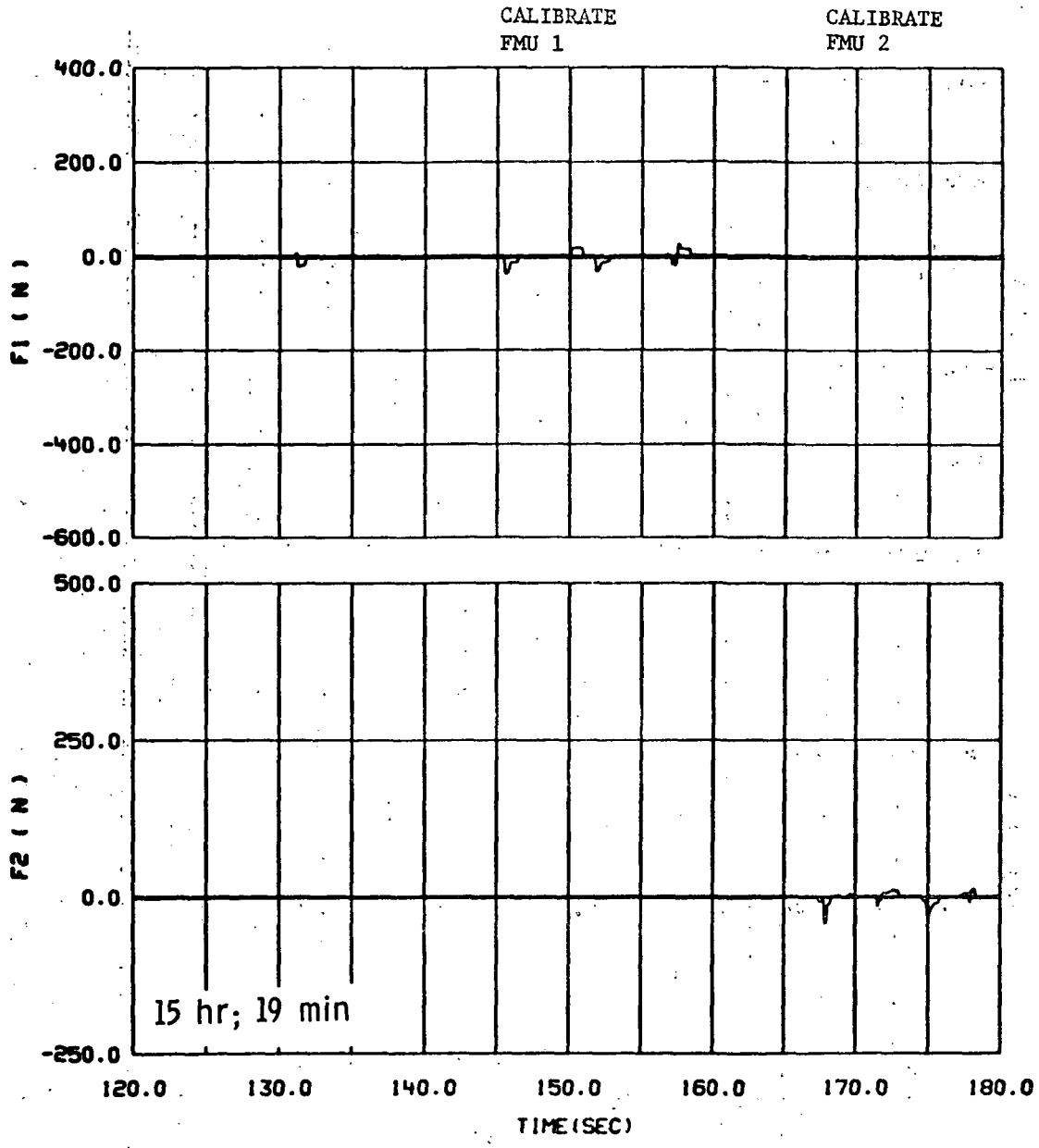

Figure 60.- Continued.

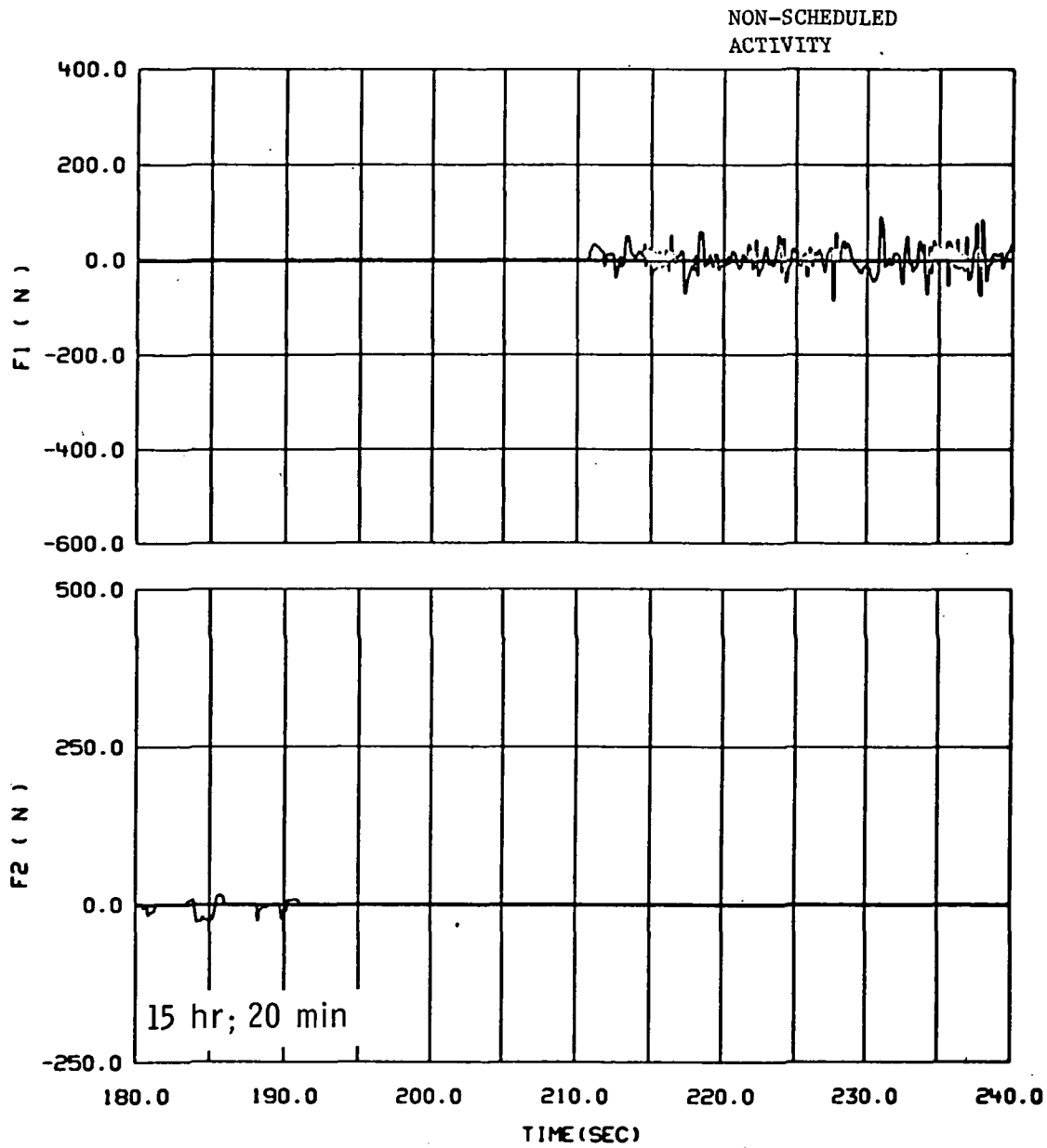

Figure 60.- Continued.

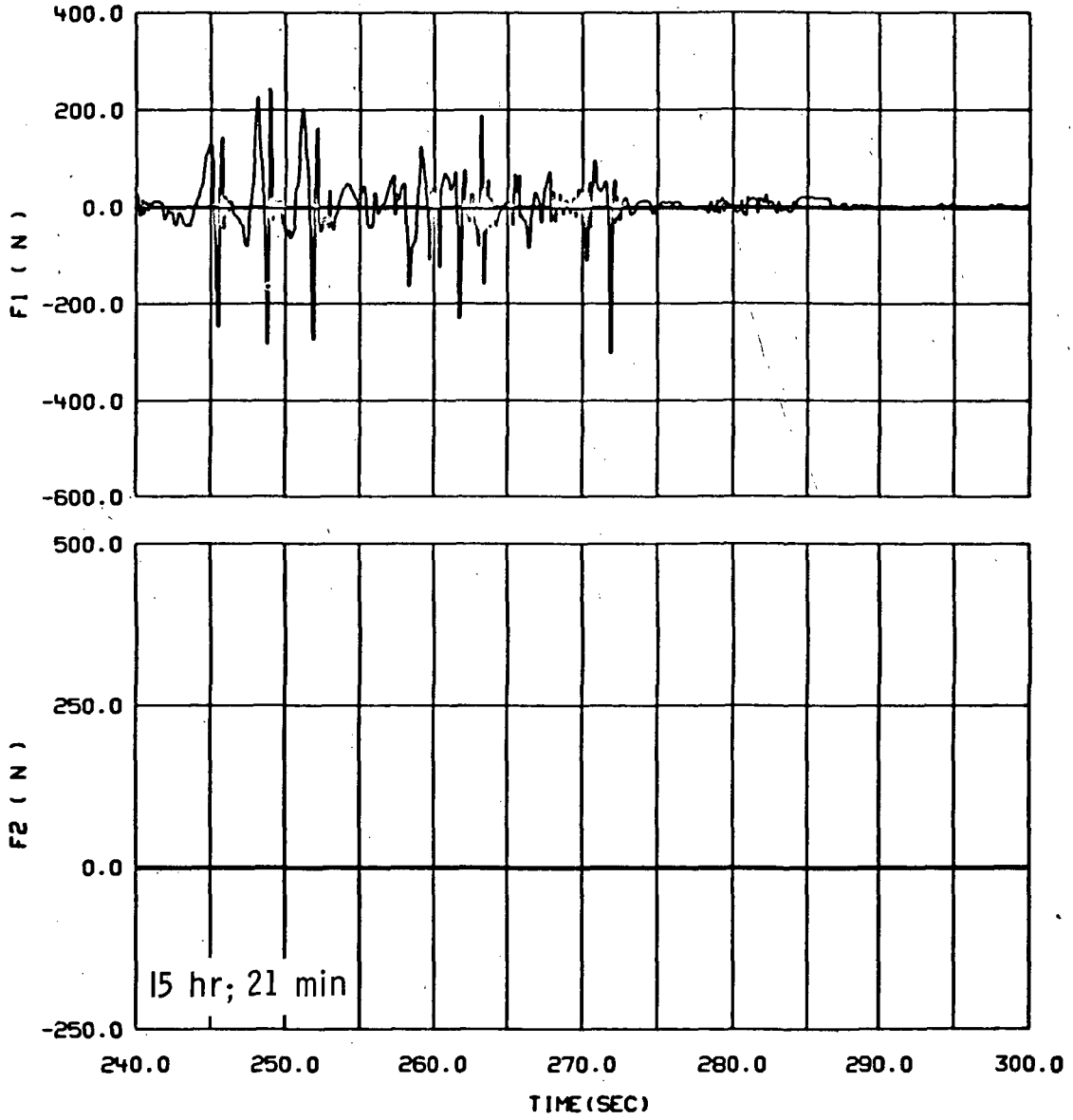

Figure 60.- Continued.

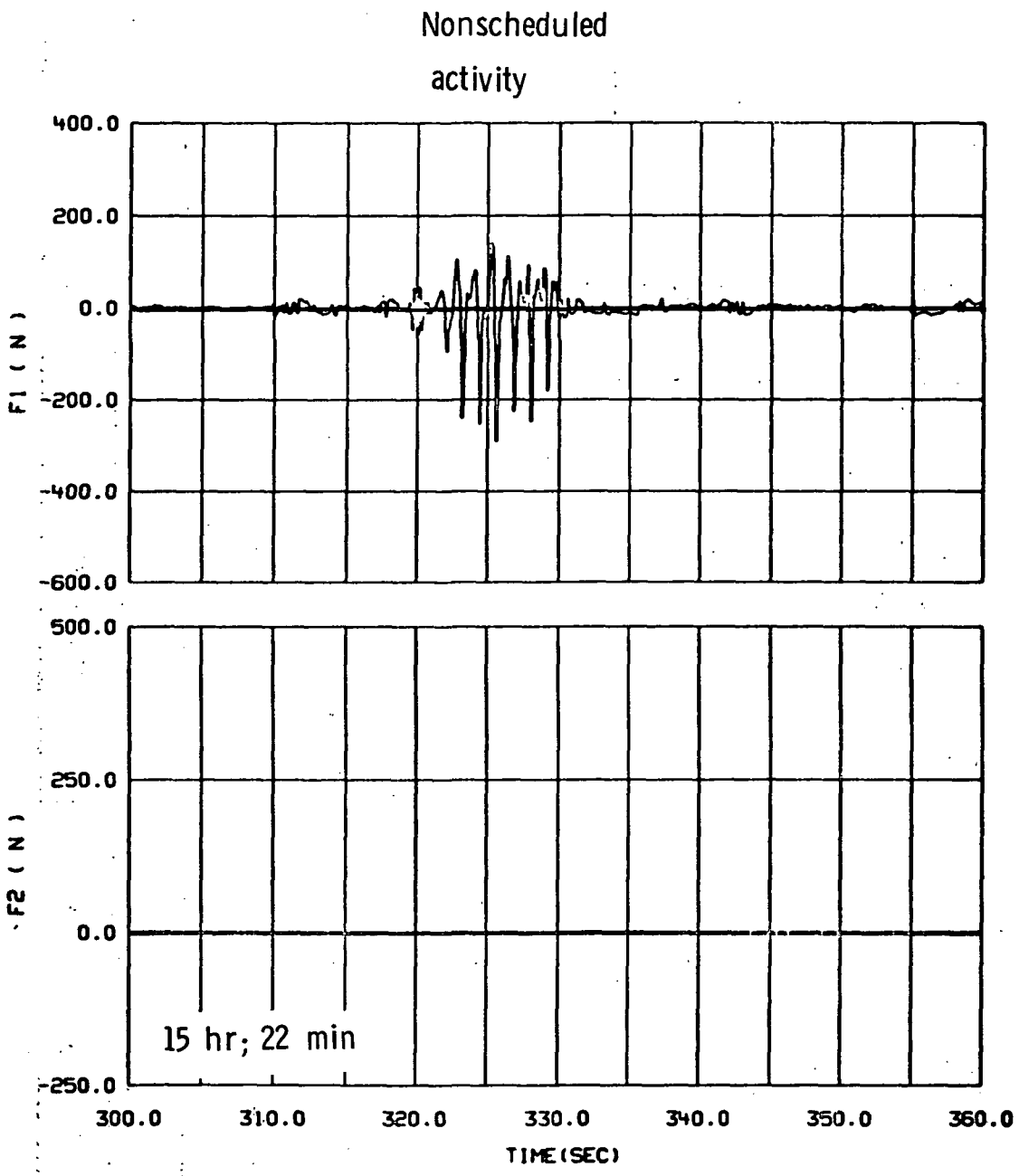

Figure 60.- Continued.

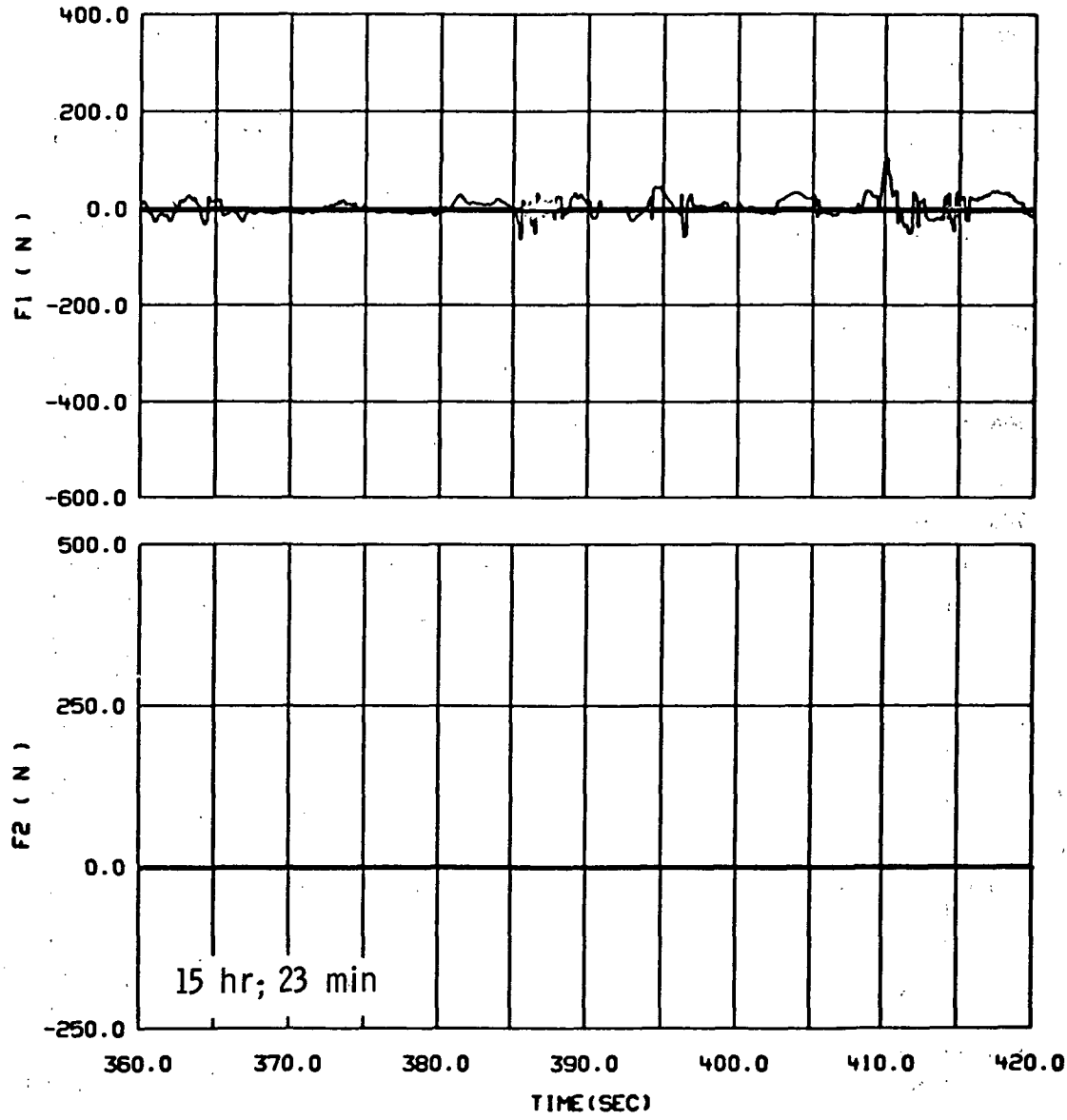

Figure 60.- Continued.

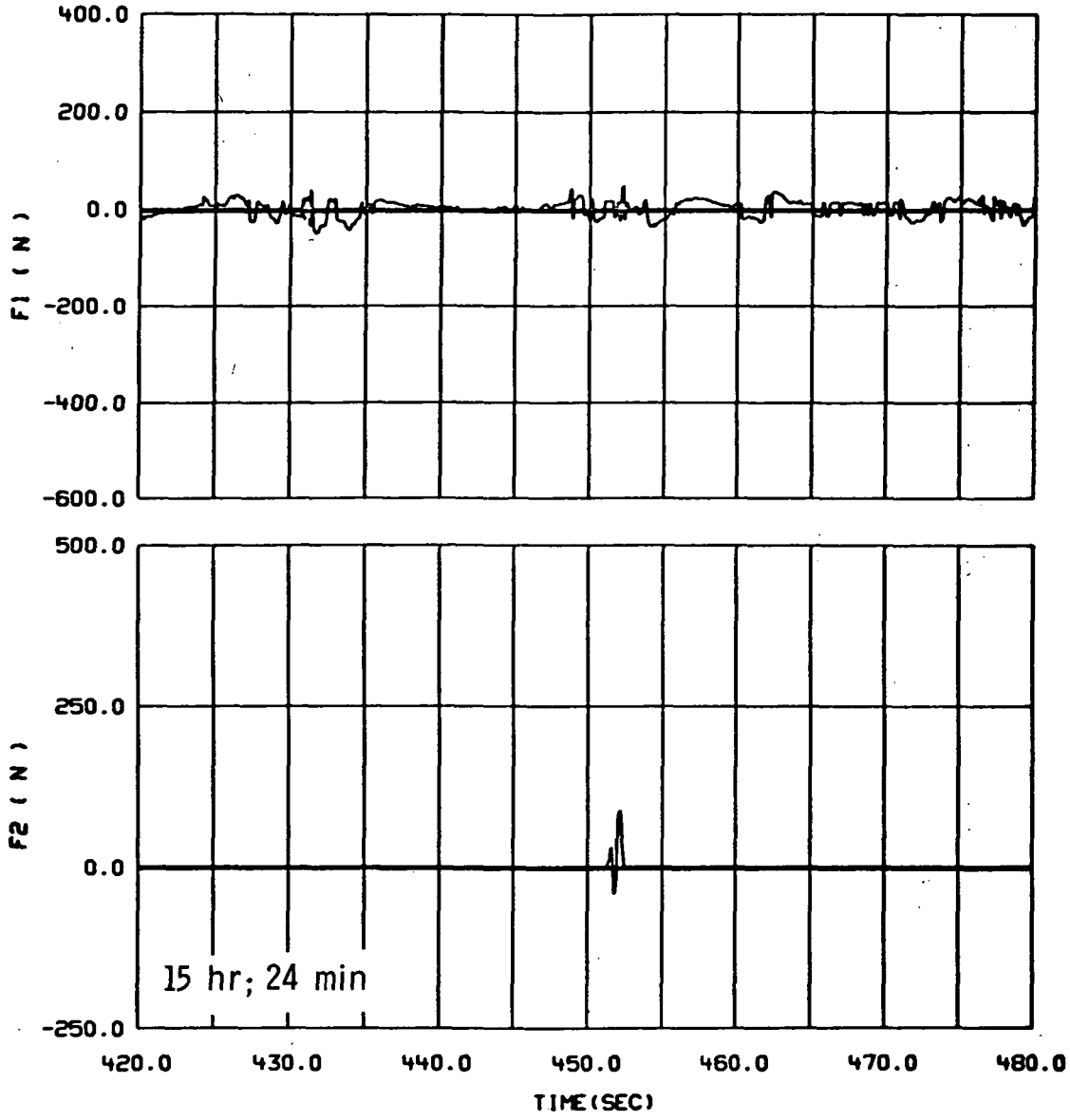

Figure 60.- Continued.

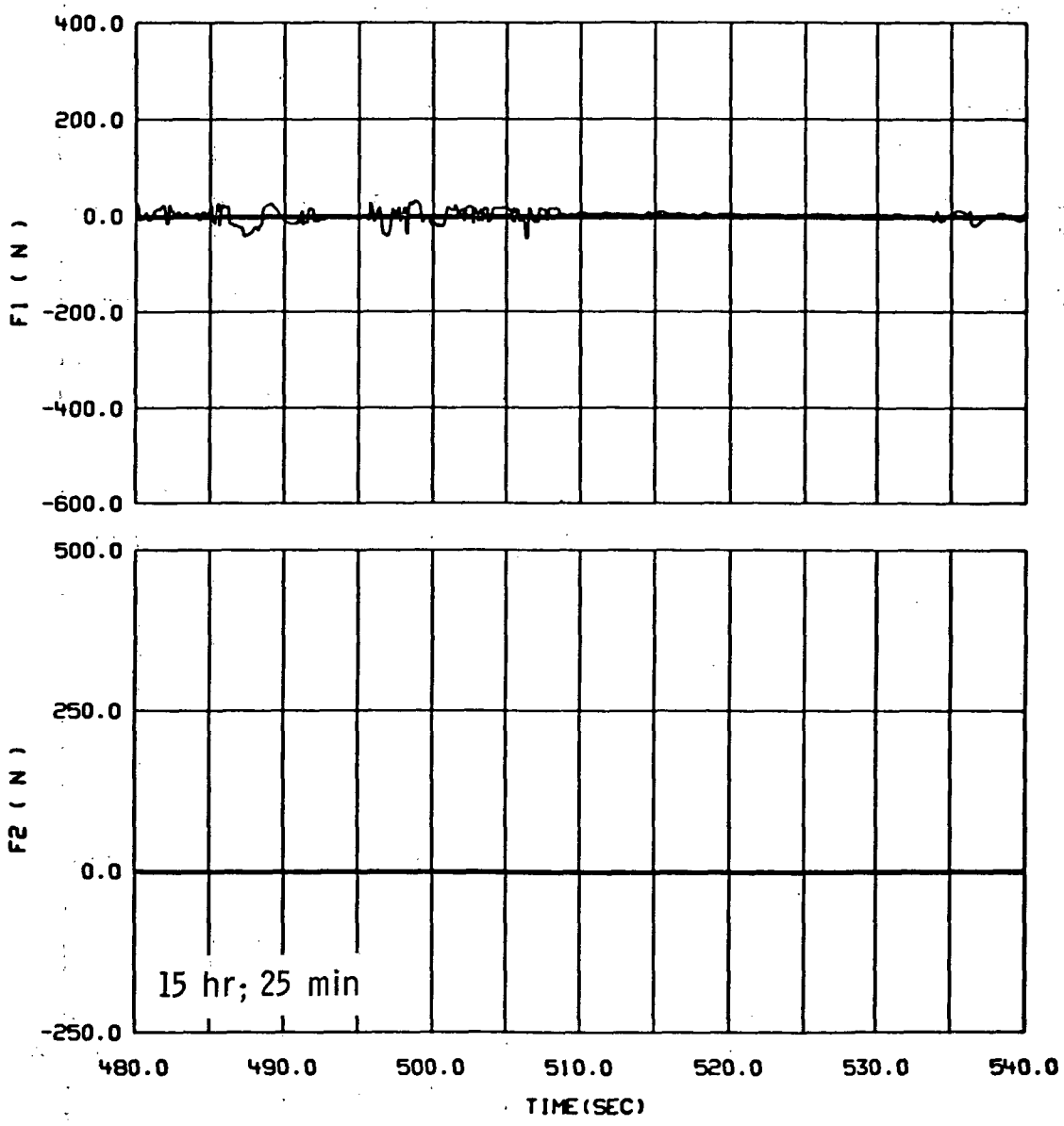

Figure 60.- Continued.

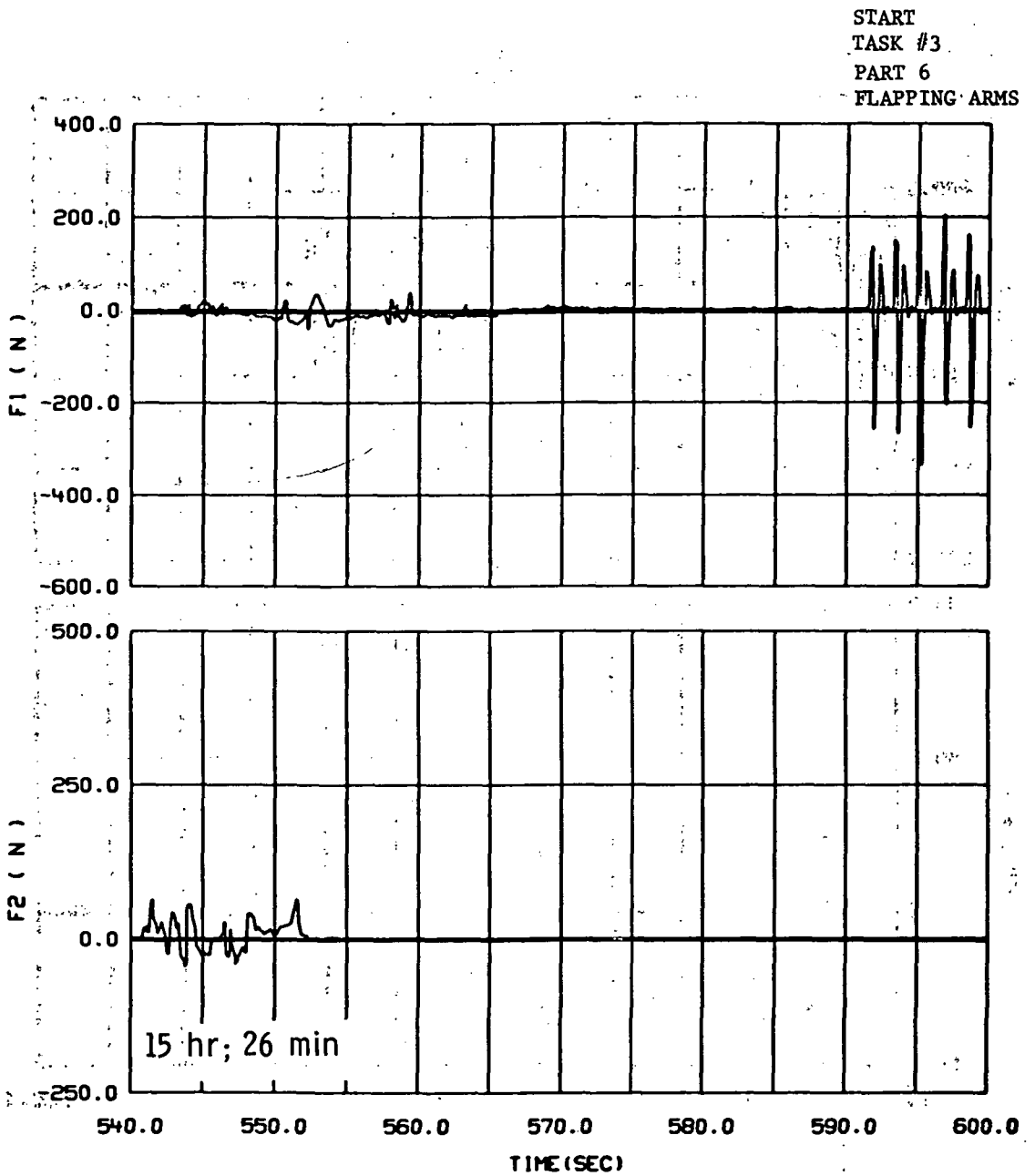

Figure 60.- Continued.

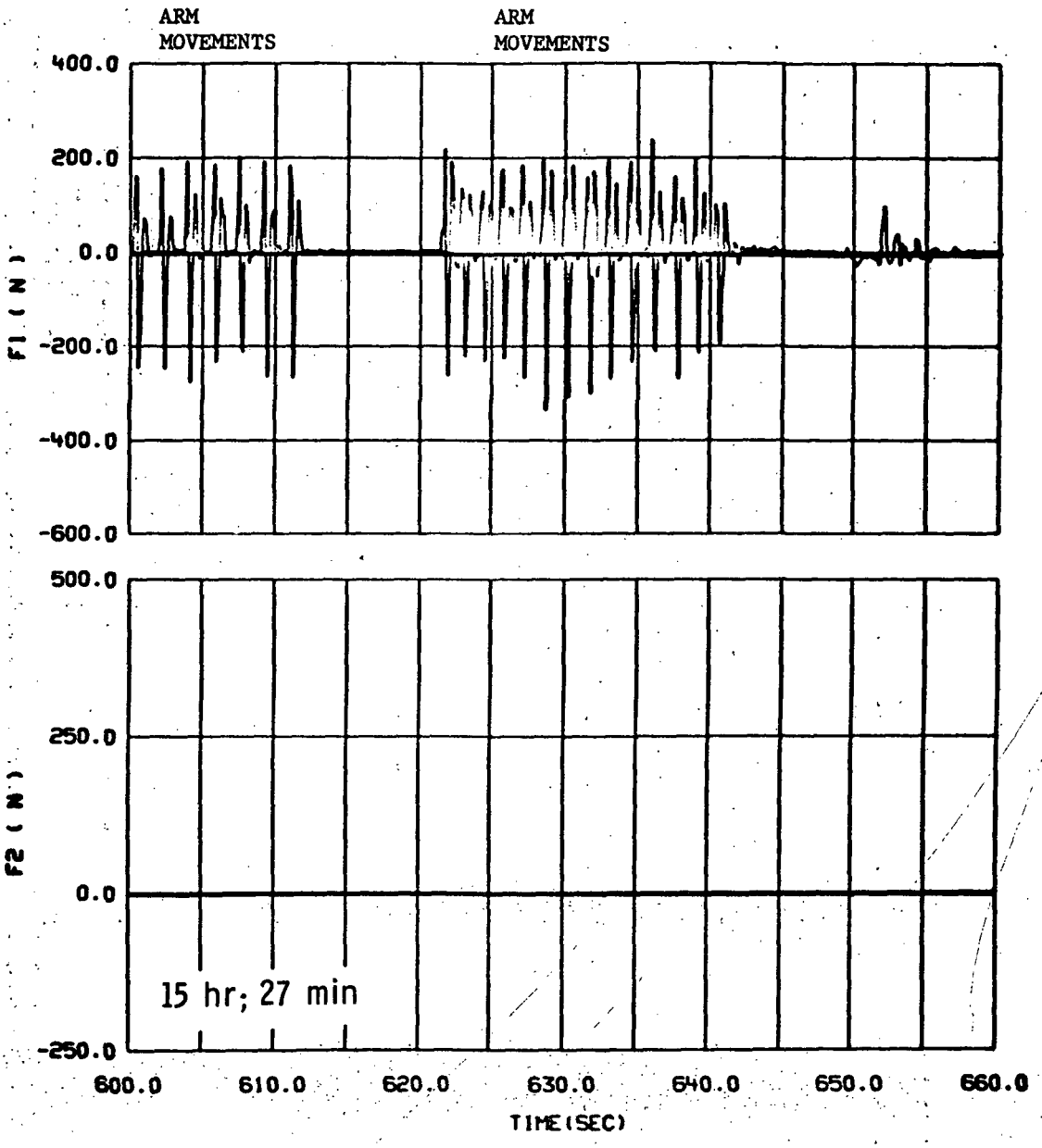

Figure 60.- Continued.

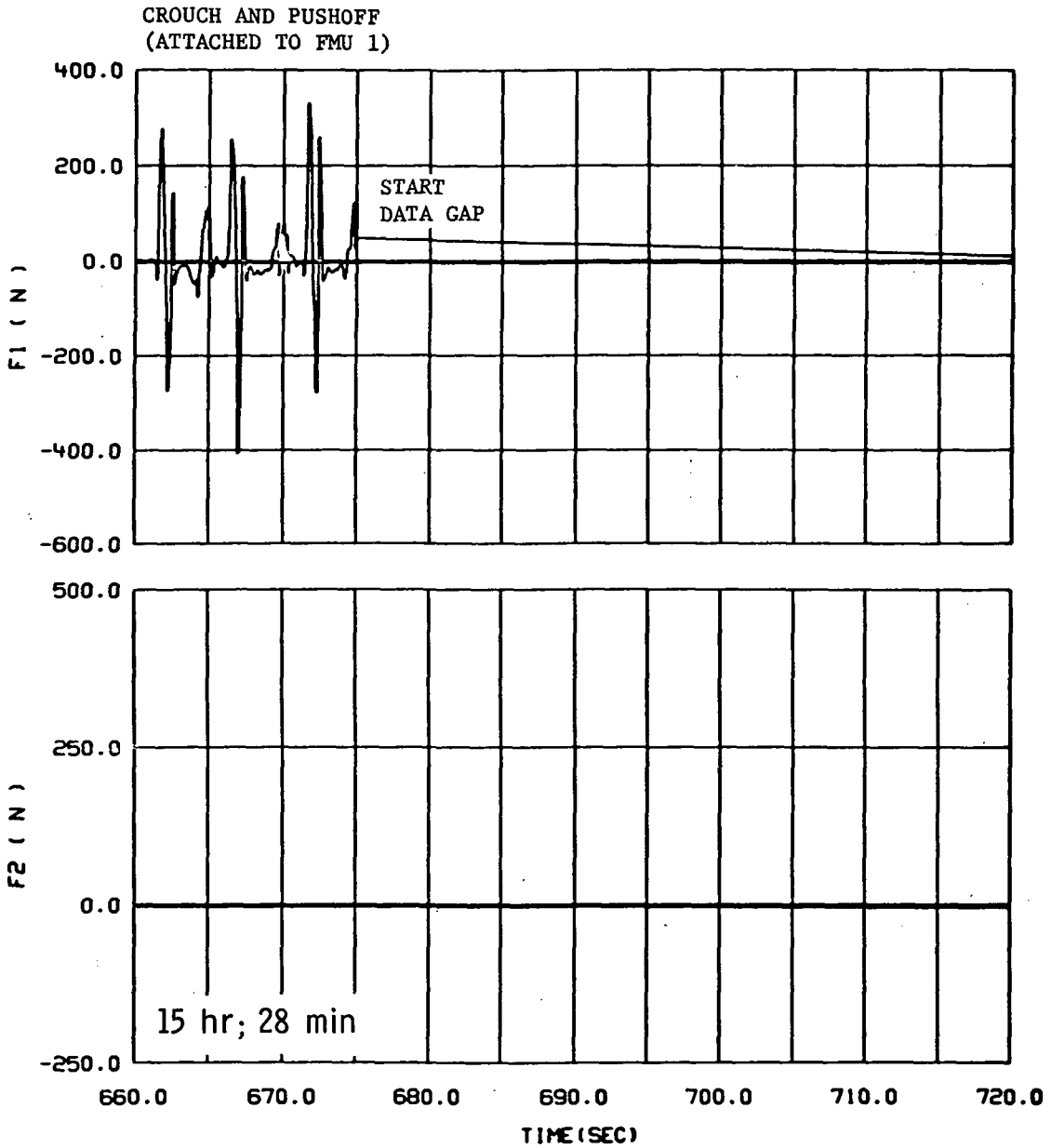

Figure 60.- Continued.

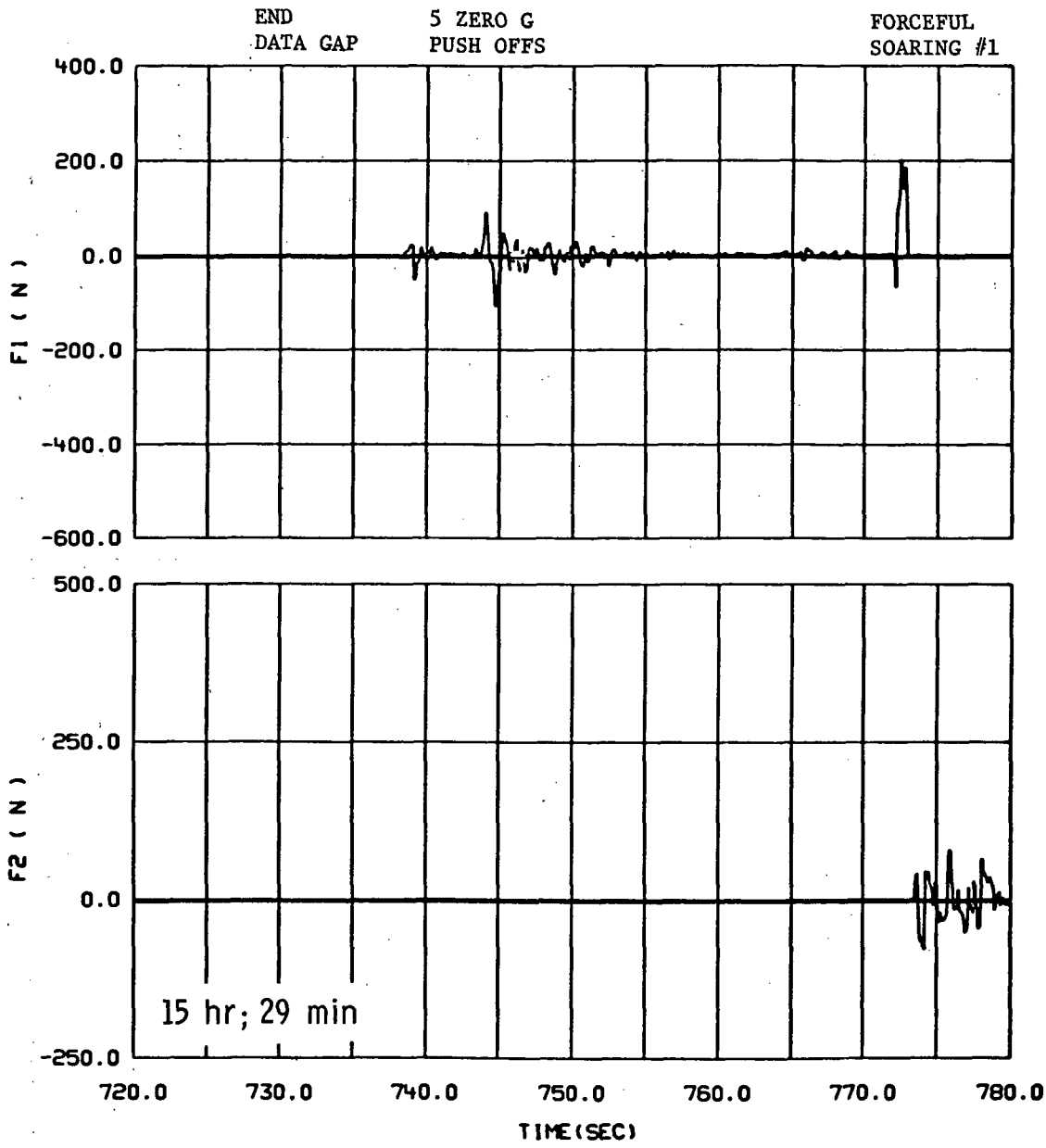

Figure 60.- Continued.

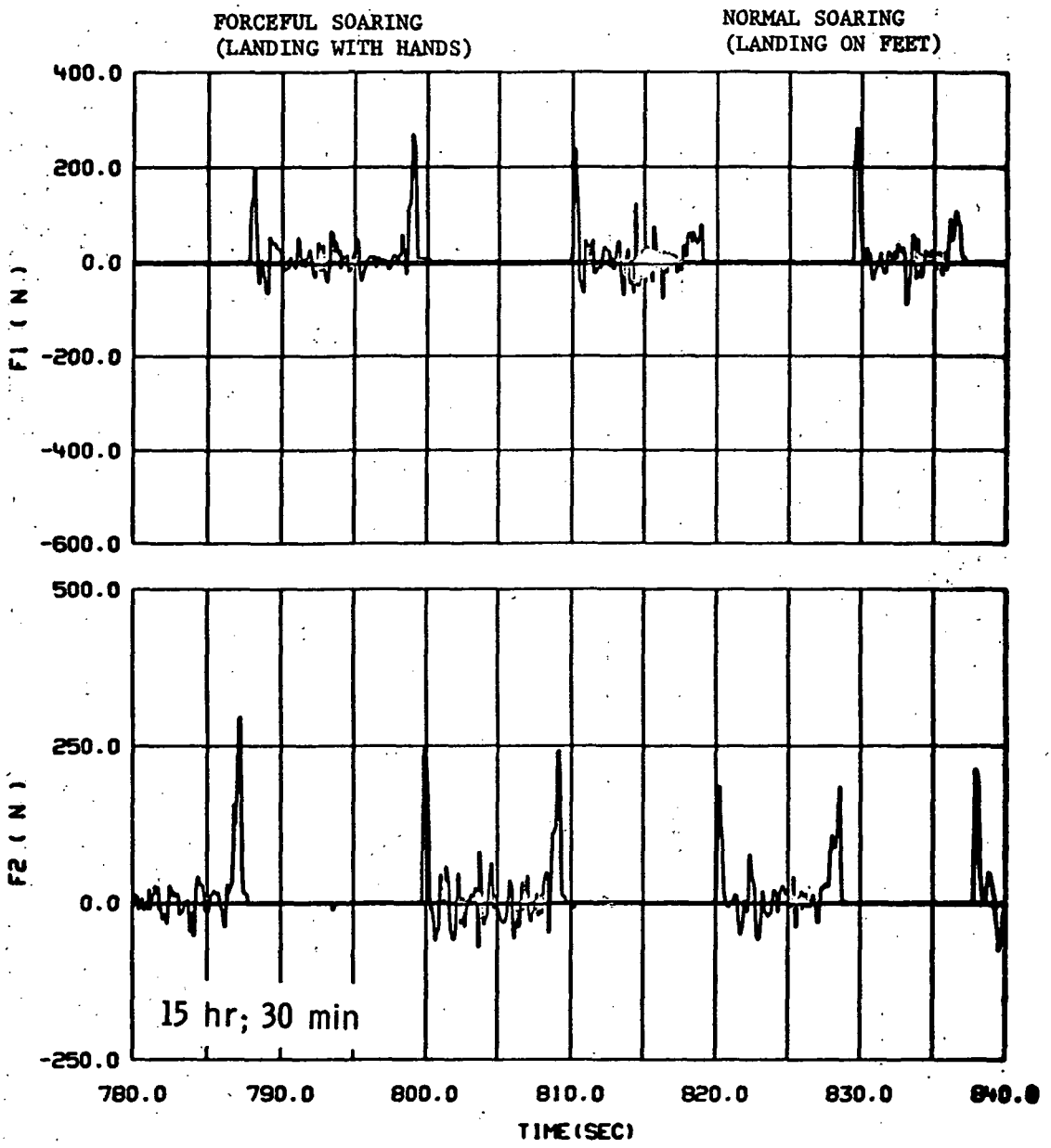

Figure 60.- Continued.

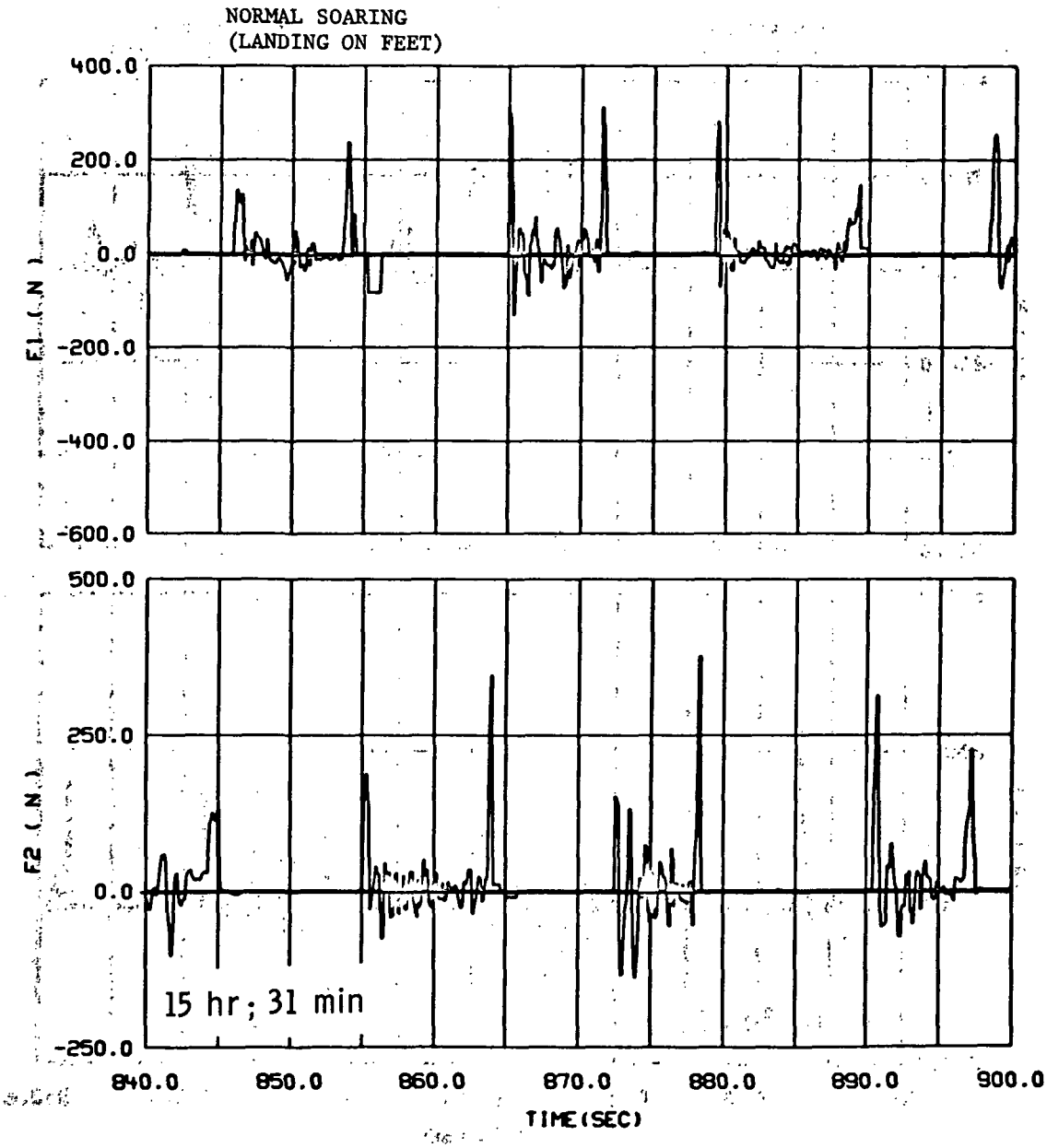

Figure 60.- Continued.

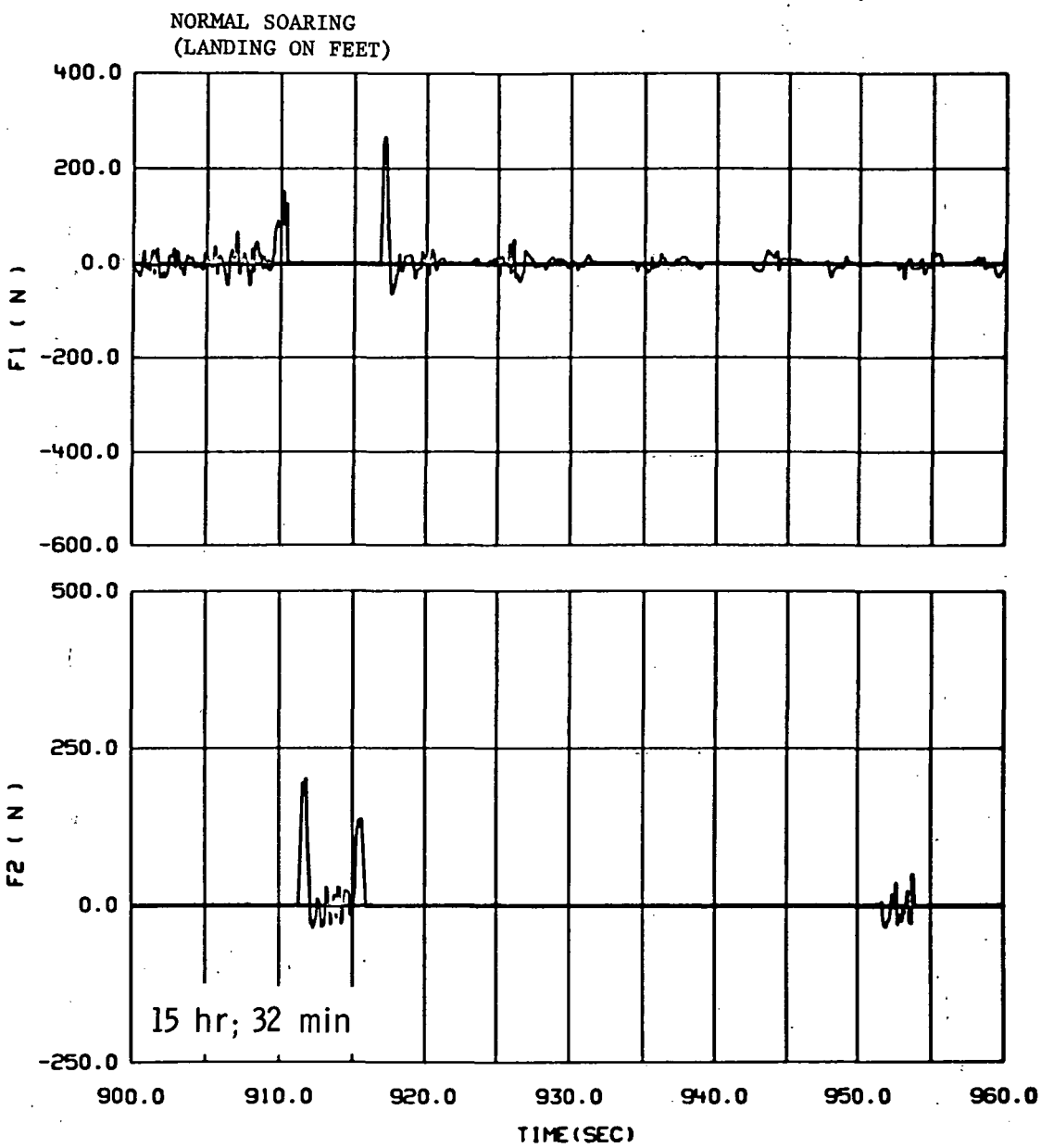

Figure 60.- Continued.

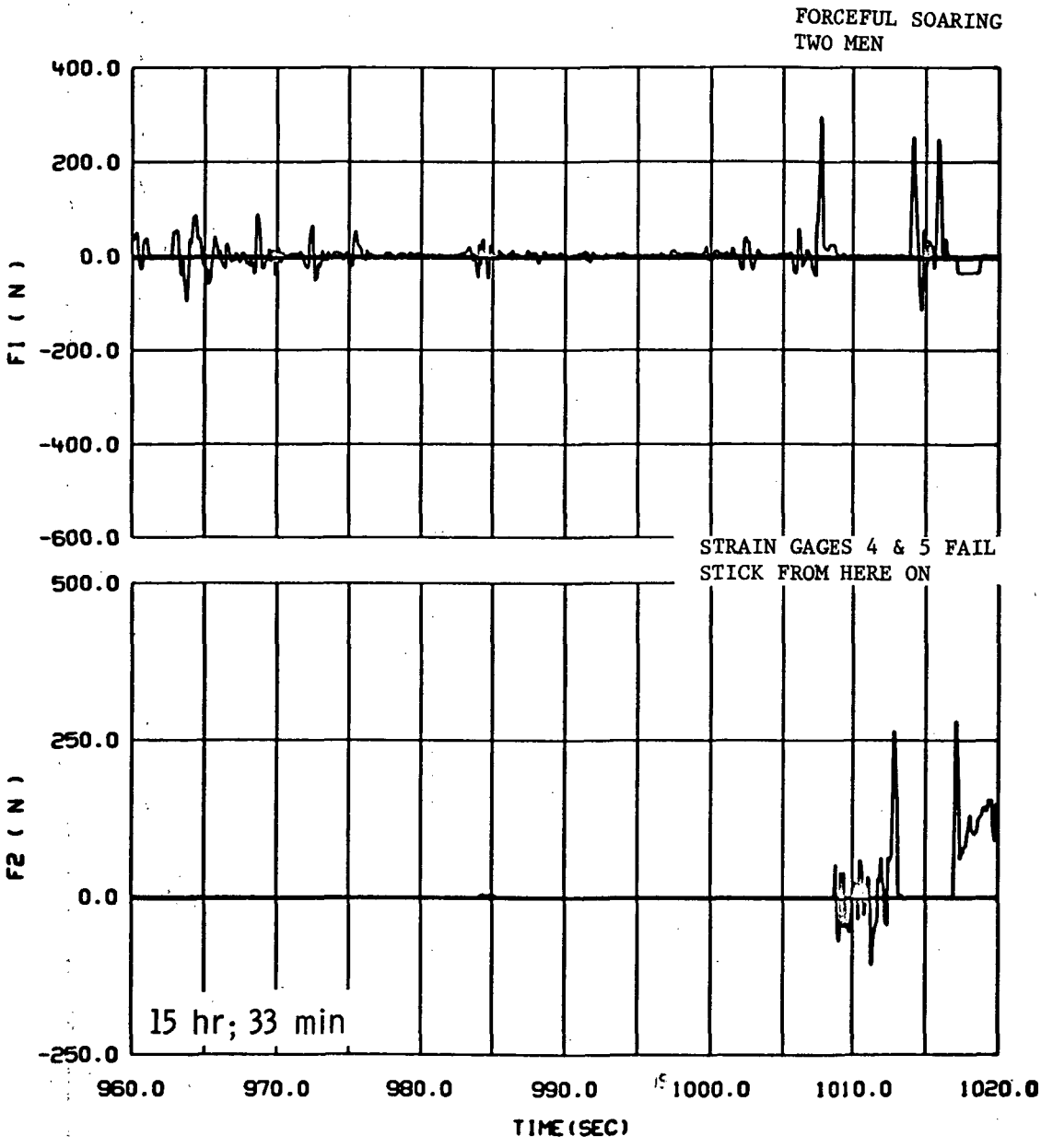

Figure 60.- Continued.

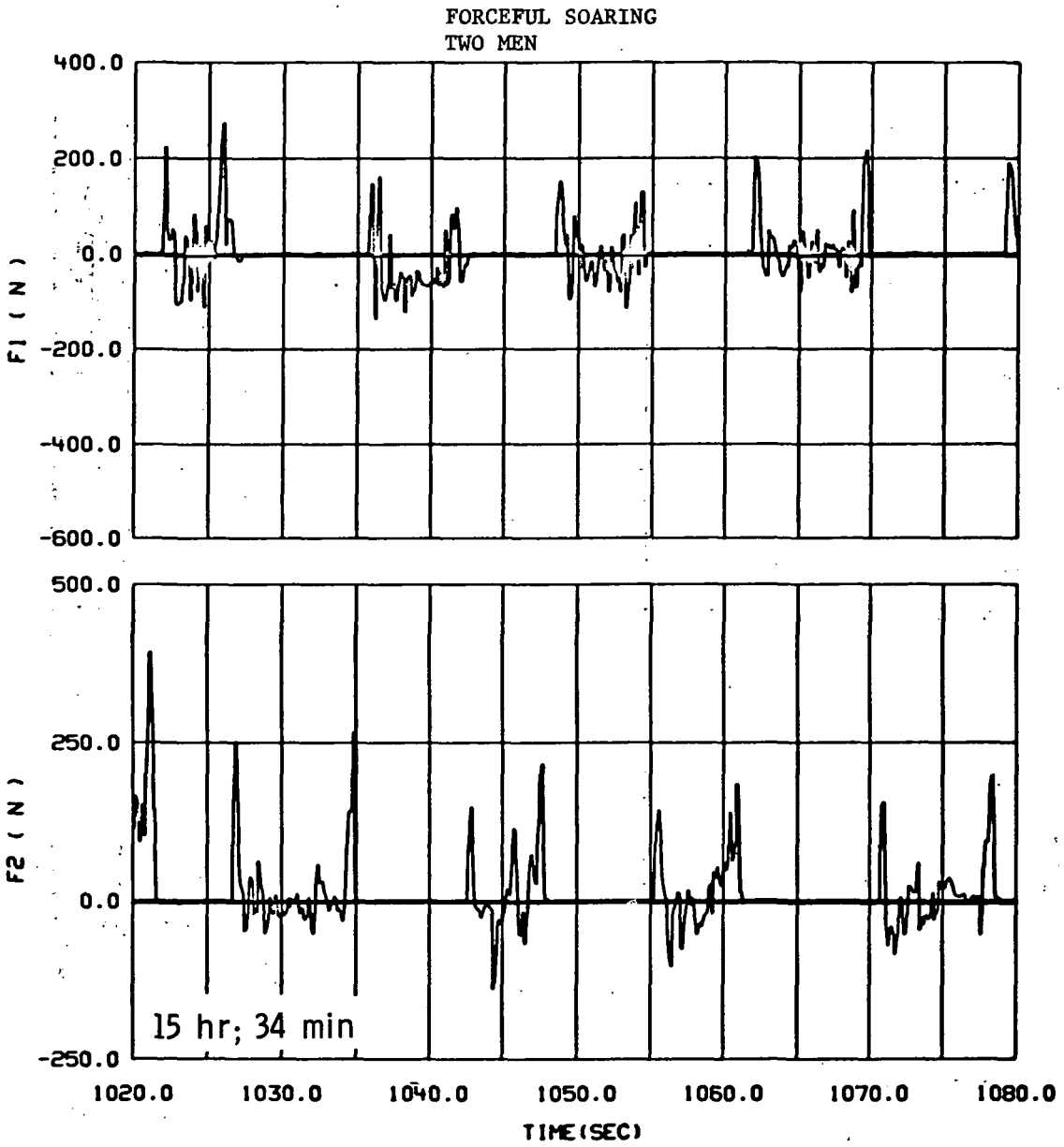

Figure 60.- Continued.

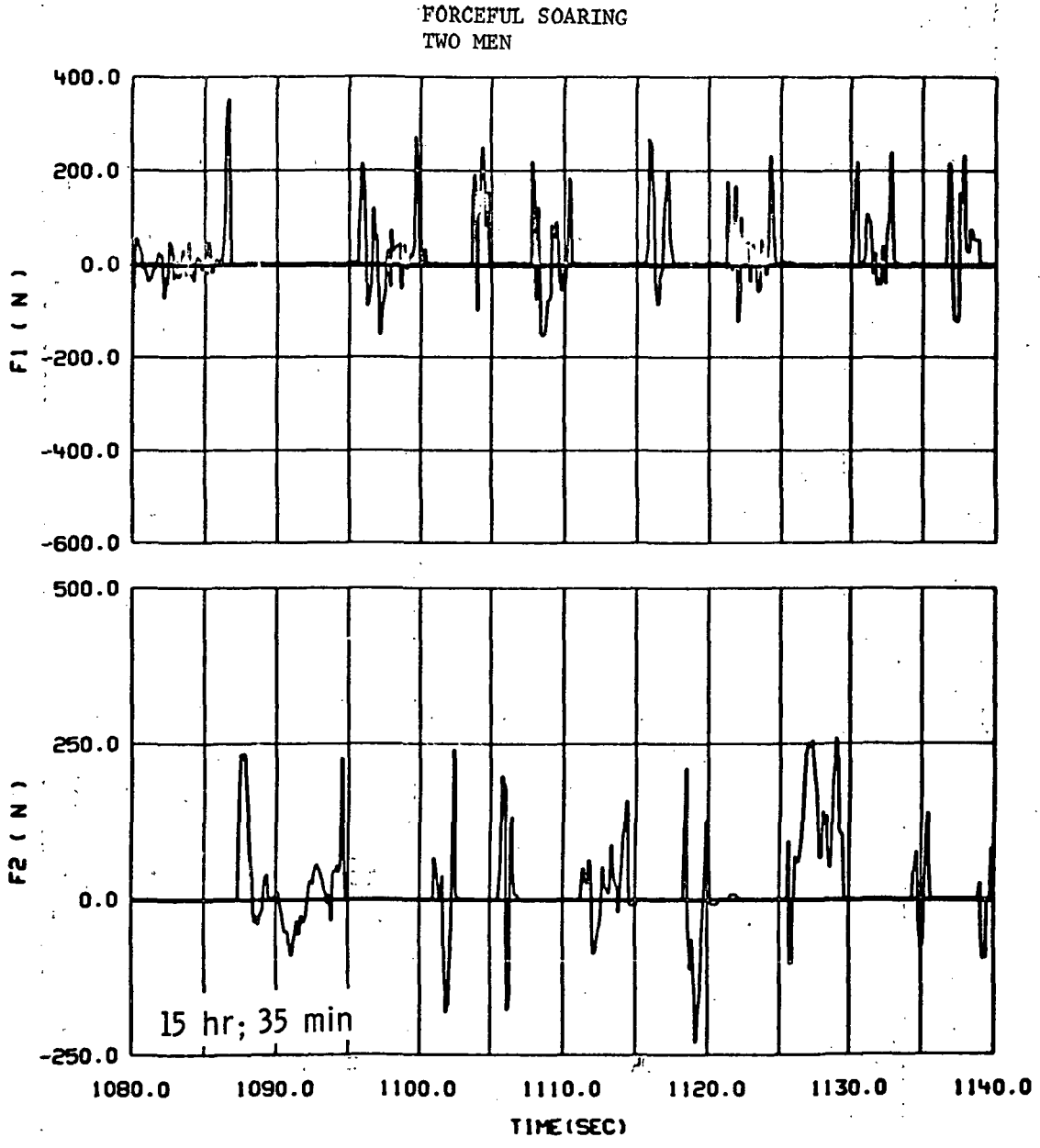

Figure 60.- Continued.

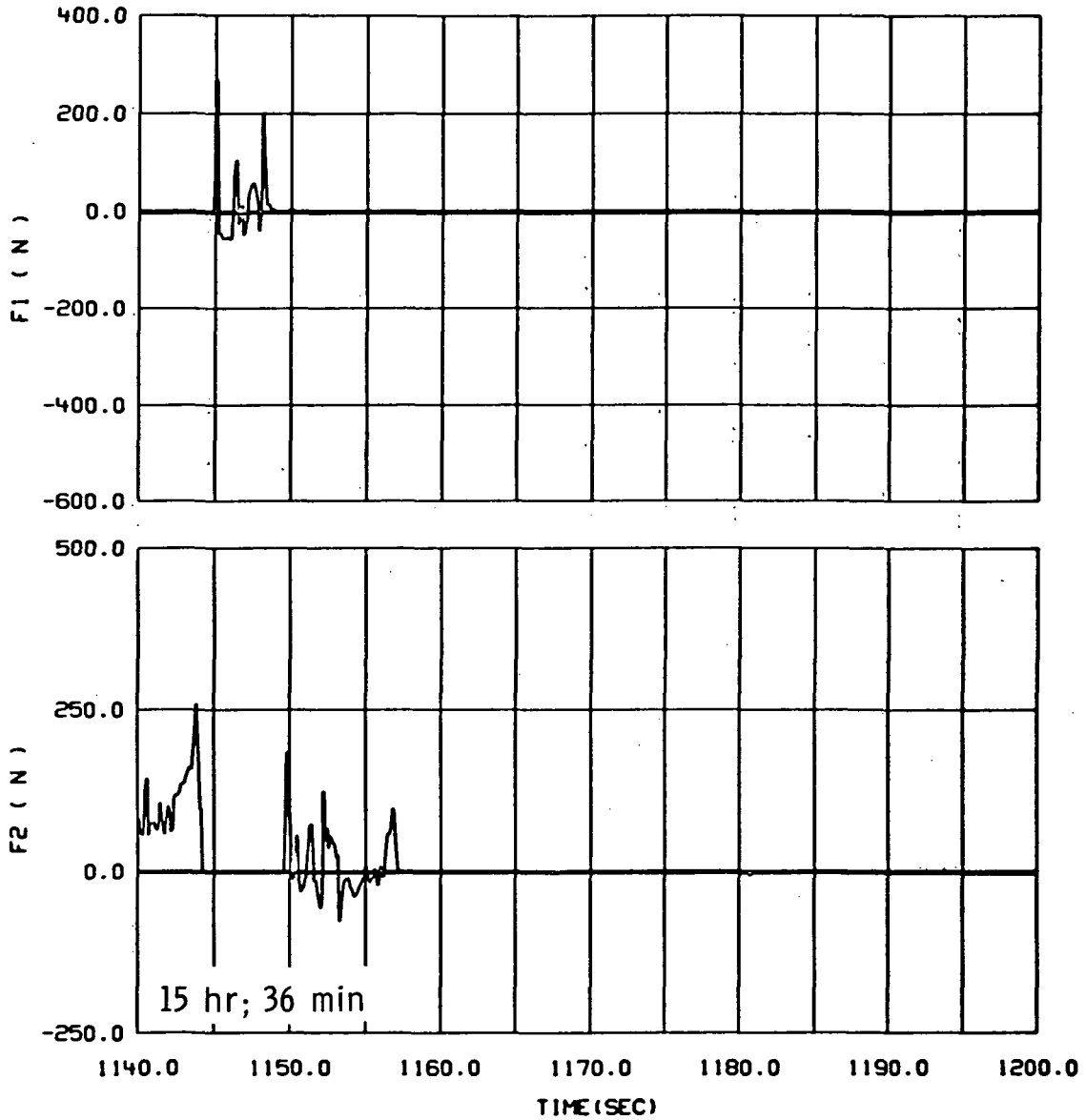

Figure 60.- Continued.

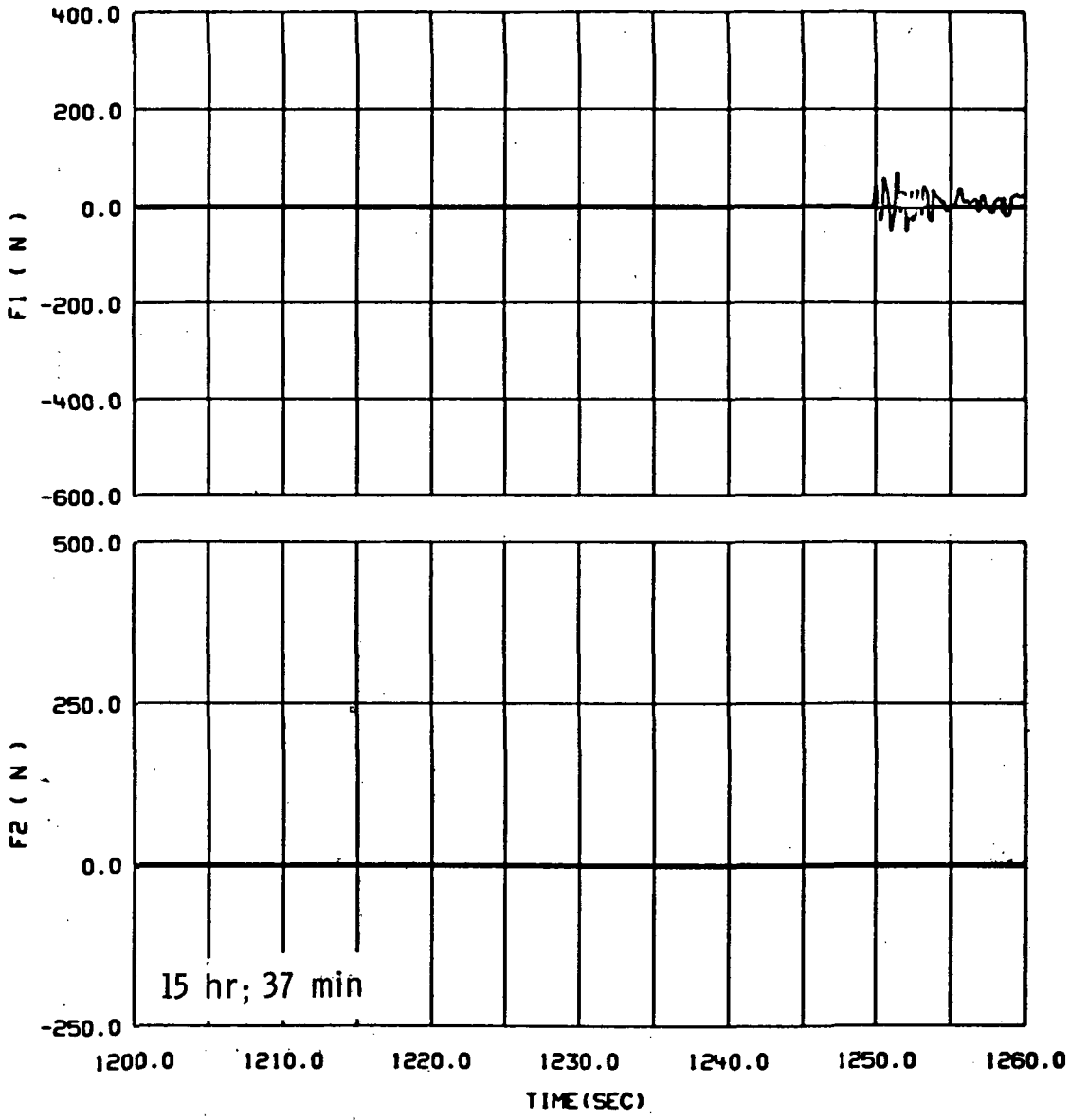

Figure 60.- Continued.

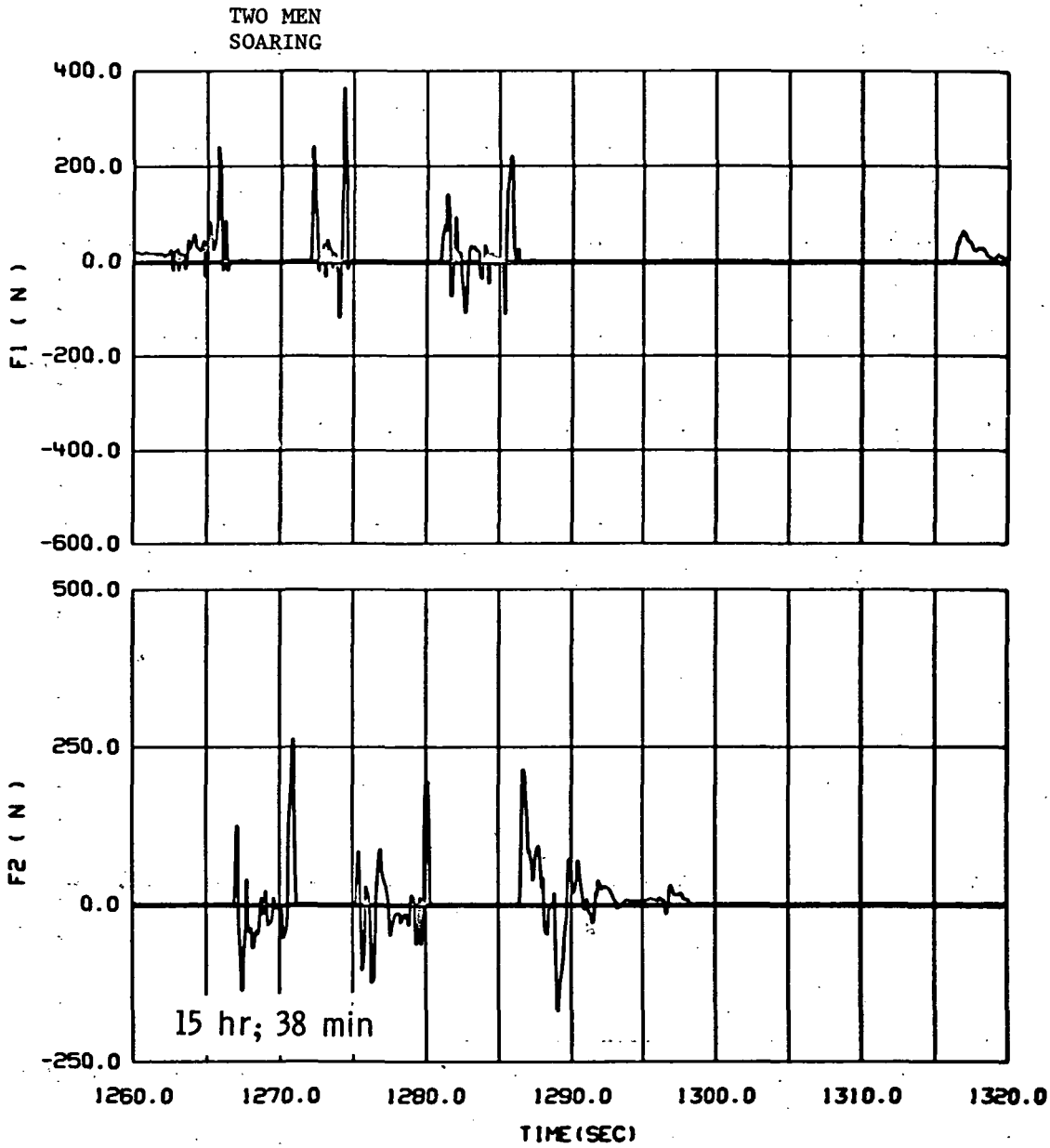

Figure 60.- Continued.

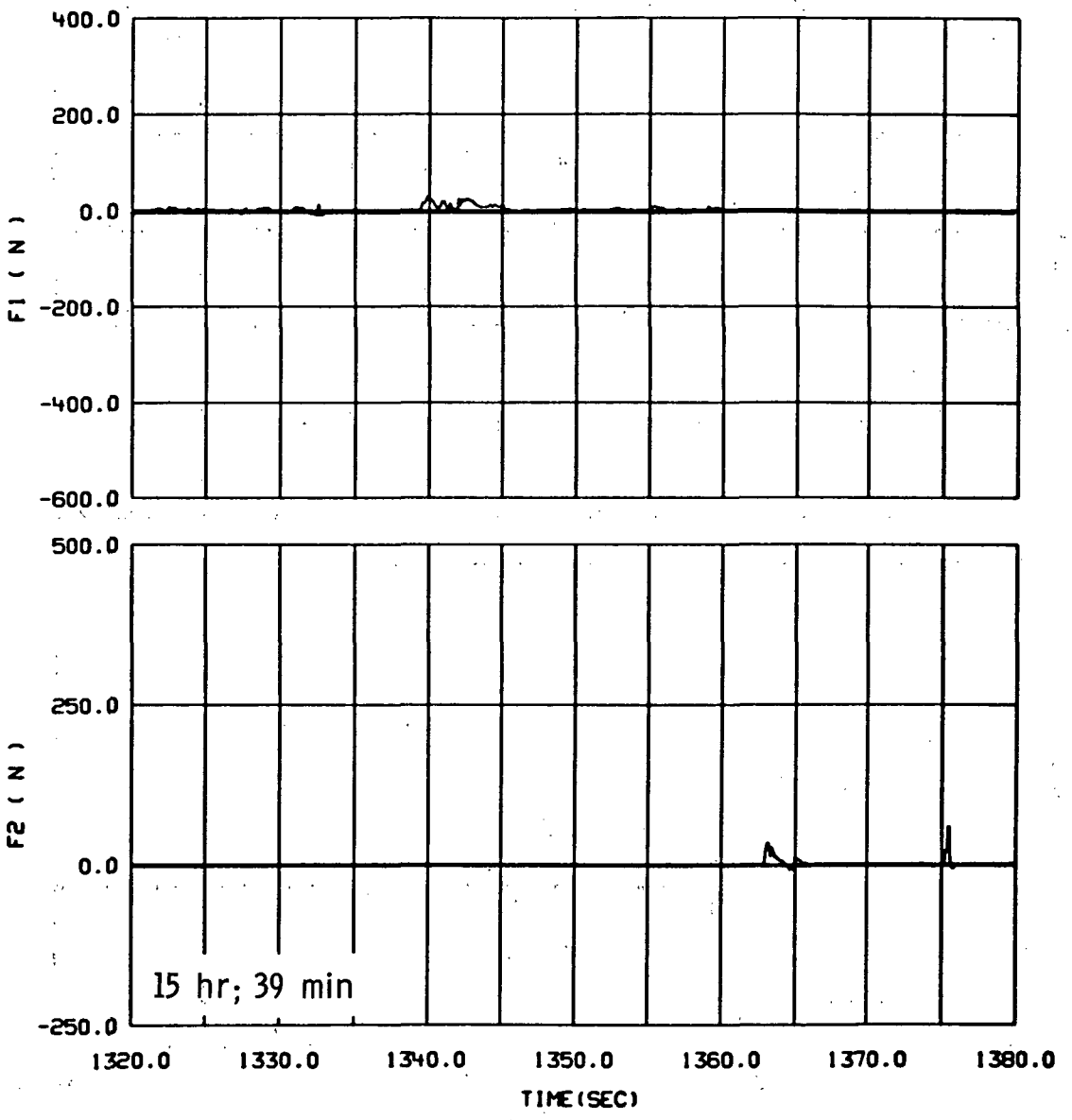

Figure 60.- Continued.

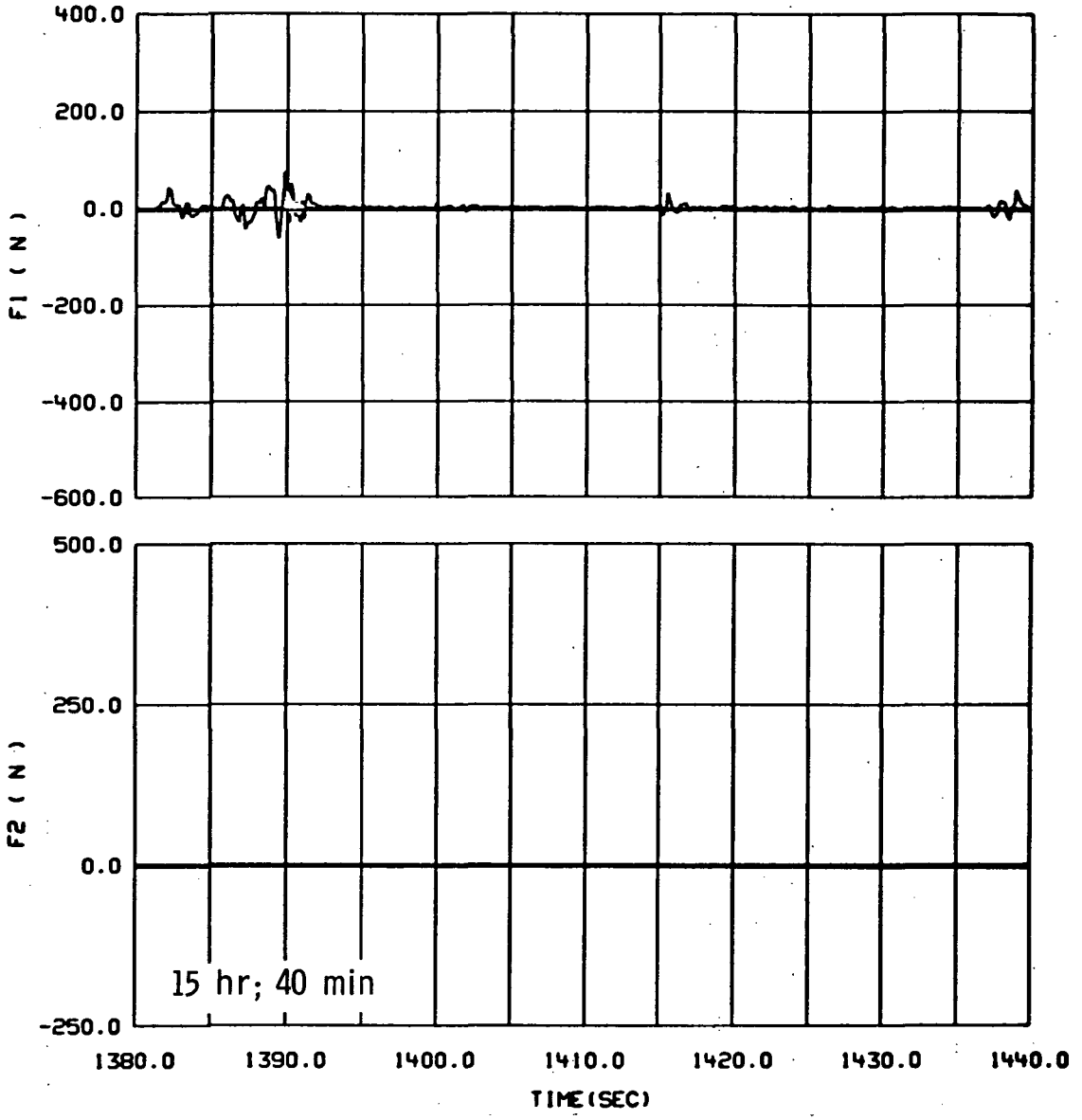

Figure 60.- Continued.

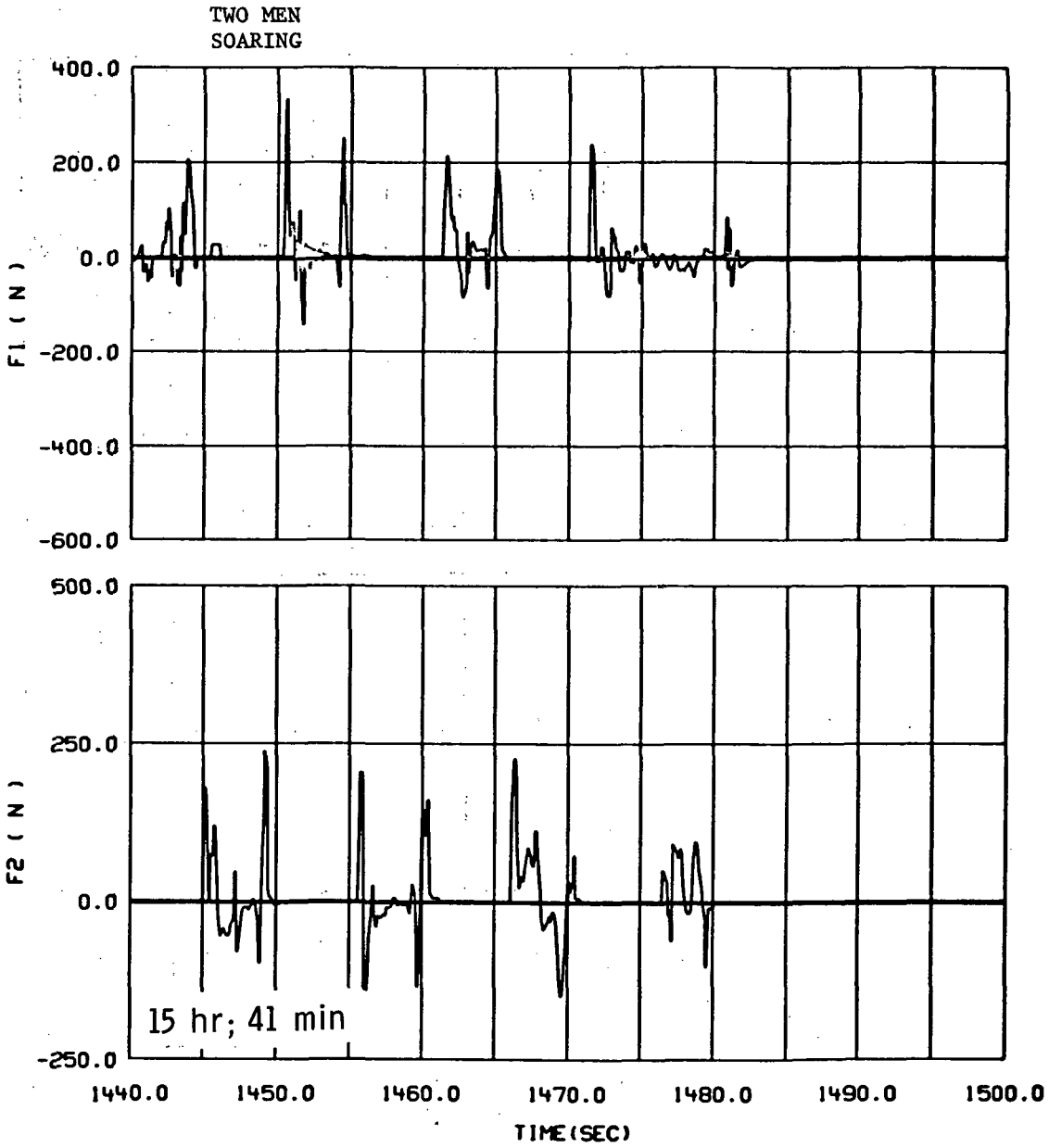

Figure 60.- Continued.

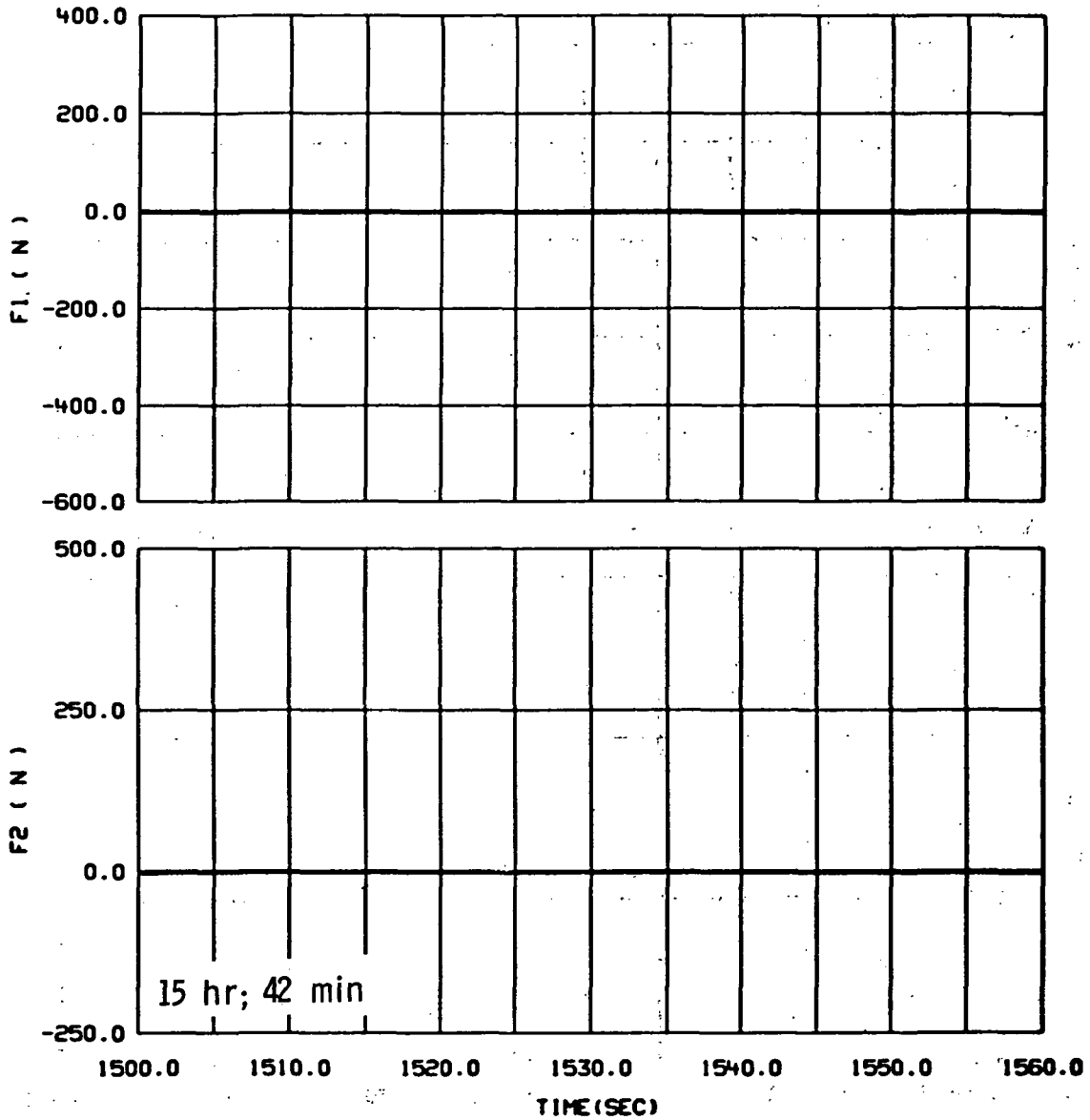

Figure 60.- Continued.

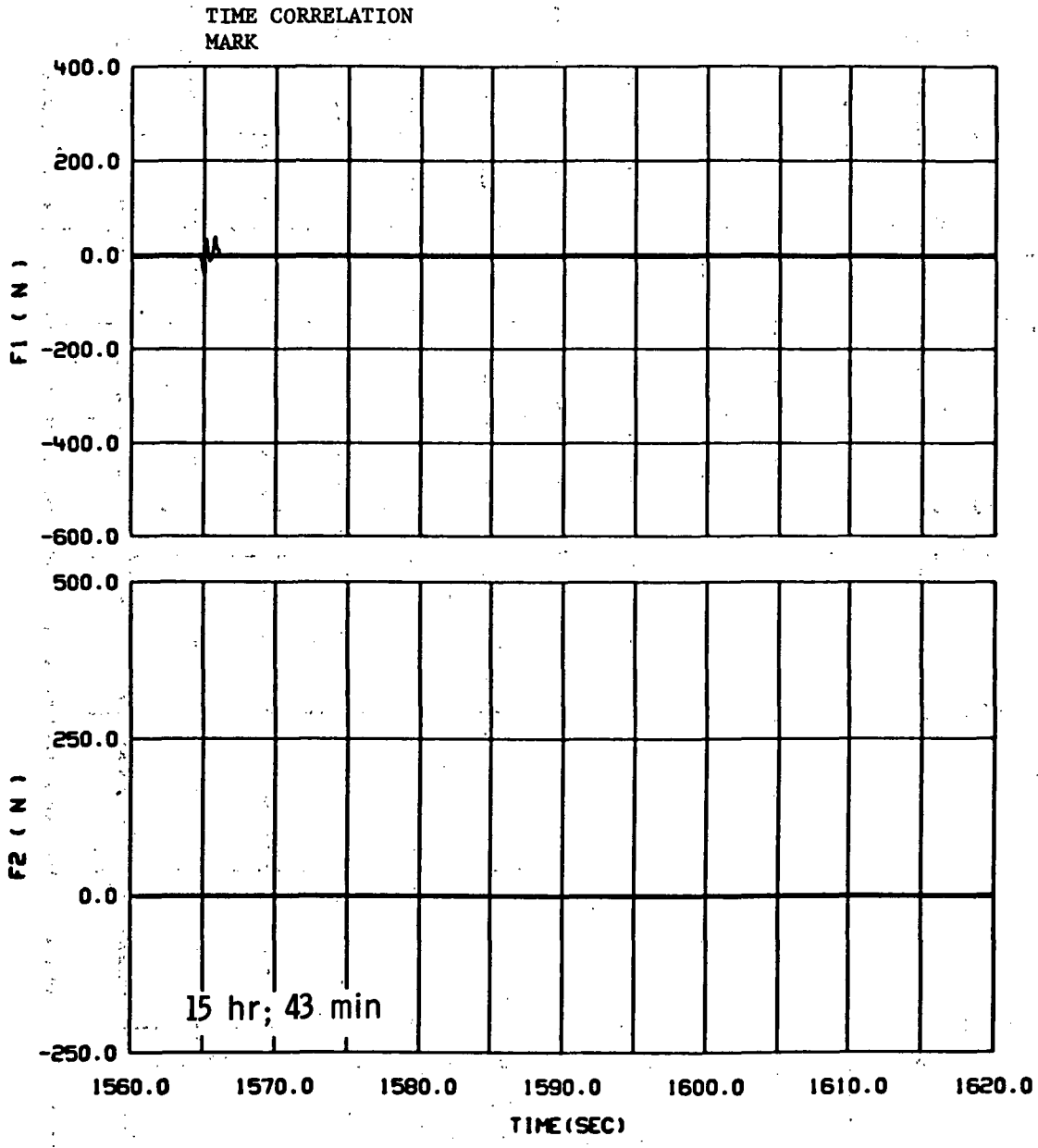

Figure 60.- Continued.

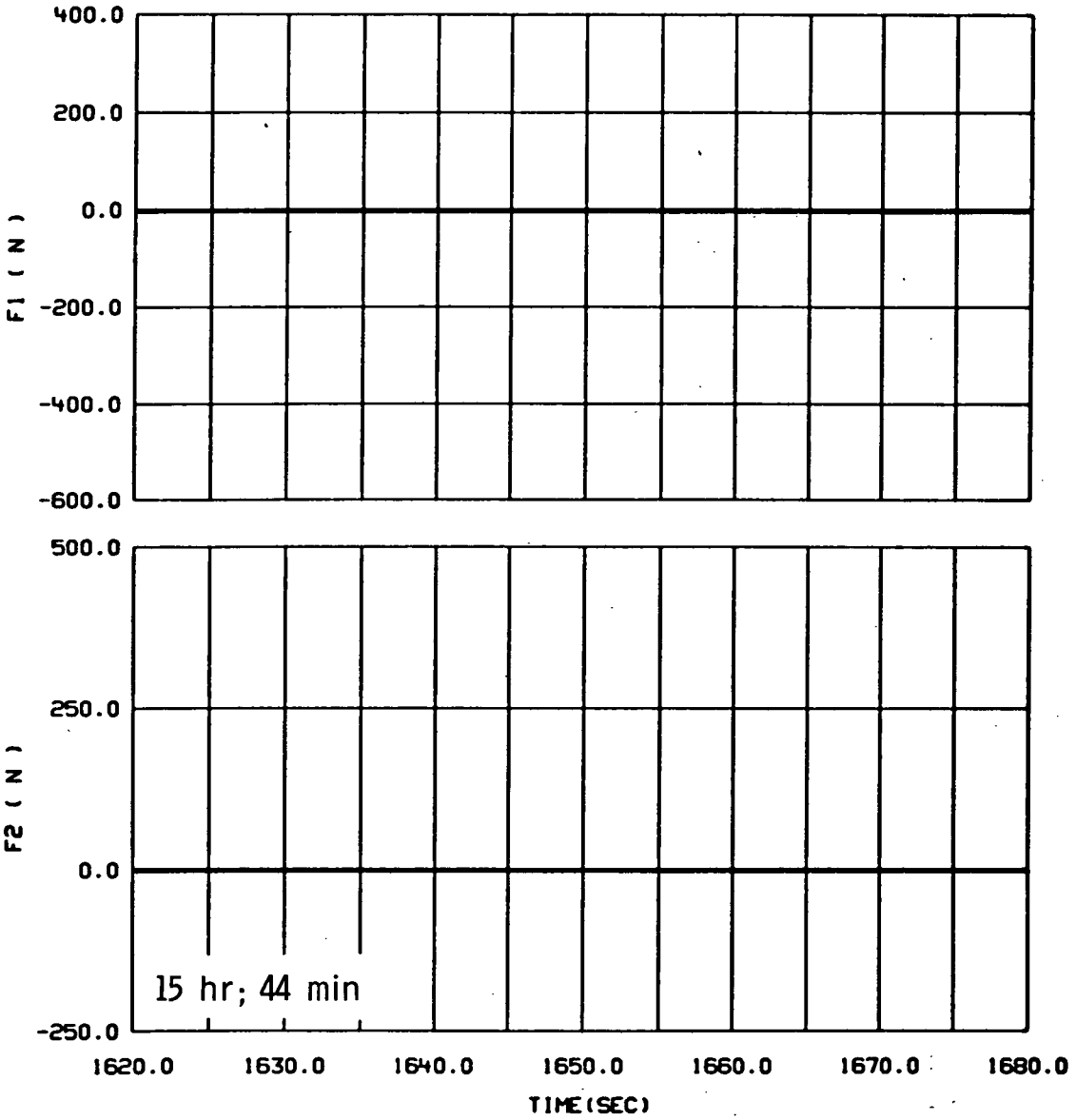

Figure 60.- Continued.

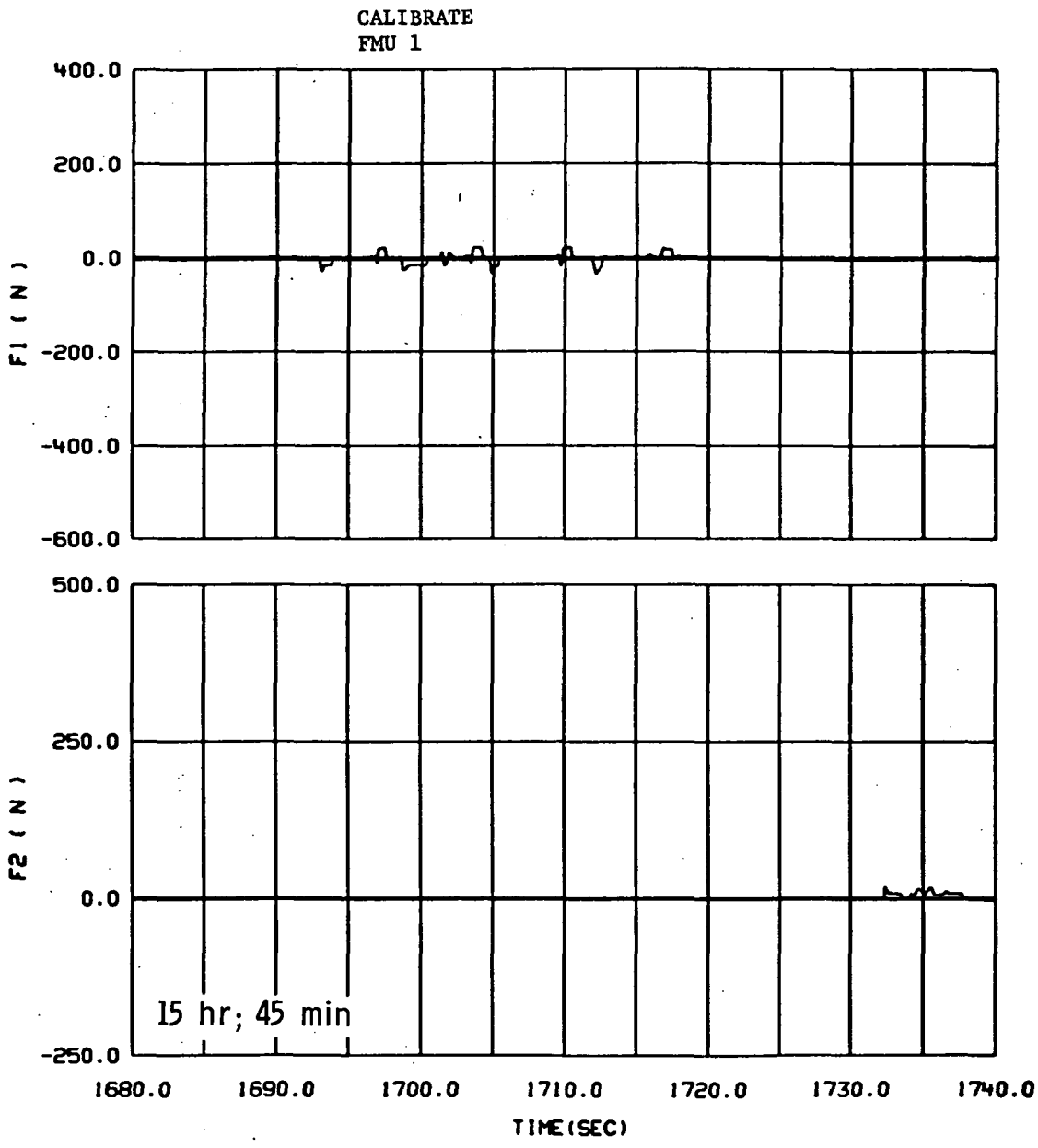

Figure 60.- Continued.

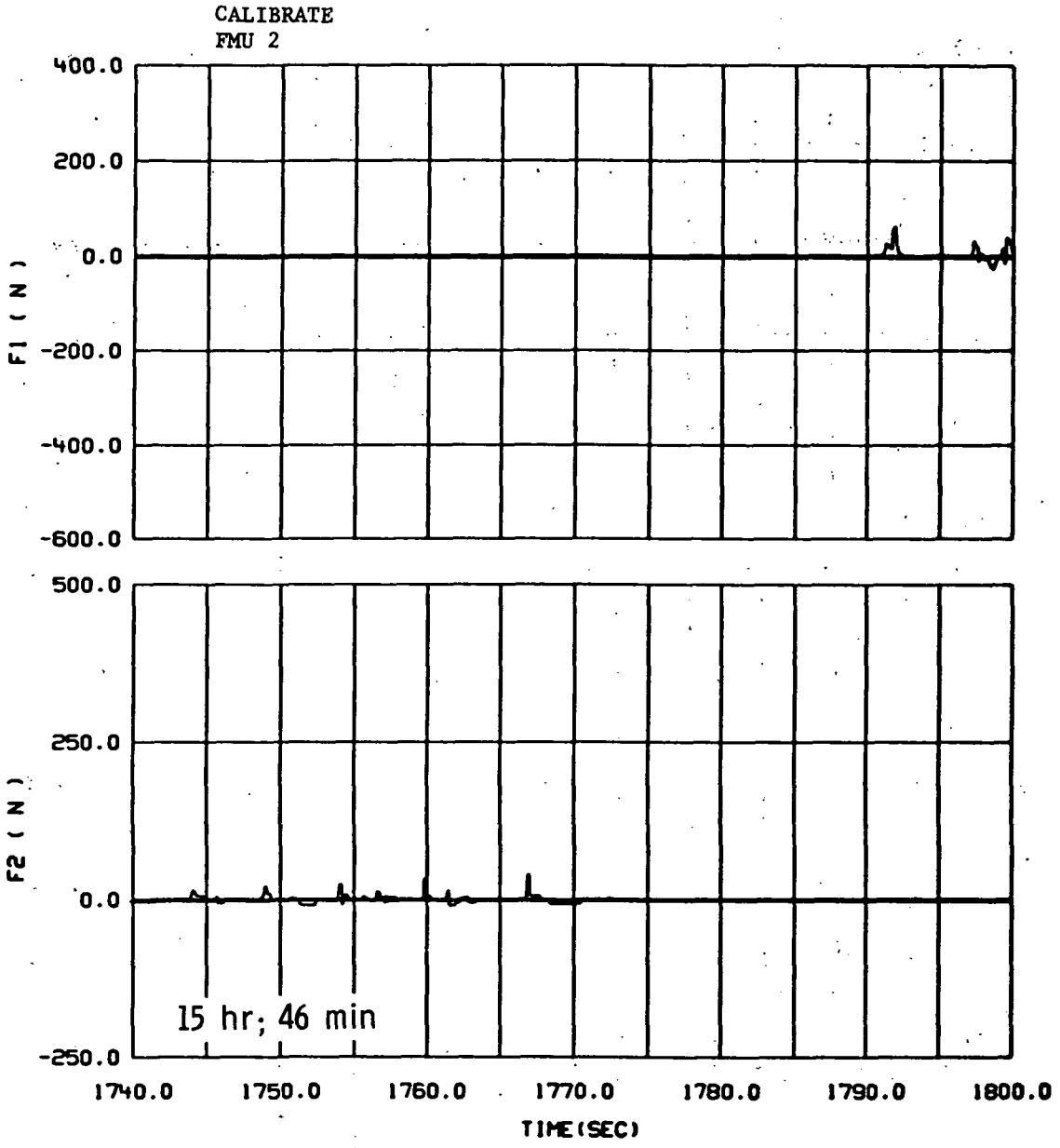

Figure 60.- Continued.

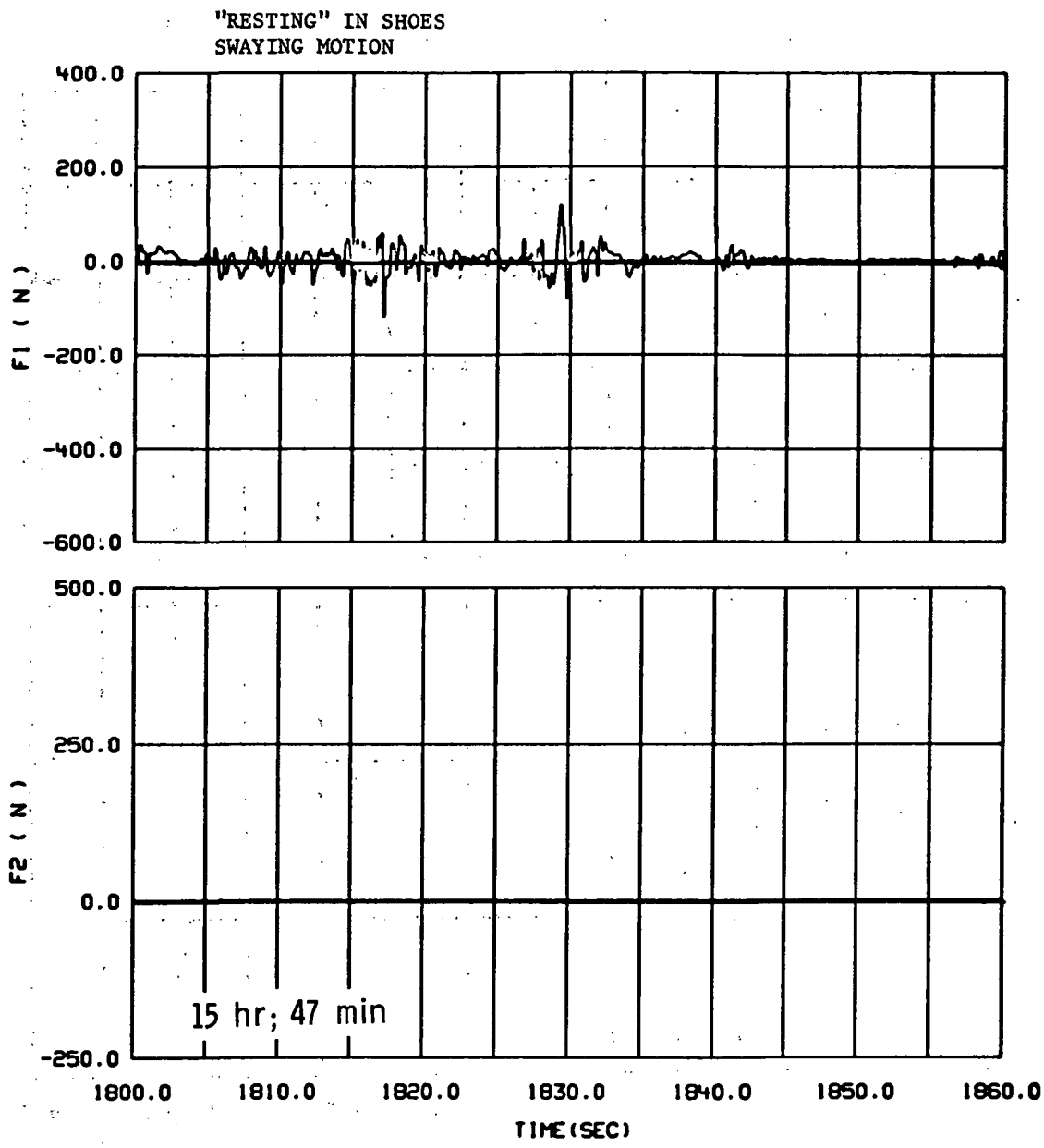

Figure 60.- Continued.

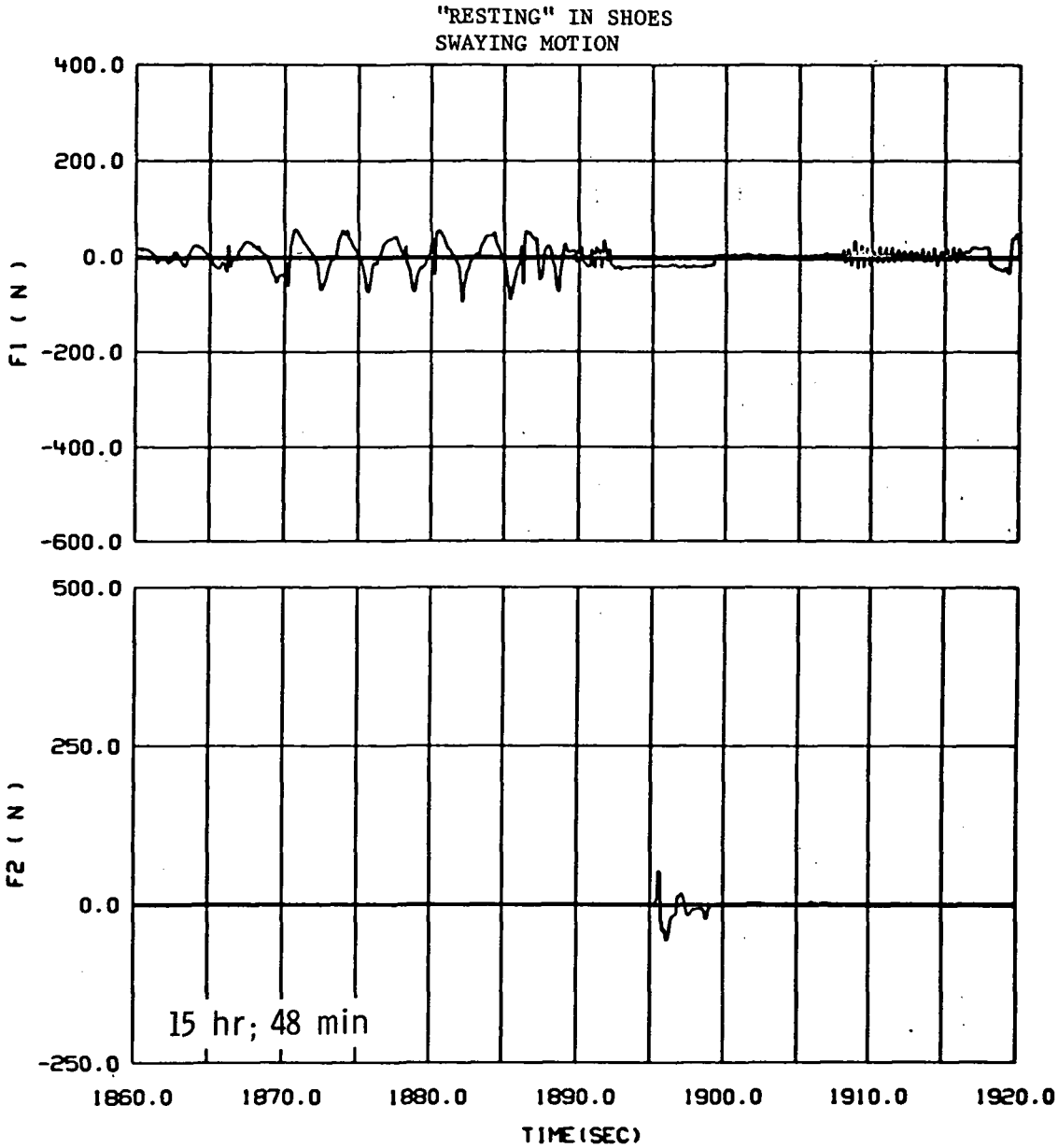

Figure 60.- Continued.

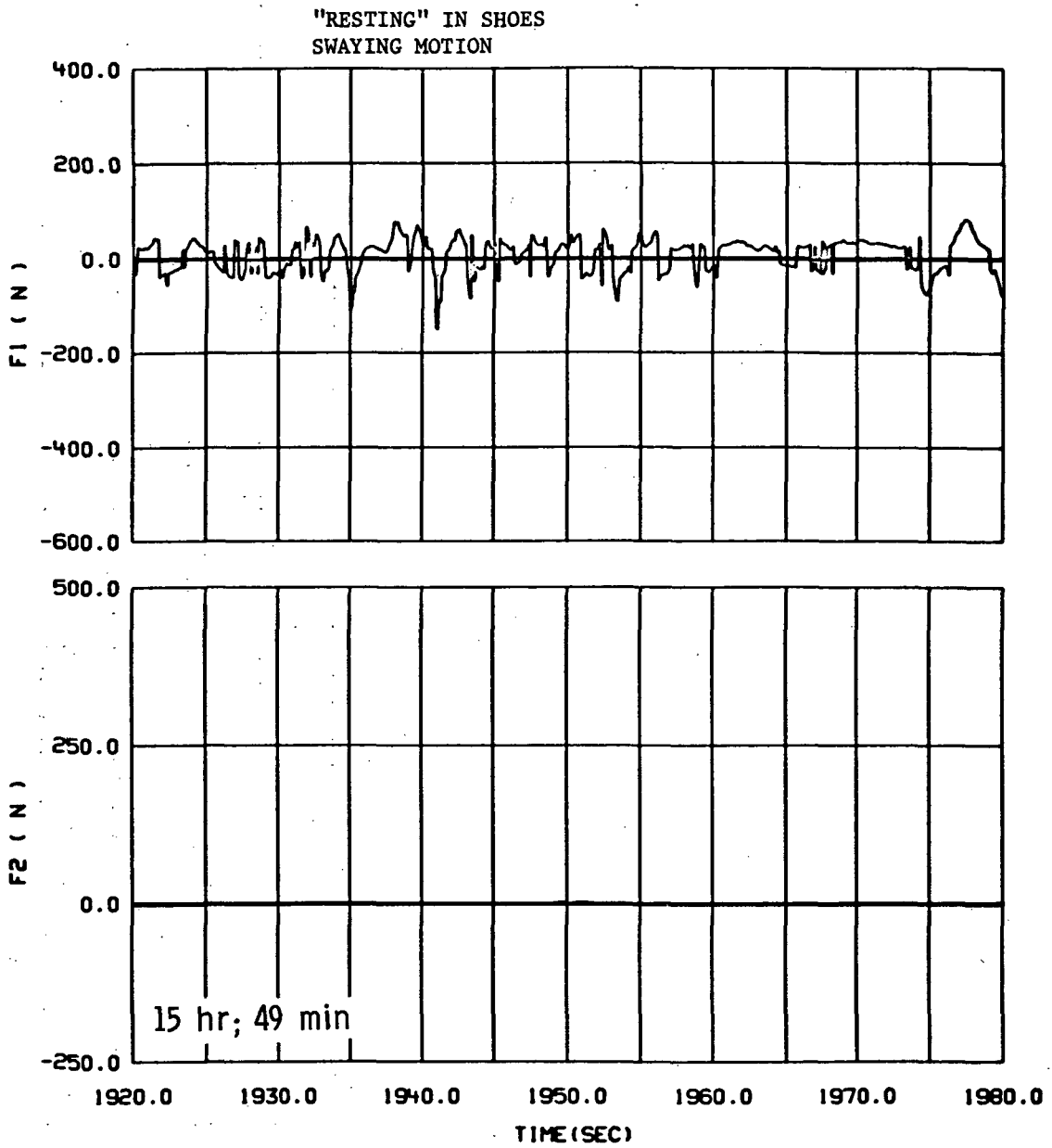

Figure 60.- Continued.

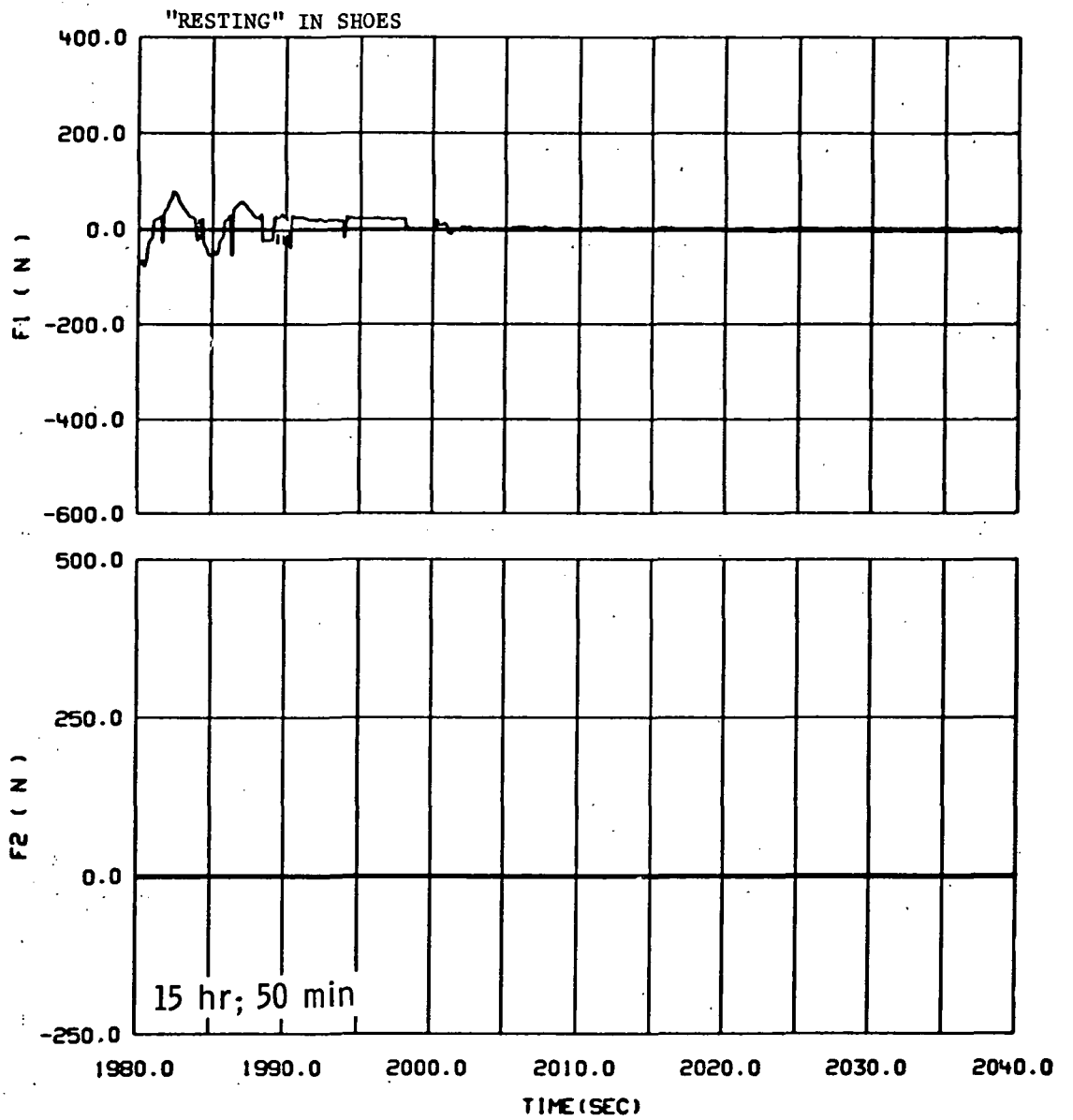

Figure 60.- Continued.

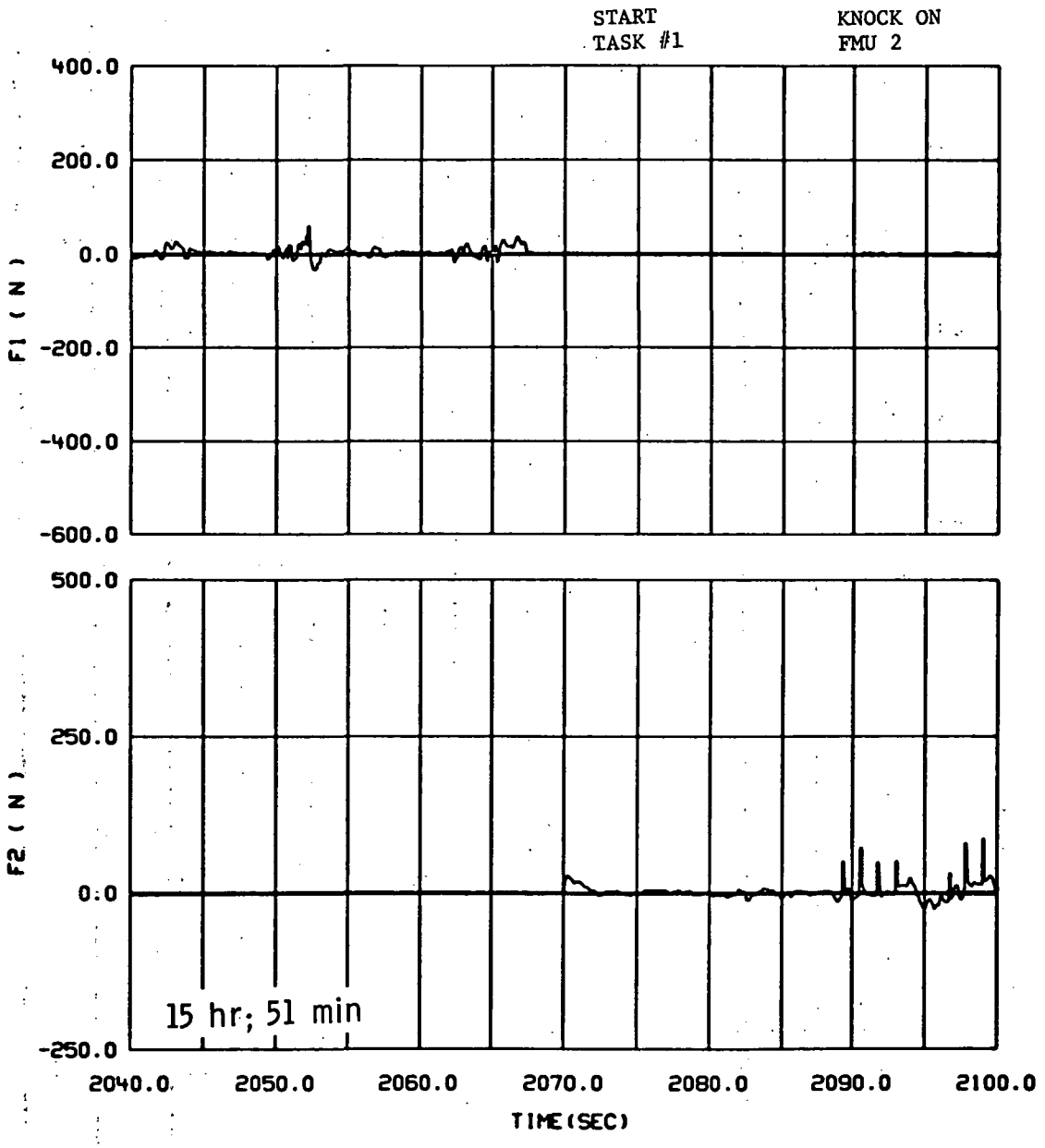

Figure 60.- Continued.

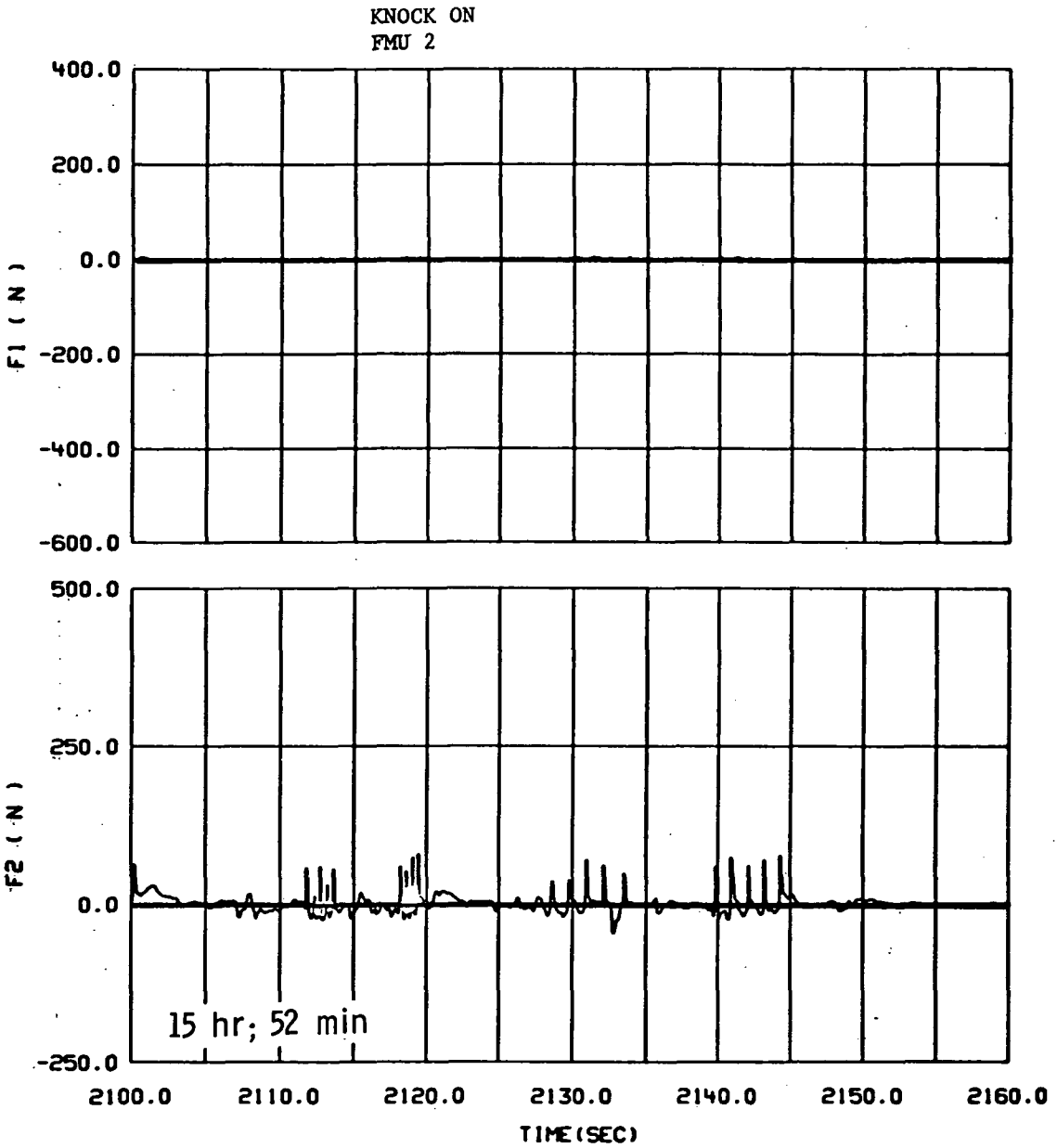

Figure 60.- Continued.

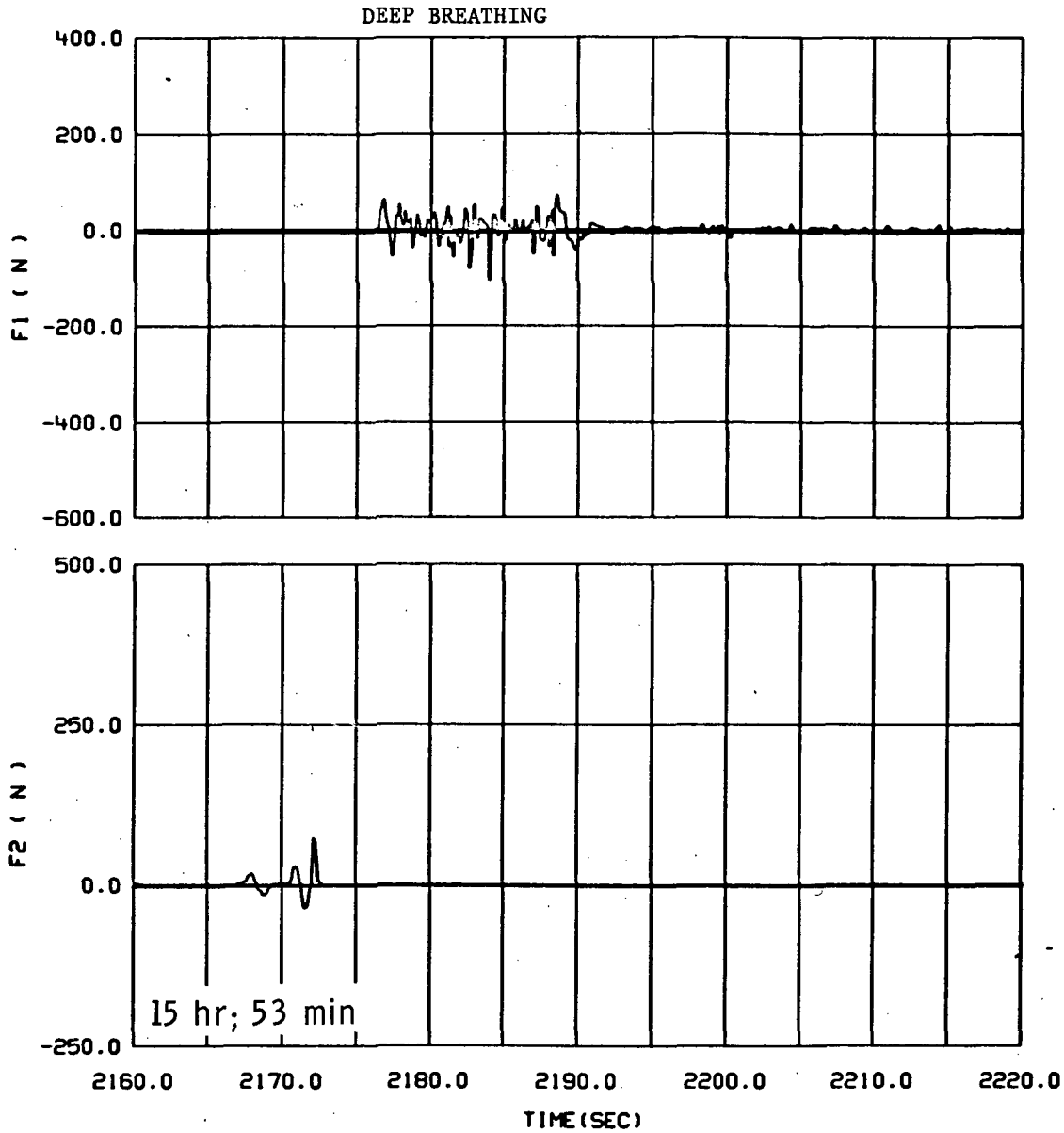

Figure 60.- Continued.

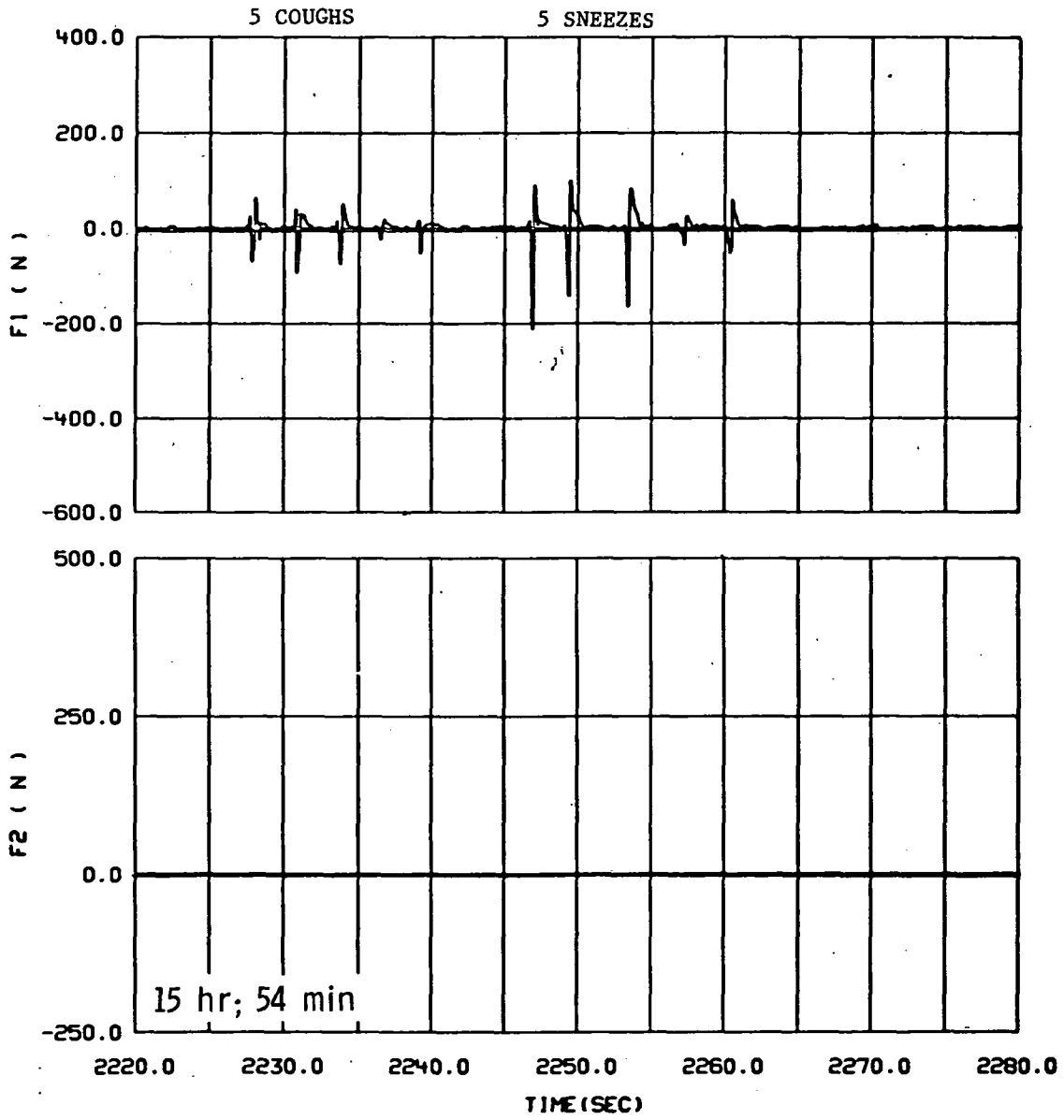

Figure 60.- Continued.

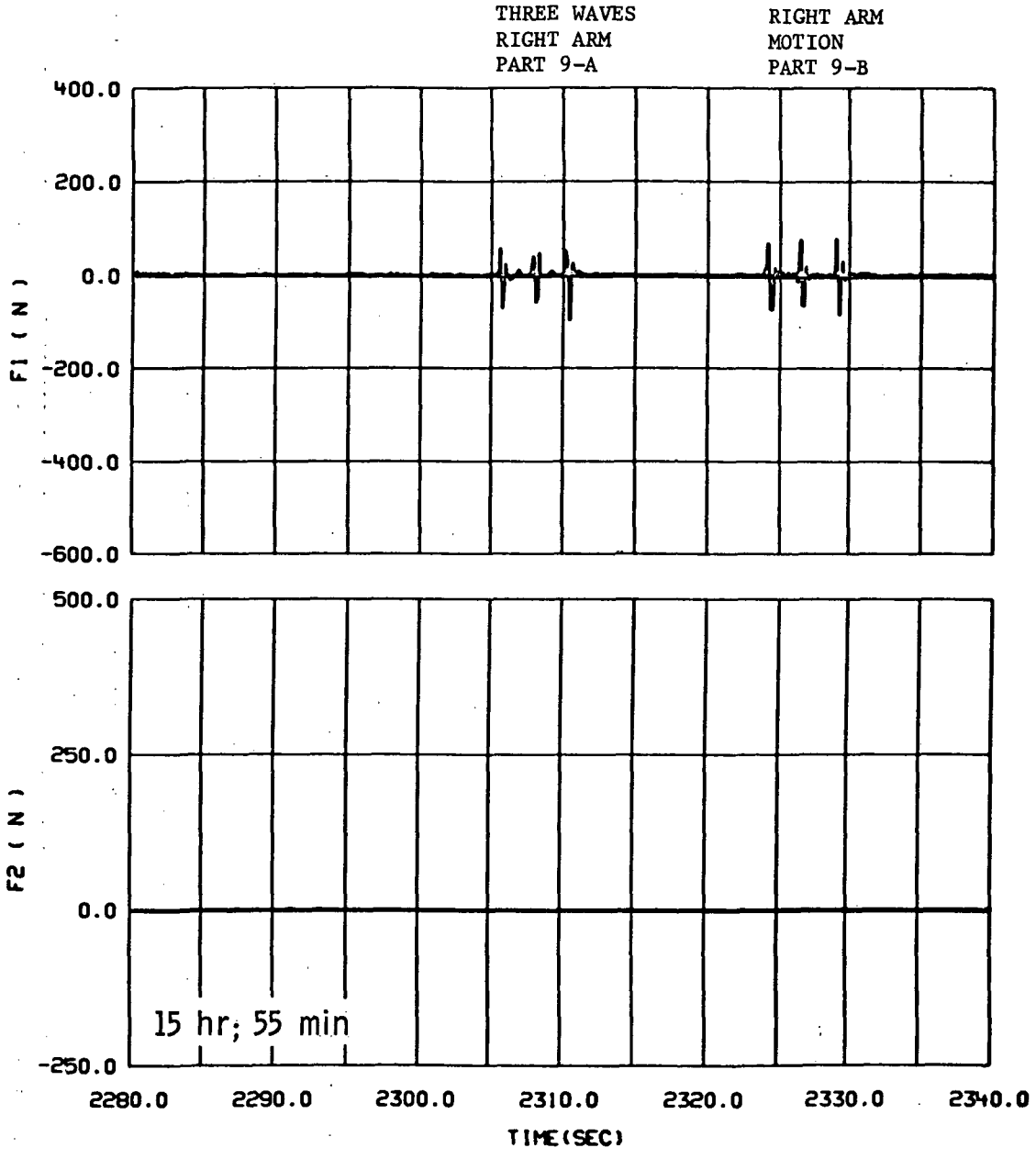

Figure 60.- Continued.

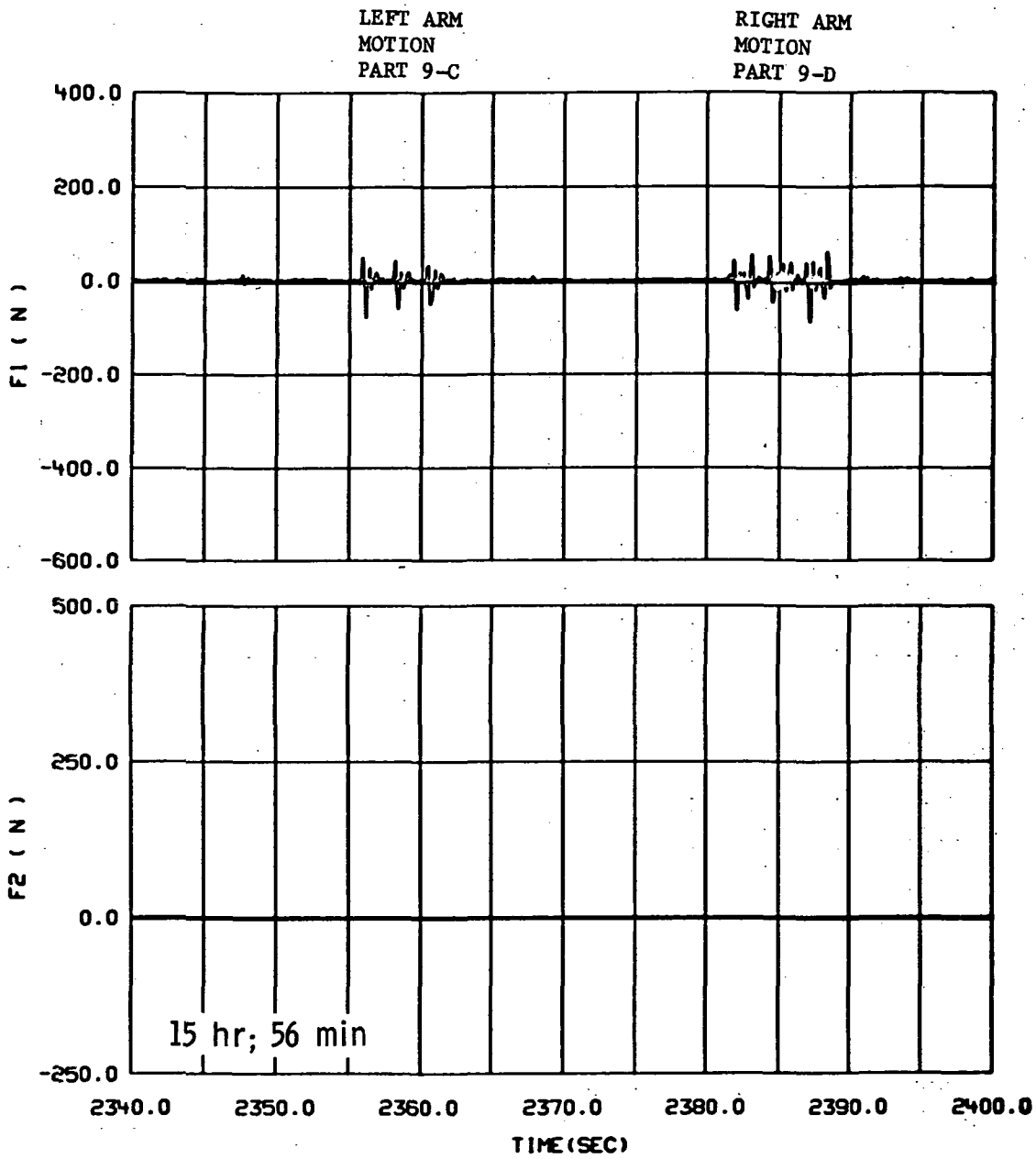

Figure 60.- Continued.

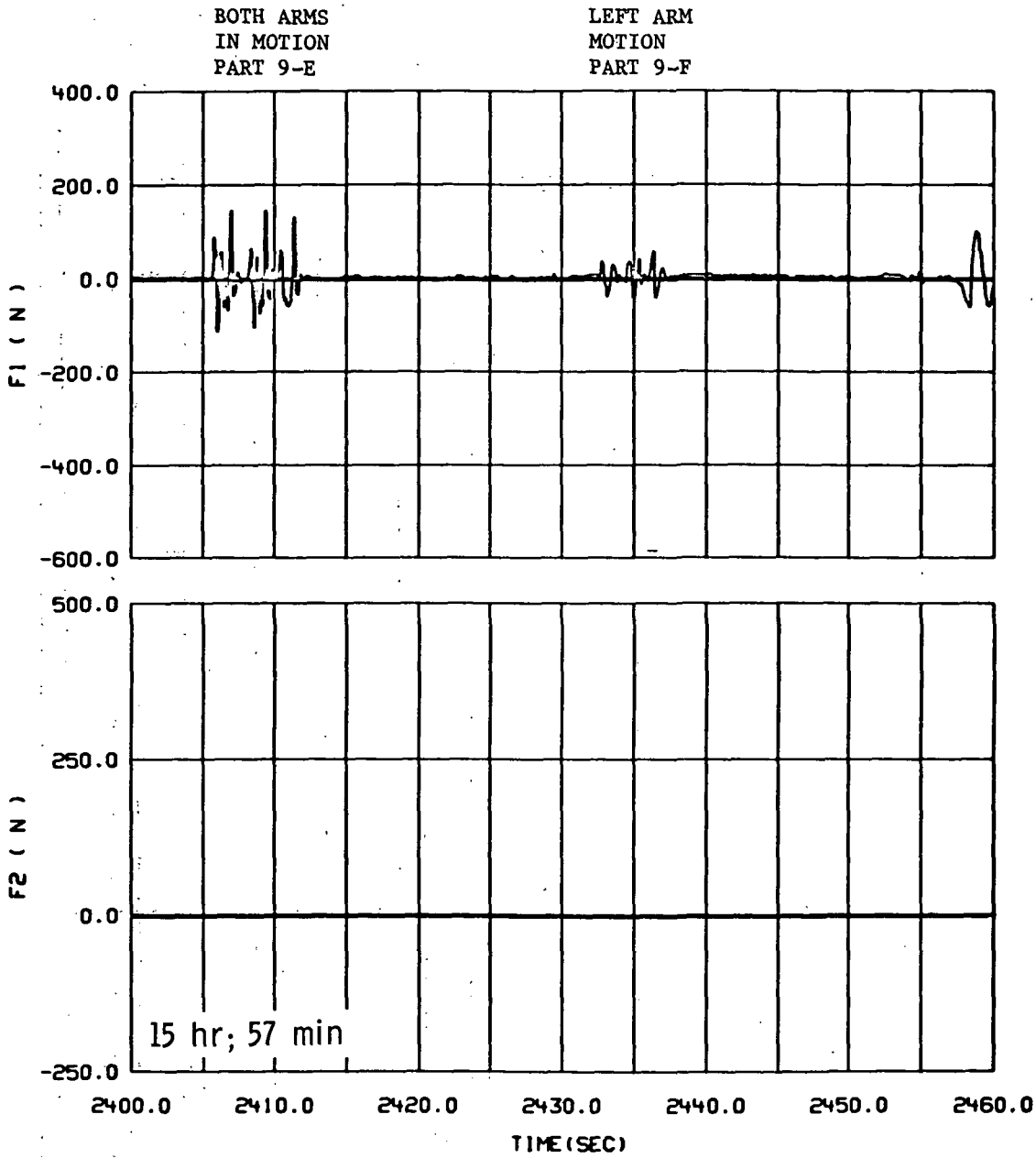

Figure 60.- Continued.

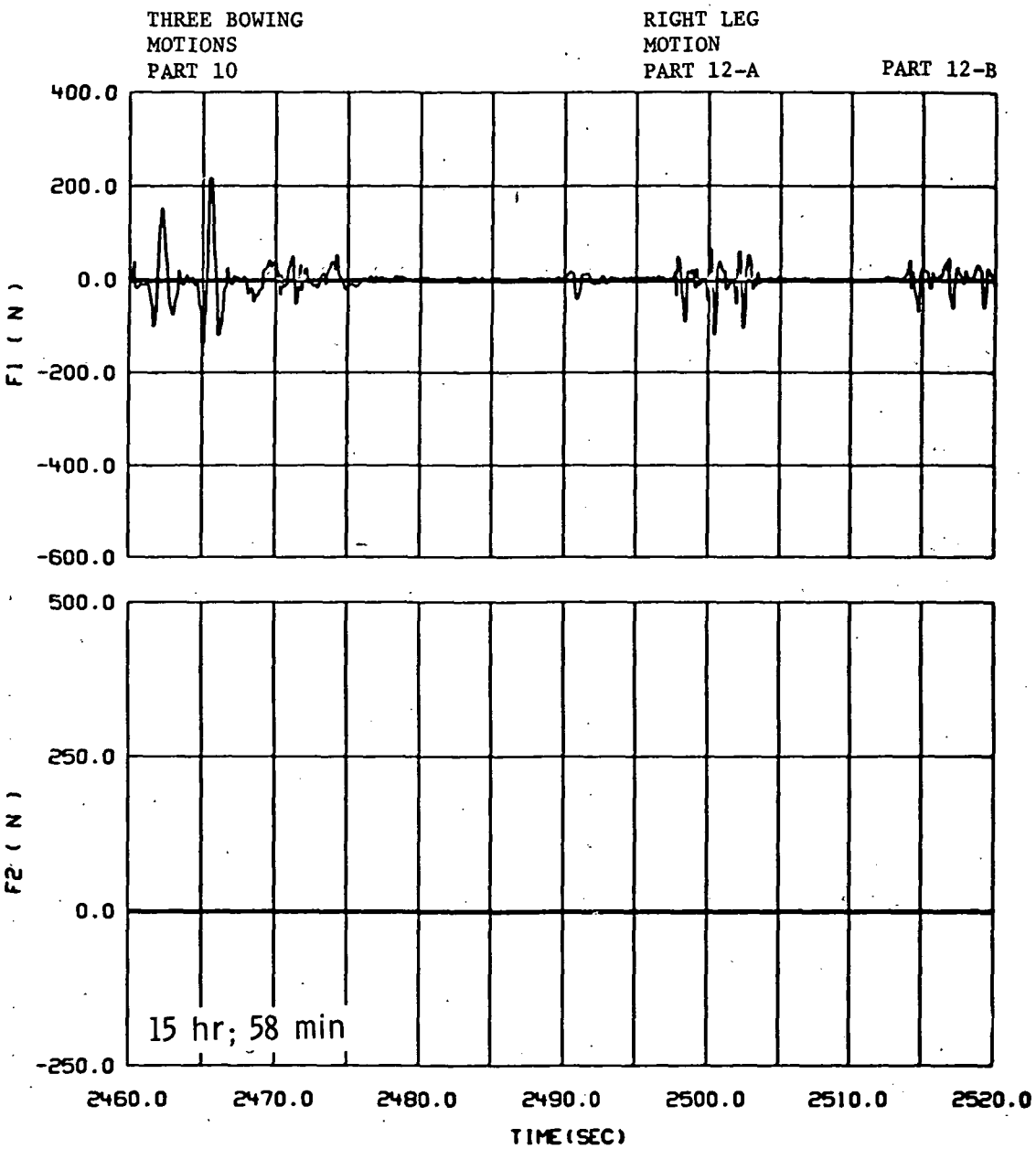

Figure 60.- Continued.

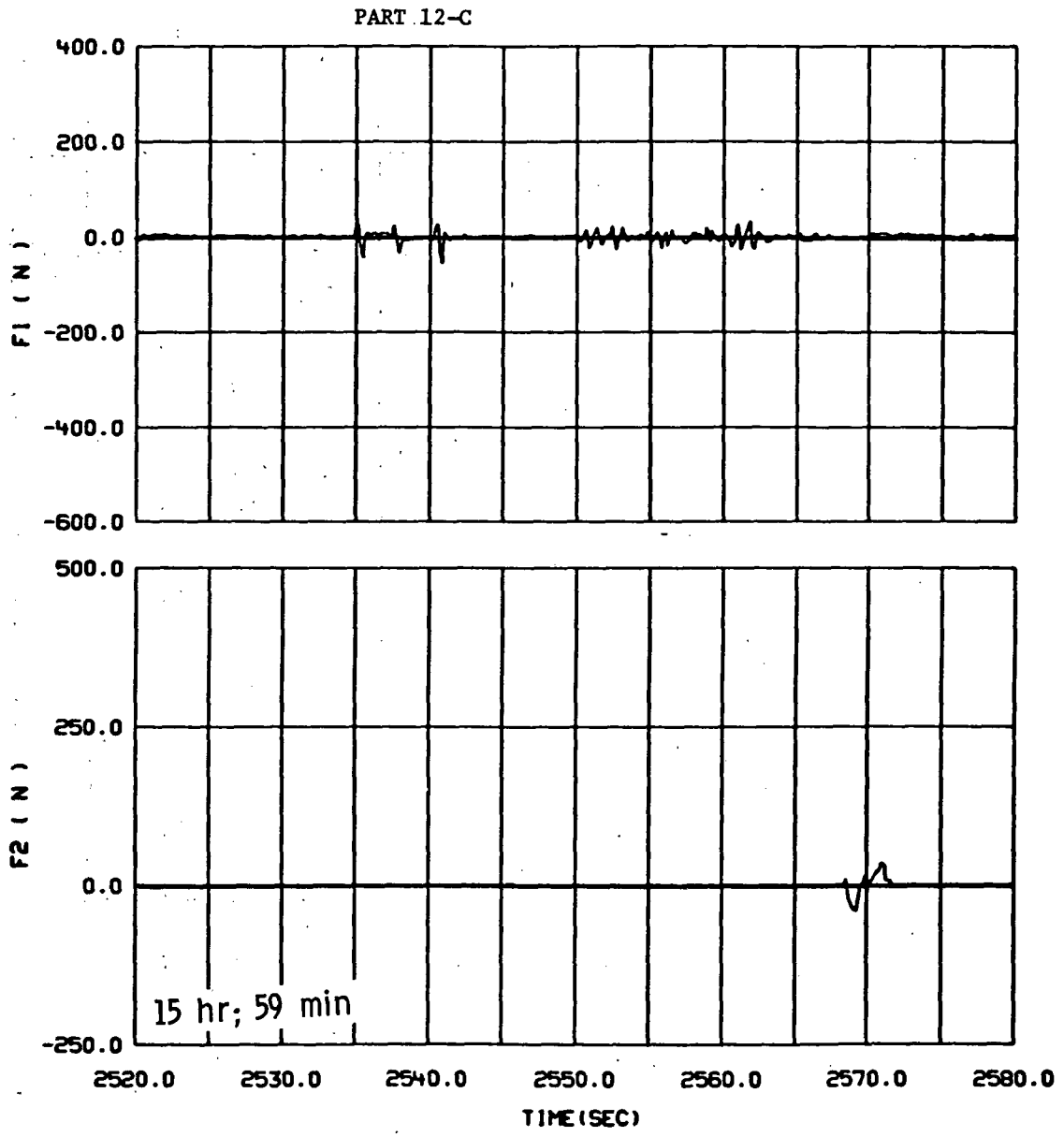

Figure 60.- Continued.

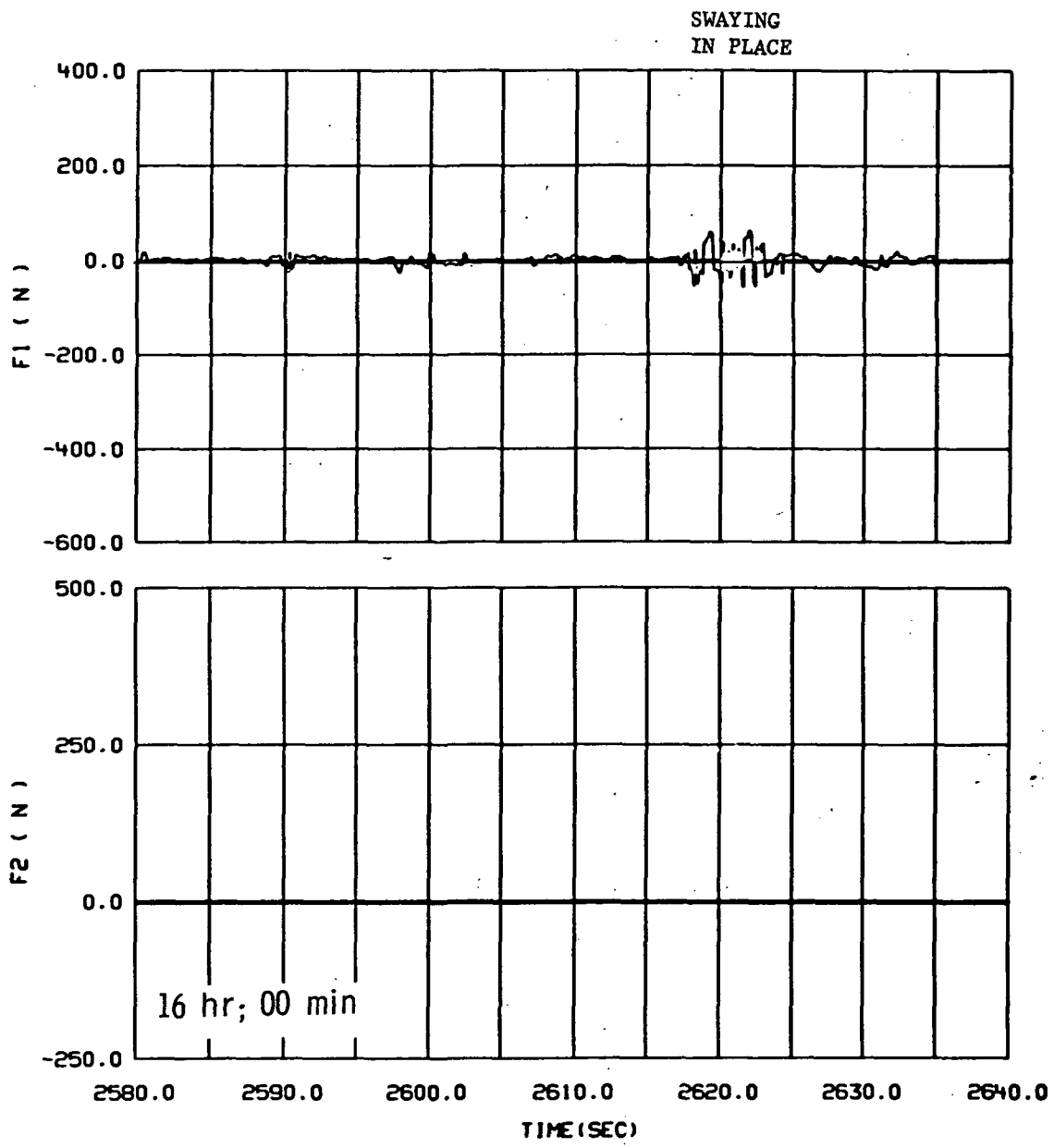

Figure 60.- Continued.

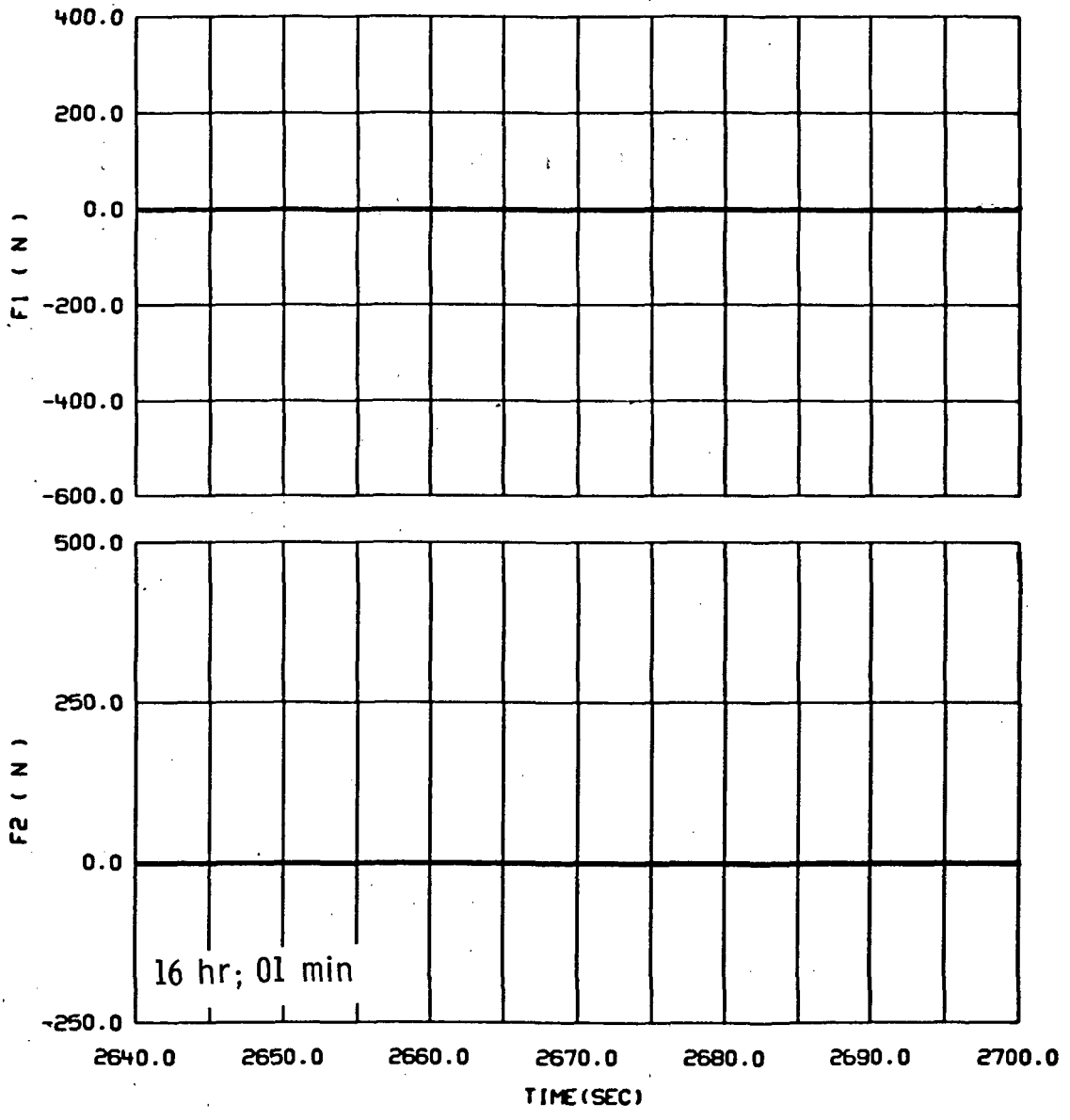

Figure 60.- Continued.

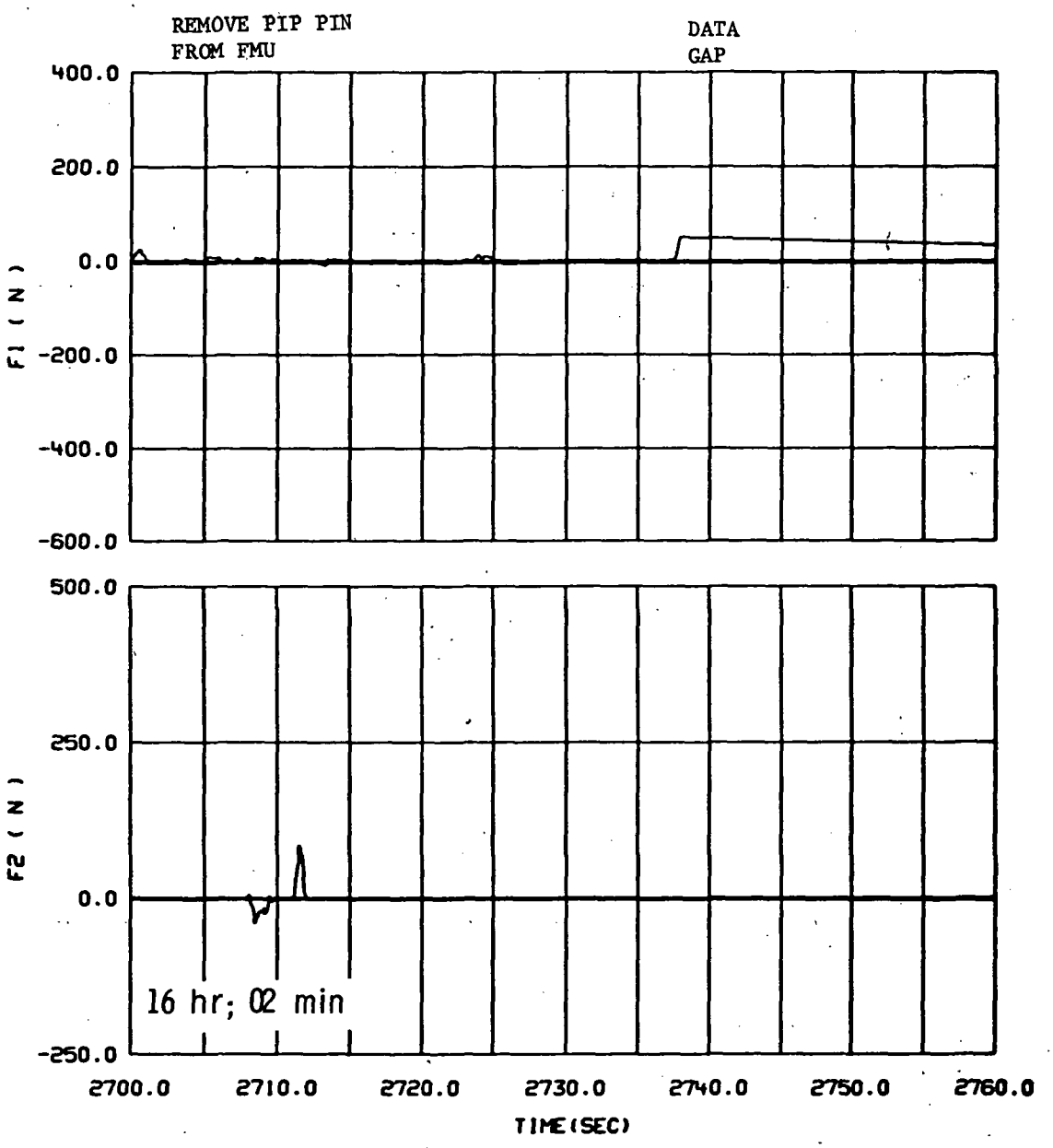

Figure 60.- Continued.

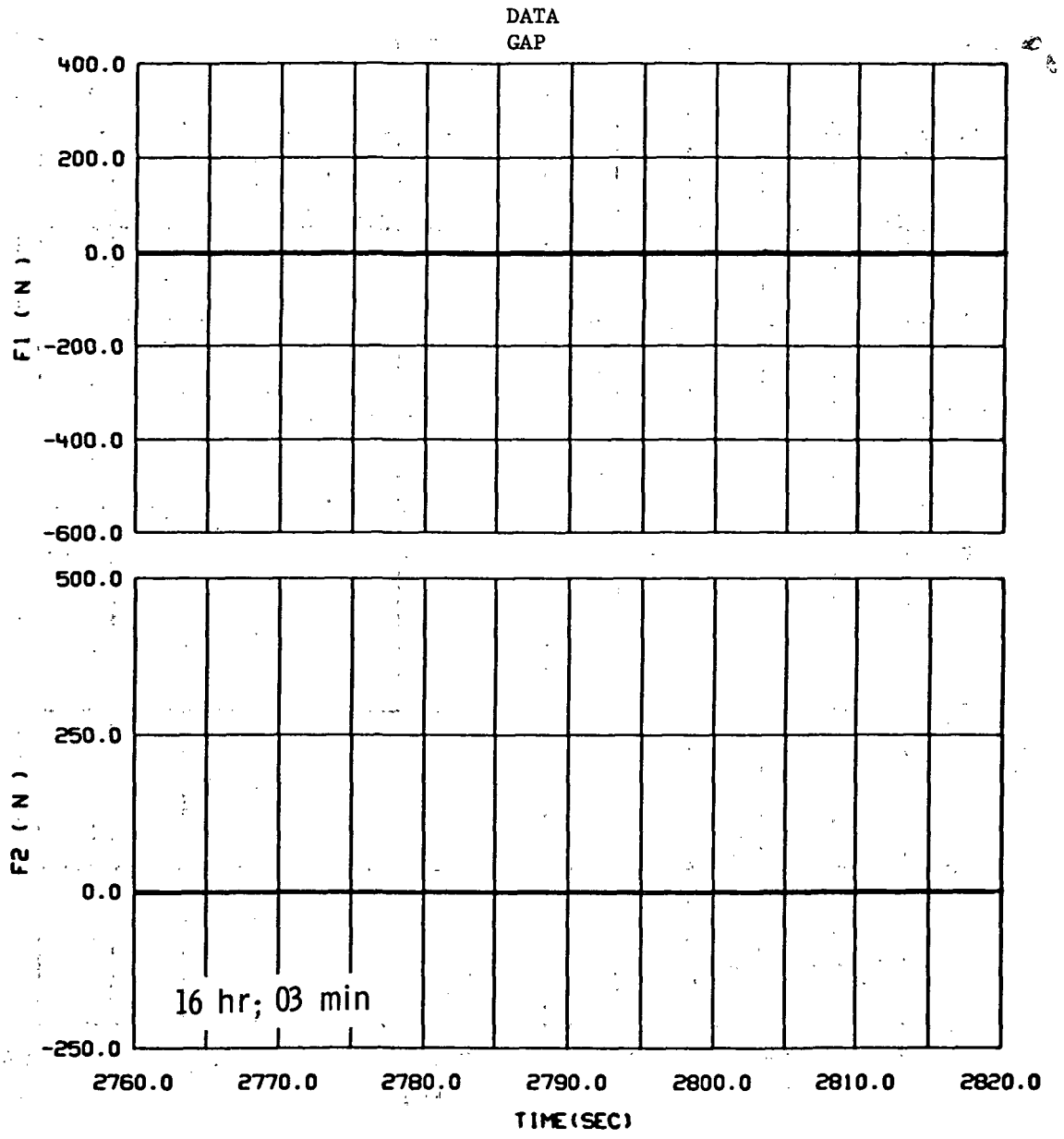

Figure 60.- Continued.

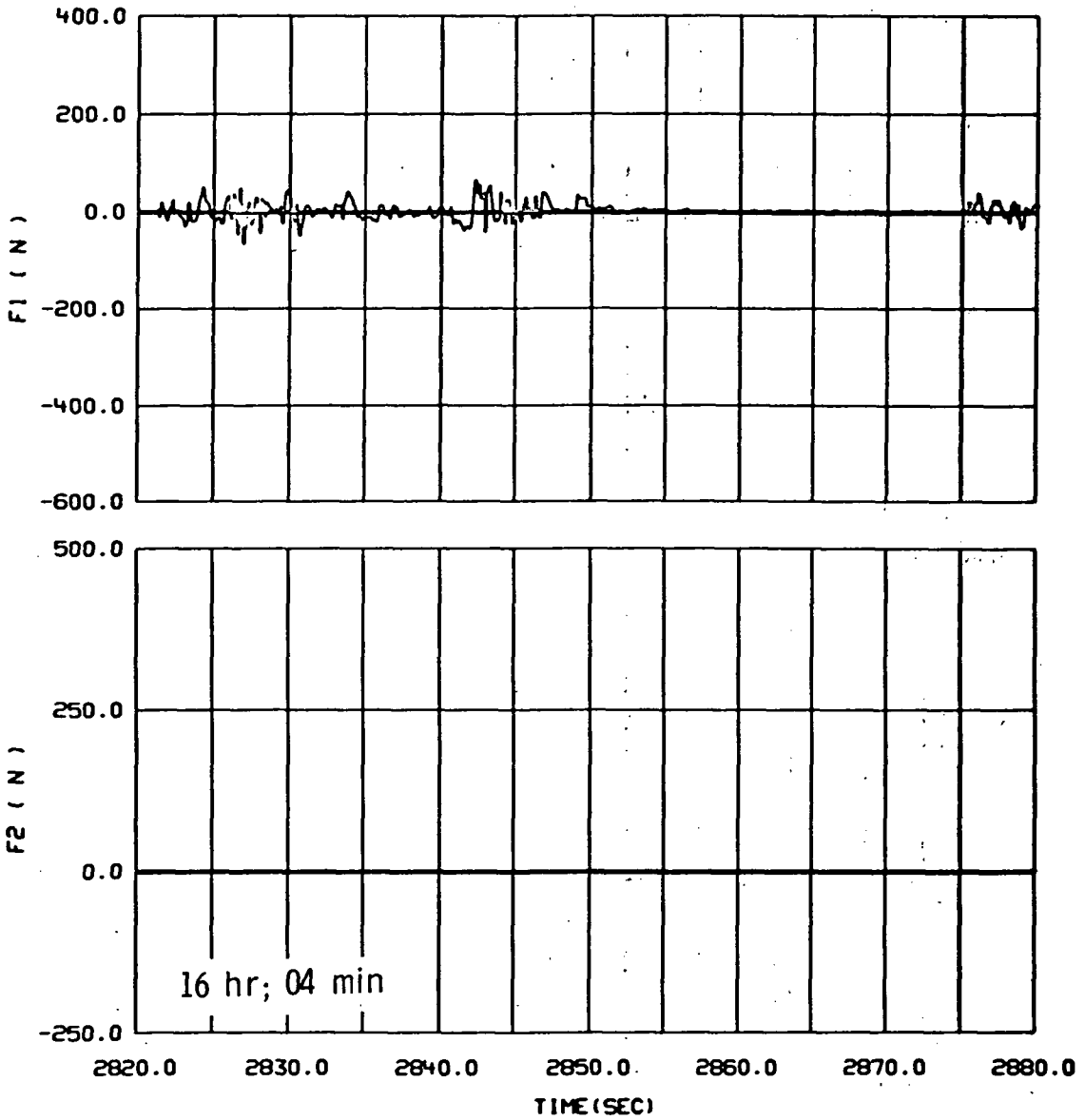

Figure 60.- Continued.

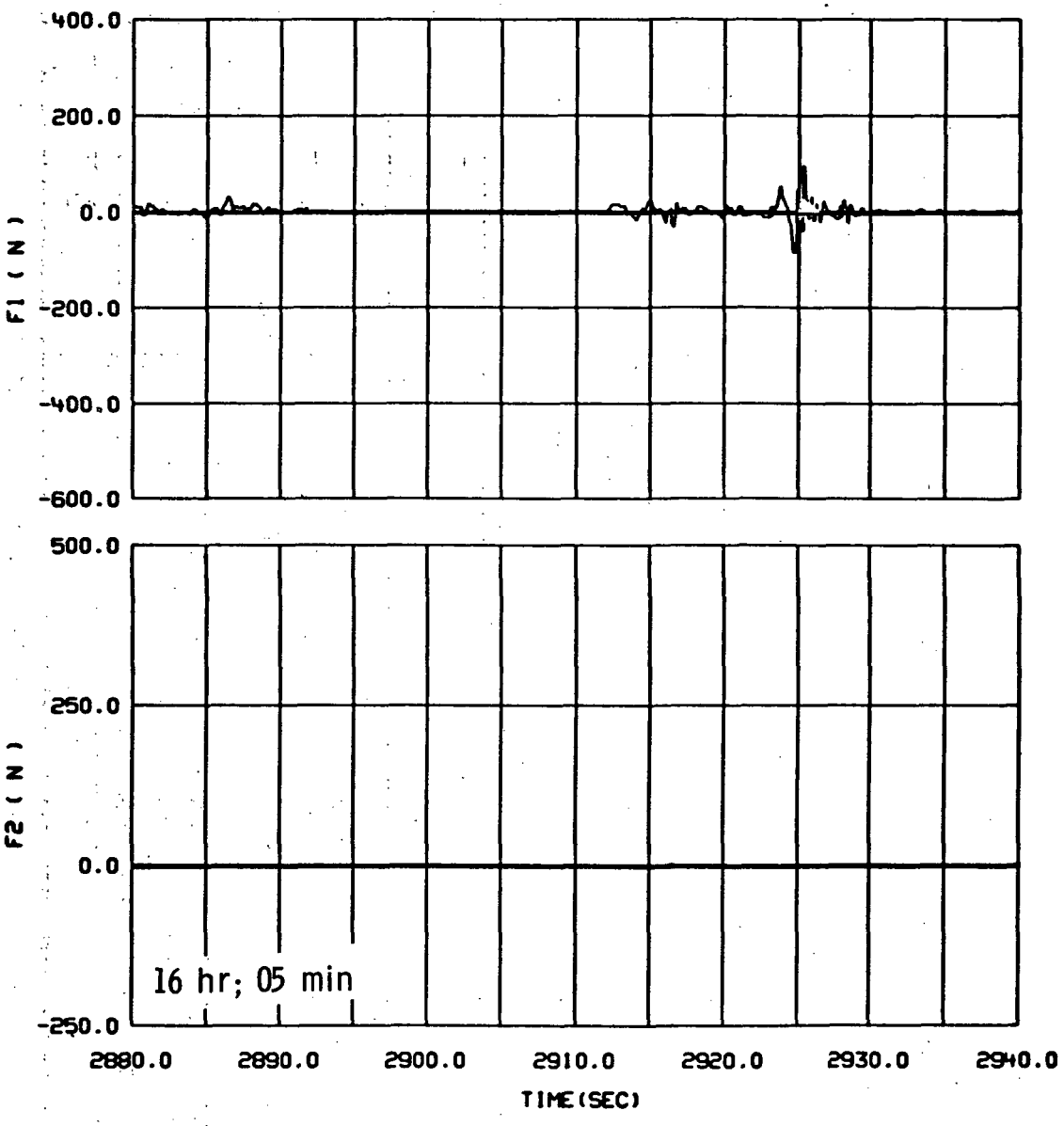

Figure 60.- Continued.

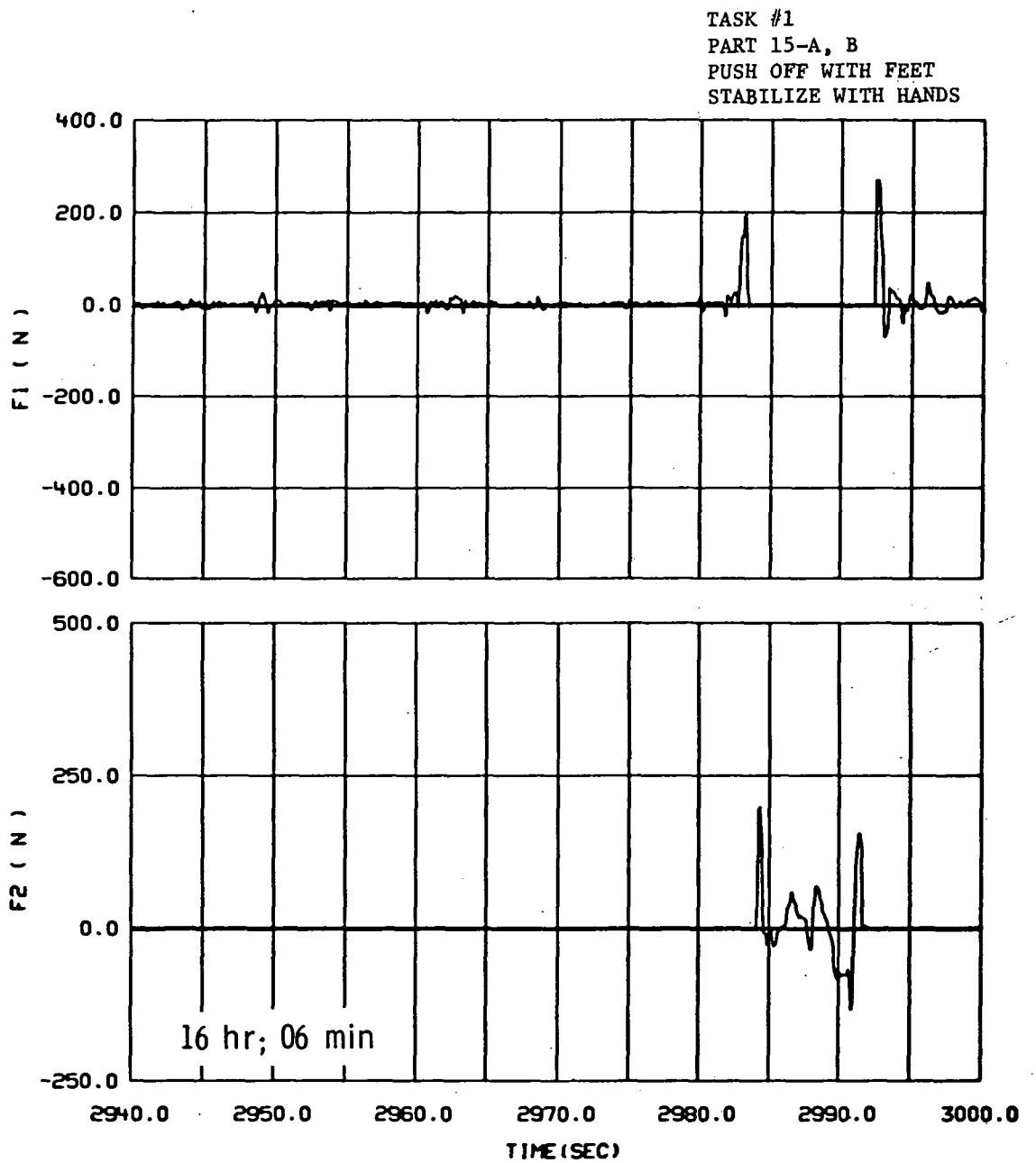

Figure 60.- Continued.

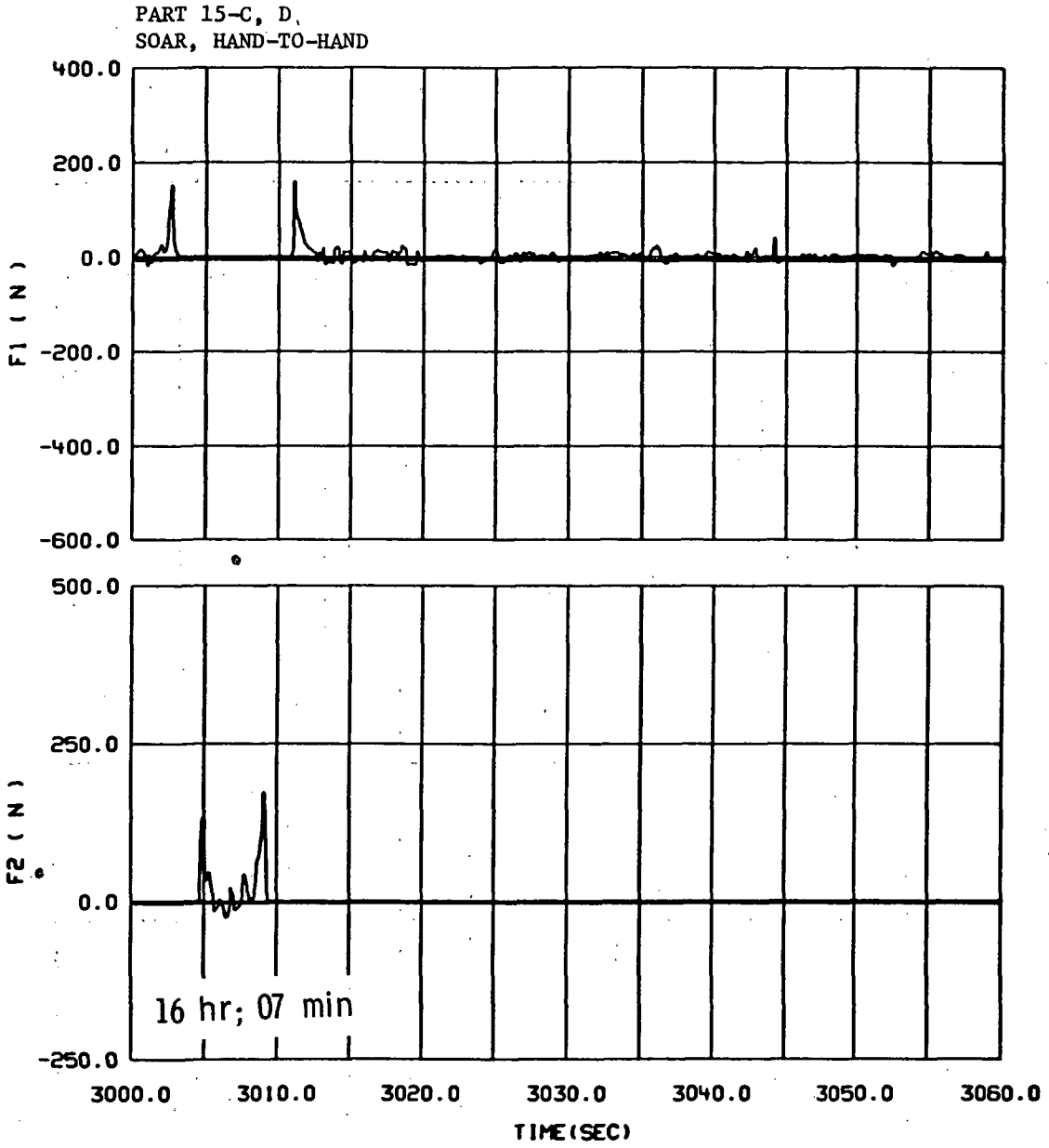

Figure 60.- Continued.

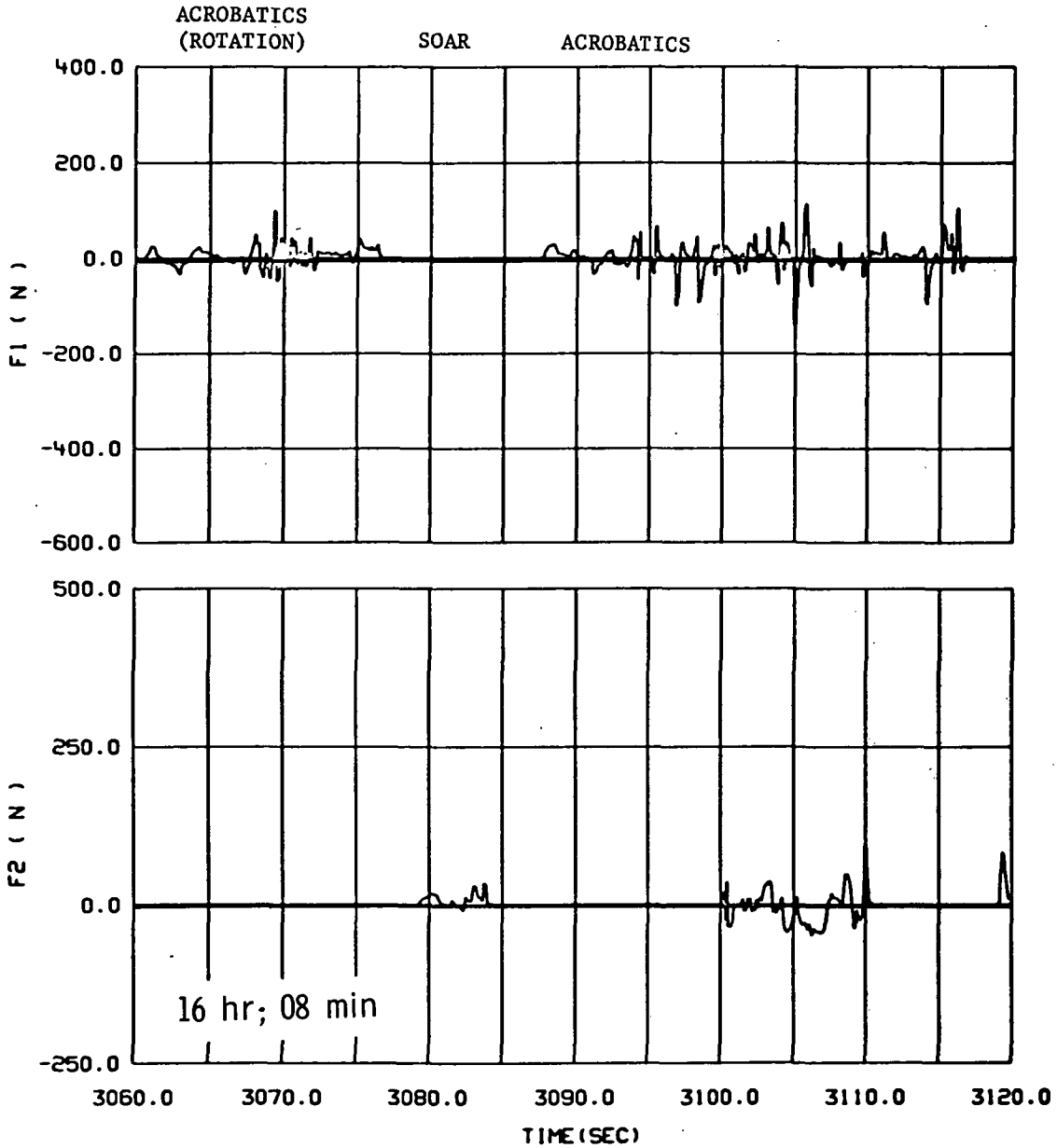

Figure 60.- Continued.

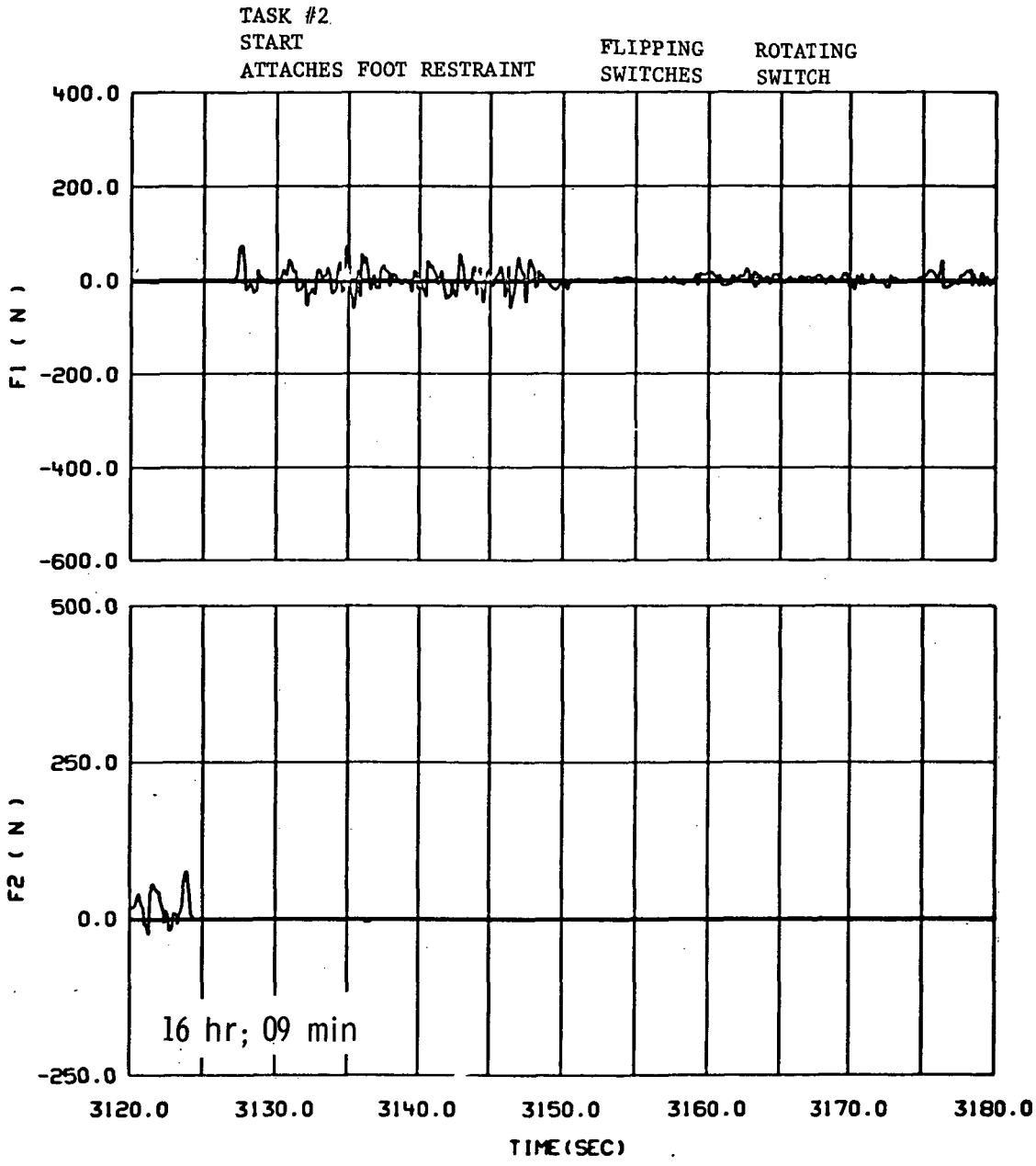

Figure 60.- Continued.

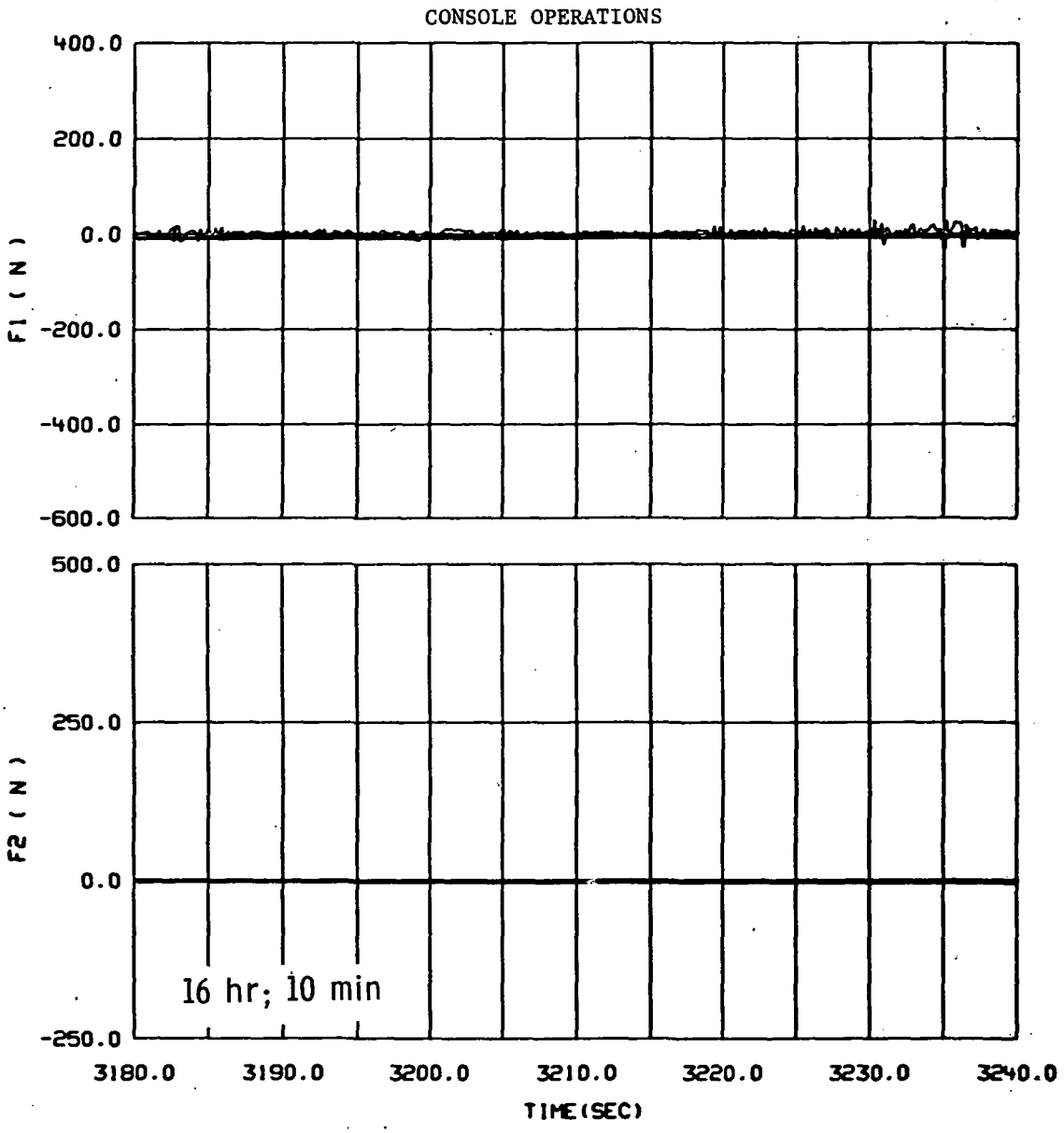

Figure 60.- Continued.

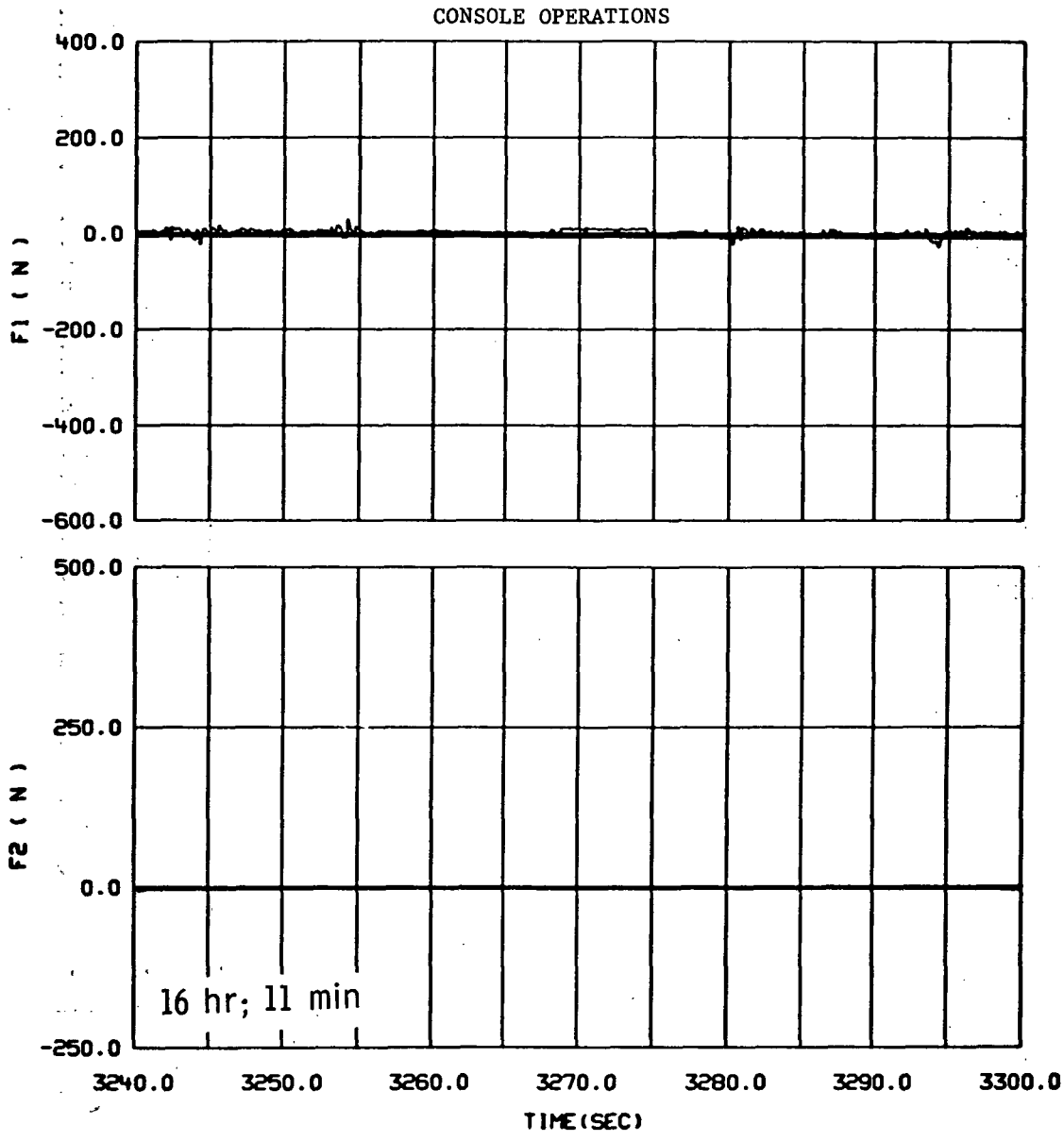

Figure 60.- Continued.

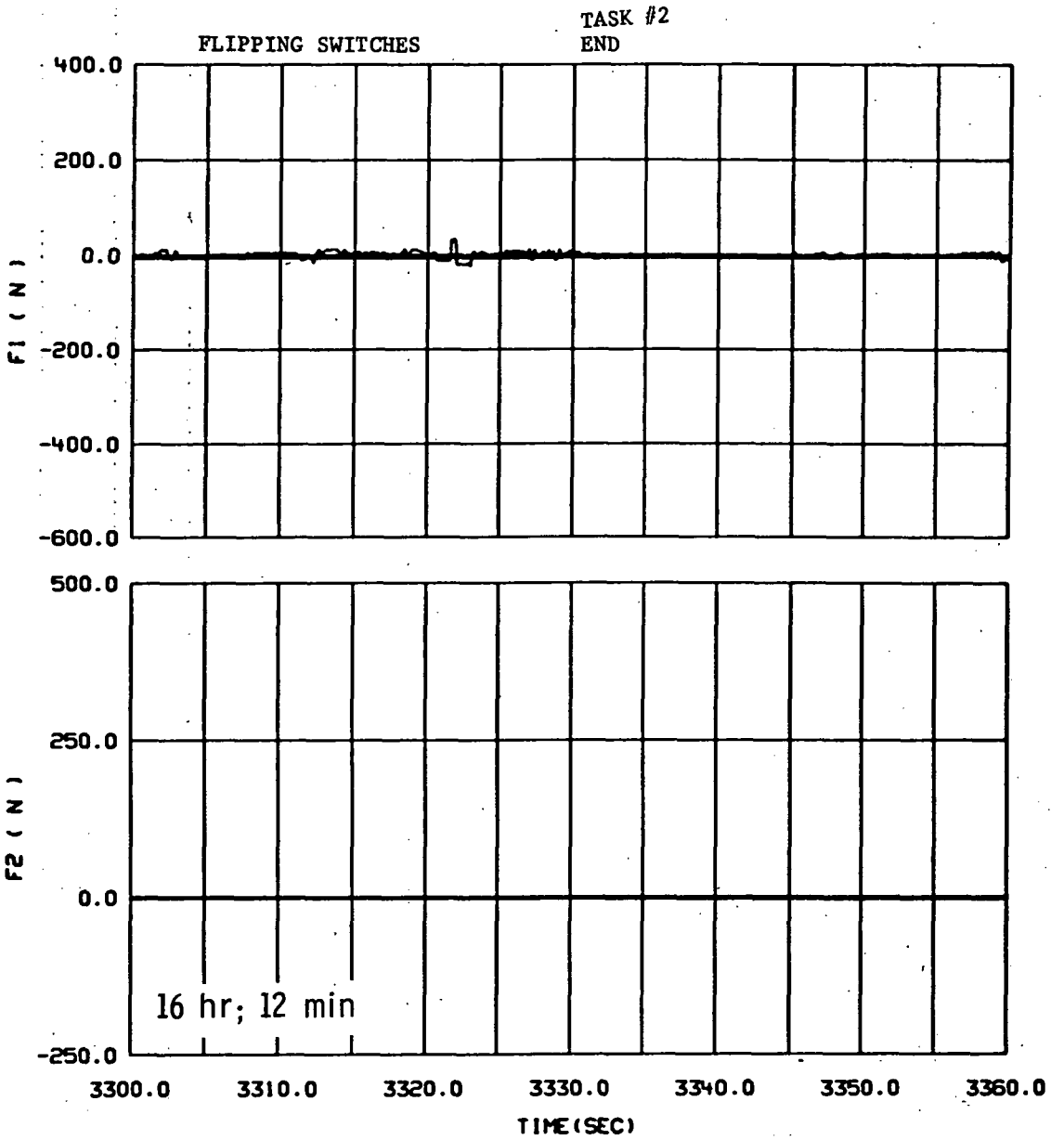

Figure 60.- Continued.

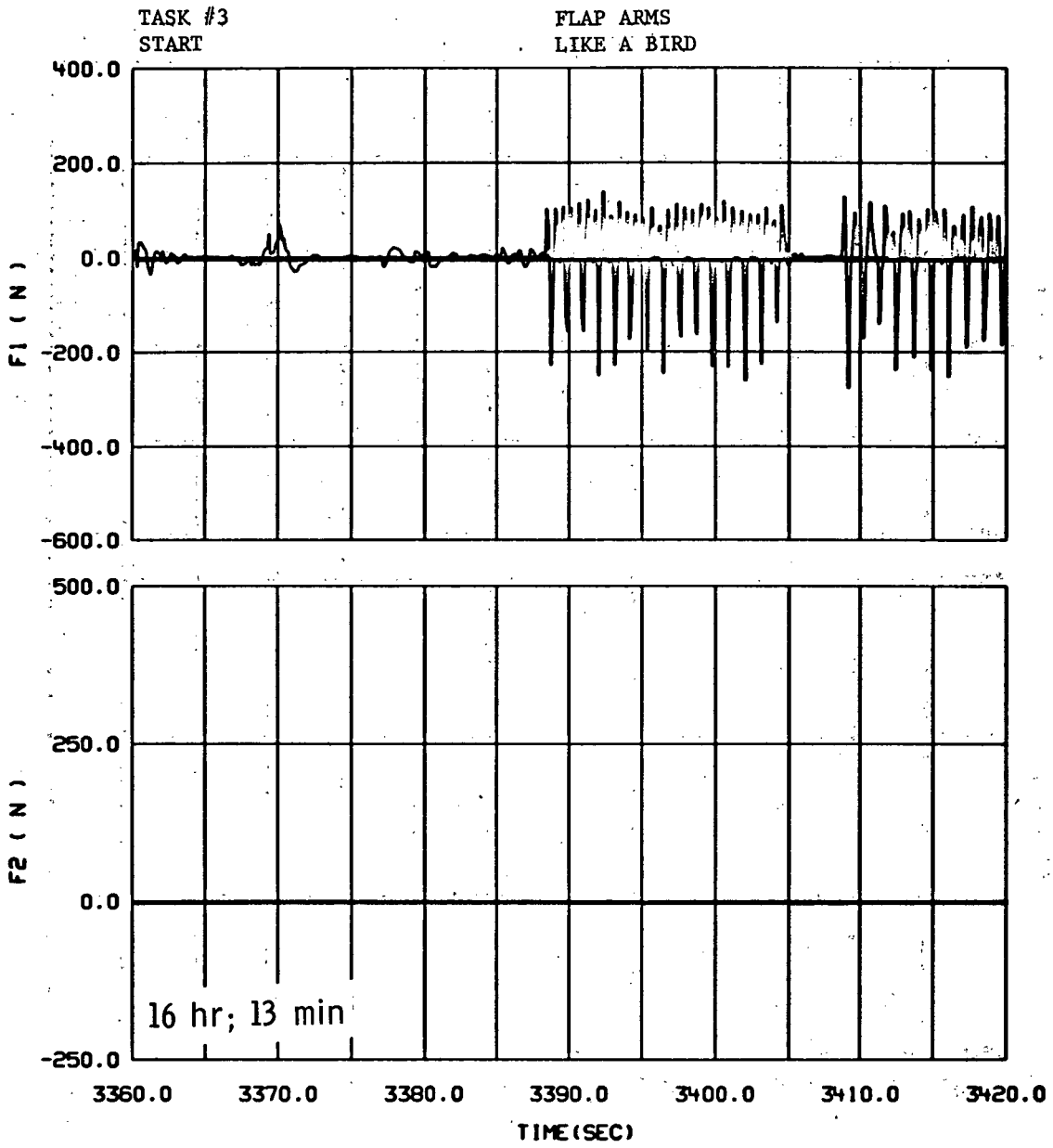

Figure 60.- Continued.

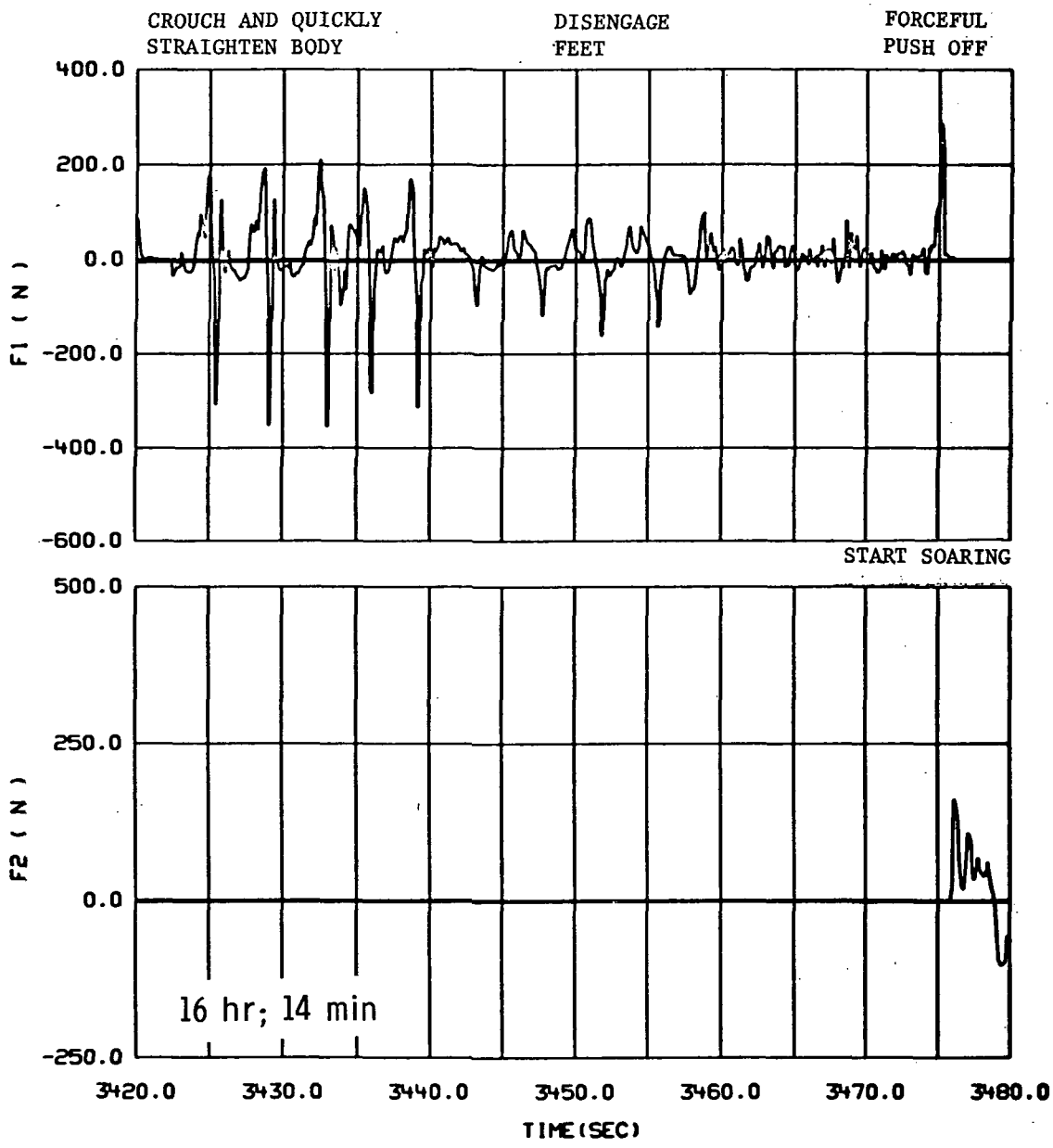

Figure 60.- Continued.

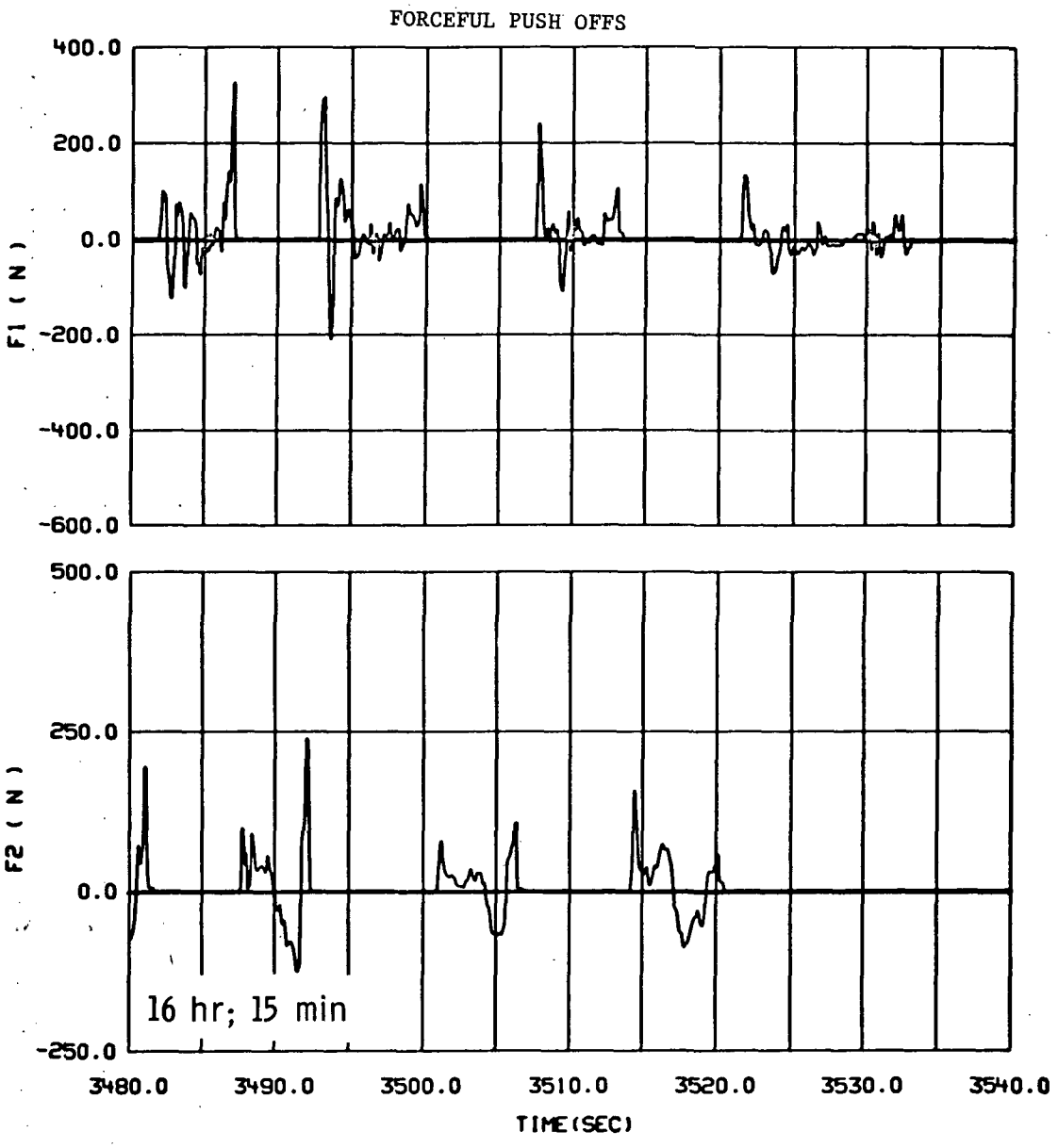

Figure 60.- Continued.

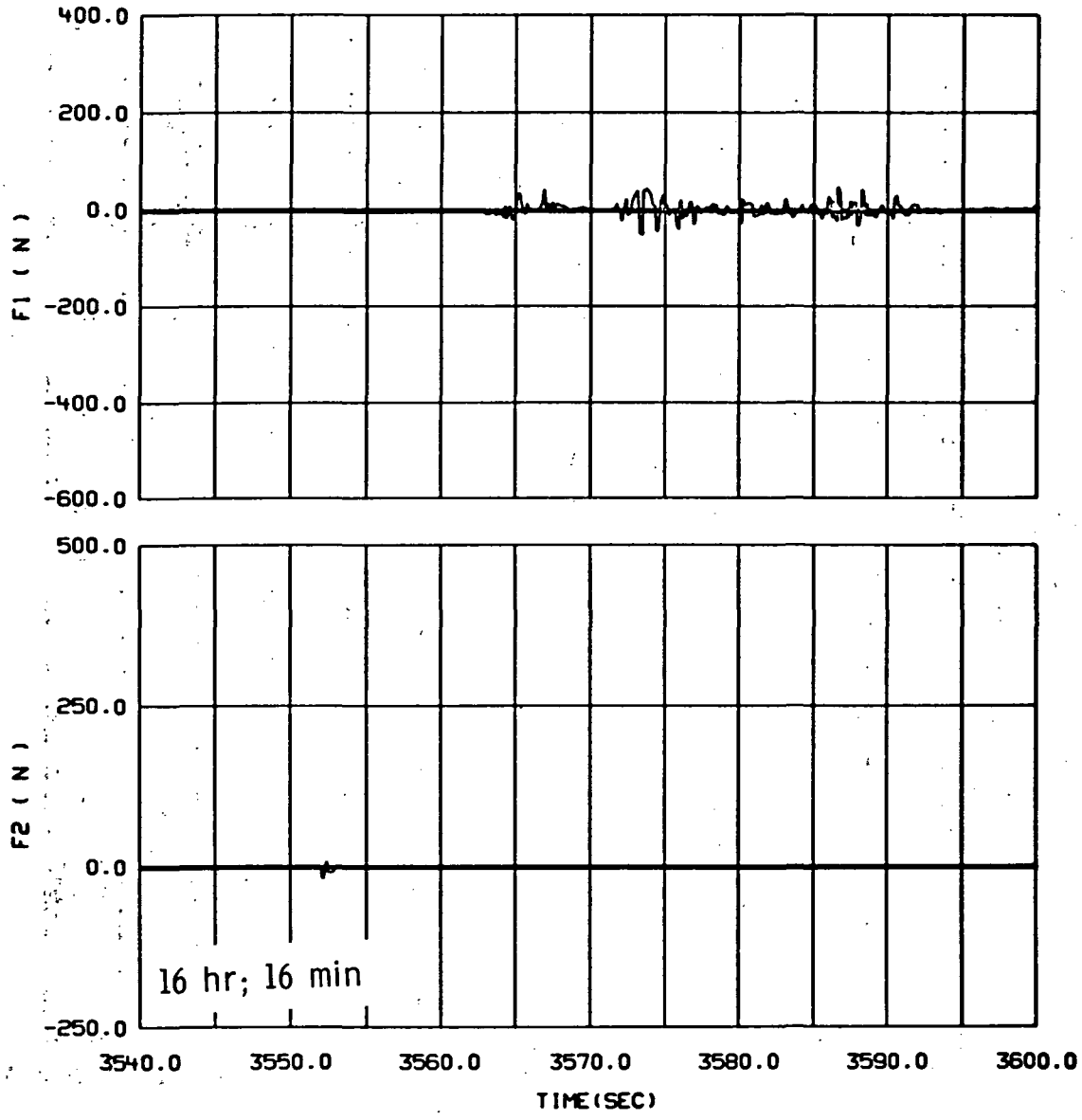

Figure 60.- Continued.

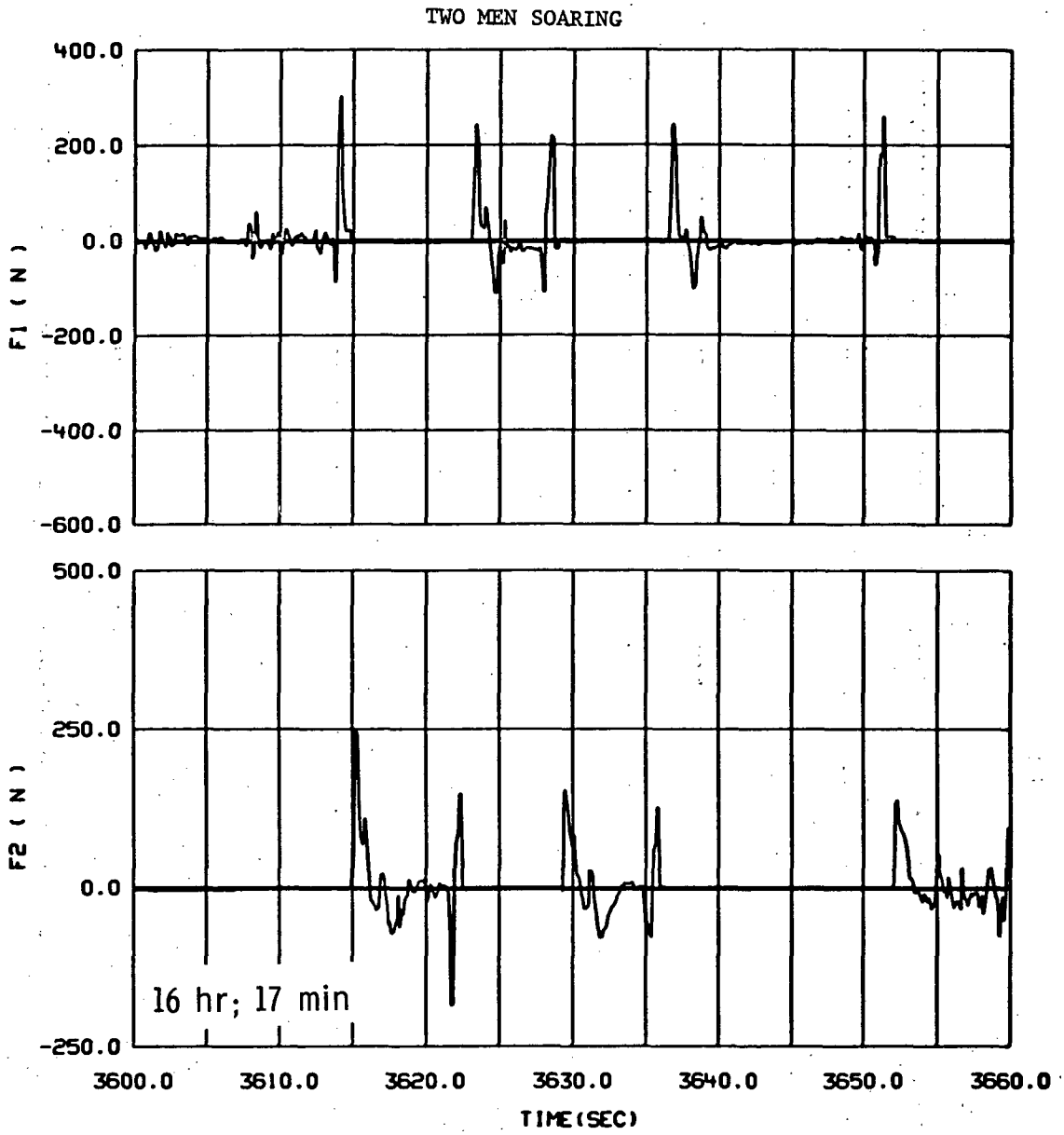

Figure 60.- Continued.

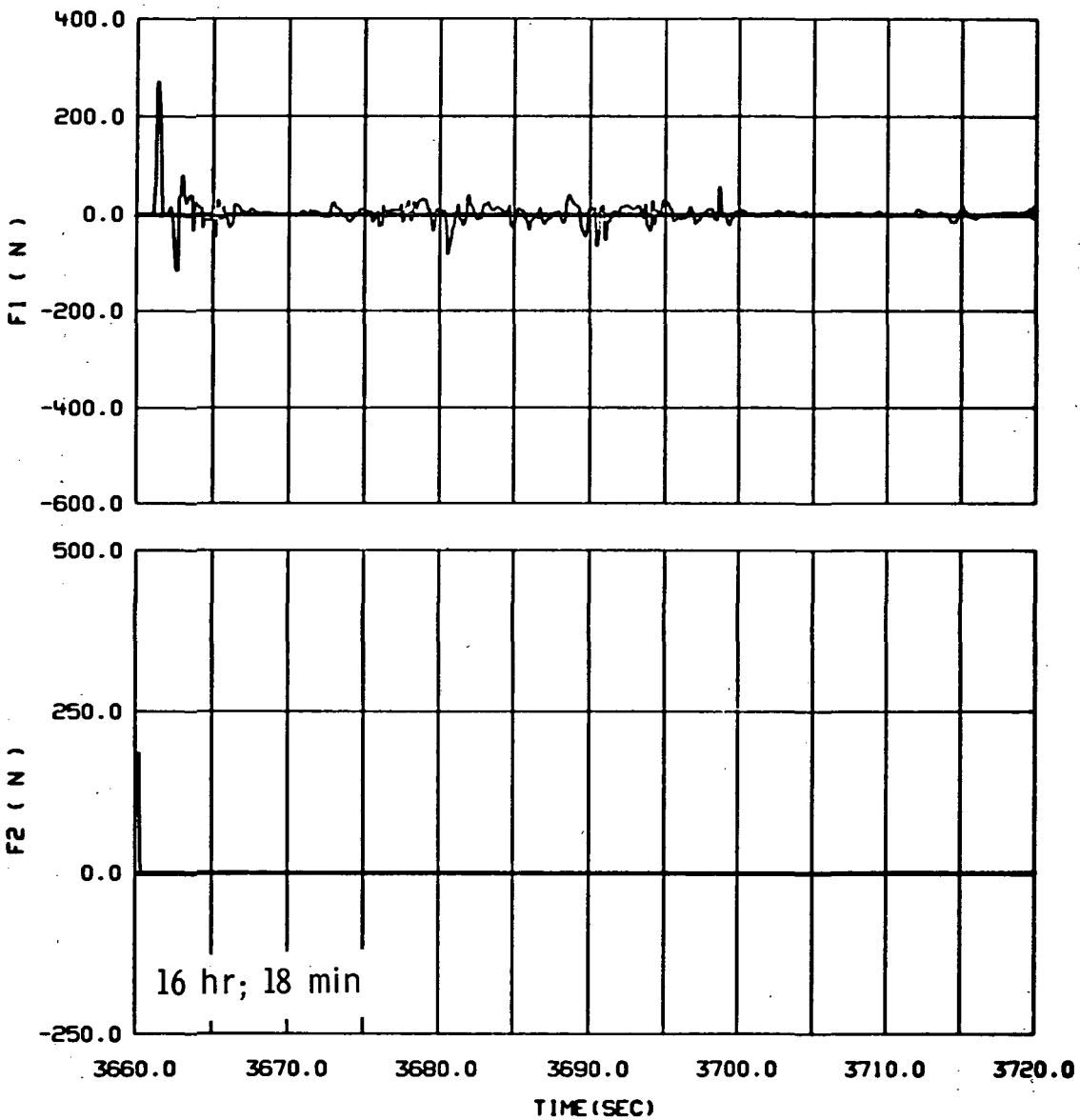

Figure 60.- Continued.

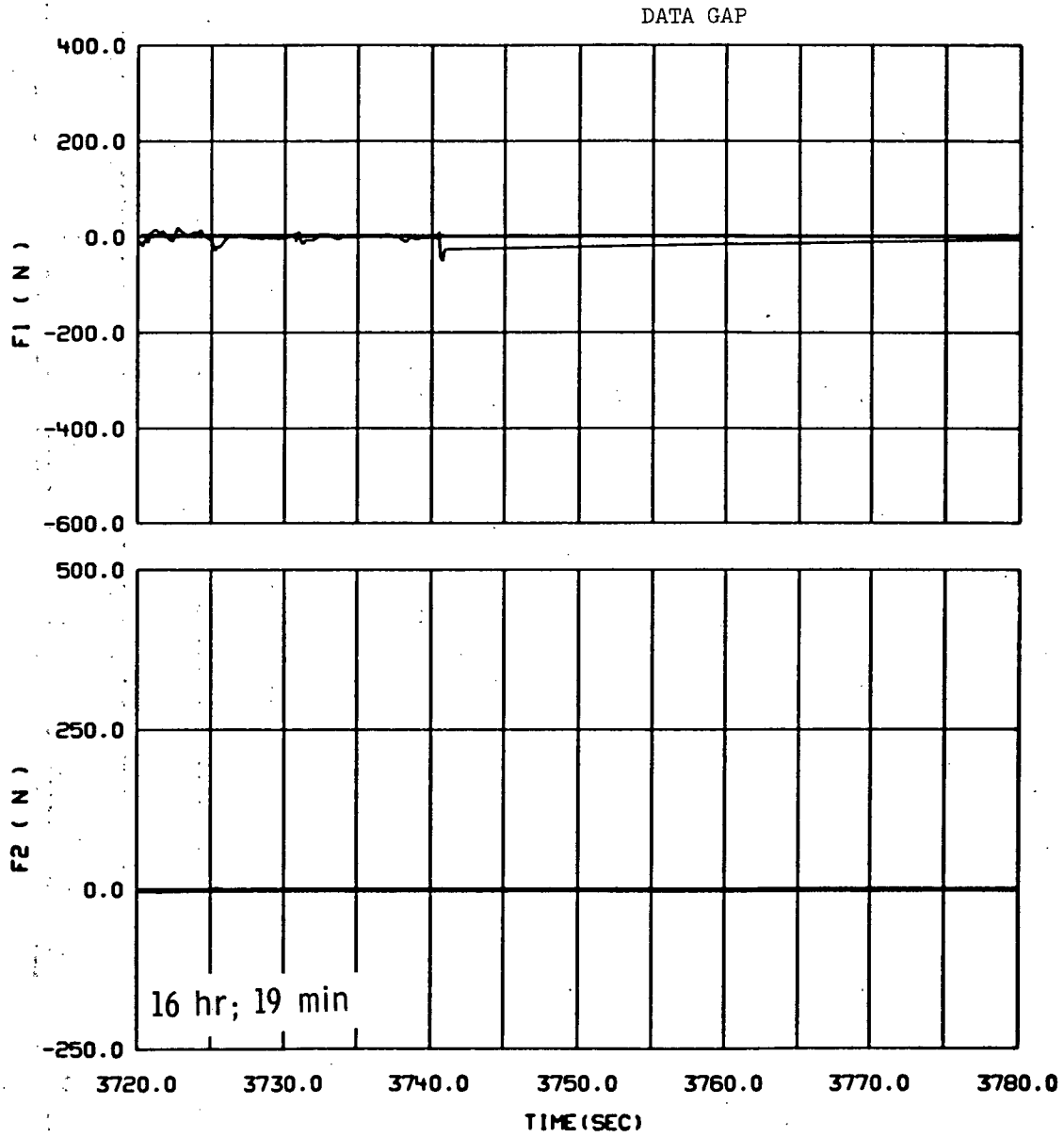

Figure 60.- Continued.

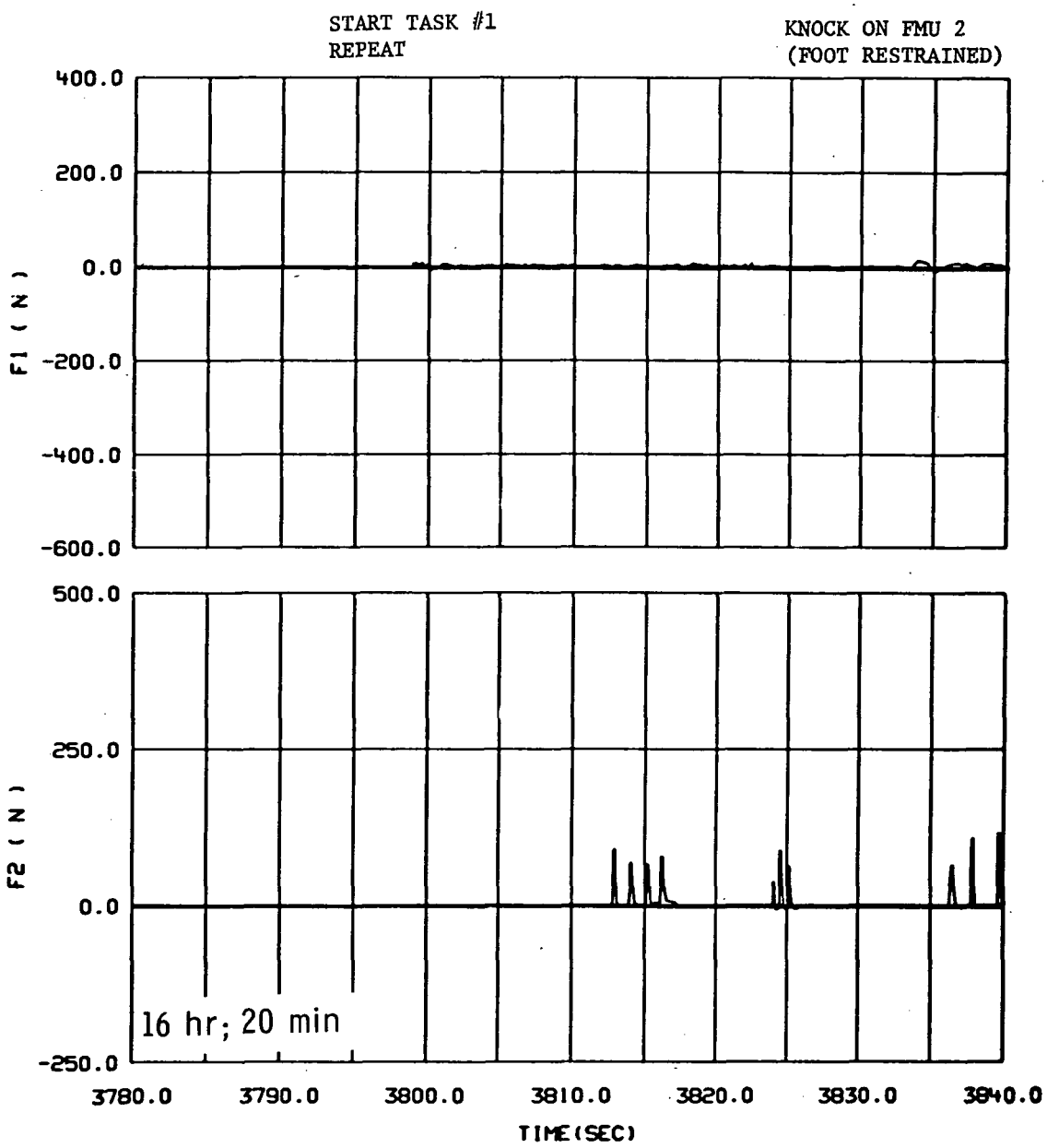

Figure 60.- Continued.

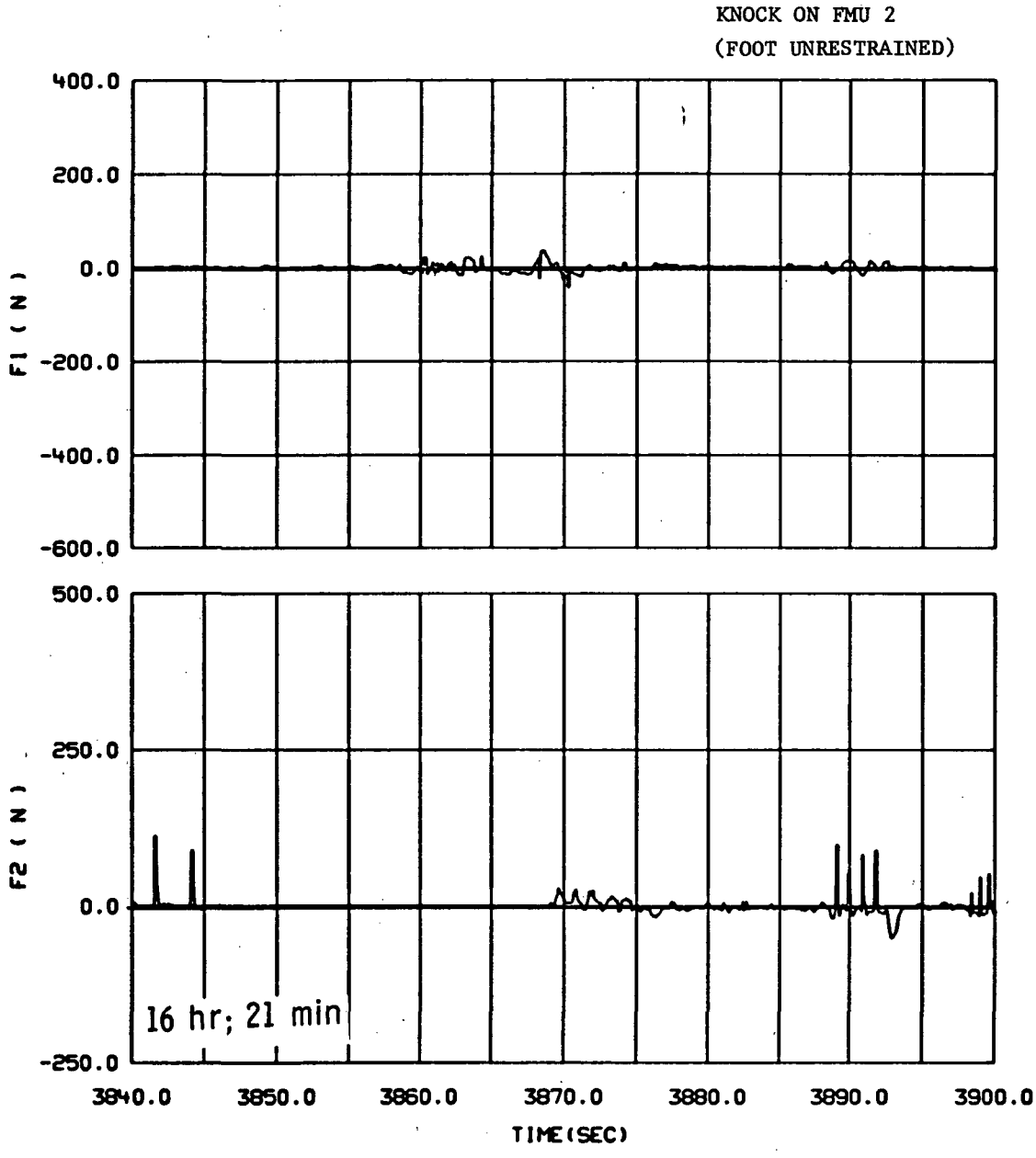

Figure 60.- Continued.

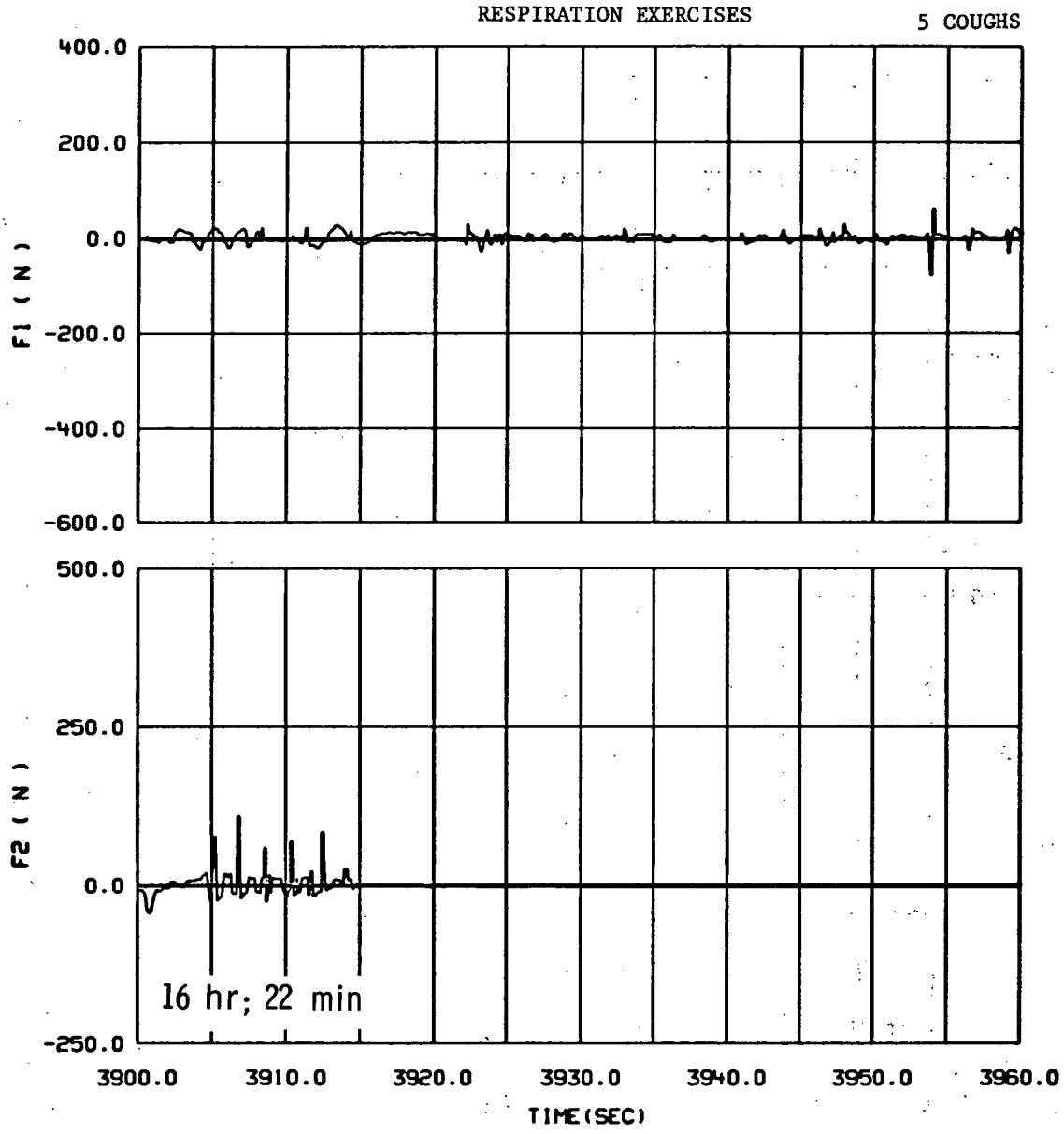

Figure 60.- Continued.

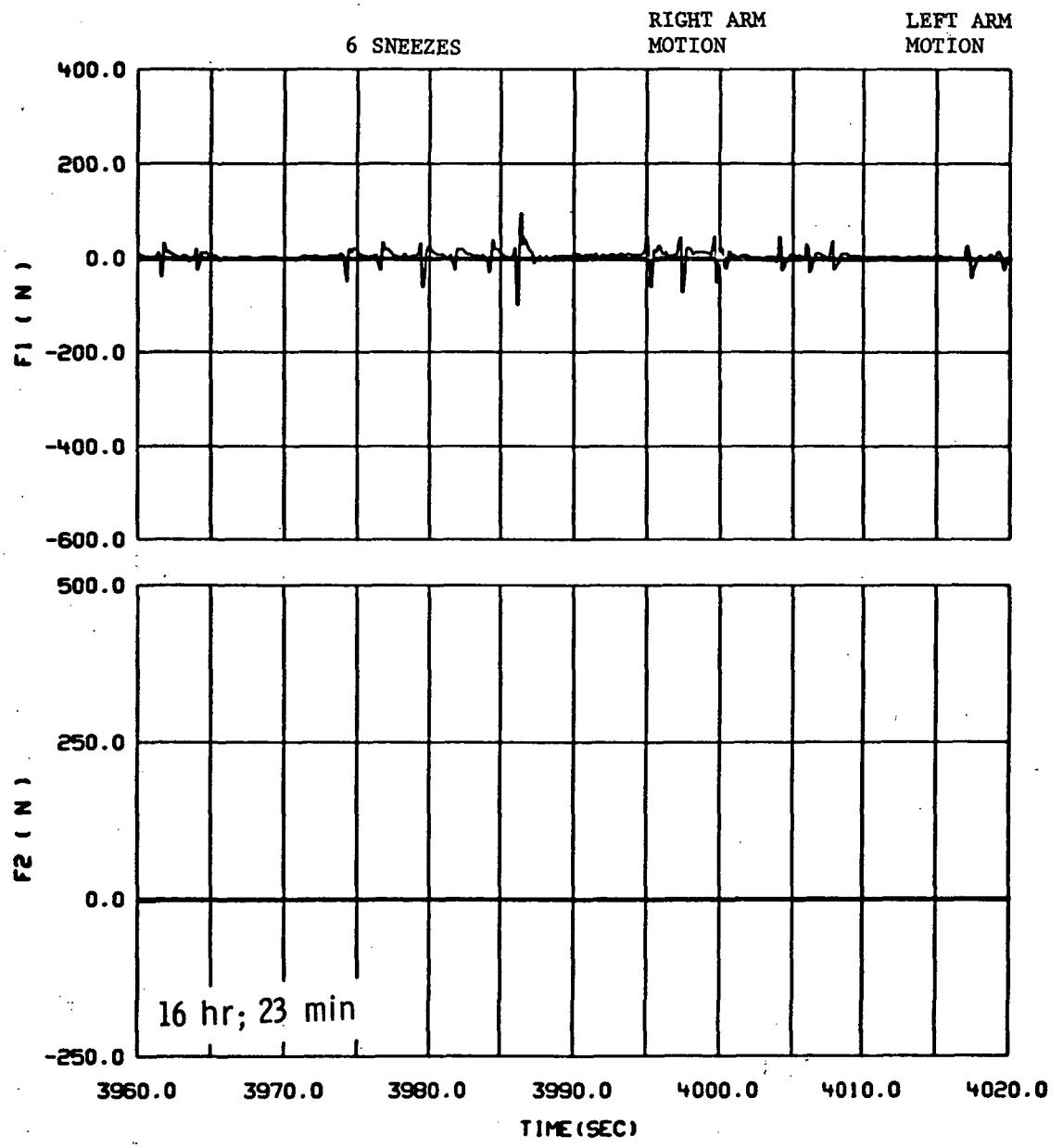

Figure 60.- Continued.

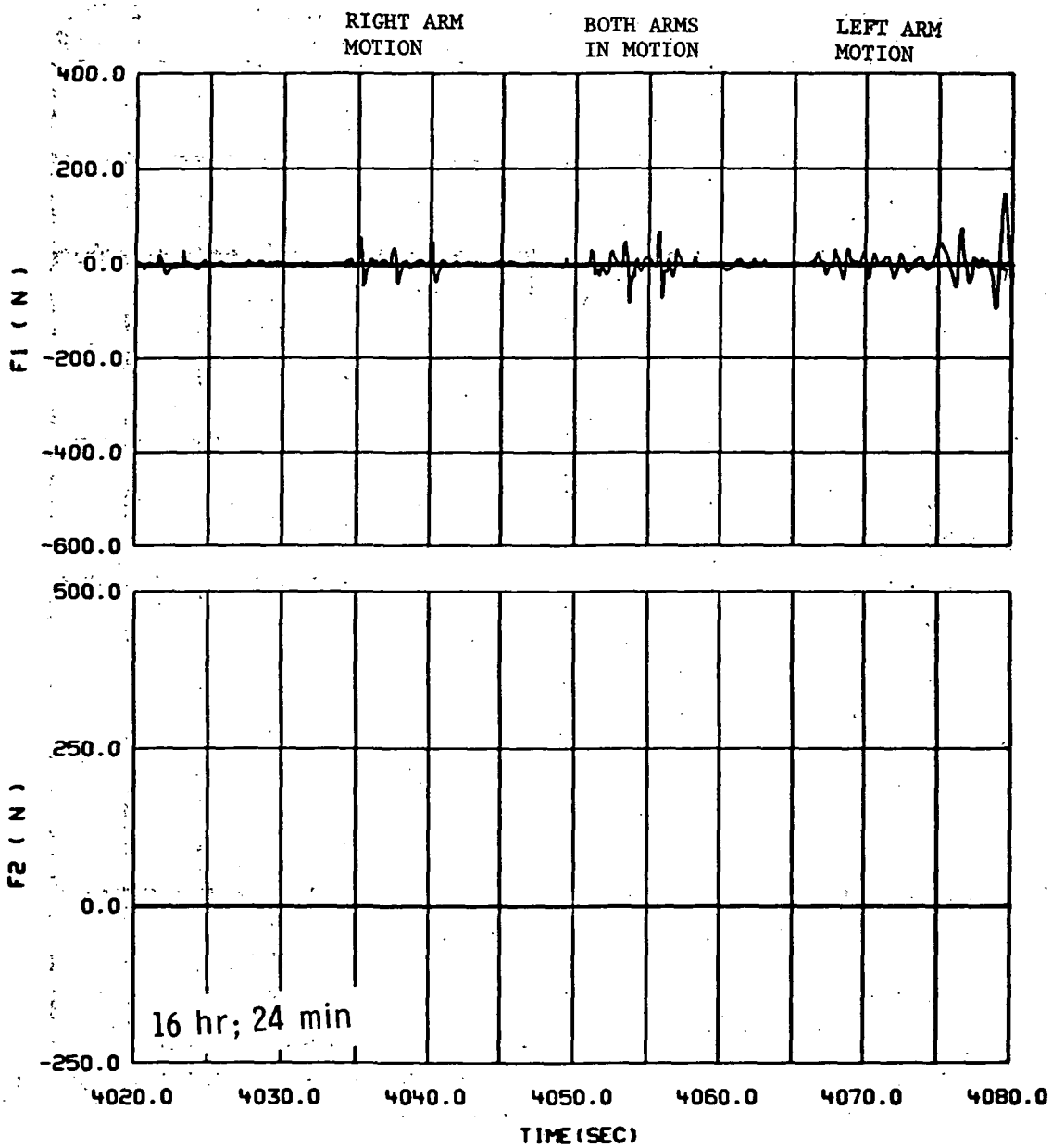

Figure 60.- Continued.

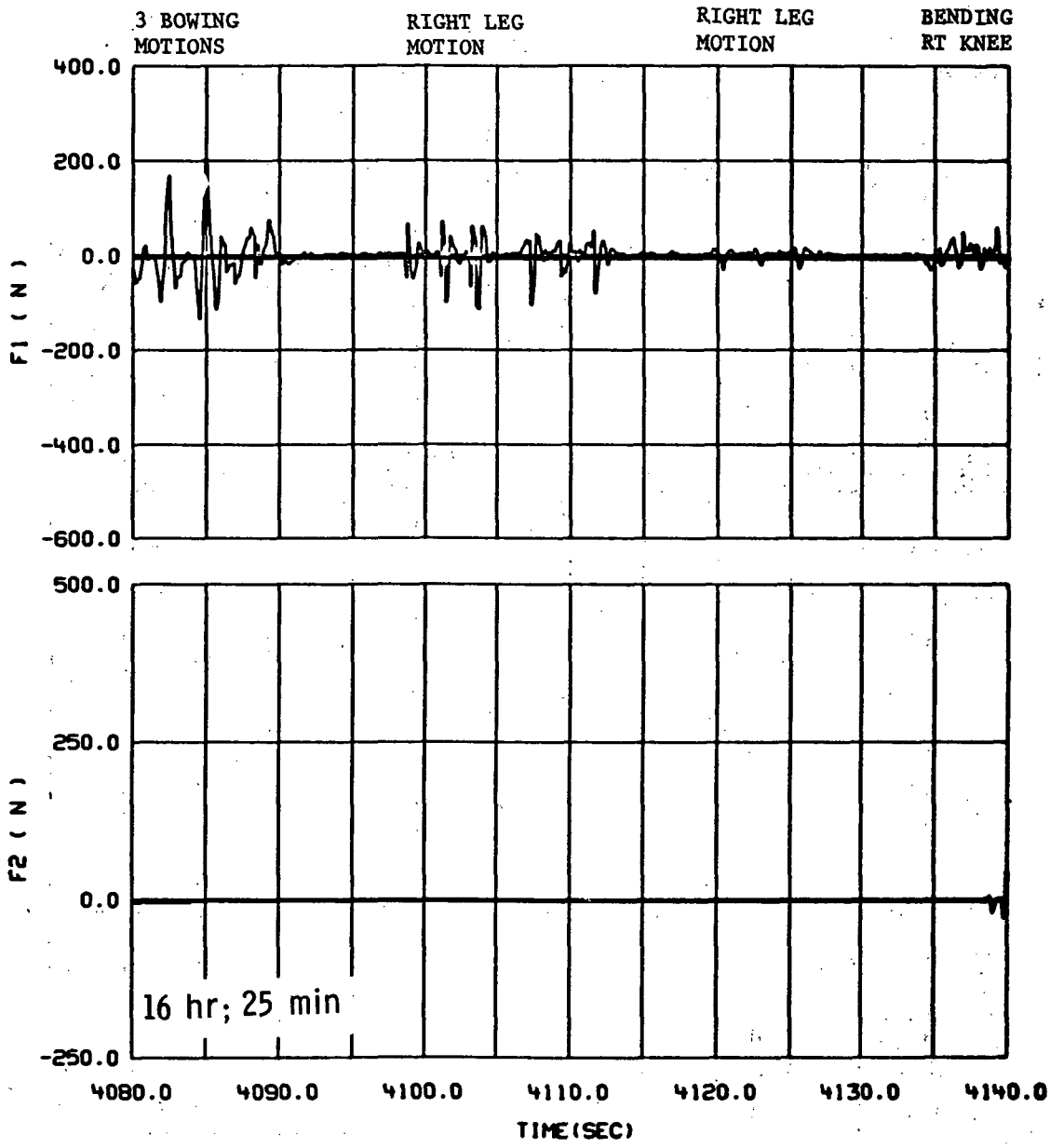

Figure 60.- Continued.

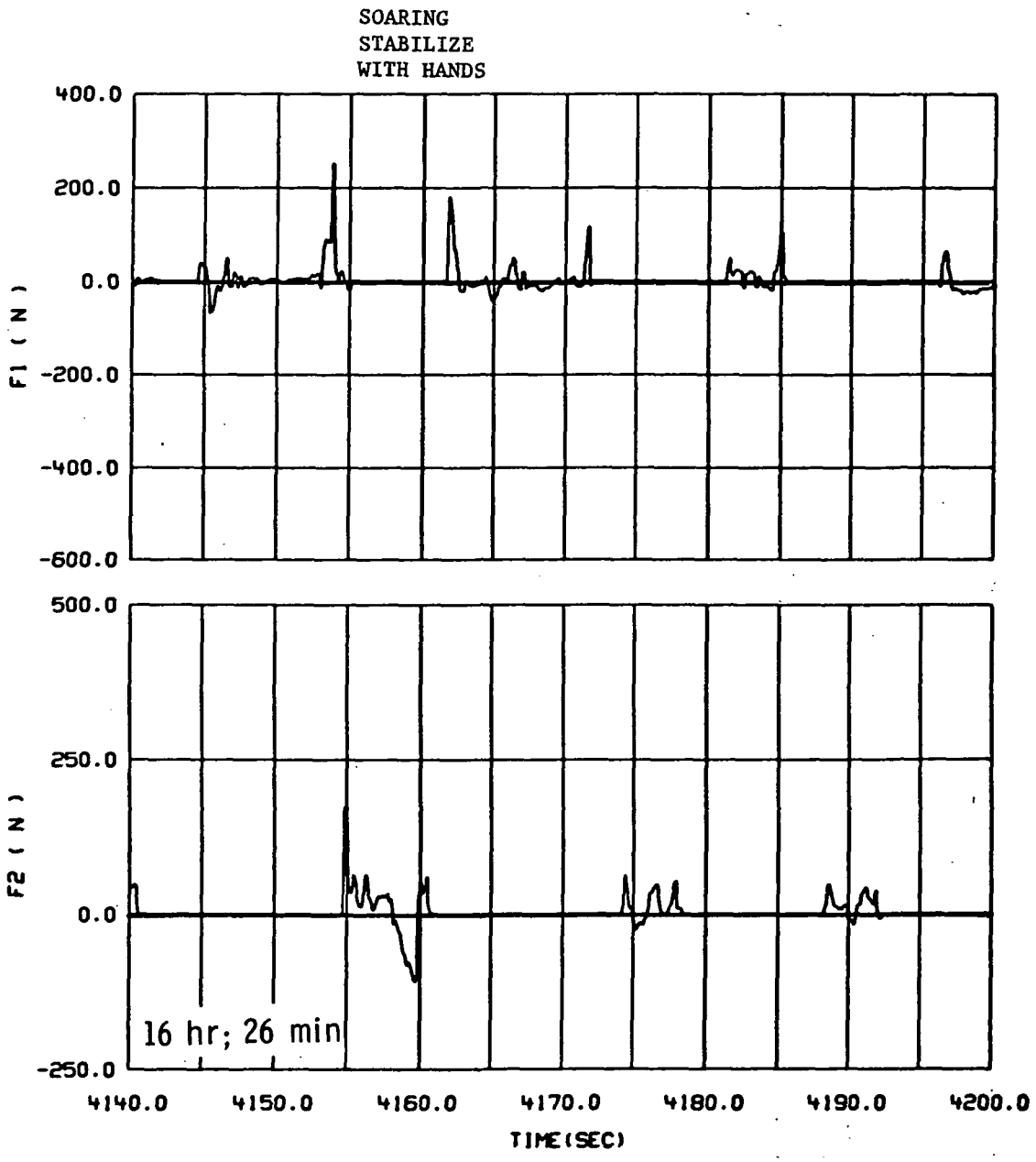

Figure 60.- Concluded.

*U.S. GOVERNMENT PRINTING OFFICE: 1976 - 635-275/83

"The aeronautical and space activities of the United States shall be conducted so as to contribute . . . to the expansion of human knowledge of phenomena in the atmosphere and space. The Administration shall provide for the widest practicable and appropriate dissemination of information concerning its activities and the results thereof."

—NATIONAL AERONAUTICS AND SPACE ACT OF 1958

NASA SCIENTIFIC AND TECHNICAL PUBLICATIONS

TECHNICAL REPORTS: Scientific and technical information considered important, complete, and a lasting contribution to existing knowledge.

TECHNICAL NOTES: Information less broad in scope but nevertheless of importance as a contribution to existing knowledge.

TECHNICAL MEMORANDUMS: Information receiving limited distribution because of preliminary data, security classification, or other reasons. Also includes conference proceedings with either limited or unlimited distribution.

CONTRACTOR REPORTS: Scientific and technical information generated under a NASA contract or grant and considered an important contribution to existing knowledge.

TECHNICAL TRANSLATIONS: Information published in a foreign language considered to merit NASA distribution in English.

SPECIAL PUBLICATIONS: Information derived from or of value to NASA activities. Publications include final reports of major projects, monographs, data compilations, handbooks, sourcebooks, and special bibliographies.

TECHNOLOGY UTILIZATION PUBLICATIONS: Information on technology used by NASA that may be of particular interest in commercial and other non-aerospace applications. Publications include Tech Briefs, Technology Utilization Reports and Technology Surveys.

Details on the availability of these publications may be obtained from:

SCIENTIFIC AND TECHNICAL INFORMATION OFFICE

NATIONAL AERONAUTICS AND SPACE ADMINISTRATION

Washington, D.C. 20546